UNIVERSITY OF SOUTHAMPTON
Faculty of Engineering and Applied Science
Department of Electronics and Computer Science

# Multilayer Mobile Communication Systems

by

Chai Phongphanphanee

B.Eng., M.Sc.

*A doctoral thesis submitted in partial fulfillment of the requirement for the award of Doctor of Philosophy at the University of Southampton*

March 2000

**Supervisor: Professor Raymond Steele**
B.Sc., Ph.D., D.Sc., CEng., FEng., FIEEE, FIEE
Department of Electronics and Computer Science,
University of Southampton

UNIVERSITY OF SOUTHAMPTON

## ABSTRACT

FACULTY OF ENGINEERING AND APPLIED SCIENCE

Department of Electronics and Computer Science

Doctor of Philosophy

# Multilayer Mobile Communication Systems

*by* Chai Phongphanphanee

The rapid growth of mobile communications establishes the need for capacity evolution methods for the cellular systems of today. One solution is to employ multilayer network that provide coverage to the same areas by several cells of different sizes. While street microcells and in-building picocells contribute strategic coverage in densely urban area, macrocells provide seamless coverage over wide areas.

We consider three approaches of deploying multilayer networks for the global system for mobile communications (GSM). The first one is frequency partitioning where a GSM allocated bandwidth is divided into subbands and each subband is allocated to each layer. The spectral efficiency of the frequency partitioning architecture is evaluated. For a typical link quality requirement (SIR $\geq$ 12 dB over 90% of the service area), the minimum bandwidth required to operate a system with a good spectral efficiency are 15 and 9 MHz, for macrocells and picocells, respectively. The minimum bandwidth for a microcells is from 2.4 MHz to 8.4 MHz depending on cell layouts. The maximum spectral efficiency of macrocells, microcells and picocells are 0.88, 1489 and 7845 Erlangs/MHz/km$^2$, respectively.

Another approach of deploying multilayer cellular systems is to allocate the entire GSM bandwidth to the macrocellular network, and to use the digital enhanced cordless telecommunication (DECT) network in street microcells and in in-building picocells. This approach is suitable for operators with relatively limited spectrum for a GSM network, however the system requires dual-mode mobile terminals, namely GSM/DECT terminals. We propose some enhancements to a DECT system, such as a minicell with an adaptive handover strategy, and an adaptive DECT-like radio interface for wireless ATM. We also evaluate a DECT system providing outdoor as well as indoor radio coverage from indoor radio ports.

The last approach is a spectrum sharing system where all cellular layers utilise the same bandwidth. In this thesis we propose fixed spectrum sharing algorithm (FSSA) and dynamic spectrum sharing algorithm (DSSA). We analyse several case studies for a FSSA system with the macrocellular cluster size of 4/12. FSSA gives better spectrum efficiency than the frequency partitioning scheme for the macrocellular system with a reuse cluster size of greater that seven. When the reuse cluster size is less than seven, the frequency partitioning gives better spectrum efficiency. The spectrum efficiency for both schemes are the same when the reuse cluster size is seven. Dynamic spectrum sharing algorithm (DSSA) provides spectrum sharing for cellular systems with dynamic channel assignment. The performance of DSSA is analysed in terms of SIR performance.

This thesis proposes a novel spectrum resource allocation protocol, namely adaptive autonomous frequency assignment (AAFA). The protocol provides frequency reuse without frequency planning and automatically assigns the spectrum resource according to the changes in the propagation environment and traffic conditions. The protocol was tested using computer simulation on different cellular layer models, and different type of services, i.e., circuit-switched service and packet data access service. Comparing with the conventional FCA system, AAFA increases the system capacity by 20% and 180% for uniform and non-uniform traffic scenarios, respectively.

# *Acknowledgements*

I would like to thank my supervisor, Professor Ray Steele, for his support, enthusiasm and guidance during my work. I would also like to thank my colleagues and staffs in the communication group, with whom I found an excellent environment for research, in particular, to Professor Lajos Hanzo for his assistance and advice. Special thanks and appreciation to

- Terry Mitchell for his radio propagation work.
- Peter Cherriman, Chin-Chun Lee, Mostafa Nofal, Matthew Au, Jason Woodard, Jeff Torrance, Mehul Metha, Bashir El-Jabu and Lie-Liang Yang for their technical assistance.
- Hee Thong How, Sheyam Lal Dhomeja, Tong-Hooi Liew and Mong Suan Yee for helpful Latex advices on the preparation of this thesis.
- Denis Harvey, the group secretary. for her adminstrative support.
- My brothers, relatives, and friends who have continuously encouraged me to finish my postgraduate study.

My deepest gratitude goes to my parents and wife for their love and support throughout the years. Finally, I thank the Thai government for their financial support.

To my parents and Lord Buddha

# Contents

# List of Tables

# List of Figures

# List of Publications

Based on the work in this thesis, the following papers were published.

1. C. Phongphanphanee and R. Steele, "GMSK for Mobile Radio", 1995/6 Research Journal, Department of Electronics and Computer Science, University of Southampton.

2. C. Phongphanphanee and R. Steele, "Enhancing the DECT system", Electronics Letters, Vol.33, No.21, Oct. 9, 1997, pp.1755-1757.

3. C. Phongphanphanee, T. Mitchell and R. Steele, "DECT Coverage of Indoor/Outdoor Environments", IEEE Communications Letters, Vol.3, No.6, June, 1999, pp.161-163.

# Chapter 1

# Introduction

In less than two decades, the number of cellular subscribers has grown from zero to over 100 million. In some countries, more than 40 percent of the population use mobile communications. Such rapid growth and new demands for high-speed multimedia services stands in clear contrast to the rather limited radio spectrum resources that have been allocated in international agreements. In conventional cellular mobile radio networks, base stations (BSs) are usually located at high elevations to provide maximum radio coverage, and a coverage by each base station is called a cell, or specifically, a macrocell. To provide seamless radio coverage over a wide area, the base stations are scattered and their cells are tessellated to provide seamless coverage. Due to spectrum scarcity, it is essential to re-use the allocated radio spectrum efficiently. Frequencies used in a given cell are reused in other cells, which are at a sufficient distance that the unavoidable interference created is within an acceptable level. The spectrum is partitioned between cells that are to form a cluster. Frequency re-use occurs when clusters of cells are tessellated. In order to model the system, cells are often represented by hexagons, and the coverage area is represented by a hexagonal grid.

As demands for services and capacity increases, conventional cells, generally called macrocells, cannot provide the required capacity, particular in urban areas. Several solutions have been already proposed to address this situation.

1. Cell splitting by sub-dividing one cell into typical three smaller cells [1, 2].

2. Using frequency hopping combined with discontinuous transmission and power control that allow the clusters to have fewer cells, and hence more frequencies per base station [3].

3. Reuse partitioning, often called underlay/overlay that have two reuse clusters [1, 2]. The smaller one is used only for communications made by users that are near to their base station and can tolerate a higher interference because their useful signal is very high, and the other clusters is used by users who are more distant from their base stations.

Although these methods allow an increase in capacity, they rely on conventional macrocells, with their large reuse cluster sizes. A solution for serving high traffic demands is to deploy small cells called microcells, where the base stations have limited transmission power with antennas below the roof-top level of the surrounding buildings. As the coverage of a microcell, typically a few city blocks, is much smaller than the coverage of a macrocell, between one and five kilometres, the available spectrum can be use more densely, and consequently the capacity increases. In addition, the cluster size required by microcells may be smaller than the macrocellular reuse cluster size, because the microcellular base station antennas are below the rooftops, and consequently, the co-channel interference is reduced by the electromagnetic shielding formed by the buildings.

Because microcells are characterised by fairly low power levels and antenna heights, they offer limited indoor coverage. Macrocells may offer better indoor coverage due to their higher antenna placements and higher transmission power, but often they do not offer sufficient indoor capacity in offices, where specific indoor systems are required to serve a large number of users. It is also essential to cope with the hard-to-predict indoor radio propagations, such as within buildings and in underground railway environments. For these difficult environments a number of different solutions have been suggested or are already in use. These include distributed antennas and conventional small picocells which yield high capacity [4, 5, 6]. The networks with microcells and picocells in addition to macrocells are called multilayer networks, because picocells and microcells have overlapping coverage with macrocells.

The research described in this thesis is concerned with the design of multilayer networks for mobile radio systems employing time division multiple access (TDMA). These include the global system for mobile communication (GSM)-based systems (i.e., GSM 900, digital cellular service at 1800 MHz, or DCS 1800, now often called GSM 1800, and personal communications service at 1900 MHz, or PCS 1900) which dominate the world's cellular market share. We studied three approaches for implementing the multilayer network. The first method is called frequency partitioning,

where the allocated GSM spectrum is divided into different subbands, and each subband is allocated to each layer. For an operator with limited bandwidth, a division of the frequency carriers between different layers leads to a significant reduction of the capacity in the macrocell layer, made even worse by losing trunking capacity. An alternative is to use a dual-mode mobile terminal which can access both GSM and the digital enhanced cordless telecommunication (DECT) system. DECT is a cordless system which is designed for indoor use, and is allocated 20 MHz of radio spectrum in the band of 1880-1990 MHz. By using DECT in picocells and street microcells, macrocells retain their frequencies and capacity. The last approach is to use a spectrum sharing scheme which allows different cellular layers reusing the same frequency band. With spectrum sharing, picocells and microcells can be deployed without sacrifying system capacity of the overlaying macrocell.

As the cell sizes become smaller, the variance of the offered traffic per cell increases. At present, the GSM network employs fixed channel allocation (FCA), where channels-to-cells assignments are semi-permanent, i.e., it can only be rearranged on a medium-term (non-realtime) basis, and thus the network can not adapt itself to the traffic variation in small cells. In order to assign channels to cells according to the traffic evolution in different cells on a realtime basis, several dynamic channel allocation (DCA) schemes have been proposed [7, 8, 9, 10, 11, 12, 13, 14, 15, 16, 17, 18, 19, 20, 21, 22, 23]. In this thesis we classify the existing DCA schemes and propose a novel DCA scheme called Autonomous Adaptive Frequency Assignment (AAFA) that is suitable for being introduced in the GSM network with both circuit-switched access and packet-switched access.

This thesis is organised as follows. Chapter 2 describes the design criteria of the GSM-like multilayer network. The design criteria are the capacity and the spectrum efficiency of macrocellular layer, street microcellular layer and inbuilding picocellular layer, which are obtained by means of mathematical analysis and computer simulation. Chapter 3 presents the deployment of a DECT/GSM system. The performance of DECT-like radio interface in the presence of frequency selective fading is described. The capacity of DECT picocellular network is investigated and the results is presented. An overlaying minicell and an adaptive handover algorithm for enhancing the capacity of DECT system is also proposed. Chapter 4 delivers a novel channel allocation scheme that is suitable for packet radio access as well as circuit-switched wireless system. Chapter 5 is dedicated to the issues of sharing spectrum between

macrocellular systems, street microcellular systems and inbuilding picocellular systems. Finally, conclusions and suggestions for further research is given in Chapter 6.

# Chapter 2

# Capacity of TDMA Mobile Radio Systems

## 2.1 Introduction

Multilayer cellular networks provide radio coverage to the same area by overlapping cells of different sizes. Three-tier cellular systems consisting of street microcell clusters and in-building picocell clusters are overlaid with macrocells, are likely to be deployed in major city centres. The arrangement is shown in Figure 2.1. In this chapter we evaluate separately the capacity of three mobile cellular layers, where each of them has a distinctive cellular environment.

The spectral efficiency, $\eta_S$ can be defined as the number of Erlangs a system can carry for an allocated bandwidth expressed in MHz over an area in km$^2$ is given by

$$\eta_S = \frac{A_{CT}}{S_T W} \cong \frac{N_{ts} G_c (1-\chi)}{2KC_s S_c B_c} \tag{2.1}$$

where $A_{CT}$ is the total traffic carried by a network, $S_T$ is the total area covered by the network, $S_c$ is the average area of each cell, $W$ is the total available bandwidth allocated to the network, $B_c$ is the equivalent bandwidth per carrier, $N_{ts}$ is the number of time slots per carrier, $\chi$ is the fraction of channels allocated for signalling, $G_c$ is the carried traffic per channel, $S_c$ is the sector area, $K$ is the number of sectors per cell site, and $C_s$ is the number of cells per cluster. The spectral efficiency can also be written as the product of three efficiencies, viz:-

$$\begin{aligned} \eta_S &= (N_{ts}/(2B_c)) \cdot (KC_sS_c)^{-1} \cdot G_c(1-\chi) \\ &= \eta_B \cdot \eta_C \cdot \eta_T. \end{aligned} \tag{2.2}$$

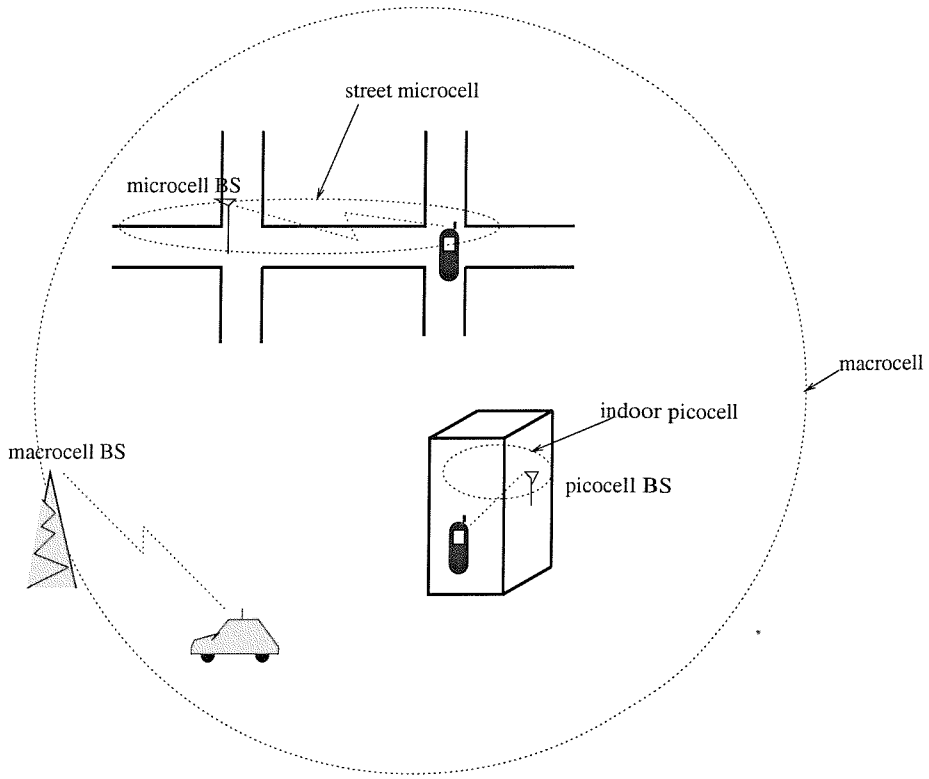


Figure 2.1: Various traffic cells in a city centre

The first factor $\eta_B$ is the bandwidth efficiency. High bandwidth efficiency can be achieved, for example in the case of speech, by using low bit rate voice coding and bandwidth efficient modulation. In mobile telephony the bandwidth efficiency is defined by the number of duplex traffic channels supported in one MHz of bandwidth. In GSM each duplex channel is represented by two time slots on two frequencies separated by a fixed frequency gap of 45 MHz (in the 900 MHz band) and of 75 MHz (in the 1.8 GHz band). In other words frequency division duplexing (FDD) is used, and therefore when a carrier is assigned to a cell, it implies that a pair of carriers is allocated to the cell.

For example, the GSM radio interface supports 8 time slots per carrier and a carrier bandwidth of 200 KHz gives $\eta_B = 8/(2 \cdot 0.2) = 20$ channels/MHz. Hence a bandwidth of 400 KHz including an uplink carrier and a downlink carrier supports eigth full rate duplex channels. We note furthermore that in a GSM system supporting half-rate channels, the number of channels per carrier is twice that of the full-rate channels and therefore the user capacity is doubled.

The second factor $\eta_C = (KC_sS_s)^{-1}$ is the spatial efficiency. High spatial efficiency can be achieved by minimising the area per cell, and/or minimising the reuse cluster size. The trunking efficiency is $\eta_T = G_c(1 - \chi)$. High trunking efficiency can be achieved by using channel assignment schemes that maximise channel utilisation, and/or minimising signalling overhead.

In the following section we discuss the principle and the characteristics of spatial efficiency, and in Section 2.3 the trunking efficiency is described in detail. Sections 2.4, 2.5 and 2.6 are devoted to determining the spectral efficiency of independent macrocellular, street microcellular and inbuilding picocellular networks, respectively. Analysis of the spectral efficiency of a TDMA cellular system with power control and slow frequency hopping are presented in Sections 2.7 and 2.8, respectively. The final section provides a summary of the main conclusion.

## 2.2 Spatial efficiency

The spatial efficiency $\eta_C$ is a primary concern of cellular system planners. The spatial efficiency can be defined in terms of the reuse efficiency per unit service area. The intense interest in small cell systems such as street microcells and inbuilding picocells can be explained by the fact that the spatial efficiency increases as the cell dimensions decrease [24]. Planners often have problems in deploying microcells as many sites need to be acquired, and provision must be made for the trunking from the sites to the remainder of the network. Another problem arises because of a significant increase in the number of handover calls. The effect of handover calls on system capacity is examined in the next section.

Among other important cellular planning factors is the efficiency of reusing the radio channel resources over the service area. This reuse efficiency, which depends on the interference environment of the network, is defined as the inverse of the reuse cluster size $C_s^{-1}(\leq 1)$.

Cellular radio links often exhibit a threshold effect, such that the link quality is acceptable provided that both the average received signal-to-noise ratio (SNR) and the average signal-to-interference ratio (SIR) exceed certain thresholds, denoted by $\text{SNR}_{min}$ and $\text{SIR}_{min}$, respectively [25]. These thresholds depend on many radio link parameters, including the modulation and coding scheme employed, the receiver structure, the measurement of transmission quality, the propagation environment,

and the fast-fading incurred as the mobile roams.

The reuse cluster size is minimized by designing the radio links to minimise $\mathrm{SIR}_{min}$. In practice, this is achieved by using error control coding, antenna diversity, adaptive equalisation, and other receiver techniques, as well as system procedures such as cell sectoring, adaptive transmitter power control, discontinuous transmission, frequency hoppings, effective handover algorithms, and macro-diversity. The main aim is to minimise the co-channel interference and have the $\mathrm{SIR} > \mathrm{SIR}_{min}$.

In high capacity cellular systems the thermal noise at the receiver can usually be neglected in comparison to the co-channel interference. In our deliberations, the system performance metric of interest is therefore the link reliability

$$\Re = \mathrm{Prob}[\mathrm{SIR} \geq \mathrm{SIR}_{min}] \tag{2.3}$$

The cluster size must be carefully chosen such that the link quality performance is satisfied, e.g. over 90% of the cell area SIR exceeds $\mathrm{SIR}_{min}$, $\Re \geq 90\%$. We noted that in GSM the working $\mathrm{SIR}_{min}$ is approximately 12 dB [26].

Hence, in order to determine the spectrum efficiency of each cellular network, the design parameters, which include cluster sizes, cell size and BS separation distances, need to be investigated. To establish a mathematical relationship between $\mathrm{SIR}_{min}$ and the reuse cluster sizes, it is necessary to model the relative geographical locations of transmitter and receivers in the multilayer cellular systems so as to account for propagation effects on the radio channels. The adjacent channel interference is ignored in this chapter. We make our calculation of reuse cluster size for the case where all cells are fully loaded, that is, all $N_c$ channels available in each cell are used simultaneously and continuously. Although this condition gives pessimistic results for reuse cluster size, it permits a simpler analysis, and the results are independent of the number of channels, and other system traffic parameters. We also examined how the cluster size can be decreased by employing power control, frequency hopping, fractional cell loading and discontinuous transmission (DTX) [26] which are features of the market-leading GSM.

## 2.3 Trunking efficiency

The trunking efficiency $\eta_T$ is represented by

$$\eta_T = G_c(1 - \chi) \tag{2.4}$$

where $\chi$ represents the fraction of channels allocated for signalling that rely on the signalling transfer protocols of each cellular system, and $G_c$ is the offered traffic per channel, i.e., the offered traffic at a sector divided by the number of channels that can be deployed in a sector. High trunking efficiency can be achieved by using channel assignment schemes that maximise channel utilisation. Dynamic channel assignment (DCA) and other flexible channel assignment procedures provide more trunking efficiency than fixed channel assignment (FCA) as the number of channels available per cell can adapt to the spatially and temporally varying offered traffic. In practice some areas are overlapped by more than one BS. In this situation the trunking efficiency can be improved if the system employs the direct retry algorithm, i.e., when a call attempt is blocked by the first choice BS, the mobile station (MS) makes another call attempt to the second choice BS, and so on [1, 2]. In this chapter we consider the simple scenario of FCA with non-overlapping cell coverage.

Network operators usually design their networks such that during the busy hour only a small percentage, say 2%, of call attempts are blocked because all the channels are in use. The grade-of-service (GOS) of cellular networks is represented not only by the probability $P_B$ that a new call attempt is being blocked, but also by the probability $P_F$ that an ongoing call is forced to terminate due to handover failure between two BSs due to the presence of excessive interference. For this reason we define the GOS for cellular networks as a combination of call blocking and call dropping;

$$\text{GOS} = P_B + \omega P_F(1 - P_B), \quad \omega \geq 1, \tag{2.5}$$

where $\omega$ is the relative penalty factor. When $\omega$ is unity, the GOS is simply the ratio of uncompleted calls. In this study we set $\omega$ to ten to accommodate our view that the occurence of a call being forced to terminated is typically considered to be less desirable, than the occurence of a new call being blocked.

To perform a quantitative study of the trunking capacity for the cellular networks, several assumptions are used. We assume that the call arrival dirtribution can be modelled by a Poisson process with rate $\lambda_c$ (calls/sec). The call arrival includes two types of traffic arrivals, namely new call arrival and handover call arrival, competing for access to $N$ channels in a cell. The total call arrival is simply the sum of a new-call arrival rate $\lambda_n$ and a handover-call arrival rate, hence we have

$$\lambda_c = \lambda_n + \lambda_h. \tag{2.6}$$

We also assume that an unencumbered call duration is exponentially distributed with

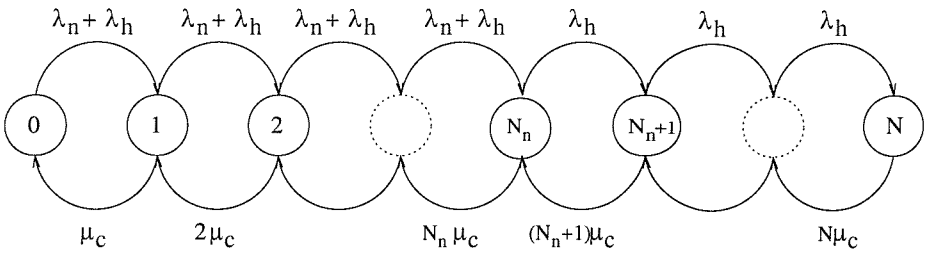


Figure 2.2: Markov model for call arrivals and departures

a mean call duration of $\mu_m^{-1}$ sec. For a given new-call arrival rate, the handover-call arrival rate and the channel service rate $\mu_c$ need to be determined. They are dependent on the new call arrival rate, the mean unencumbered call duration, the cell size and the mobiles' mobility.

Let $N$ be the total number of traffic channels assigned to a cell. We employ a handover priority with $N_g$ channels being reserved for handovers only. With the block-call cleared policy, we model the system as an $(N+1)$-state Markov chain process, and each state is labelled by an integer $i$ ($i$ = 0,1,2,..,$N$), representing the number of busy channels, and $N_n = N - N_g$ is the number of channels being used for either new calls or handover calls (see Figure 2.2). Let $p_i$ be the probability that the system is in state $i$. The steady state probability in state $i$ is

$$p_i = \begin{cases} p_0(\lambda_n + \lambda_h)^i/(\mu_c^i i!) & \text{if } i \le N_n, \\ p_0(\lambda_n + \lambda_h)_n^N \lambda_h^{i-N_n}/(\mu_c^i i!) & \text{if } N_n < i \le N, \end{cases} \tag{2.7}$$

where

$$p_0 = \left[ \sum_{i=0}^{N_n} \frac{(\lambda_n + \lambda_h)^i}{\mu_c^i i!} + \sum_{i=N_n+1}^{N} \frac{(\lambda_n + \lambda_h)_n^N \lambda_h^{i-N_n}}{\mu_c^i i!} \right]^{-1}. \tag{2.8}$$

The probability that a new call is blocked is given by

$$P_B = \sum_{i=N_n}^{N} p_i, \tag{2.9}$$

and the probability that a handover is being blocked is given by

$$P_{fh} = p_N. \tag{2.10}$$

The channel service rate $\mu_c$ is decomposed into two rates according to

$$\mu_c = \mu_m + \mu_h, \tag{2.11}$$

where $\mu_m^{-1}$ is the mean unencumbered call duration and $\mu_h$ is the outgoing handover rate per calling terminal. Since call completion and call handover are disjoint events, Equation 2.11 is justified. The mean number of ongoing calls in a cell is given by

$$E[C] = \sum_{i=1}^{N} ip_i. \tag{2.12}$$

Under the condition of mobility equilibrium and uniformity among cells, the incoming handover call arrival rate is equal to the outgoing handover call arrival rate, which is given by [27, 28]:

$$\lambda_h = E[C]\mu_h. \tag{2.13}$$

In conventional cellular networks having large cells handovers between BSs during a call are rare, i.e., $\lambda_h \ll \lambda_n$ and $\mu_h \ll \mu_m$, and the number of mobiles in a cell is significantly higher than the number of BS channels $N$. Hence the GOS is approximated by the probability of a call being blocked given by the Erlang-B formula, which is derived for the assumption of an infinite subscriber population. Furthermore, Poisson distributed call arrivals of rate $\lambda_c$ calls/s, and an exponentially distributed call duration with a mean call duration of $\mu_m^{-1}$, s/call are assumed. The Erlang-B formula is given by

$$P_B = \frac{(\lambda_c/\mu_m)^N/N!}{\sum_{k=0}^{N}(\lambda_c/\mu_m)^k/k!}, \tag{2.14}$$

where $\lambda_c \approx \lambda_n$ is the new call arrival rate and $\mu_m$ is the call departure rate.

As the microcells and picocells are much smaller than the conventional macrocell, the probability that MSs experience handovers during a call is higher in these small cells. Furthermore, the channel holding time in the cell is a fraction of the call duration. Consequently, there is a greater chance of forced termination of a call due to an unsuccessful handover attempt. In this case the probability $P_F$ of forced termination, and the probability $P_{fh}$ that a handover attempt fails are also important performance measures.

A call which is not blocked will be eventually forced into termination, if it succeeds in each of the first $(l-1)$ required handover attempts but fails on the $l$th [29]. Therefore

$$P_F = \sum_{l=1}^{\infty} P_{fh}[P_N(1-P_{fh})^{l-1}P_H^{l-1}] = \frac{P_{fh}P_N}{1-P_H(1-P_{fh})}, \tag{2.15}$$

where $P_N$ is the probability that a new call, which is not blocked will require at least one handover before call completion because of the mobile crossing a cell boundary,

while $P_H$ is the probability that a call, which has already had a successful handover will require another handover before completion. These two parameters rely on the cell size and the mobility of the MSs.

We let the random variable $T_m$ denote the unencumbered call duration. The random variable $T_m$ is assumed to be exponentially distributed with a mean value $\overline{T_m} = \mu_m^{-1}$, i.e.,

$$f_{T_m}(t) = \mu_m e^{-\mu_m t}. \tag{2.16}$$

We define the random variable $T_n$ as the time from the onset of a call to when the MS leaves the cell, while still engaged in a call. The time during which a mobile resides in the cell after a handover is denoted by $T_h$. We develop a mathematical model and expressions for the PDFs $f_{T_n}(t)$ and $f_{T_h}(t)$. The random variable $T_n$ is approximated by an exponential distribution with a mean of $\overline{T_n} = \mu_n^{-1}$, i.e.,

$$f_{T_n}(t) = \mu_n e^{-\mu_n t}. \tag{2.17}$$

Similarly, the random variable $T_h$ is also approximated by an exponential distribution with a mean value of $\overline{T_h} = 1/\mu_h$, i.e.,

$$f_{T_h}(t) = \mu_h e^{-\mu_h t}. \tag{2.18}$$

References [28, 27] suggest that $\mu_h$ is approximated by the mean boundary crossing rate per mobile $\mu_b$, which is given by the reciprocal of the mobile's mean dwelling time in a cell $\overline{T_h}$. For a mobility model, where cells are circular with radius $R$ and mobiles are uniformly distributed in the system moving in straight lines at an average speed $E[v_s]$ with direction uniformly distributed between 0 and $2\pi$, the mean boundary crossing rate $\mu_b$ is approximated by [28]

$$\mu_h \approx \mu_{bc} = (2E[v_s])/(\pi R). \tag{2.19}$$

For a highway microcell model, where BSs are linearly separated on a one-dimentional highway section with distance $R_L$ and where the average mobile speed is $E[v_s]$, we have [30]

$$\mu_h \approx \mu_{bl} = E[v_s]/L_{h\mu}. \tag{2.20}$$

When a model of rectilinear street microcells [31] is considered, we have

$$\mu_h \approx \mu_{bs} = (L_{s\mu}/(2E[v_s]) + P_c P_d \overline{T_d})^{-1}, \tag{2.21}$$

where $L_{s\mu}$ is a horizontal BS separation distance (equal to a vertical one), $P_c$ is the proportion of pedestrians leaving a microcell by road crossing, $P_d$ is the proportion of pedestrians delayed at the intersection in a cell of those who are trying to cross and $\overline{T_d}$ is the average delay time a pedestrian spends waiting at the intersection to cross the road. More detail about these parameters can be found in reference [31]. Using the circular cell model with radius $R$, the average remaining dwelling time in the call initiated cell is [27]

$$\overline{T_n} = 8RE[1/v_s]/(3\pi), \tag{2.22}$$

and therefore we have

$$\mu_n = 3\pi/(8RE[1/v_s]). \tag{2.23}$$

For the linear highway microcell model we have

$$\mu_n = 1/\overline{T_n} = L_{h\mu}/(2E[1/v_s]), \tag{2.24}$$

and the rectilinear street microcell model gives

$$\mu_n = ((2E[1/v_s])/L_{s\mu} + P_c P_d \overline{T_d})^{-1}. \tag{2.25}$$

The expectations $E[v_s]$ and $E[1/v_s]$ depend on the PDF $f(v_s)$. If the velocity $v_s$ is uniformly distributed between $1/V_{max}$ and $V_{max}$, and $V_{max}$ is much larger than 1 m/s, we have

$$E[v_s] \approx V_{max}/2, \tag{2.26}$$

and

$$E[1/v_s] \approx \ln V_{max}/E[v_s]. \tag{2.27}$$

The probability $P_N$ that a new call will need at least one handover is [29, 31]

$$\begin{aligned} P_N &= \Pr\{T_m > T_n\} = \int_0^\infty [1 - F_{T_m}(t)] f_{T_n}(t) dt \\ &= \int_0^\infty e^{-\mu_m t} f_{T_n}(t) dt \\ &= (\mu_n)/(\mu_m + \mu_n). \end{aligned} \tag{2.28}$$

For a call which has experienced a successful handover the channel is held until the call is completed, or the mobile moves out of the cell again before call completion. Because of the memoryless property of the exponential distribution the remaining message duration of a call after handover has the same distribution as the unencumbered

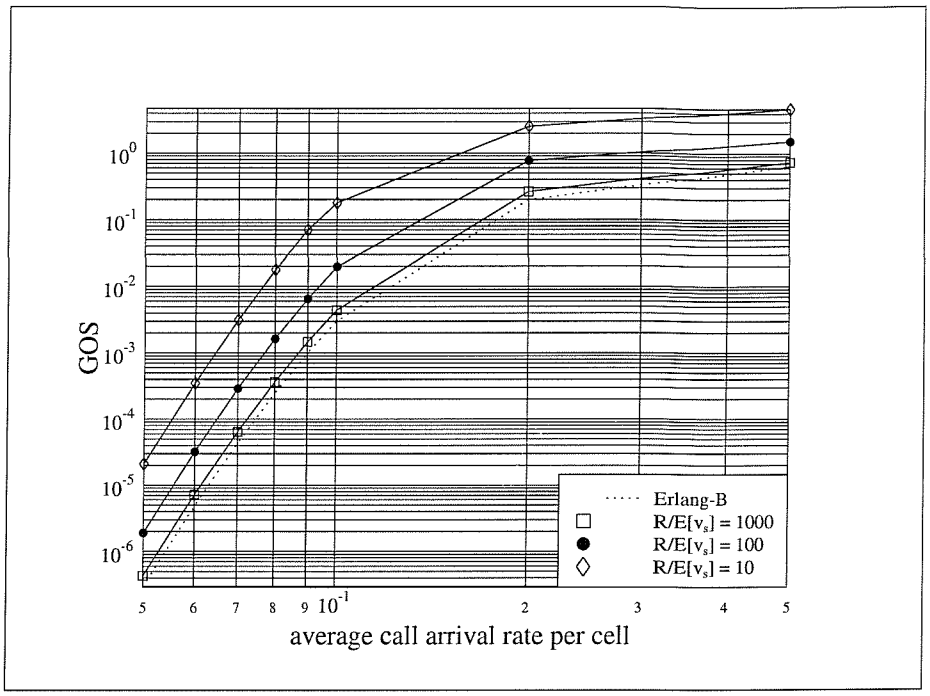


Figure 2.3: Variation of GOS as function of call arrival rate per cell for the circle cell model

message duration. The probability $P_H$ that a call, which has already been handed over successfully, will require another handover before completion is

$$\begin{aligned} P_H &= \Pr\{T_m > T_h\} = \int_0^\infty [1 - F_{T_m}] f_{T_h}(t) dt \\ &= \int_0^\infty e^{-\mu_m t} f_{T_h}(t) dt \\ &= (\mu_h)/(\mu_m + \mu_h). \end{aligned} \tag{2.29}$$

Figure 2.3 shows the relation of the GOS against the call arrival rate per cell for different ratios of the cell radius to an average mobile speed $R/E[v_s]$. The average unencumbered call duration was 120 s, no handover priority was used ($N_g = 0$) and the number of channels per cell was 22, which corresponded to the number of traffic channels for a GSM system with three carriers being assigned to each cell. We observed that the lower bound GOS is reliant on the blocking probability $P_B$ given by the Erlang-B formula. For GOS=2% the traffic capacity per cell decreased by 4%, 30% and 40% relative to the traffic capacity given by the Erlang-B curve, i.e., the upperbound capacity, when the $R/E[v_s]$ ratio was 1000, 100 and 10, respectively. Using the GSM parameters, such as the number of traffic channels and signalling channels for a given number of transceivers, the fraction of channels $\chi$ allocated for

| Transceivers/sector | **1** | **2** | **3** | **4** | **5** |
|---|---|---|---|---|---|
| Total no. of channels ($N_c$) | 8 | 16 | 24 | 32 | 40 |
| No. of signalling channels ($N_{sc}$) | 1 | 2 | 2 | 2 | 3 |
| No. of traffic channels ($N_{tc}$) | 7 | 14 | 22 | 30 | 37 |
| $\chi$ | 0.125 | 0.125 | 0.083 | 0.063 | 0.075 |
| **Sector capacity** | 2.9 | 8.2 | 15 | 22 | 28 |
| $G_c$ | 0.41 | 0.57 | 0.68 | 0.73 | 0.76 |
| $\eta_T$ | 0.36 | 0.50 | 0.62 | 0.68 | 0.70 |
| Transceivers/sector | **6** | **7** | **8** | **9** | **10** |
| Total no. of channels ($N_c$) | 48 | 56 | 64 | 72 | 80 |
| No. of signalling channels ($N_{sc}$) | 3 | 3 | 3 | 3 | 3 |
| No. of traffic channels ($N_{tc}$) | 45 | 53 | 61 | 69 | 77 |
| $\chi$ | 0.063 | 0.05 | 0.047 | 0.042 | 0.038 |
| **Sector capacity** | 35.5 | 43 | 50 | 58 | 66 |
| $G_c$ | 0.79 | 0.81 | 0.82 | 0.84 | 0.86 |
| $\eta_T$ | 0.74 | 0.77 | 0.78 | 0.80 | 0.83 |

Table 2.1: Traffic capacity in Erlang and trunking efficiency $\eta_T$ for a set of full rate traffic channels (Erlang-B formula, 2% blocking)

signalling is obtained from the ratio of the number of allocated channels for signalling to the total number of channels [26]. The upperbound offered traffic per channel $G_c$ which satisfies the required GOS ($GOS = 2\%$) is obtained using the Erlang-B formula which is tabulated against the number of transceivers in Table 2.1. The trunking efficiency $\eta_T$, given by $\eta_T = G_c(1 - \chi)$ is shown for different numbers of transceivers per sector. The more transceivers a sector has, the higher the trunking efficiency. We will use the upperbound trunking efficiency given by Table 2.1 in the spectral efficiency calculation for the rest of this thesis.

## 2.4 Capacity of macrocellular networks

### 2.4.1 Site layout and reuse planning

The cellular layout of a conventional macrocellular system is commonly described by tessalated hexagonal cells [32]. We consider a cellular system, where each BS employs directional antennae giving three sectors per cell. The cellular layout of sectorised macrocells is shown in Figure 2.4, where the relation between the separation distance

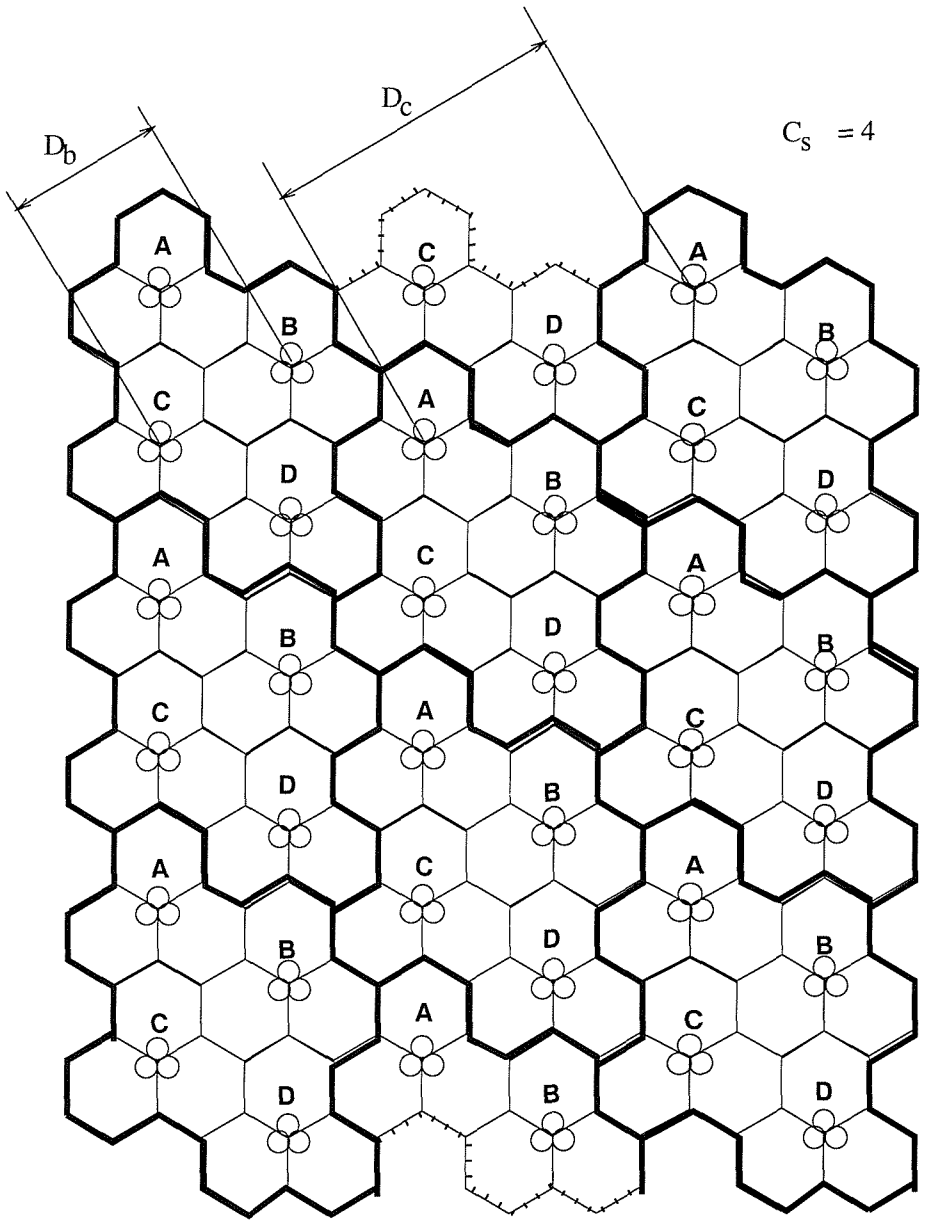


Figure 2.4: The macrocell layout with 3 sectors per cell and 4 cells per cluster. Each BS is labelled by its allocated frequency set

between adjacent BSs, $D_b$, and the outer radius of a sector, $R$, is given by

$$D_b = 3R \tag{2.30}$$

The nearest co-channel cell-site separation is given by

$$D_c = D_b\sqrt{C_s} \tag{2.31}$$

where $C_s$ is the number of cell sites per cluster.

In conventional cellular networks, the received signal power, averaged over multi-path fading is [33, 34]

$$P_R = \frac{P_T A\, V}{d^\gamma} \tag{2.32}$$

where $P_T$ is the transmitted signal power (assuming no power control), $A$ is the median path loss, and for a frequency of 1.8 GHz and a BS to mobile distance separation $d$, $A$ is given by

$$A(\text{dB}) = \begin{cases} -133.8 & \text{if } d < 5\,\text{km} \\ -137.5 & \text{if } d \geq 5\,\text{km} \end{cases} \tag{2.33}$$

and $\gamma$ is a propagation exponent given by

$$\gamma = \begin{cases} 3.8 & \text{if } d < 5\,\text{km} \\ 3.4 & \text{if } d \geq 5\,\text{km} \end{cases} \tag{2.34}$$

and $V$ is a log-normal shadow fading random variable in dBs with zero-mean and a standard deviation of $\sigma_\xi$ (6 dB).

The coverage area of each cell can be approximated by a circle of radius $R$. In order to provide coverage in each sector, the antenna gain is given by

$$G(\theta) = 10\gamma \log(\cos\theta) \quad (\text{dB}) \tag{2.35}$$

where $\theta$ is the angle between the mobile position vector and the antenna direction vector as shown in Figure 2.5. By considering the direction of antenna, the received signal can be calculated by substituting $d$ in Equation (2.32) by,

$$d_{eq} = \frac{d}{\cos\theta} \tag{2.36}$$

### 2.4.2 Signal-to-interference ratio

In downlink BS-to-MS transmissions, a mobile receives a signal from its desired BS plus co-channel interference (CCI) from other BSs. The average CCI level from the

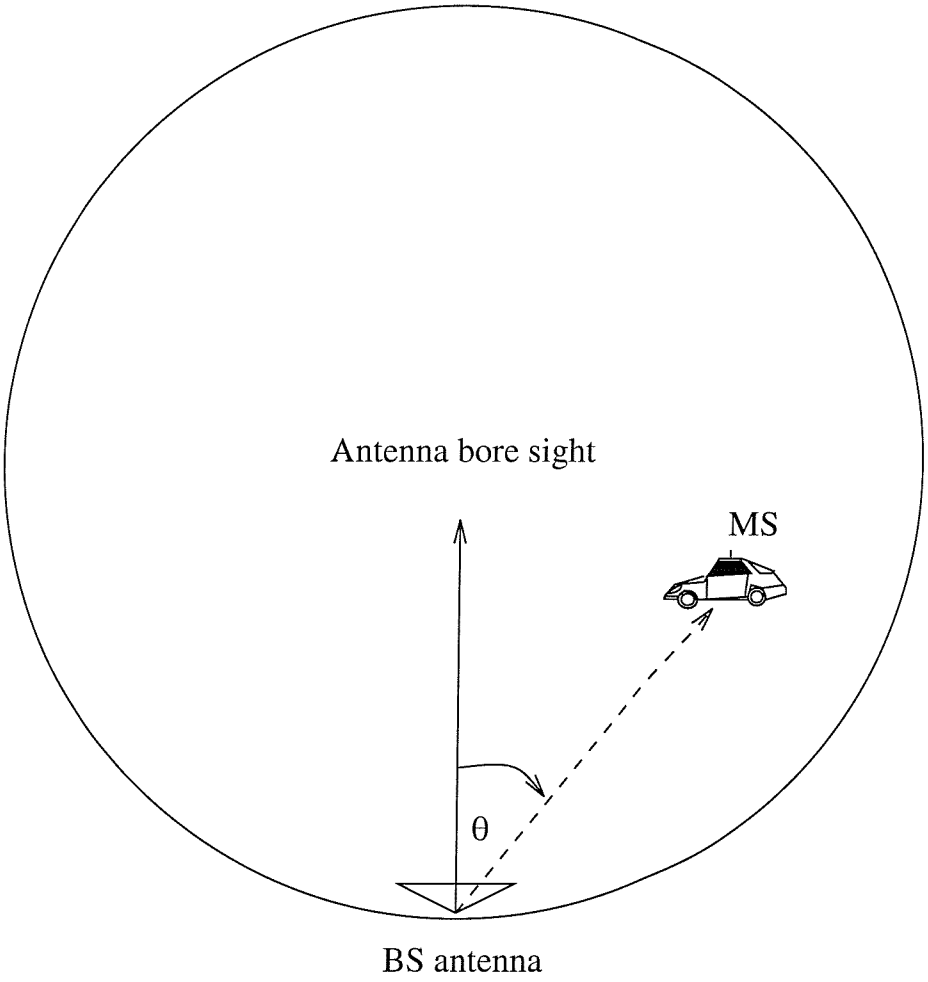


Figure 2.5: The directional antenna used in macrocell layout with 3 sectors per cell and 4 cells per cluster.

closet co-channel cells, the first tier, tends to be about 9 dB more than that of the more distance co-channel cells. Among the first tier interferers, the cell where antenna bore sight is directed toward the cell being interfered with causes more significant CCI than the cell whose antenna direction is away from the cell being interfered with, see Figure 2.6. So for our estimates of SIR, it is reasonable to approximate all first-tier interferers by two first-tier co-channel sectors [35].

In MS-to-BS uplink transmissions, a BS receives a signal from its desired mobile plus CCI from other mobiles. The uplink SIR is similar to the downlink SIR and may be approximated by [36]

$$\text{SIR} \approx \frac{A_0 V_0/(d_{eq})^{\gamma_0}}{\sum_{i=1}^{M} A_i V_i / D_i^{\gamma_i}} \tag{2.37}$$

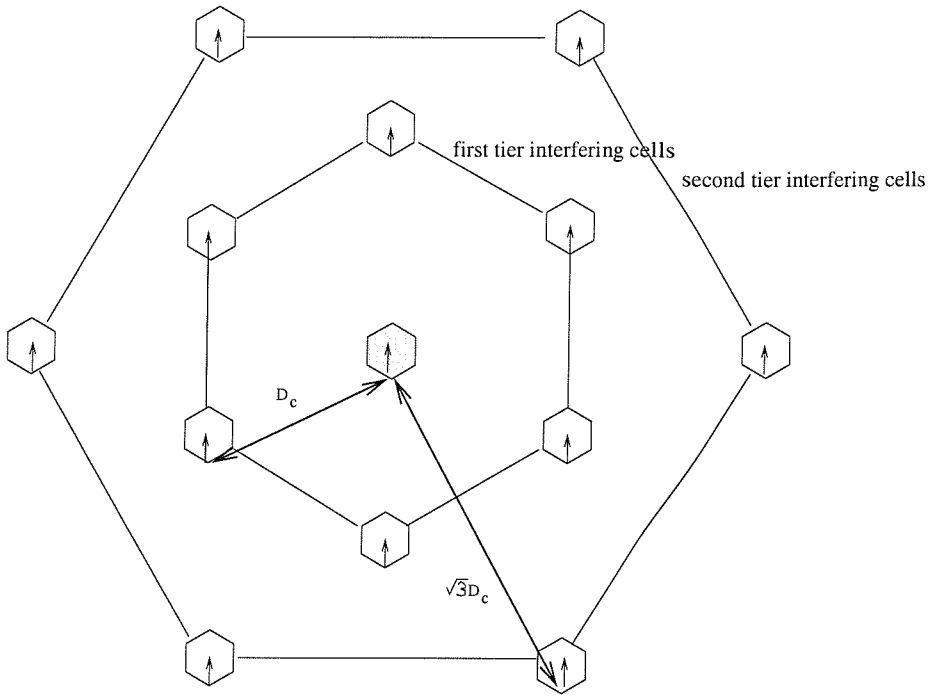


Figure 2.6: Macrocell interference scenario. The small arrows represent a direction of BS antennae.

where $D_i$ is the distance to the $i$th interferer from the BS, $V_0$ is the shadow fading random variable of the desired signal, $V_i$ is the shadow fading random variable of the $i$th interferer, $A_0$ is the median path loss of the desired signal, $A_i$ is the median path loss of the $i$th interferer, $\gamma_0$ is the path loss exponent of the desired signal and $\gamma_i$ is the pathless exponent of the $i$th interferer. The standard deviation parameter for $V_0$ and $V_i$ is denoted by $\sigma_\xi = 6$ (dB).

### 2.4.3 Approximation method

The following simplifying approximations were used in order to analytically derive the expression for the variation of $\Re$ (defined by Equation 2.3) as a function of $C_s$.

1. $D_i \approx D_c$ (See Figure 2.6).

2. $\sum_{i=1}^{M} V_i \approx V_I$ (M = 2 for both downlink and uplink), where the decibel value of $V_I$ is Gaussian distributed (i.e., the sum of lognormal variables is approximated by another lognormal variable) with mean $\mu_I$ and standard deviation $\sigma_I$, are both derived using Fenton's method [37].

3. The desired mobile position is uniformly distributed within a circle of radius R, i.e., the probability density function (PDF) of $d_{eq}$ is approximated by $f(d_{eq}) = d_{eq}/(2R^2)$, $0 < d_{eq} \leq 2R$.

4. $d_{eq}$ is below 5 km, and $D_c$ is over 5 km, hence $A_0 = 133.8$, $A_i \approx A_I = 137.5$, $\gamma_0 = 3.8$ and $\gamma_i \approx \gamma_I = 3.4$

From these approximation, we have

$$\text{SIR} = \Lambda(d_{eq})\frac{V_0}{V_I} \tag{2.38}$$

where

$$\Lambda(d_{eq}) = \frac{A_0\,(3R)^{\gamma_I} C_s^{\gamma_I/2}}{A_I\,(d_{eq})^{\gamma_0}}. \tag{2.39}$$

The reliability is given by

$$\Re = \int_0^{2R} f(d_{eq})\Gamma(d_{eq})\;\mathrm{d}\,d_{eq} \tag{2.40}$$

where

$$\Re(d_{eq}) = Z\left[\frac{\Lambda(d_{eq})_{dB} - (\text{SIR}_{min})_{dB} - \mu_I}{\sqrt{\sigma_\xi^2 + \sigma_I^2}}\right] \tag{2.41}$$

and $Z(\beta) \equiv 0.5[\text{erf}(\beta/\sqrt{2}) + 1]$.

### 2.4.4 Simulation method

A total of 13 macrocell sectors, including the desired macrocell and 12 co-channel interferers, were located according to Figure 2.6 where the middle cell is the desired macrocell. A directional antenna resides in each macrocell sector. For a specified reuse cluster size, macrocell radius and shadow fading statistics, we can estimate the distribution of SIR [by Equation (2.37)] by randomly generating many thousands of sets of mobile positions in each macrocell sector with their shadow-fading variable, i.e., in each simulation trial, we derive the set of distance parameters $d_{eq}$ and $\{D_i\}$, and the set of lognormal variables $V_0$ and $\{V_i\}$ [36]. The mobile positions are uniformly distributed within the hexagonal cells. Up to second tier interferers are considered ($M = 12$). The co-channel cell-site separations are $D_c$ and $\sqrt{3}D_c$, for first and second tier interferers, respectively. We perform simulations for a range of reuse cluster sizes to find the relationship between $\Re$ and $C_s$. By arranging for the received power at the BS receiver and at the mobile receiver to be above the thermal noise by at

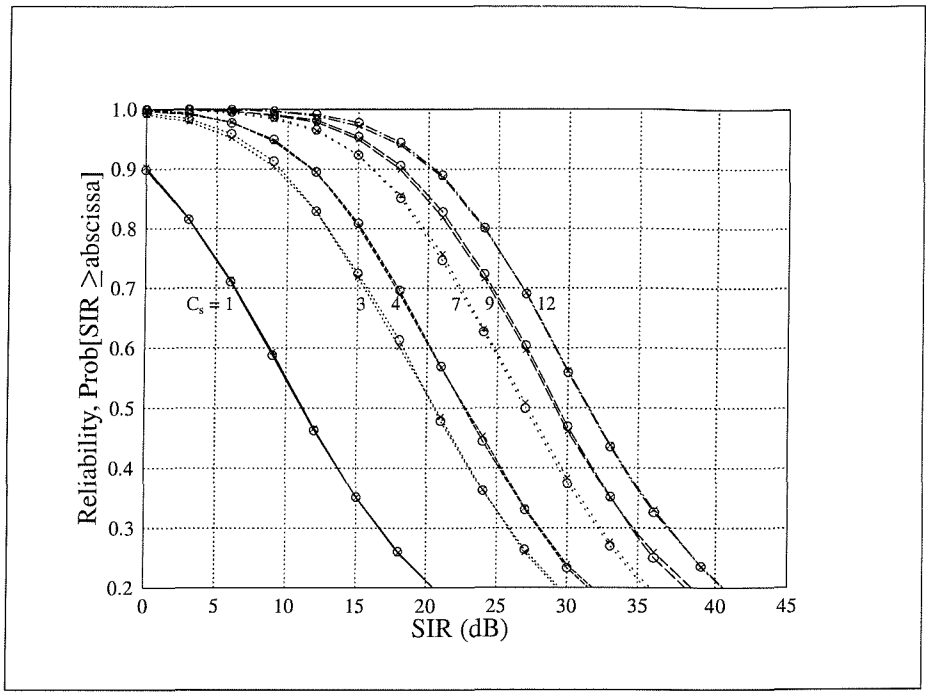


Figure 2.7: Reliability against $\text{SIR}_{min}$ for different cluster sizes, $D_b = 1$ km.

least $\text{SNR}_{min}$, we performed simulations over a range of separation distances between adjacent BSs, $D_b$, to show the relationship between $\Re$ and $D_b$.

### 2.4.5 Results

Figure 2.7 shows the simulation results of the uplink and downlink SIR performance for different reuse cluster sizes with a BS separation distance of 1 km. Uplink and downlink results are represented by crosses and circles, respectively, and their SIR performances are shown to be identical. Though the reliability curves of the system with higher reuse cluster size is higher than the one with lower reuse cluster size, all curves have the same smoothed shape. For all reuse cluster sizes, and the reliability values between 20% and 90%, the reliability is improved by 3.5% for each one dB decreasing of $\text{SIR}_{min}$.

Figure 2.8 shows the relation of the reliability versus the reuse cluster size for $\text{SIR}_{min}$ of 12 and 18 dB. Generally, a cellular system is required to operate with 90% reliability for good service quality, i.e., 90% of calls in progress have acceptable radio link quality. The reliability increases with the bigger reuse cluster size because the

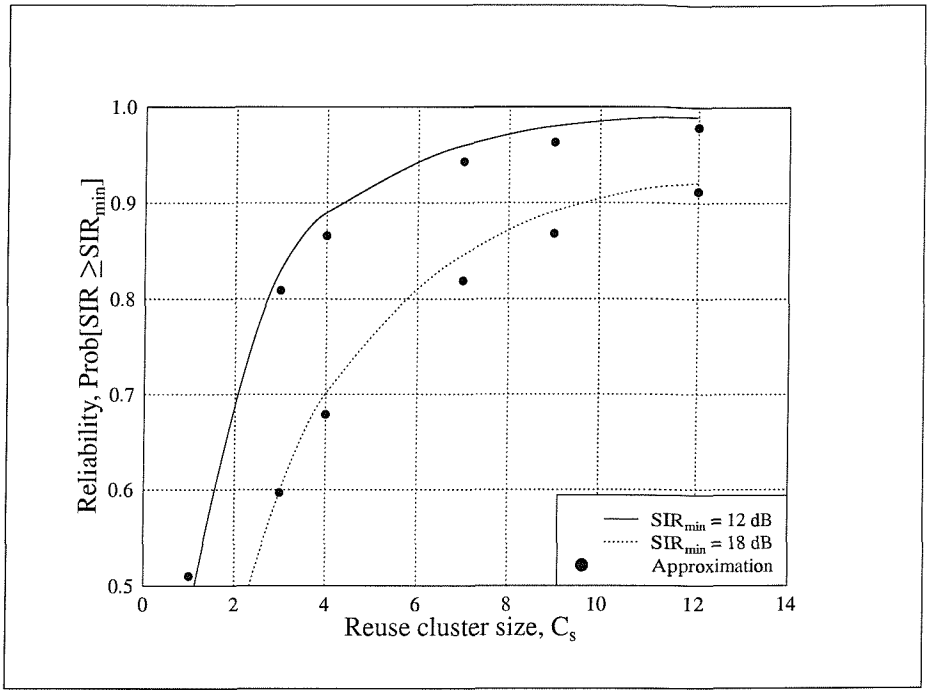


Figure 2.8: Reliability against reuse cluster size for conventional sectorised cellular system, $D_b = 1$ km.

reduction of co-channel interference improves the SIR performance. For fully loaded cells, with 90% reliability and an $\text{SIR}_{min} = 12$ dB, the reuse cluster size is $C_s \approx 4$, and for $\text{SIR}_{min} = 18$ dB, the reuse cluster size is $C_s \approx 9$. A cellular system with higher $\text{SIR}_{min}$ requires a larger reuse cluster size than a system with lower $\text{SIR}_{min}$, and, consequently, provides smaller system capacity. The simulation results illustrated by Figure 2.9 demonstrate that $\Re$ marginally decreases, as the separation distance $D_b$ between adjacent BSs increases from 1 km to 10 km, but it remains near-constant, when $D_b$ is in excess of 10 km.

The spectrum efficiency $\eta_S$ is given by Equation (2.2), as the product of the bandwidth efficiency $\eta_B$, the spatial efficiency $\eta_C$ and the trunking efficiency $\eta_T$. As described in Section 2.1, the bandwidth efficiency is independent of each cellular system. For GSM systems the bandwidth efficiency is $\eta_B = 20$. If we assume that the sector radius, derived from Figure 2.3, is 1 km, the BS separation distance is 3 km, and the sector area $S_c = 3.14$ km$^2$. Accordingly, the spatial efficiency of a four-cell reuse cluster and three sectors per cell is $\eta_C = (12 \cdot 3.14)^{-1}$. Table 2.1 tabulates the upperbound trunking efficiency, $\eta_T$, against the number of transceivers per sector

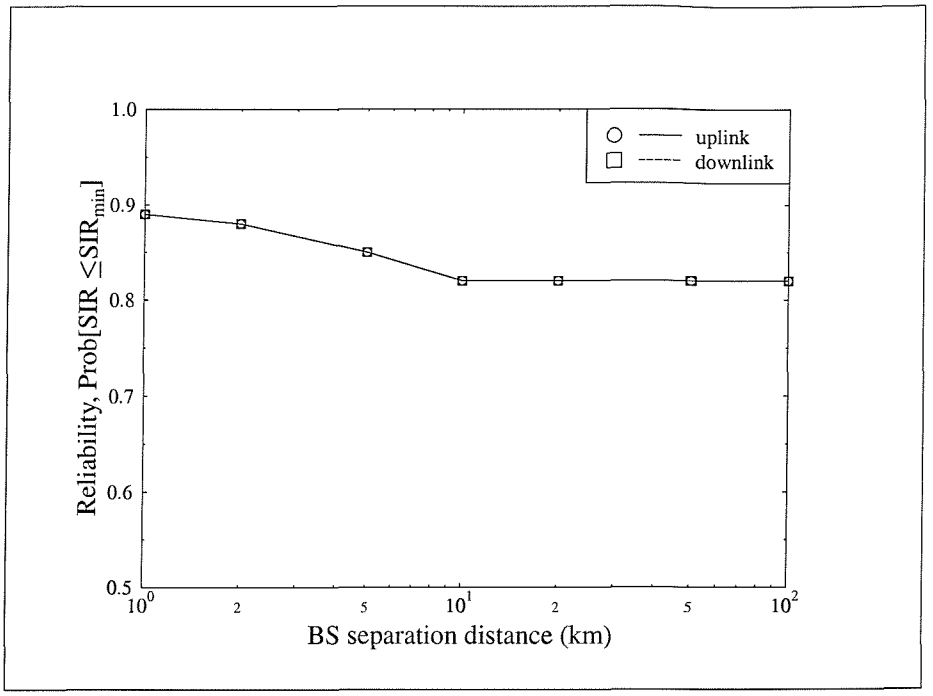


Figure 2.9: Reliability against BS separation distance for $\mathrm{SIR}_{min} = 12$ dB and $C_s = 4$

$N_{trx}$. In general the number of transceivers per sector is equivalent to the number of allocated carriers per sector. Therefore the total number of carriers allocated to the network is:

$$N_{tc} = N_{trx} K C_s, \tag{2.42}$$

where $K$ is the number of sector per cell site and $C_s$ is the reuse cluster size, and the corresponding bandwidth is given by

$$W = 2 N_{tc} B_c, \tag{2.43}$$

where$B_c$ is the equivalent bandwidth per carrier ($B_c = 0.2$ MHz for GSM).

Figure 2.10 shows the relationship of the spectral efficiency to the allocated bandwidth for macrocellular networks. The curve is not smooth at certain data points since the increasing number of channels used for signalling lowers the spectrum efficiency. However it can be approximated by a two-slope linear graph with a breakpoint at an allocated bandwidth of 15 MHz. It can be seen that to avoid a significant drop of the spectral efficiency, the bandwidth allocated to a macrocellular network should be maintained at least 15 MHz, and that corresponds to the spectral efficiency of 0.65 Erl/Mhz/km$^2$.

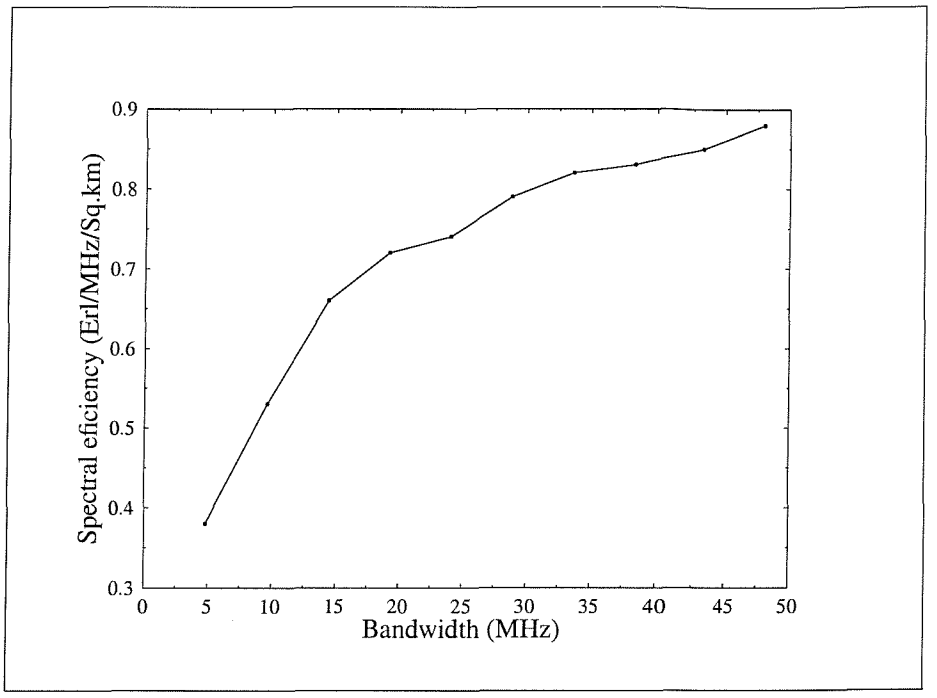


Figure 2.10: Spectral efficiency (in Erlangs/MHz/km$^2$) against allocated bandwidth for a GSM network with $D_b = 3$ km

## 2.5 Urban microcellular networks

### 2.5.1 Site layout and reuse planning

One way of increasing the system capacity in the urban areas is to employ microcells characterised by the low transmitter powers that cover only a few town blocks and where the antenna is located below the rooftops. The propagation characteristics of microcells are not only a function of the propagation exponent and radiated power, but also depends on the town layout of street networks, types of buildings and vegetation [32]. Due to the street canyon effect, there exists a clear distinction between the line-of-sight (LOS) and non line-of-sight (NLOS) interference [38]. Hence, we address the problem of cell planning separately for LOS and NLOS scenarios. In the LOS scenario, we consider the reliability performance where mobiles are located in LOS areas. In the NLOS scenario, the NLOS mobiles are considered.

The town layout used in our studies is a Manhattan street microcell model which is a pattern of rectilinear streets [39, 24]. Figure 2.11 shows half-block coverage microcells which were planned with three cells per cluster, and full-block coverage

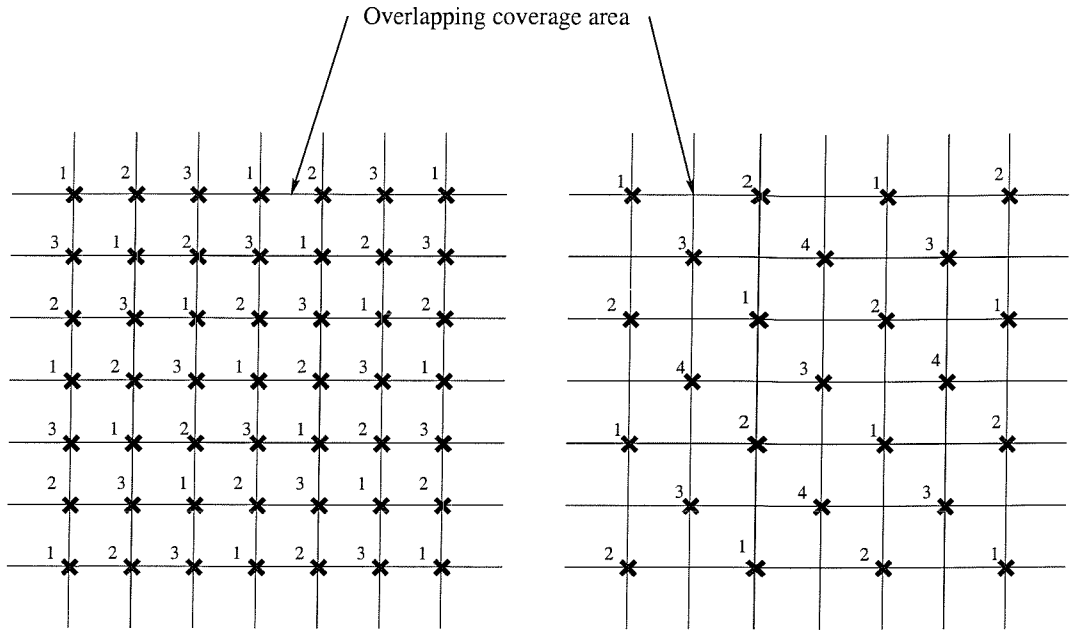


a) Half block coverage (1-D) microcell layout

b) Full block coverage (2-D) microcell layout

Figure 2.11: Microcell configurations, a) half-block coverage, b) full-block coverage

microcell which were planned with four cell per cluster. Each microcell BS is labelled by its frequency sets. A microcell BS is located at each intersection in order to provide maximum cell coverage, although it causes the maximum co-channel interference as line-of-sight LOS interferences are from all four directions.

### 2.5.2 LOS reuse structure

The LOS exists between microcells whose BSs are along the same road so that there is no man-made structure obstructing the signal propagation. The relation between the LOS separation distance between adjacent BSs, $D_{b_{LOS}}$, and the LOS distance to the cell boundary along a street of a microcell, $R_{LOS}$, is given by

$$D_{b_{LOS}} = 2R_{LOS}. \tag{2.44}$$

We characterise LOS microcell layouts in to two categories, one dimensional layout (1-D) and two dimensional layout (2-D). The microcell layout is characterised as one dimensional when no LOS area with more than two microcells overlapping, i.e., only one neighbouring microcell at a cell border on each street (see Figure 2.11 a).

The two dimensional layout is the condition when more than two cells overlap the same area (see Figure 2.11 b). The one dimensional layout includes highway microcells, half-block coverage microcells. The full block coverage microcell network are two dimensional. The reuse cluster size of the one dimensional layout is given by

$$C_{s_1} = \frac{D_c}{D_{b_{LOS}}} \tag{2.45}$$

and the reuse cluster size of the two dimensional layout is given by

$$C_{s_2} = \left(\frac{D_c}{D_{b_{LOS}}}\right)^2 \tag{2.46}$$

where $R_{LOS}$ is the LOS distance to the microcell boundary and $D_c$ is the minimum LOS co-channel separation.

In order to calculate the SIR we use simple propagation models for the received signal power and we assume that all calls are made when BS and its MS are in LOS. The received power, average over multipath fading is modelled by a smooth two-slope path loss model as

$$P_R = P_T \frac{AV}{d^2[1 + (d/B)^2]} \tag{2.47}$$

where $A = (\lambda/4\pi)^2$, $B = 4h_b h_m/\lambda$ is the breakpoint distance [36], $h_b$ and $h_m$ are the BS and mobile antenna heights, respectively, $\lambda$ is the wavelength, $d$ is the base-mobile separation, and $V$ is a zero-mean lognormal variable with a standard deviation of 4 dB [40]. That is, the median path loss (taken over shadow fading, $V$) approximately follows an inverse square-power law before the breakpoint (e.g. before 216 m at 1800 MHz with $h_b = 6$ and $h_m = 1.5$ m) and an inverse fourth-power law after the breakpoint.

As in the macrocellular analysis, we focus on a first-tier interference model with fully loaded cells. As our microcells use omnidirectional antennae, we have $M = 2$ LOS interferers, as illustrated in Figure 2.12. The amount of interference from NLOS interferers is very small and negligible as the LOS path loss is lower than the NLOS path loss by more than 20 dB due to significant corner loss. The SIR is given by

$$\text{SIR} = \frac{\frac{V_0}{d^2[1+(d/B)^2]}}{\sum_{i=1}^{M} \frac{V_i}{D_i^2[1+(D_i/B)^2]}} \tag{2.48}$$

where $0 < d < R$, $D_i$ is the distance between the desired mobile and the $i$th interfering BS for the downlink, or the distance between the desired BS and the $i$th interfering MS for the uplink, and $V_0$ and $V_i$ are lognormal shadow fading random variables.

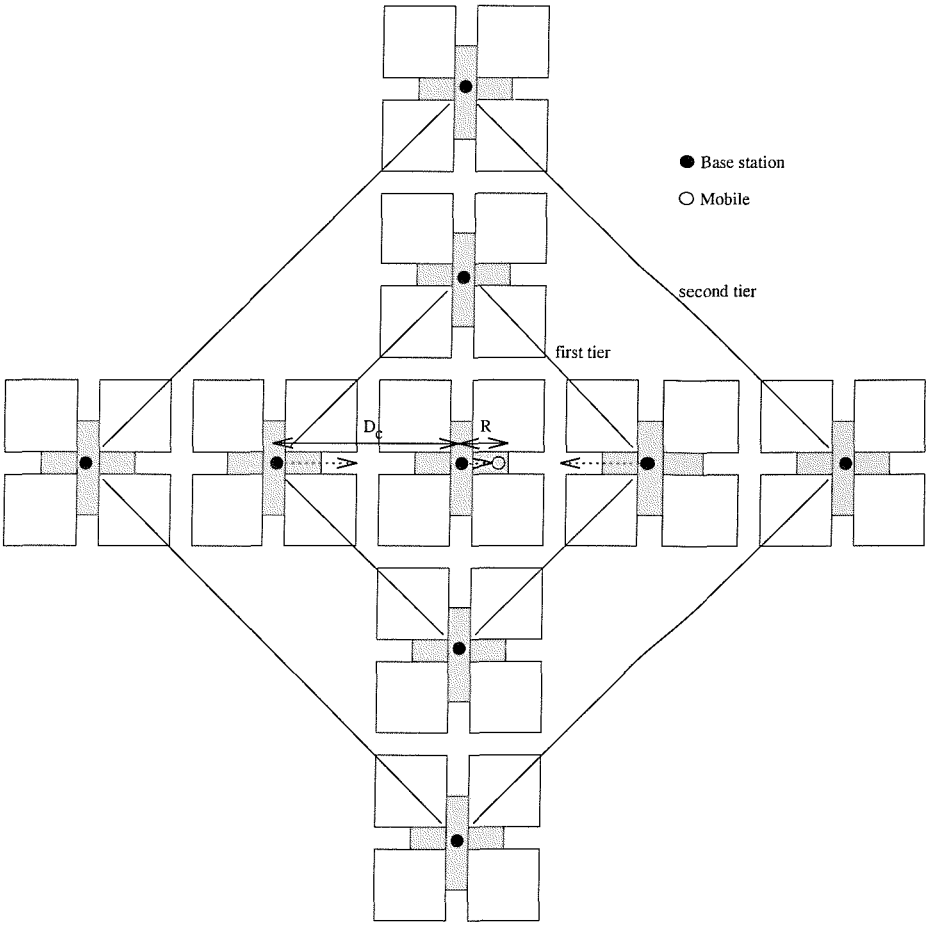


Figure 2.12: LOS interference scenario ($D_c = 4R$), shading represents a BS service area

We can estimate the distribution of SIR using a simulation similar to that for the conventional cellular system, but with the mobile and BS positions according to LOS microcellular model. We locate a microcell and its co-channel interferers as shown in Figure 2.12. Up to the second tier interferers are considered (M = 8), with the co-channel cell-site separation distance of $D_c$ and $2D_c$, for the first and second tier interferers, respectively. Mobiles are randomly located with uniform distribution over cross-shaped microcell service areas. We also produced $\Re$ versus $C_s$ results based on the analytical approximation method described in Section 2.4, but with $D_i = D_{c_{LOS}}$ and $f(d) \approx 1/R_{LOS}$, $0 < d < R_{LOS}$, and

$$\Lambda(d) = \frac{D_i^2[1 + (D_i/B)^2]}{d^2[1 + (d/B)^2]} \tag{2.49}$$

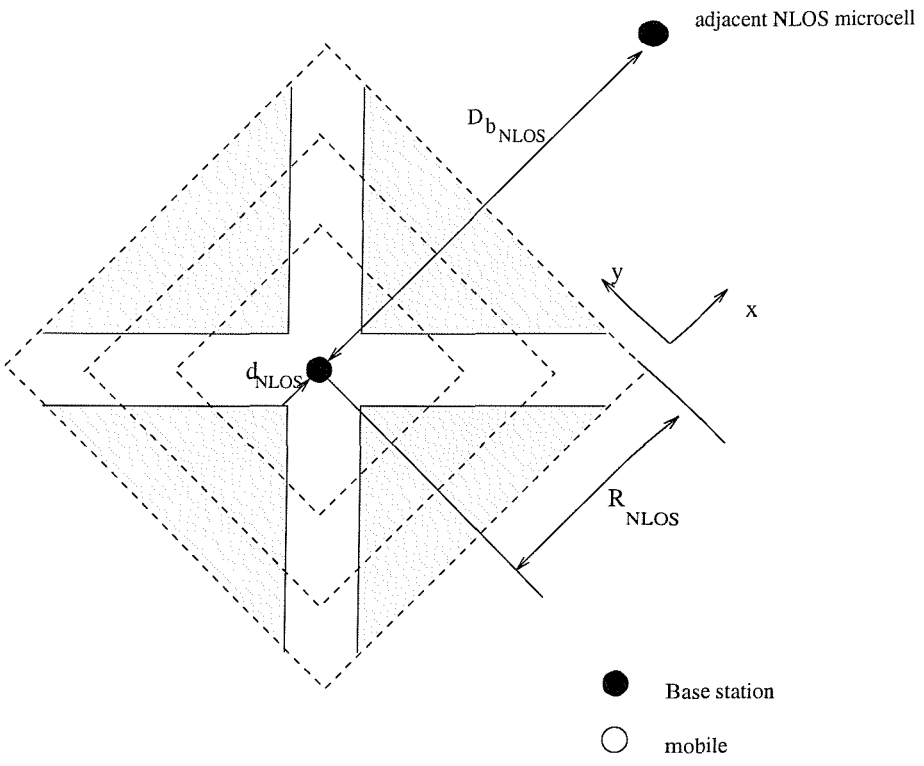


Figure 2.13: NLOS microcell propagation

### 2.5.3 NLOS reuse structure

Whereas LOS transmissions to BS antennas mounted in the streets implies MSs on the streets who can "see" their BSs, NLOS transmissions refer to MSs who are either out of sight around a corner, or within a building. The relation between the NLOS separation distance between adjacent BSs, $D_{b_{NLOS}}$, and the NLOS distance, $R_{NLOS}$ to the microcell boundary shown in Figure 2.13, is given by

$$D_{b_{NLOS}} = 2R_{NLOS}. \tag{2.50}$$

The nearest NLOS co-channel cell site separation is $D_{c_{NLOS}} = D_{b_{NLOS}}\sqrt{C_s}$. For NLOS conditions, path loss contours can be approximated by square diamonds as illustrated in Figure 2.13. We use a simple empirical model [36] for the approximate received power at a location on these square diamond which is given by

$$P_R = P_T \frac{AV}{d^\gamma} \tag{2.51}$$

where $A = .0015$, $d$ is the shortest distance from the BS to the edge of the square diamond on which the mobile is located, $\gamma = 3.8$, and $V$ is a lognormal variable, with

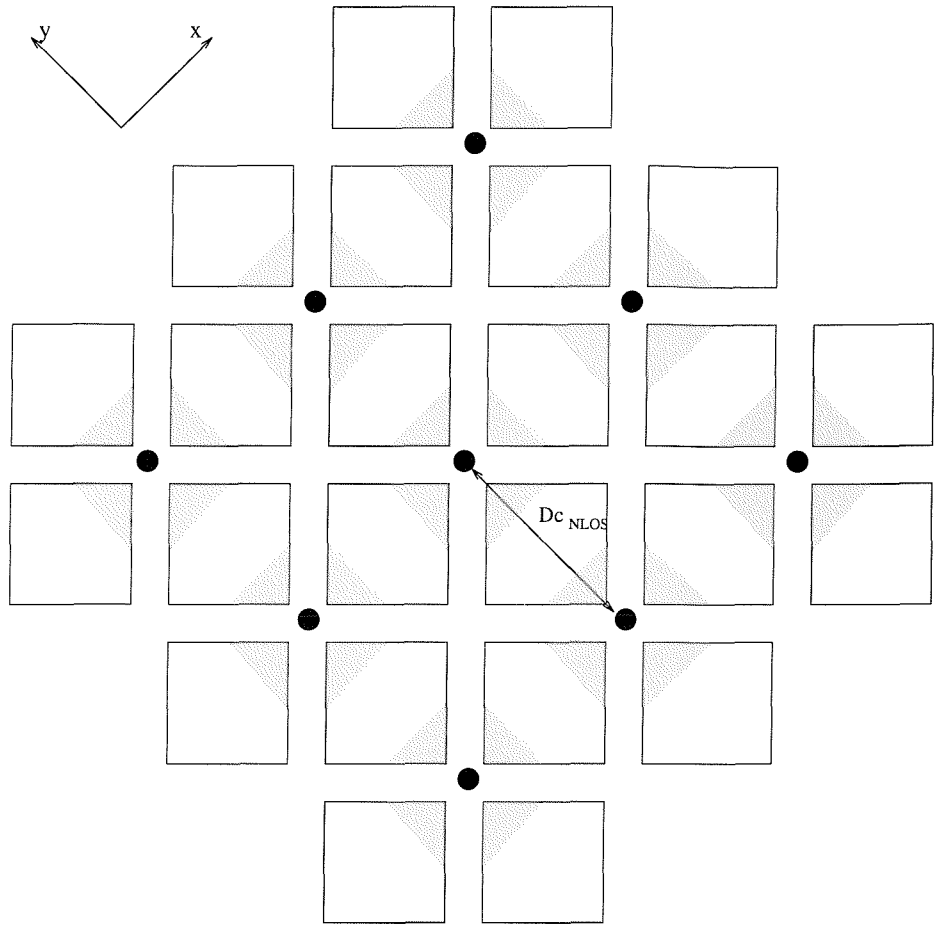


Figure 2.14: NLOS interference scenario, shading represents NLOS service area

a standard deviation parameter, typically, of about 5 dB [40]. Notice $A$ is the of low value to allow for the high attenuation experience by NLOS transmissions.

We assume that if a mobile has NLOS to its BS, it will have no LOS condition to another BS, restricting the interference. However, in real urban environments, with less than ideal street blocks, a mobile will sometimes have NLOS to its BS and LOS with a candidate BS for handover, but with insufficient signal power to cause a handover to that other BS.

As in our conventional cellular analysis, we focus on a first-tier interference model with fully loaded cells. Hence, we have $M = 8$ NLOS first tier interferers as shown in Fig. 2.14. The SIR is given by

$$\text{SIR} \approx \frac{V_0/d^\gamma}{\sum_{i=1}^{M} V_i/D_i^\gamma} \tag{2.52}$$

where $d_{min} < d < R_{NLOS}$; $D_i = \max(|x_i|, |y_i|)$ where $(x_i, y_i)$ is the coordinate (based

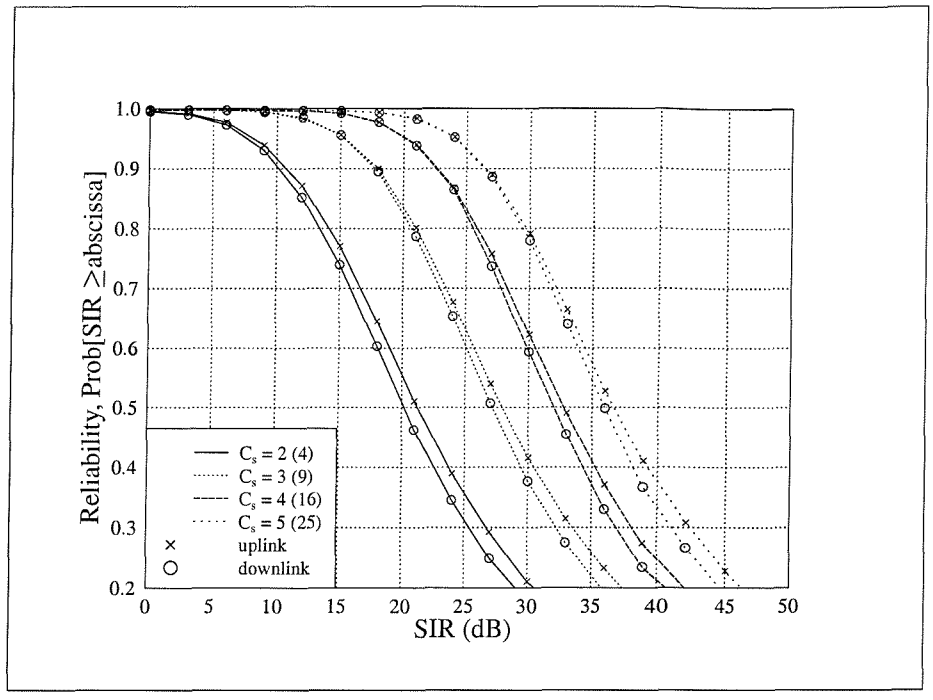


Figure 2.15: Reliability against SIR for street microcellular system (LOS), $D_b$ = 200m.

on the coordinate system shown in Figure 2.14) of the desired mobile with reference to the $i$th co-channel microcell site in the first tier, and $V_0$; $\{V_i\}$ are the shadow-fading variables as defined in Section 2.4.

The simulation similar to that for the conventional cellular system is used to estimate the distribution of SIR [via Equation (2.52)], but with the NLOS microcell model. The desired microcell and its interferers are illustrated in Figure 2.14. Mobiles are randomly positioned with uniform distribution over each NLOS microcell areas.

We can determine $\Re$ versus $C_s$ based on the analytical approximation method describe in Section 2.4, but with the following differences: $f(d) \approx 2d/(R^2_{NLOS})$, $d_{min} \leq d \leq R_{NLOS}$, $d_{min} \ll R_{NLOS}$; and we have

$$\Lambda(C_s, d) = \left(\frac{4R^2_{NLOS}C_s}{d^2}\right)^{\gamma/2} \tag{2.53}$$

### 2.5.4 Results

Figure 2.15 shows the simulation results of the uplink and downlink SIR performance for different reuse cluster sizes in the 1-D and 2-D microcell arrangements. The $C_s$

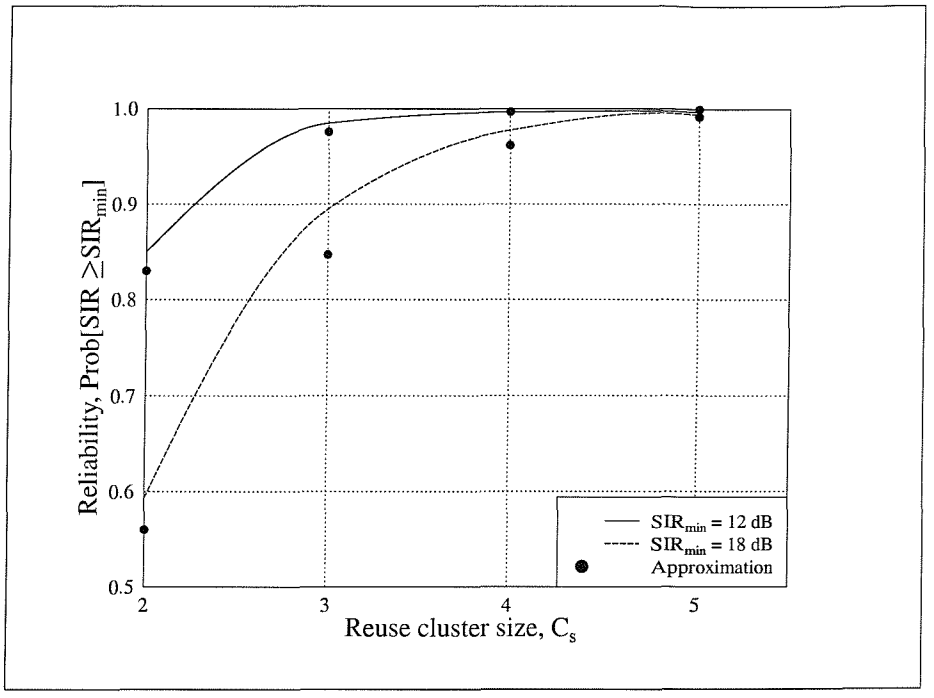


Figure 2.16: Reliability against reuse cluster size for street microcellular system (LOS), $D_b = 200$m.

values in bracket indicates the reuse cluster sizes of the 2-D microcell layout while the values outside are for 1-D microcell layout. The microcell BS separation distance $D_b$ is set to 200 m. The SIR performance of the NLOS microcell layout is shown in Figure 2.18. The uplink and downlink SIR performance of the LOS and NLOS microcells are approximately the same. Figure 2.16 and 2.19 show the variation of the reliability as a function of the reuse cluster sizes for LOS and NLOS microcell layouts, respectively. The reuse cluster size of 2 and 4 are required to achieve the 85% reliability (SIR$_{min}$ = 12 dB), for 1-D and 2-D LOS microcell layouts, respectively. With SIR$_{min}$ = 18 dB, the required reuse cluster size are 3 and 9 for 1-D and 2-D LOS microcell layout, respectively. Figure 2.19 shows that the required reuse cluster size for NLOS microcell layout with SIR$_{min}$=12 and 18 dB are 7 and 12, respectively.

Figure 2.17 shows the relation of the reliability to the separation distance between BSs for LOS microcell layout with $C_s = 4$. Increasing the BS separation distance improves the reliability because the LOS pathless exponent is higher at greater distances. However, in the case of NLOS microcell layout Figure 2.20 shows that the reliability is constant with the variation of the BS separation distance.

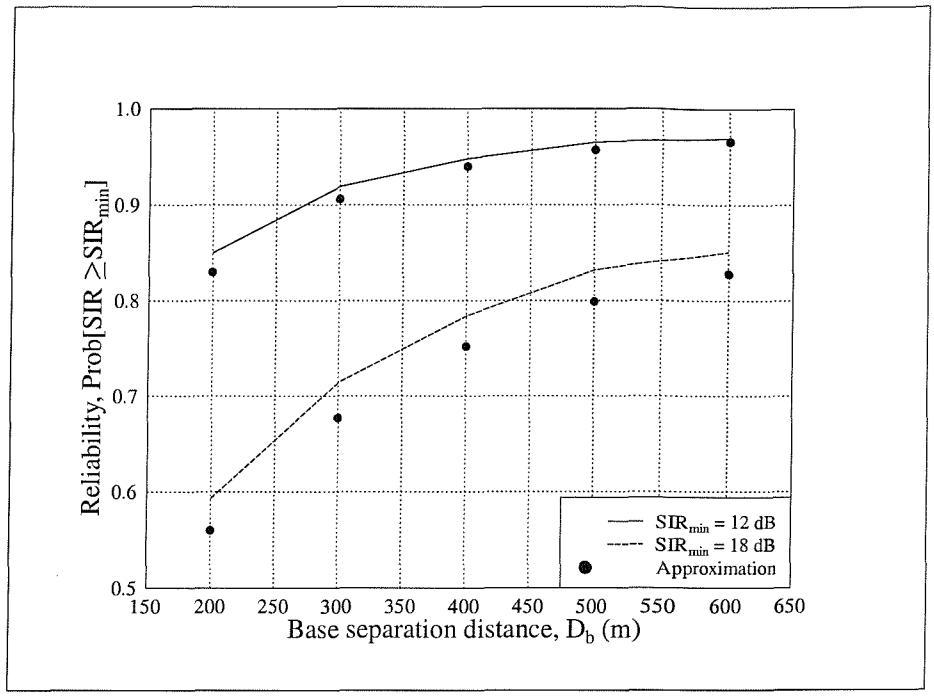


Figure 2.17: Reliability against base separation distance for street microcellular system (LOS), $C_s = 4$.

When the minimum LOS separation distance between adjacent BSs is 200 m, the service areas are .0112 and 0.2 km$^2$ for LOS and NLOS microcells, respectively. The street width is set to 28 m. The reuse cluster size is 2, 4 and 7 for 1-D LOS, 2-D LOS and NLOS, respectively. Figure 2.21, 2.22 and 2.23 show the relationship of spectral efficiency with the allocated bandwidth for 1-D LOS, 2-D LOS and NLOS microcells, respectively. Although the spectral efficiency increases with the higher allocated bandwidth, the rate is less when the bandwidths are wider than 2.4 MHz, 4.8 MHz and 8.4 MHz for 1-D LOS, 2-D LOS and NLOS, respectively. We conclude that a microcellular network should be allocated with at least 2.4 MHz, 4.8 MHz and 8.4 MHz giving the spectral efficiency of 1100, 550 and 180 Erl/MHz/km$^2$, for 1-D LOS, 2-D LOS, and NLOS microcellular network, respectively, and each cell is equipped with at least three transceivers.

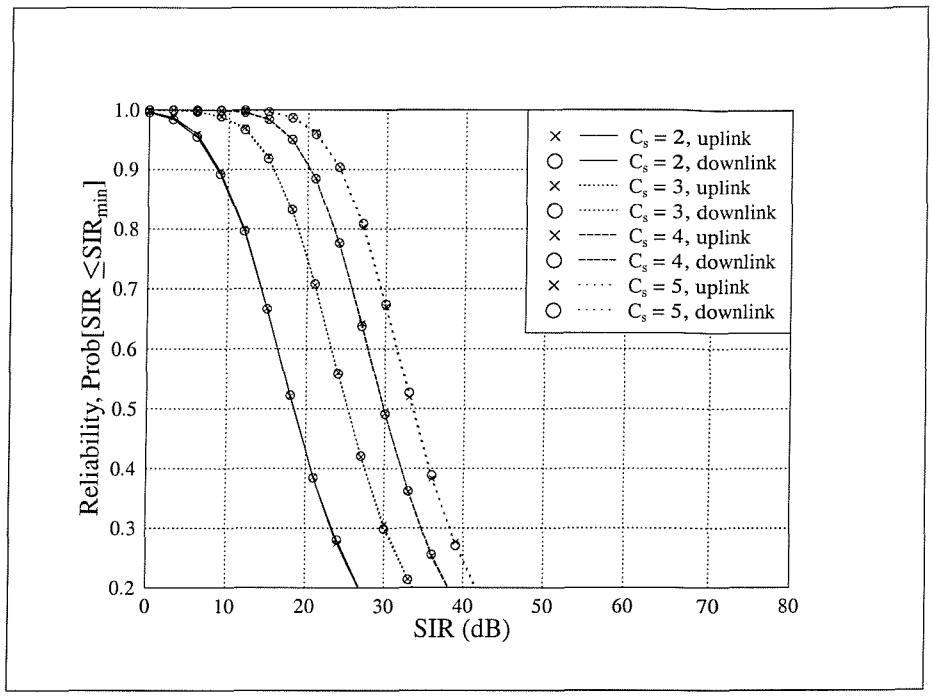


Figure 2.18: Reliability against $\text{SIR}_{min}$ for street microcellular system (NLOS), $D_b$ = 200m.

## 2.6 Indoor picocell networks

An indoor picocellular models that is representative in the way that hexagonal cells and rectilinear cells are used for macrocell and street microcell calculations, respectively, is a rectangular floor with square offices on either side of a central corridor. We sought a model of a square multistorey buildings, and on each floor there are offices about a rectilinear pattern of corridors. Our proposed model is shown in Figure 2.24. The streets are 28 metres wide including 4 metre wide pavements on each side. Each building is 72 metres square with 9 floors and contains four corridors and 144 square offices on each floor. The dimensions of the model are arbitrary, but we consider reasonably representative. We chose actual lengths in order to do simulations. In to this model we placed on each floor, nine BS antennae were located in the positions shown by the dots in Figure 2.24. The BS antennae were located in the middle of each office area in order to minimize the reflection path along corridors and street canyons. The minimum horizontal BS separation is given by

$$D_{bh} = W_o + W_c \tag{2.54}$$

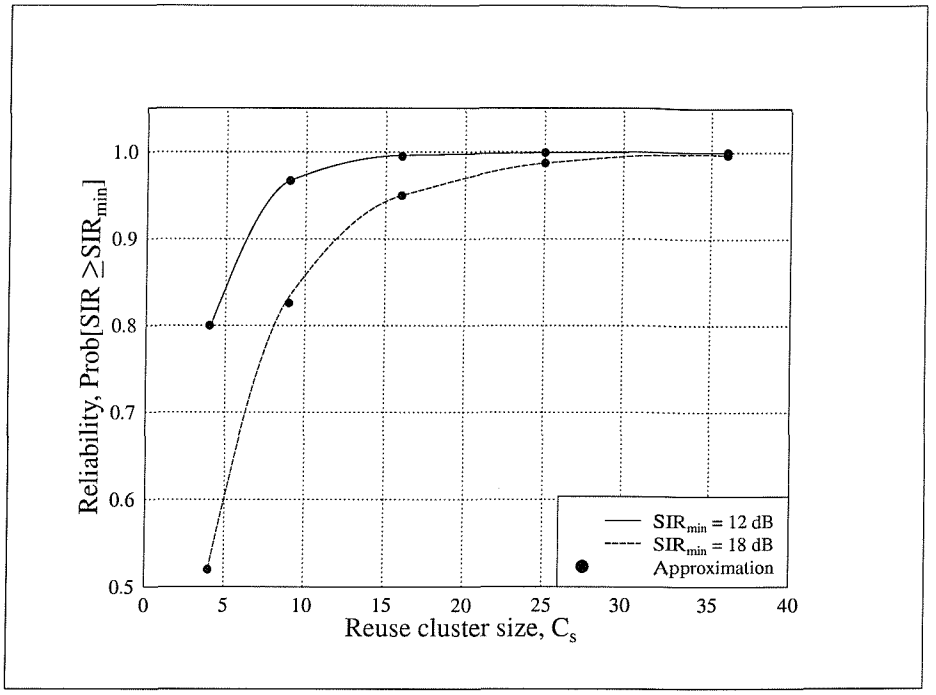


Figure 2.19: Reliability against reuse cluster size for street microcellular system (NLOS), $D_b = 200$m.

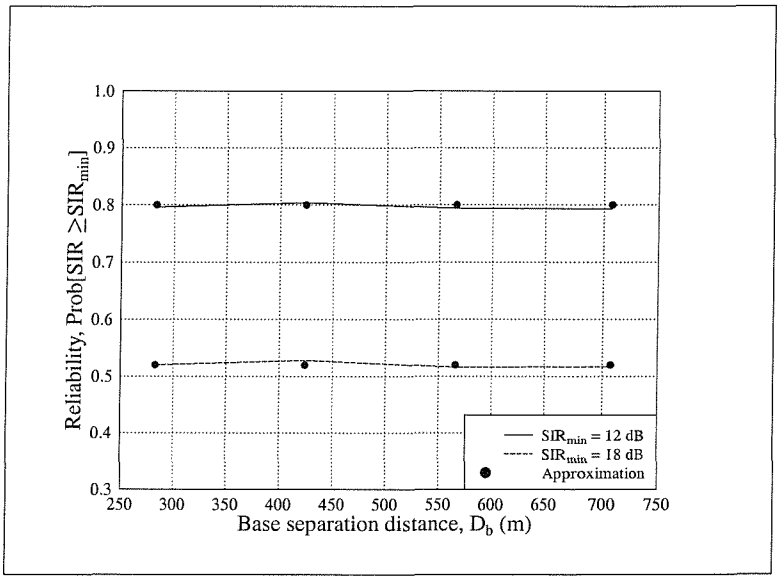


Figure 2.20: Reliability against BS separation distance for street microcellular system (NLOS), $C_s = 4$.

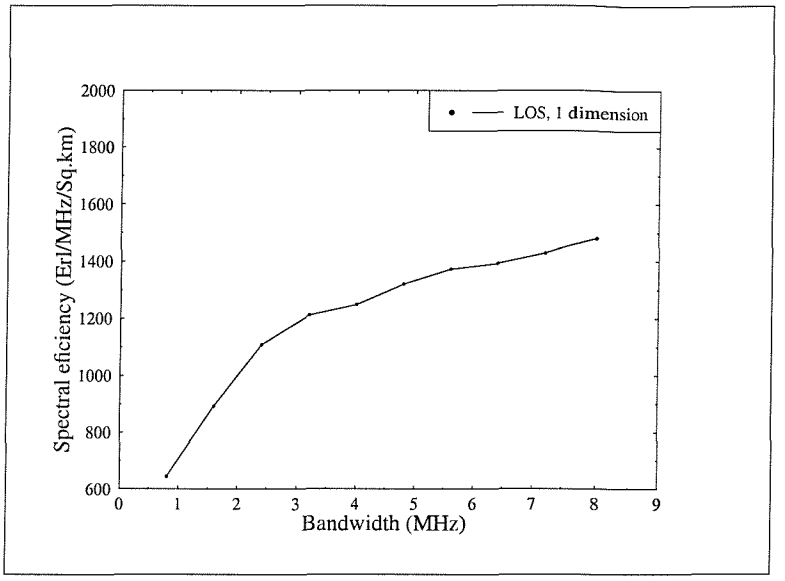


Figure 2.21: Spectral efficiency (in Erlangs/MHz/km$^2$) against radio bandwidth allocated for one dimensional LOS microcell layout, $D_b = 100$m.

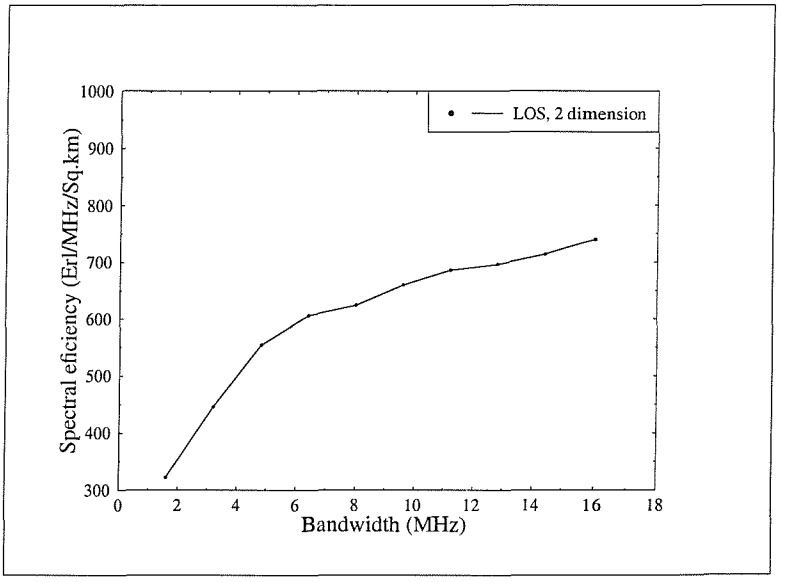


Figure 2.22: Spectral efficiency (in Erlangs/MHz/km$^2$) against radio bandwidth allocated for two dimensional LOS microcell layout, $D_b = 200$m.

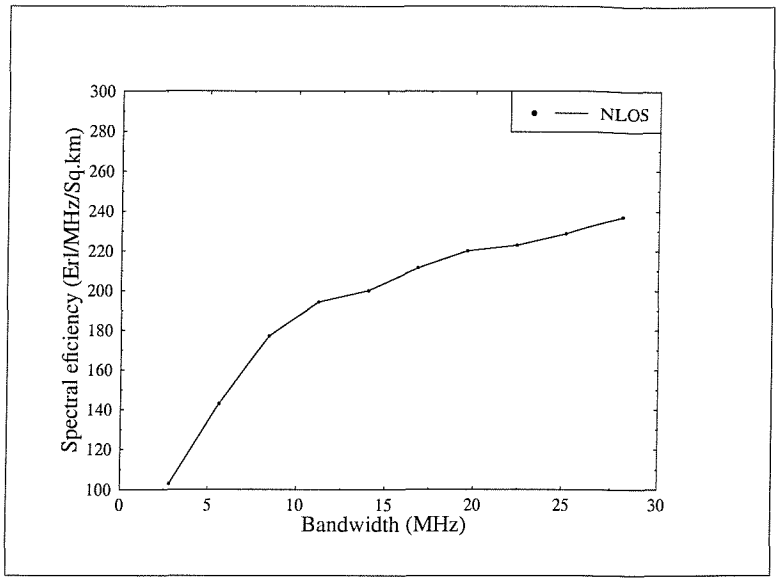


Figure 2.23: Spectral efficiency (in Erlangs/MHz/km$^2$) against radio bandwidth allocated for NLOS microcell layout, $D_b = 200$m.

where $W_o = 20$ (m) is the width of each office area, $W_c = 2$ (m) is the corridor width. The cell radius is approximated by

$$R = \frac{W_o}{\sqrt{2}} \tag{2.55}$$

The vertical BS separation is given by

$$D_{bv} = H_f \tag{2.56}$$

where $H_f = 3$ (m) is the floor height.

The vertical reuse is $N_v$, and on each floor, four picocells per cluster is used as shown in Figure 2.25, where the frequency planning of picocells is characterised by $C_s = 4N_v$ cells per cluster. The nearest horizontal co-channel cell-site separation is given by

$$D_{ch} = 2D_{bh} \tag{2.57}$$

and the nearest vertical co-channel cell-site separation is

$$D_{cv} = N_v D_{bv} \tag{2.58}$$

where $N_v = 3$ is the vertical reuse distance. In order to reduce co-channel interference from picocells in adjacent building, we gave adjacent buildings different frequency planning pattern as illustrated in Figure 2.25.

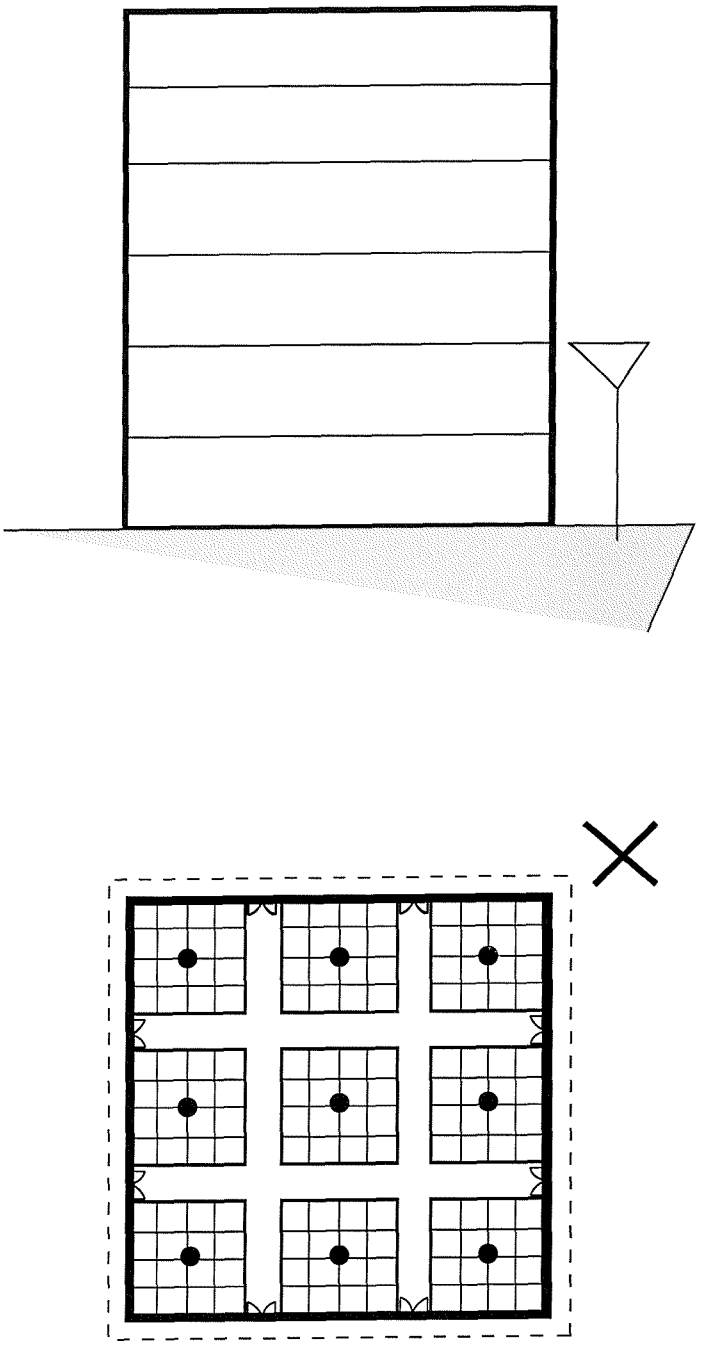

Figure 2.24: Picocells and microcells layout in plan and elevation

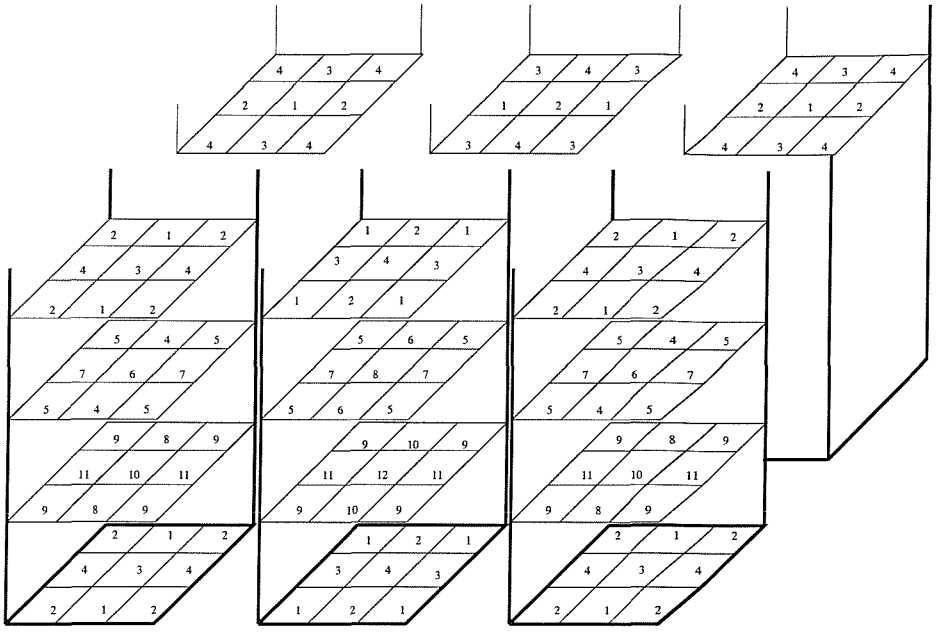

Figure 2.25: The picocell frequency allocation chart. Each picocell is labelled by the frequency set allocated to its BS

### 2.6.1 Signal-to-interference ratio

The Motley-Keenan model, from COST 231 [41] is an empirical model which takes into account the attenuation due to walls and floors in the direct path between transmitter and receiver. The path loss (dB) predicted by this model is given by

$$L\,(\text{dB}) = L_0 + 10\gamma \log(d) + \sum_{i=1}^{I} N_{w_i} L_{w_i} + \sum_{j=1}^{J} N_{f_j} L_{f_j} \tag{2.59}$$

where $L_0$ denotes the loss at the reference point (at 1 m), $\gamma$ is the power decay index and $d$ represents the transmitter-to-receiver horizontal path length, $N_{w_j}$ and $N_{f_i}$ are the number of walls and floors of different kind that are traversed by the transmitted signal, and $L_{w_i}$ (dB) and $L_{f_i}$ (dB) represent their corresponding losses factors. The values proposed for these parameters are as follows:

$$\begin{aligned} L_0 &= 20\log(4\pi/\lambda)\ (\text{dB}) \\ \gamma &= 2 \\ L_f &= 15\ (\text{dB}) \\ L_w &= 3\ (\text{dB}) \end{aligned} \tag{2.60}$$

In order to calculate SIR we simplify the Motley-Keenan model to

$$L\,(\text{dB}) = L_0 + 10\gamma \log(d) + L_w \frac{d}{W_r} + L_f N_f \tag{2.61}$$

where $W_r = 5$ (m) is the room width and $N_f$ is the transmitter-to-receiver floor difference. The received power averaged over multipath fading is given by

$$P_R = P_T \frac{AV}{d^\gamma 10^{\frac{(L_w d/W_r)+L_f N_f}{10}}} \tag{2.62}$$

where $A = 10^{-L_0/10}$ is the free-space path loss at 1 m, and $V$ is a zero-mean lognormal variable, with a standard deviation of 4 dB [32].

For the picocellular environment with fully loaded cells, we focus on a first tier interference model as illustrated in Figure 2.25. The interference between buildings is neglected. The SIR is given by

$$\text{SIR} = \frac{\frac{V_0}{d^\gamma 10^{\frac{L_w d}{10W_r}}}}{\sum_{i=1}^{M_h} \frac{V_i}{D_i^\gamma 10^{\frac{L_w D_i}{10W_r}}} + \sum_{j=1}^{M_v} \frac{V_j}{D_j^\gamma 10^{\frac{(L_w D_j/W_r)+L_f N_v}{10}}}} \tag{2.63}$$

where $M_h = 3$ is the number of horizontal interferers, $M_v = 2$ is the number of vertical interferers, $N_v$ is the vertical reuse distance, $0 < d < R$, $D_i$ is the horizontal distance between the desired mobile and the $i$th horizontal interfering BS for the downlink, or the distance between the desired BS and the $i$th mobile for the uplink; $D_j$ is the horizontal distance between the desired mobile and the $j$th vertical interfering BS for the downlink, or the distance between the desired BS and the $j$th mobile for the uplink; and $V_0$, $V_i$ and $V_j$ are shadow fading variables.

We produce $\Re$ versus SIR results based on the analytical approximation method described in Section 2.4, but with $D_i = D_{ch}$; $D_j = D_{cv}$; $f(d) \approx 2d/R^2$, $0 < d < R$;

$$\Lambda(d) = d^{-\gamma} D_{ch}^\gamma 10^{(D_{ch}-d)\frac{L_w}{10W_r}} \tag{2.64}$$

and

$$\begin{aligned} V_I &\approx \sum_{i=1}^{M_h} V_i + 10^{\frac{10\gamma \log D_{ch} L_w (D_{ch}-1)/W_r - L_f N_v}{10}} \cdot \sum_{j=1}^{M_v} V_j \\ &\approx \sum_{i=1}^{M_h} V_i + \sum_{j=1}^{M_v} \hat{V}_j \end{aligned} \tag{2.65}$$

where $\hat{V}_j$ is a lognormal distribution with a mean (in dB) of

$$\mu_p = 10\gamma \log D_{ch} - 10\gamma \log D_{cv} + L_w(D_{ch} - D_{cv})/W_r - L_f N_v, \tag{2.66}$$

and a standard deviation of 4 dB. The mean and standard deviation of $V_I$ are also derived by Fenton's method [37].

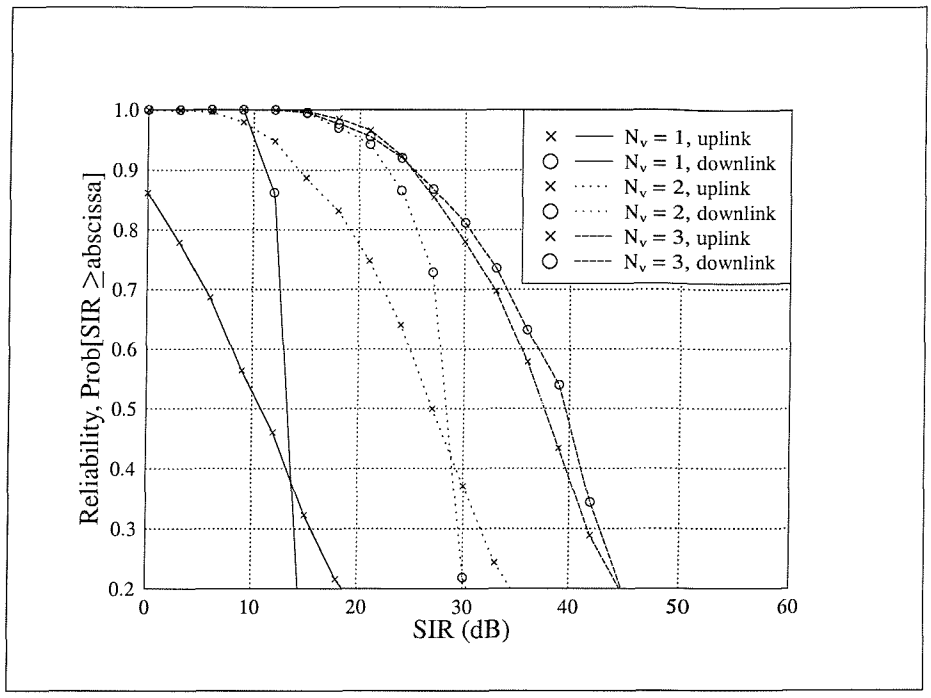


Figure 2.26: Reliability against SIR for inbuilding picocellular system (LOS).

The distance $D_{cv}$ is given by

$$\begin{aligned} D_{cv} &= E[\sqrt{N_v^2 D_h^2 + r^2}] \\ &= \int_0^R \sqrt{N_v^2 D_h^2 + r^2} f(d) \mathrm{d}r \end{aligned} \tag{2.67}$$

where $N_v$ is the vertical reuse cluster size, $D_h$ is the floor height, $R$ is the cell radius and $r$ is the horizontal distance from the interfering transmitter.

### 2.6.2 Results

Figure 2.26 shows the simulation results of the SIR performance for different vertical reuse cluster size. The uplink performance is found to be the limiting case, as BS positions are vertically aligned in our model, and therefore the distance from the desired BS to the vertical interfering MS may be shorter than to the desired MS. Figure 2.27 shows the relation of the reliability to the reuse cluster size. To achieve a reliability of 90% with $\mathrm{SIR}_{min}$ = 12 dB, the required vertical reuse cluster size is two. However, with $\mathrm{SIR}_{min}$=18 dB, the vertical reuse cluster size of three is required to achieve the reliability of 90%. Figure 2.28 shows the curve of spectral efficiency versus bandwidth for our building model. The spectral efficiency increases with the

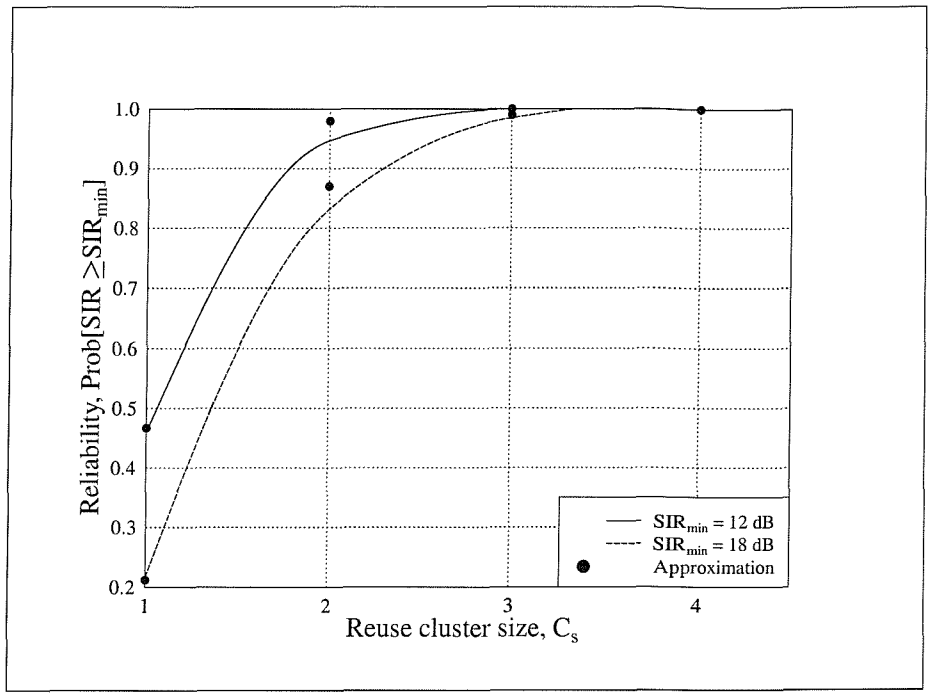


Figure 2.27: Reliability against reuse cluster size for the inbuilding picocellular system (LOS).

higher allocated bandwidth. However, this increase is smaller for bandwidths greater than 9 MHz. We conclude that a picocellular network should be allocated at least 9 MHz to achieve good spectral efficiency (at least 6000 Erl/MHz/km$^2$) and each cell being equipped with three transceivers.

## 2.7 Effect of power control

We consider a simple but suboptimum form of power control which relies on the received signal strength indicator (RSSI) to measure channel quality. The RSSI power control ensures that signal transmissions are received at the BSs or MSs at some fixed received power level, $P_R$, i.e., perfect power control. The following SIR analysis is applicable to both uplink and downlink SIR performance. The transmitted power from the $i$th interferer is,

$$P_{Ti} = \frac{P_R}{L(x_{0i}, y_{0i})} \tag{2.68}$$

where $L(x, y)$ is the path loss, including shadow fading, and $(x_{0i}, y_{0i})$ is the coordinate of the $i$th interferer with reference to the interfered station (either BS or MS). For

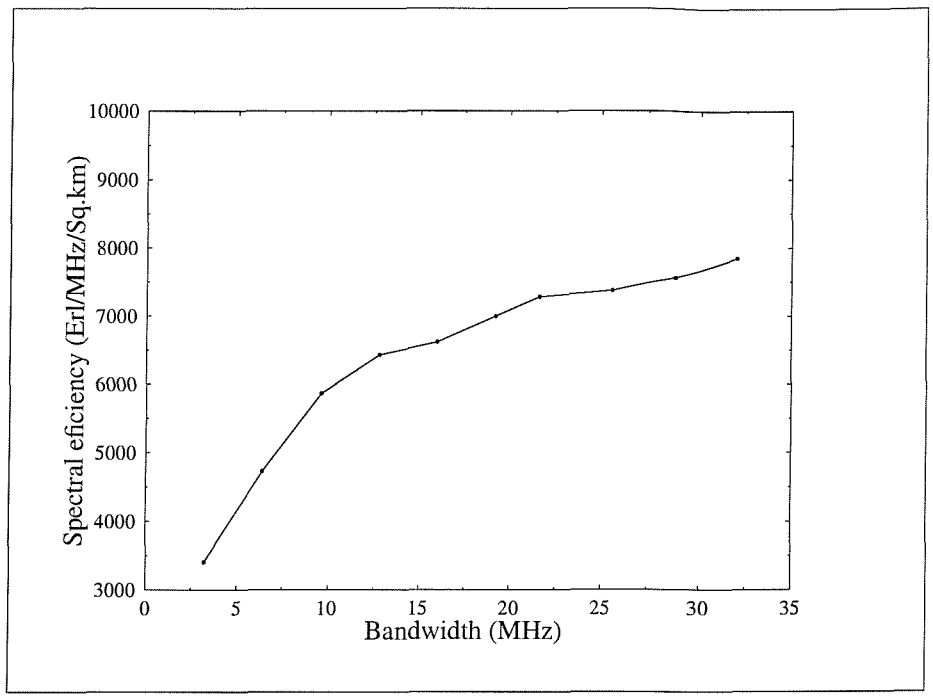


Figure 2.28: Spectral efficiency (in Erlangs/MHz/km$^2$) against radio bandwidth allocated for inbuilding picocellular network

conventional macrocells, $L(x_{0i}, y_{0i})$ is given by

$$L(x_{0i}, y_{0i}) = \frac{A_{0i}V_{0i}}{d_{eq_{0i}}^{\gamma_0}} \tag{2.69}$$

By focusing on only the two first tier interferers (for $M = 2$),

$$\text{SIR} = \frac{P_R}{\sum_{i=1}^{M} P_{Ti}L(x_i, y_i)} = \left[\sum_{i=1}^{M} \frac{L(x_i, y_i)}{L(x_{0i}, y_{0i})}\right]^{-1} \tag{2.70}$$

where $(x_i, y_i)$ is the coordinate of the $i$th interfering MS for uplink SIR, or BS for downlink SIR with reference to the desired BS or MS, respectively. The SIR for the macrocellular system is represented by

$$\text{SIR} = \left[\sum_{i=1}^{M} \frac{A_i V_i d_{eq_{0i}}^{\gamma_0}}{A_{0i}V_{0i}D_i^{\gamma_I}}\right]^{-1}. \tag{2.71}$$

The following simplifying approximations are used in order to produce $\Re$ versus $\text{SIR}_{min}$ analytically.

1. $D_i \approx D_c$.

2. The interfering mobiles is uniformly distributed within a circle of radius R, i.e., the PDF of $d_{eq}$ is approximated by $f(d_{eq}) = d_{eq}/(2R)^2$, $0 < d_{eq} \leq 2R$.

3. $d_{eq0i} \approx E[d_{eq}]$ which is given by

$$\begin{aligned} E[d_{eq}] = \mu_d = &= \int_0^{2R} d_{eq} f(d_{eq}) \mathrm{d}d_{eq} \\ &= \left(\frac{4R}{3}\right) \end{aligned} \tag{2.72}$$

4. $1/V_{0i} \approx E[1/V_0]$, which is given by

$$E[1/V_0] = \mu_v = \int_{-\infty}^{\infty} \frac{1}{v} f(v) \mathrm{d}v \tag{2.73}$$

where the PDF $f(v)$ is lognormally distributed with a decibel mean of zero and a standard deviation $\sigma = 6$dB, and is represented by

$$f(v) = \frac{10}{v\sqrt{2\pi} \ln 10\sigma} \exp\left(\frac{-(10 \ln v / \ln 10)^2}{2\sigma^2}\right), 0 \leq v < \infty \tag{2.74}$$

5. $\sum_{i=1}^{M} V_i \approx V_I$ (M = 2, for both downlink and uplink), where the decibel value of $V_I$ is Gaussian with a mean $\mu_I$ and a standard deviation $\sigma_I$, both being derived using Fenton's method [37].

6. We assume that $d_{eq0i}$ is below 5 km and $D_c$ is above 5 km, hence $A_{0i} = A_0 = 133.8$, $A_i \approx A_I = 137.5$, $\gamma_{0i} = \gamma_0 = 3.8$, and $\gamma_i \approx \gamma_I = 3.4$.

By using the above approximation, we have

$$\mathrm{SIR} = \Lambda_p / V_I \tag{2.75}$$

where

$$\Lambda_p = \frac{A_0 (3R)^{\gamma_I} C_s^{\gamma_I/2} \mu_d^{\gamma_0} \mu_v}{A_I}. \tag{2.76}$$

The reliability is given by

$$\Re_p = Z\left[\frac{(\Lambda_p)_{dB} - (\mathrm{SIR}_{min})_{dB} - \mu_I}{\sigma_I}\right] \tag{2.77}$$

### 2.7.1 Results

Section 2.4 has shown that a macrocellular network with an SIR of 12 dB requires a reuse cluster sizes of four in order to achieve good reliability. Figures 2.29 shows the reliability performance as a function of SIR for the macrocellular network employing

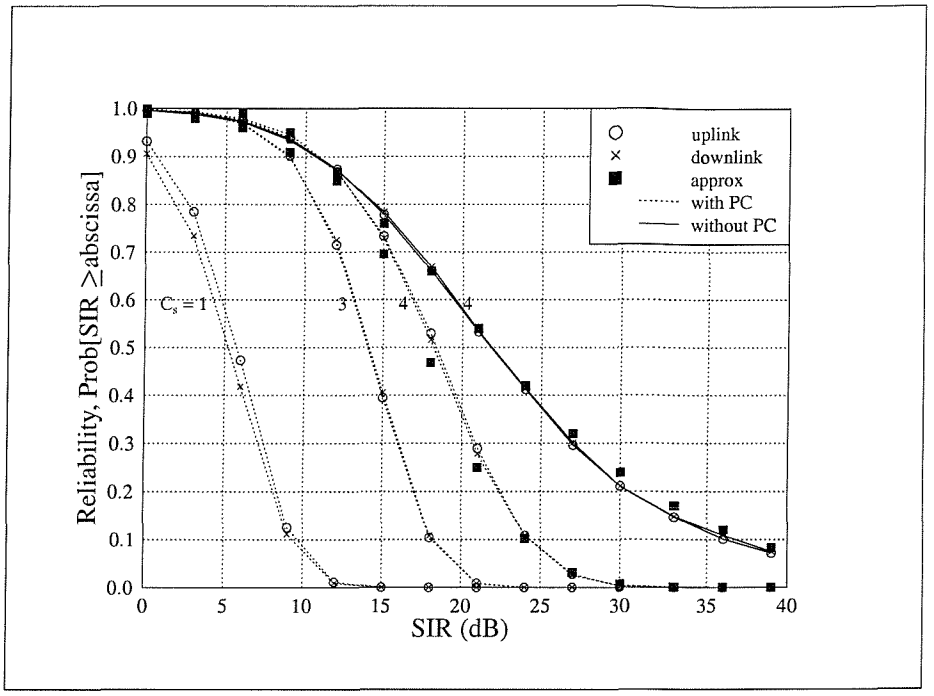


Figure 2.29: Reliability against SIR for different cluster sizes in a macrocellular network employing power control, and $D_b = 1$ km.

power control with different reuse cluster sizes, represented by the dash curves, and compares them with the reliability performance of the four-cell cluster system without power control, represented by the solid curve. The results show that the power control does not increase the system capacity, as the require reuse cluster is still four, however, for the same reuse cluster size, the reliability curve of power-control system is lower than the curve of the non power-control system for unnecessarily high SIRs, i.e., the SIRs having less than 90% reliability. This indicates that the power control reduces the number of calls with unnecessary high SIRs, and therefore the global interference is also reduced. The reduction of transmission power by power control also increases battery life of mobile handsets.

## 2.8 Effect of frequency hopping and fractional loading

The SIR performance of a TDMA system with frequency hopping and power control is now investigated. In the previous section, we assumed that the system is fully

loaded, i.e., all radio channels allocated to each cell are in use and no DTX was used. Here we consider the situation when the system is partially loaded and voice activity detection (VAD) and a discontinuous transmission are employed. We define voice activity factor, VAF, as an average speech activity, and a load fraction, LF, as the proportion of the average cell traffic load to the number of traffic channels assigned to a cell. Both parameters are valued between zero and unity. We assume that the number of frequencies of each hopping sequence is enough to enable the reduction of the average interference, and to thereby improve the SIR performance for all users.

The following analysis is the extension of the analysis of the TDMA system with power control in the previous section. We use slow frequency hopping where the transmission frequency remains the same during the transmission of the whole frame burst. Since the transmission frequency changes in each hop, the interferers change too. By assuming that the amount of interference is uncorrelated at each hopping frequency, the average interference over $N_f$ hopping carriers is given by

$$I = \frac{1}{N_f} \sum_{j=1}^{N_f} I_j \tag{2.78}$$

where $I_j$ is the interference level at each hop. According to the previous macrocell assumption, the maximum number of first tier interferers, $M$, is 2. In the system employing the fractional loading and the discontinuous transmission, each connected mobile stop transmission from time to time and changes its transmission carrier periodically, therefore, the number of active first tier interferers fluctuates from 0 to 2. From Section 2.7, the interference level is

$$\begin{aligned} I_j &= P_R \textstyle\sum_{i=1}^{k} \left[ \frac{A_i V_i d_{eq_{0i}}^{\gamma_0}}{A_{0i} V_{0i} D_i^{\gamma_I}} \right] \\ &= \frac{P_R A_i E[d_{eq}^{\gamma_0}] E[1/V_0]}{A_0 D_c^{\gamma_I}} \textstyle\sum_{i=1}^{k} V_i \end{aligned} \tag{2.79}$$

where $k$ is the number of first tier interferers.

For simplicity when there is no first tier interferer, we assume that there is always one active second tier interferer, i.e., the co-channel cell site separation distance is twice that of the first tier. The term $\sum_{i=1}^{k} V_i$ can be represented by a function of $V_i(k)$ given by

$$V_i(k) = \begin{cases} 2^{\gamma_0} V_i, & \text{for } k = 0 \\ V_i & \text{for } k = 1 \\ \sum_{i=1}^{2} V_i & \text{for } k = 2 \end{cases} \tag{2.80}$$

As $k$ is a random variable with PDF

$$p_k(k) = \begin{cases} \nu^2\zeta^2, & \text{for } k = 2 \\ 2\nu\zeta(1-\nu\zeta), & \text{for } k = 1 \\ (1-\nu\zeta)^2, & \text{for } k = 0 \end{cases} \tag{2.81}$$

where $\nu$ and $\zeta$ represent the voice activity (VAF) and the load fraction, respectively, $V_i(k)$ is approximated by a lognormally distributed random variable $V_j$ with a decibel mean $\mu_j$ and variance $\sigma_j^2$ given by

$$\begin{aligned} \mu_j &= E[V_j]_{(dB)} = \textstyle\sum_{k=0}^{M} \mu_k p_k(k) \\ \sigma_j^2 &= E[V_j^2] - E^2[V_j] = \textstyle\sum_{k=0}^{M} \sigma_k^2 p_k(k) \end{aligned} \tag{2.82}$$

where $\mu_k$ and $\sigma_k^2$ are the mean and variance of $V_i(k)$, viz:-

$$\mu_k(\text{dB}) = \begin{cases} 10\gamma_0 \log 2, & \text{for } k = 0 \\ 0 & \text{for } k = 1 \\ \mu_{k=2} & \text{for } k = 2 \end{cases} \tag{2.83}$$

and

$$\sigma_k^2(\text{dB}^2) = \begin{cases} \sigma_\xi^2, & \text{for } k = 0 \\ \sigma_\xi^2, & \text{for } k = 1 \\ \sigma_{k=2}^2 & \text{for } k = 2. \end{cases} \tag{2.84}$$

The mean $\mu_{k=2}$ and variance $\sigma_{k=2}^2$ can be obtained by Fenton's method [37]. From Equations (2.78) and (2.79) the average interference $I$ can be expressed as

$$I = \frac{P_R A_I \mu_d^{\gamma_0} \mu_v}{N_f A_0 D_c^{\gamma_I}} \sum_{j=1}^{N_f} V_j \tag{2.85}$$

By approximating $\sum_{j=1}^{N_f} V_{I_j}$ to the lognormally distributed random variable $V_f$ with mean $\mu_f$ and standard deviation $\sigma_f$ derived by Fenton's method, the average SIR of the system employing fractional loading and DTX over $N_f$ hopping carriers is given by

$$\text{SIR} = \frac{\Lambda_f}{V_f} \tag{2.86}$$

where $\Lambda_f$ is

$$\Lambda_f = \frac{N_f A_0 D_c^{\gamma_I}}{A_i \mu_d^{\gamma_0} \mu_v} \tag{2.87}$$

The reliability $\Re$ is therefore given by

$$\Re = Z\left[\frac{(\Lambda_f)_{dB} - (\text{SIR}_{min})_{dB} + \mu_f}{\sigma_f}\right] \tag{2.88}$$

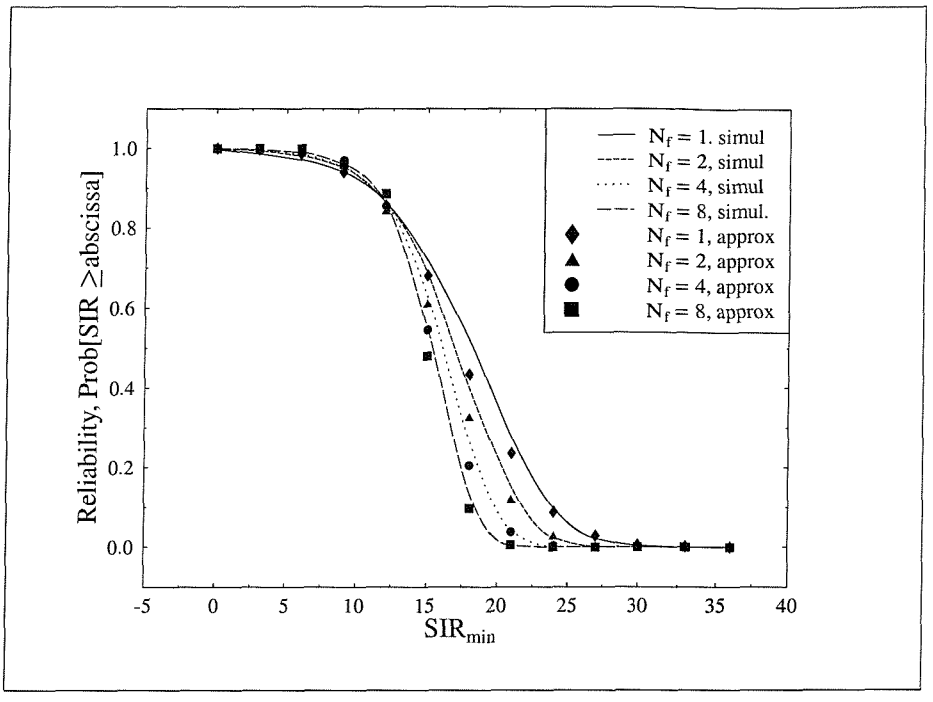


Figure 2.30: Reliability against SIR for macrocellular system with four-cell reuse cluster employing power control and frequency hopping over $N_f$ carriers

### 2.8.1 Results

Figure 2.29 shows the reliability as a function of $\text{SIR}_{min}$ for the macrocellular network employing power control and frequency hopping with $C_s = 4$, $D_b = 1$ km, and full loading. The four-cell cluster structure allows the network with $\text{SIR}_{min} = 12$ dB to operate with a reliability of 90%. To calculate the SIR for the frequency hopping, we average the interference levels over the hopping frequencies. As the number of hopping frequencies increases, the reliability for the SIR less than $\text{SIR}_{min}$ (12 dB) increases, and it decreases for the SIR greater the $\text{SIR}_{min}$. Consequently, with a significant number of hopping frequency, all calls will have the same SIR = $\text{SIR}_{min}$, because of the interference diversity produced by the frequency hopping.

The relationship of the reliability to the product of the voice activity factor $\nu$ and the load fraction $\zeta$ is shown in Figure 2.31. For the curve of a single cell cluster, the reliability increased exponentially as the product of the load fraction and the VAF decreases. Fractional loading is the arrangement in which the single cell cluster is employed, and the number of transceivers in a sector is less than the number of allocated carriers. For 50% voice activity, the reliability of 90% can be achieve with

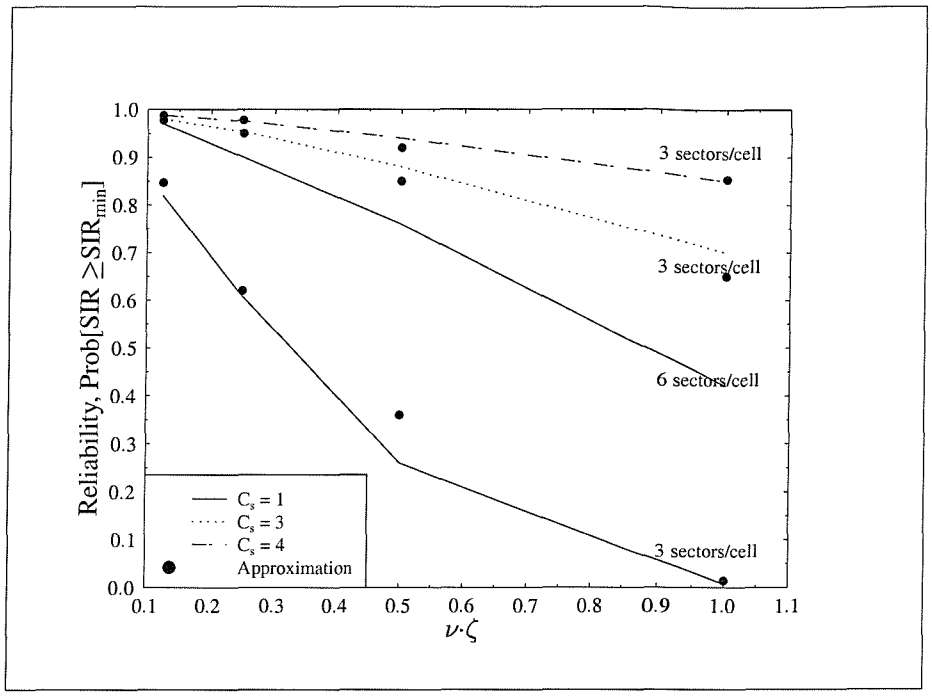


Figure 2.31: Reliability against the fraction of the traffic load for the frequency hopping system with four hopping frequencies ($N_f = 4$)

the single cell cluster and fractional loading of 25%, and therefore the capacity of the fractional loading system is the same as the four-cell cluster system, i.e., both have the same number of transceiver per sector which is a one-fourth of the total number of carriers. However the system capacity of the fractional loading system is halved, if VAD is not employed.

The capacity of the fractional loading can be increased by applying more sectors per cell, for example, six sectors per cell is achieved by using directional antennas of 60 degree. The simulation results for the fractional loading with six sectors per cell is shown in Figure 2.31. The system capacity of the fractional loading system with six sectors per cell is twice the capacity of the fractional loading system with three sectors per cell and the four-cell cluster system, as the 90% reliability is maintained at a loading of 50%, assuming 50% voice activity.

## 2.9 Conclusion

We have analysed the capacity in terms of its spectral efficiency of a TDMA mobile cellular system having a macrocellular network, a street microcellular network and an inbuilding picocellular network. The investigation has made use of the latest propagation model that we know for each type of cellular environments. The mobile cellular networks we envisage is characterised by the following attributes.

1. The macrocellular network is formed by a hexagonal grid. Each cell site is sectorised with three sectors per cell.

2. The microcellular network is utilised in a dense urban rectilinear street grid environment. The cell-site antennae are located at street level, well below the rooftops of the surrounding buildings, e.g., on lampposts and at intersections and along streets.

3. The inbuilding picocellular network is installed in a square building with four corridors and 144 square offices. Each floor has nine office areas and also nine cell-sites, where each cell site is located in each office area.

4. A TDMA system such as GSM, is assumed, and the traffic is speech.

We focused on the reference case of fixed channel allocation with fully loaded cells, i.e., all channels are in used and no DTX is used. For a typical link quality requirement (SIR $\leq$ 12 dB over 90% of the service area) the macrocellular reuse cluster size is four, and the maximum spectral efficiency for the macrocellular network is 0.88 Erlangs/MHz/km$^2$. The required reuse cluster size for 1-D LOS, 2-D LOS and NLOS microcellular networks are two, four and seven, respectively. The maximum spectral efficiency for the microcellular network is 1480, 740 and 237 Erlangs/MHz/km$^2$, for 1-D LOS, 2-D LOS and NLOS microcell arrangement, respectively. The required reuse cluster size for inbuilding picocellular network is eight, and the spectral efficiency for our inbuilding model is 7845 Erlangs/MHz/km$^2$. Those mentioned figures of the maximum spectral efficiency were based on BSs with ten transceiver per BS. For BSs with two transceiver, the figure is only 60 percent of the maximum figure, due to the loss of trunking capacity.

In our analysis of the application of power control and frequency hopping we found that the capacity did not directly improve, as the required reuse cluster size is unchanged. However, the global radio interference are reduced by power control as each

MS and BS minimises its transmission power. We also concluded that the fractional loading allows the network to use smaller reuse structures due to the interferer diversity characteristics of frequency hopping. If a single-cell cluster is used, the system capacity is soft and frequency planning is not required. However, the system's load must be controlled in order to maintain the required $\mathrm{SIR}_{min}$.

In the macrocellular network with three and six sectors per cell, the single cell cluster can provide satisfactory link quality with 25% and 50% fractional loading, respectively, assuming a 50% voice activity factor.

# Chapter 3

# Cordless Telecommunication Systems

## 3.1 Introduction

Throughout the 1970s and early 1980s, analogue cordless telephones designed and manufactured in the Far East dominated the European market. As these cordless telephone often operated at frequencies allocated to other users and the potential of interference was high, a situation not approved of by regulatory authorities. Europe reacted to this situation by creating four new cordless telecommunication (CT) standards, starting with CT1.

The specification of CT1 was originated by the European posts and telecommunications (CEPT) standards body, and it was adopted quickly within Europe with the exceptions of UK and France. However, due to the difficulty of applying integrated technology, CT1 handsets were expensive. A key reason for this difficulty was because CT1 was specified to provide excellent speech quality equal to that of copper based local loop. The UK, believing that the cost of handsets was too high, developed their own CT1 variant, as did France. Needless to say they were incompatible, and a new single standard was required urgently. However, yet again alternative solutions came to the fore, named, CT2 [32], CT3 [42] and the digital enhanced cordless telecommunication (DECT) [42].

The driving force for CT2 came out of the UK. CT2 was the result of development work undertaken by a consortium of companies including Ferranti, Plessey, Shaye

and STC. Due to lack of co-ordination, products launched by these companies exhibited differences. However, under the encouragement and the sponsorship of DTI, they reached an agreement to work toward a standard known as the "common air interface" (CAI). There were two key standards for CT2: BS6833 which defined the signalling and speech encoding between the handset and the BS; and MPT1344 which defined the radio parameters to a sufficient degree to allow the equipments from various manufacturers to work together. While CT2 was already available, the European standard in the form of DECT was still only a draft specification. The lack of European standard at the time led a number of European public telephone operators adopting CT2 telepoint in trials. In the UK, Hutchison's Rabbit service was one example. Due to regulatory limitations, CT2 allows two-way conversations within the home or offices but only outgoing calls when employed in outdoor Telepoint environments. CT2 was not concerned for the Telepoint market, but that was where it was increasingly used. As with CT3 below, CT2 was rejected as the basis of the European standard, and was eventually abandoned.

CT3 (DCT900) was developed by the Swedish telecommunications manufacturer Ericsson and was based on an early DECT specification. There are similarities with CT2 but CT3 allowed full two-way access no matter where the phone was being used, i.e., in the home, in the offices or in a telepoint node. However CT3, was abandoned in 1991 when it was not accepted as the European cordless standard.

The DECT standard was developed within the European Telecommunications Standard Institute (ETSI). It was initially conceived in the mid-1980s as a domestic cordless phone standard for European. However, by the time the standard was finalised and published in 1992, the scope of the standard had broadened beyond domestic cordless phones, to include cordless business telephones (or so-called wireless PBX) and a radio alternative to wired subscriber accesses in public telephone network known as wireless local loop (WLL). Since 1993, DECT has been a mandatory standard throughout the European Union. Member countries have set aside radio frequencies in the 1.88-1.9 GHz for DECT systems. The DECT has also been adopted for use in many countries outside the EU, making it one of the most widely use standard for cordless communications. The DECT systems are characterised by having a relatively simple radio link in that forward error correction (FEC) coding, interleaving, channel equalisation and power control are not used, as it is designed for short-range communications in buildings and their immediate environments and are essentially

consumer products, being low cost, light weight, and inexpensive to buy and operate. By contrast, the radio interface protocols are sufficiently complex to support dynamic channel allocation(DCA).

This Chapter is organised into three sections. In the first section, we proposed a minicell with an adaptive handover strategy to enhance the DECT system operating in an indoor office environment. In the next section, a joint street microcellular/office picocellular environment is postulated and a DECT system providing outdoor as well as indoor radio coverage from indoor radio ports is examined. The objective of this study is to demonstrate that radio coverage of city streets and offices can be achieved in certain situations by locating DECT radio ports (RPs) indoors, avoiding outdoor microcellular sites. The last section presents a study of wireless ATM implementation using DECT-like radio interface. ATM or asynchronous transfer mode is the most popular standard for carrying multimedia traffic over wires. It supports various applications with different bandwidth requirements, and provide an efficient mean to guarantee the quality of service (QoS) requirements as specified by the applications [43, 44]. Clearly, it is desirable to extend ATM to the wireless link. In this section, we design a DECT-like radio interface that encapsulates a single 53-byte ATM cell (packet), in one radio packet. The performance of the radio protocol is investigated under indoor and outdoor radio environment using Rayleigh fading model.

## 3.2 Enhancing the indoor DECT system

In this discourse we consider a modified DECT system operating in both an indoor environment and an outdoor environment. We make three essential changes to the conventional DECT specification. The first is that we allow the deployment of a minicell that is able to provide overlay radio coverage of a number of indoor picocells. The minicellular radio port (RP) is characterised by having a fixed transmitter power level that is within the DECT specifications, and operates using a fixed carrier. The second modification involves an adaptive handover (HO) algorithm which adjusts the number of available channels at the minicellular RP that are reserved exclusively for HO as a function of the average traffic load at the minicellular RP. No channels are reserved exclusively for HO at the picocellular RPs. The third modification enables the portables to re-synthesis to an adjacent time slot, instead of the conventional DECT portable that re-synthesises over a period of two slots. There are other minor

differences that we will mention later, and for this reason we use the term DECT-like for our proposed system.

### 3.2.1 System model

There are 10 radio carriers and 12 TDD channels pairs per carrier. Most of these carriers are assigned to the picocellular RPs in the building, while the remaining ones are used by the minicellular RPs. The carriers occupy the frequency band 1880 to 1990 MHz. The building used in our investigation has three open-plan floors each 100 by 100m, and the room height is 3m. On each floor there are 25 picocellular RPs in a square matrix of columns and rows. Each row or column has RPs spaced 10, 20, 20, 20 and 20m from a wall in a rectilinear grid arrangement. The minicellular RP antennas are located in the centre of the floors at ceiling level and are able to provide complete coverage of the floors, and collectively of the building. Picocellular RPs have a single transceiver that is capable of hopping from one carrier to another within a guard time as dynamic channel assignment (DCA) is used. The minicellular RPs uses a fixed single carrier with 24 slots, i.e. it is a DECT RP operating in fixed channel allocation (FCA) mode. All RPs are synchronised. Calls may be made from both moving and stationary users, be they at their desks or nomadic. In our simulations the moving users walk at 1m/s and constitute 10% of the total user base. The direction that the users travel is uniformly distributed over $(0, 2\pi)$, and the directions change according to an exponential distribution with a mean of 20s. The locations of portables are uniformly distributed throughout the building, and each user offers a traffic load of 0.2 Erlang. Calls arrive according to a Poisson distribution with a mean interarrival time of 600s. The probability distribution of the call duration is exponentially distributed with a mean duration of 120s.

A simple law of path loss in dB versus distance $d$ in m between a RP and a portable is [32]

$$PL = L(\nu) + 10n\,log_{10}(d) + kF$$

where $L(\nu)$ is a clutter loss factor and is typically 30dB, $n$ is the decay index and a suitable value is 3.5, $k$ is the number of floors between the RP and the portable, and $F$ is the floor attenuation and a value of 15 was used in our simulations. The shadowing random variable is uniformly distributed in the range -10 to +10dB [45]. As the office environment is relatively static the floor space may be arbitrarily divided into a mosaic of tessellated squares of side 2m, and in the simulations the shadow fading may be

set to a fixed value for transmissions with a particular RP. Thus for each square there are a number of shadow fading levels in dB, one for each RP. To accommodate the Rayleigh fading the range of fades we assume have a lower fading margin compared to outdoor macrocells, namely, 10dB to 20dB. The lower figure is when the RP employs antenna diversity, a situation we consider to prevail. Accordingly the call set-up signal-to-interference ratio (SIR) threshold, $SIR_{su}$, is 21dB, after taking into account that the receiver sensitivity is 10dB above the noise floor, and to this we add 1dB, and a further 10dB to allow as the fast fading margin. The receiver sensitivity is -83dBm. The simulation records SIR and transmitted power for both the up-link and down-link of each call in progress.

Each RP has at least one beacon signal in order for a portable to establish a call with a RP. At system initialisation, a minicellular RP transmits its beacon on slot 0. RP number one $RP_1$ selects an arbitrary frequency and slot number for its beacon transmission. $RP_2$ observes the channel used by $RP_1$ for its beacon, and selects a different one. This procedure of each RP being activated, listening to what channels are being used for beacons, and then selecting the one that has the lowest signal level, continues until all RPs are transmitting beacon signals. The TDD frame has 12 slots during which a RP may transmit signals, and 12 slots when it may receive signals from the portables. At start-up, and following beacon transmission, each RP scans the up-link slots on each carrier in succession seeking any portable attempting an access.

A portable at start-up scans the available carriers and on identifying the one giving the highest received level, synchronises to obtain the data within its slots, seeking the beacon channel. The beacon data informs the portable of the name of the RP transmitting this beacon, and the slots it has available for access. Accesses then ensues. After a short period when the system is fully operational, each portable becomes synchronised to the network and within its protocol structure forms a matrix where the columns are the TDMA slot numbers and the rows are the carriers. From this a matrix a channel list is formed, where a channel is represented by the combinations of a slot and a carrier, and the ranking in the list is in terms of the received signal strength indicator (RSSI). Channels having an RSSI > -50dBm are considered to be busy.

A portable periodically examines the strongest beacon it receives in case it is paged. It also examines other channels in order to keep its list up to date. This is achieved

by tuning to each carrier in turn and measuring the RSSI in each slot. When a connection is requested by either the network (via paging) or by the portable, the latter selects an available slot having the lowest RSSI associated with the strongest beacon. If no suitable channel can be found the portable examines the channels of the next strongest beacon, and so on. For an access attempt by a portable to be successful the RP must correctly receive the access message, and then give the portable permission to proceed.

In the simulation the messages are deemed to be correctly received if the SIR values exceed a system threshold of 21dB. A portable initiates a handover (HO) when the SIR $<$ 21dB, when a time-out counter starts. The portable attempts to access another channel, i.e. a HO, if for the new channel the SIR$\geq$ 21dB. The call is maintained if this is achieved before the time-out, set at 10s, occurs. A portable always attempts to HO to a picocellular RP. If this cannot be accomplished, it examines the broadcast control channel from a minicellular RP. If the minicell has a channel available, a picocellular RP-to-minicellular RP HO occurs. Otherwise the call is dropped. Portables communicating with the minicellular RP continue to monitor the channels in the picocellular RPs, and they seek a HO to a picocellular RP when this is possible. Notice that the minicellular RP supports HO failure in the RPs, but it does also support new calls, if no picocellular RP channels are available in the vicinity of the portable making the access attempt.

### 3.2.2 Adaptive algorithm for minicellular access

To ensure that sufficient channels are available to support HO failure between picocellular RPs we assign $N_h$ channels at a minicellular RP exclusively for HO [31, 46] For $N_h$ channels at a minicellular RP, $N - N_h$ channels may be used for HO or for new calls. The average traffic load A at a minicellular RP is measured over a period T. Starting with $N_h$=0, we update $N_h$ at the i-th interval according to,

$$N_{h,i} = \begin{cases} N_{h,i-1} - n_d, & A \leq A_t \\ N_{h,i-1} + n_u, & A > A_t \end{cases}$$

where $A_t$ is a system parameter. As we want to keep the probability to HO failure from picocellular RPs to a minicellular RP low, say 0.5%, the choice of $A_t$ is 5.23 Erlangs, determined from the Erlang-B formula, for 12 channels, and a blocking probability

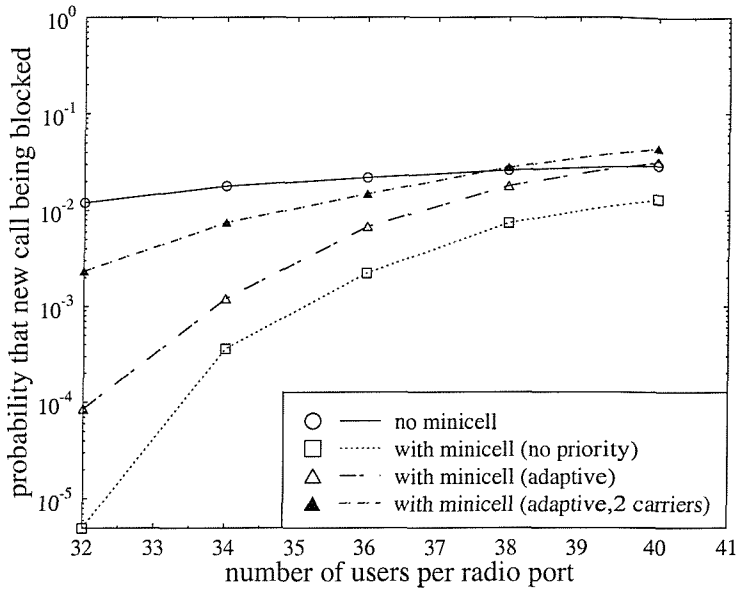


Figure 3.1: Blocking probability performances for different scenarios when 10% of the users are moving

of 0.5%. The parameters $n_d$ and $n_u$ are positive integers, and

$$0 \leq N_{h,i} \leq N_{h,max} .$$

### 3.2.3 Results

In our simulation we arranged for a portable to update its channel list before selecting the access channel. A portable was allowed to make up to 10 access attempts to get a channel. A HO was instigated when the SIR <21dB. A portable was also allowed to try up to ten times to find a channel during a particular HO process before time-out occurred and the call was dropped. The adaption time T was set to 10s. This was sufficiently long to measure the average traffic load at a minicell. The SIR on all links was measured and HO checks performed every second. The parameters $N, N_{h,max}, n_u$ and $n_d$ were set to 12, 6, 4 and 2, respectively.

The performance parameters used were the probability of a new call being blocked

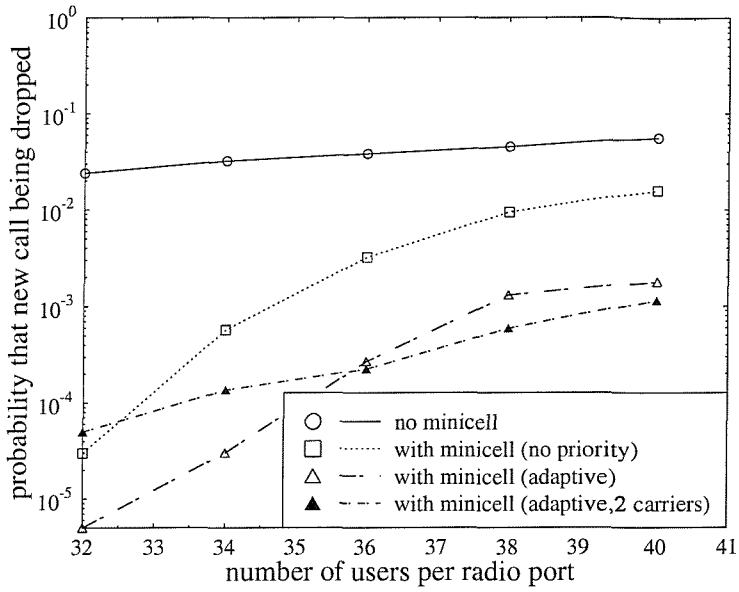


Figure 3.2: Dropping probability performances for different scenarios when 10% of the users are moving

$P_b$, the call dropping probability $P_d$ and the grade-of-service (GOS). Specifically

$$P_b = N_{block}/N_{arrival} \tag{3.1}$$

where $N_{block}$ was the number of calls being blocked and $N_{arrival}$ was the total number of call arrivals,

$$P_d = N_{drop}/(N_{arrival} - N_{block}) \tag{3.2}$$

where $N_{drop}$ was the number of calls being dropped, and

$$\text{GOS} = (N_{block} + \omega N_{drop})/N_{arrival} \tag{3.3}$$

where $\omega$=10 is an arbitrary number to accommodate our view that dropping a call is more serious than a new call being blocked.

In our first simulation we only used picocellular RPs. There was no minicellular RP. Consequently all 10 carriers were assigned to the picocellular RPs. The next simulation had one minicellular RP that used one carrier, with an antenna located at the centre of each floor transceiving the same signals. Consequently there were nine

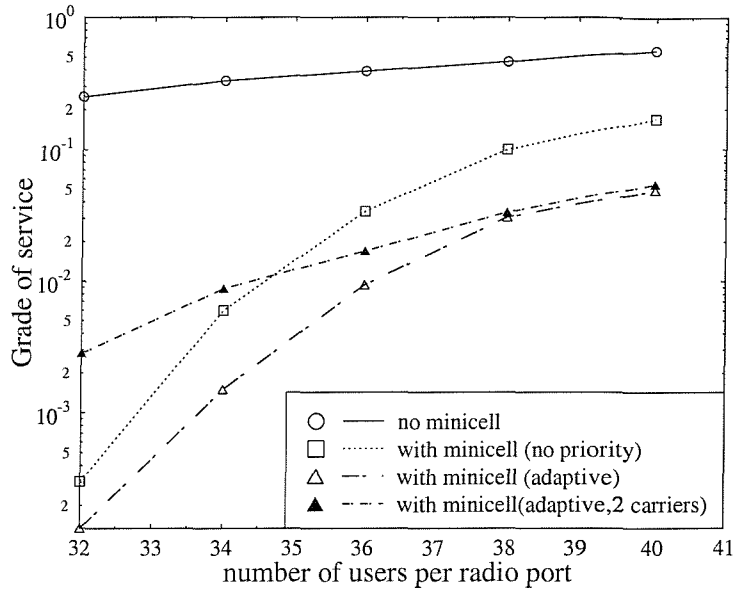


Figure 3.3: GOS performance comparisons with 10% of users moving

carriers for the picocellular RPs. However, the minicellular RP did not reserve any channels exclusively to support HOs. The next simulation was the same as the second simulation, except that the adaptive HO algorithm for the minicellular RP was used. Finally we investigated the situation when the picocellular RPs shared eight carriers, and three minicellular RPs shared two carriers. On floors 1 and 3 the minicellular RPs used the same carrier i.e. FCA, while the minicellular RP on floor 2 had its own carrier.

Figure 3.1 shows the variation of $P_b$ with the number of users per RP for our four simulations. The curves are for 10% of the users moving at 1m/s. The minicellular RP, or the picocellular RPs, provided an enhanced performance with low numbers of users due to the presence of picocellular-to-minicellular HOs. With larger number of users the effect of the minicellular RP was minimal. The curves for $P_d$ are displayed in Figure 3.2. Without the minicellular RP the value of $P_d$ was some 2 to 5per cent over the user range of 32 to 40 users per picocellular RP. However, deployment of a minicell significantly improved performance, and for 32 users per RP, $P_d < 10^{-5}$ when only one minicellular RP was used. For 40 users, the adaptive algorithm yielded

an order of decrease in $P_d$ of ten compared to the deployment of the basic minicell. The GOS curves in Figure 3.3 show similar trends, where the GOS is seen to be significantly enhanced by employing the only one minicellular RP using the adaptive algorithm. The reason why the performance is better with one minicell rather than three minicells using two carriers in a FCA mode, is that in the former there are more carriers for the picocellular RPs who are operating in a DCA mode.

### 3.2.4 Conclusion

We conclude by noting that for a particular GOS we are able to support significantly more users by adding a minicellular RP with the adaptive algorithm compared to the simple picocellular cluster in an inbuilding environment of the type described. The exact mixture of picocells operating in a DCA mode and minicells using the adaptive algorithm in a FCA mode, on the network performance depends on the specific environment. However, we advocate this mixture of cells and channel assignments in order to enhance a given network's performance.

## 3.3 City centre model for DECT coverage evaluation

The objective of this section is to demonstrate that radio coverage of city streets and offices can be achieved in certain situations by locating DECT radio ports (RPs) indoors, avoiding outdoor microcell sites.

The common street microcell model is a pattern of rectilinear streets [39, 24]. Indoor picocellular models may be a rectangular floor with square offices on either side of a central corridor. We sought a combined indoor and street model, and the one conceived includes the rectilinear street pattern model, with the addition of square buildings containing offices about a rectilinear pattern of corridors. A section of our proposed model is shown in Figure 3.4. This model, although arbitrary a model of this type must be, is selected to have reasonable correspondence to dimensions that can be encountered. There are 100 equal size city office blocks. The streets are 28 metres wide including 4 metre wide pavements on each side. Each building is 72 metres square and contains four corridors and 144 square offices. The corridor walls have a penetration loss of 8 dB. The glass doors between the corridors and the

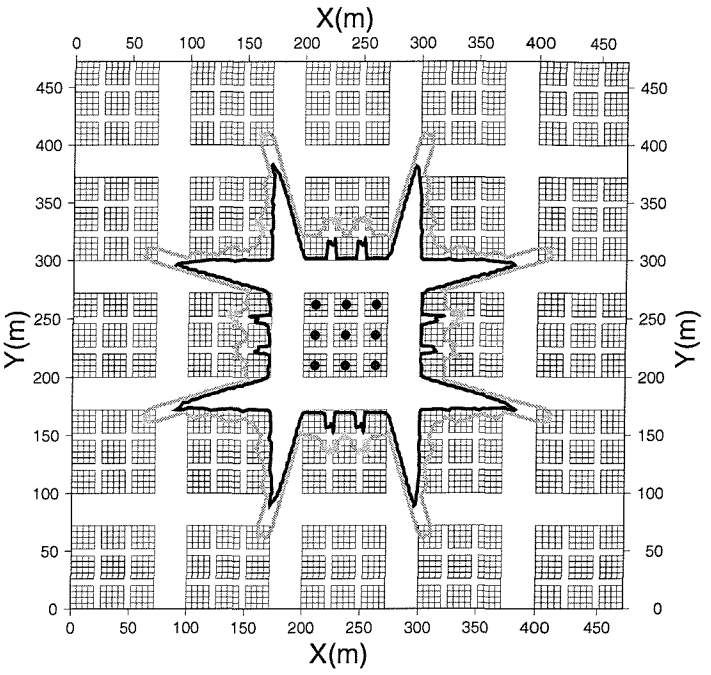


Figure 3.4: A 5x5 section of our 10x10 block city model. Dots indicate RP positions. Also shown are the composite 96 dB(black) and 117 dB(grey) path loss coverage contours from all 9 indoor picocellular RP positions in the central city block.

street have a 4 dB loss. The other exterior surfaces have a 12 dB loss, while the internal office partitions have a loss of 3 dB. The penetration losses in our model for walls are similar to those published in references [47, 48, 49, 50, 51], e.g., Owen and Pudney [51] reported the measured loss of plaster-board walls to be 3 to 4 dB, and 7 to 9 dB for breeze-block or brick. We have assumed that the propagation model's internal partition walls are made of plaster-board and the corridor walls are made of brick. We consider a network where nine RPs are located on the ground floor of each building. The black dots in Figure 3.4 show the position of the RPs in the central building. Observe that we have not considered buildings which are predominantly covered with tinted metal windows that can have penetration losses up to 30 dB [49]. This would effectively isolate the inbuilding system from the street areas.

### 3.3.1 Propagation model

A simple path loss law in dB as a function of the horizontal distance d in metres between an RP and a portable is $L_{dist} + L_{walls}$, where $L_{dist}$ is the distance dependent dual slope path loss

$$L_{dist} = \begin{cases} 20log(4\pi d/\lambda), & \text{if } d < 4h_1h_2/\lambda \\ 20log(4\pi d^2/\lambda) - 20log(4h_1h_2/\lambda), & \text{if } d \geq 4h_1h_2/\lambda \end{cases} \quad (3.4)$$

and $\lambda$ is the wavelength, $h_1$ and $h_2$ are the office RP and portable antenna heights above ground, set to 2 m. The loss $L_{walls}$ is the sum of the penetration losses of the walls intersected by the path joining the RP and the portable.

### 3.3.2 System model

To setup a call, the signal-to-interference ratio (SIR) must be above $\text{SIR}_{min}$ at the receiver. In order to achieve a bit error rate (BER) of $10^{-3}$, we assume that the SIR must be at least 10 dB. In addition to this, to compensate for Rayleigh fading we allow an extra SIR margin of 10 dB, assuming the RP employs antenna diversity, and to this we add 1 dB giving the $\text{SIR}_{min}$ of 21 dB. The noise floor of a DECT receiver [42] is -93 dBm, therefore the minimum desired signal power and the minimum interference power the portable can receive is -72 dBm and -93 dBm respectively, corresponding to path losses of 96 dB and 117 dB, respectively, for an RP transmitter power of 24 dBm. Returning to Figure 3.4, the area within the 96 dB path loss contour is the total signal coverage from the indoor RPs and the 117 dB contour indicates the region where interference from the RPs is above the noise floor. RPs are located in every building in the same interior positions as shown by the black dots in Figure 3.4, thus providing total indoor and outdoor coverage in the city centre model.

Indoor users are located randomly within the ground floor of buildings where 10 % of them are moving during their calls. The travelling directions of the indoor users are random and uniformly distributed over $(0, 2\pi)$. The directions are changed at each random interval which is exponentially distributed with a mean of 30 seconds. Indoor users walk at a constant pace of 1 m/s. Outdoor users are randomly located on the footpaths around the buildings. Only 10 % of them stand still while making their calls. The speeds of the outdoor users are normally distributed with a mean and variance of 1.0 and 0.5 m/s, respectively. Their speeds are regularly updated at time intervals of 1 s. The minimum and maximum speed is 0 and 2 m/s, respectively. When the

users reach a destined junction, we randomly pick the new destined junction from the surrounding junctions. All adjacent junctions have equal probability of being chosen. We use a wrapping technique which allows users to leave one edge of the city model and enter at the opposite edge of the city. We do not allow users to move in or out of buildings during their calls.

Every indoor and outdoor user offers traffic loads of 200 and 50 mErlang, respectively. Calls arrive according to a Poisson distribution with the arrival rate related to the total offered traffic. The call duration is exponentially distributed with a mean of 100 s. We consider 10 radio carriers and 12 TDD channel pairs per carrier. By default, all carriers are assigned to all RPs. The carriers use the frequency band 1880 to 1990 MHz. Each RP and mobile transceiver is capable of hopping from one carrier to another within the guard time. We assume that all RPs and portables have acquired synchronisation. Each RP is always active on at least one channel, where its system information and RP identification are broadcasted. This data is in the control field of each transmitted packet, allowing a portable to identify and lock to the system. The portable keeps listening to the RP with the strongest signal for a possible incoming call.

Dynamic channel allocation is performed at the portable which measures the interference level of each channel; the portable lists and sorts these channels from least to the most interfered one, is produced and updated continuously. When the portable wants to initiate a call, it selects the least interfered channel from its list, and tries to access the channel. If a RP slot is free and both uplink (measured at RP) and downlink (measured at portable) SIRs are above $SIR_{min}$, the channel is assigned for a call. If the channel cannot be accessed, the portable can repeat the access procedure for a maximum number of 10 times. When the portable fails to establish a link within 10 tries, the call is blocked.

If during the call the SIR falls below $SIR_{min}$, the portable initiates a handover procedure which is the same as the new call initiation procedure. However, the portable cannot use the current traffic time slot as traffic packets are being transmitted. If a handover cannot be executed immediately, the portable repeatedly retries during a five second timeout period. After this the call is terminated.

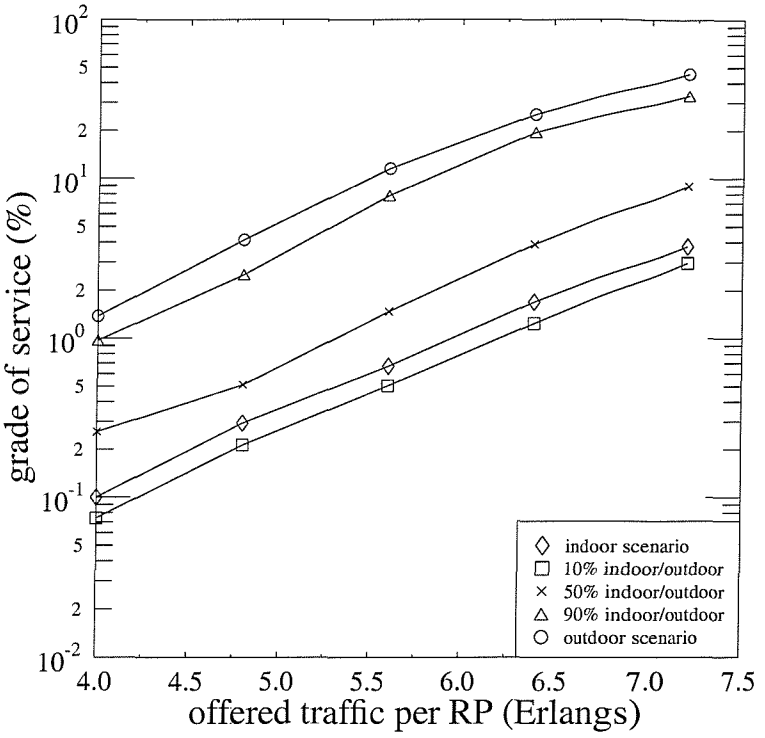


Figure 3.5: GOS performance comparison

### 3.3.3 Results

The probability of a new call being blocked $P_b$, the probability of a call being forced to terminate $P_d$, and the grade-of-service GOS are given by Equations 3.1, 3.2 and 3.3, respectively. The unit of average offered traffic per RP in Erlang is the sum of offered indoor traffic per RP ($A_i$) and the outdoor traffic per RP ($A_o$), where $A_i = N_i * A_{pi}/N_{RP}$ and $A_o = N_o * A_{po}/N_{RP}$, respectively, and $N_i$ and $N_o$ are the total number of indoor and outdoor potential users, $A_{pi}$ and $A_{po}$ are the offered traffic of each indoor and outdoor user, and $N_{RP}$ is the total number of RPs.

We performed simulations for five different traffic distribution scenarios, the indoor scenario where all calls were from indoor users, the outdoor scenario where all calls were from outdoor users, and the mixed indoor/outdoor scenario where the percentage of calls being made by outdoor users were 10 %, 50% and 90 %. Figure 3.5 shows the

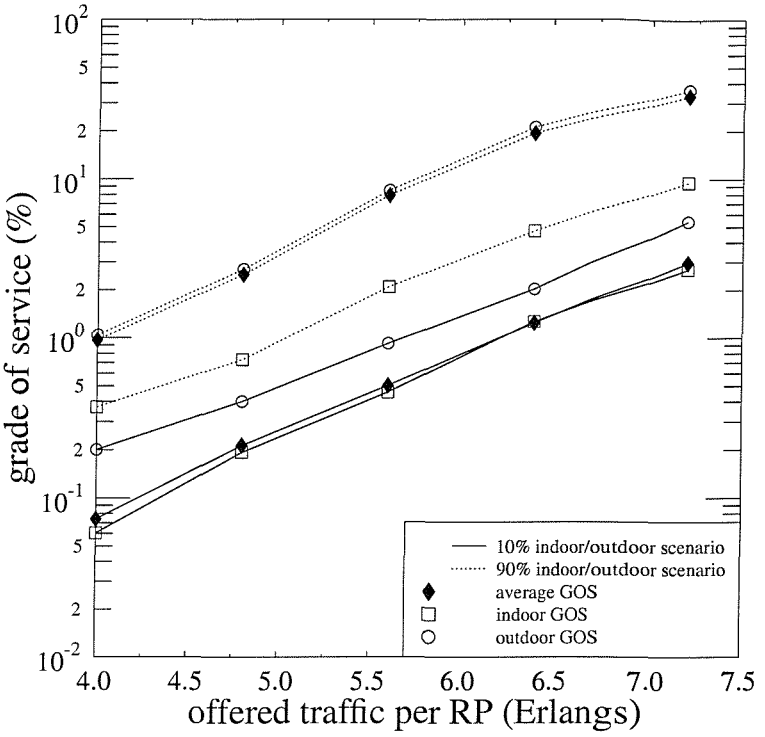


Figure 3.6: GOS performance of indoor calls and outdoor calls

variation of GOS with the offered traffic per RP. The GOS for the indoor scenario was between 0.1 % and 4 % for offered traffic of 4 to 7.2 Erlangs per RP. To achieve a GOS of 2 %, the network capacity for the indoor scenario was 6.6 Erlangs per RP or 5940 Erlangs per km$^2$. There were 900 RPs per km$^2$. The capacity of the outdoor scenario was 4.2 Erlangs per RP or 3780 Erlangs per km$^2$, which was about 64 % of the indoor scenario. The capacity of the 10 % indoor/outdoor scenario was 6.9 Erlangs per RP or 6210 Erlangs per km$^2$, which was marginally higher than the indoor scenario, while for the 90 % indoor/outdoor scenario the capacity was 4.6 Erlangs per RP or 4140 Erlangs per km$^2$, namely some 70 % of the capacity of the indoor scenario. For the 50 % indoor/outdoor scenario, the capacity was 5.9 Erlangs per RP or 5310 Erlangs per km$^2$, i.e., approximately 90 % of the indoor scenario. The network capacity of the mixed indoor/outdoor scenario when a small percentage of calls were made outdoors

was best. This was because the global interference was reduced as those connections made from outside the buildings benefited from a lower downlink interference, while the indoor connections experienced a lower uplink interference. Note that the best GOS was achieved, when 10 % of the calls were outdoor to outdoor calls.

Figure 3.6 shows that in the 10 % indoor/outdoor scenario the overall GOS was close to those of the indoor calls, as most calls were made indoors, whereas in the 90 % indoor/outdoor scenario the overall GOS was close to those of the outdoor calls, as most calls were made outdoors. In general, the GOS of calls being made outdoors was inferior to the GOS of indoor calls because the outdoor calls were more likely to be prematurely terminated than were the indoor ones due to the higher handover rate for outdoor users. However, for the mixed indoor/outdoor scenario when a small percentage of the calls were made outdoors, the average handover rate was low, and the overall GOS was improved due to the benefit of lower global interference. We also observe in Figure 3.6 that for the 10 % indoor/outdoor scenario the GOS of the outdoor calls was worse than the average GOS. In contrast, for the 90 % indoor/outdoor scenario the GOS of the indoor calls relative to the average GOS improved.

### 3.3.4 Conclusion

We conclude by noting that for our urban model the indoor DECT network provided seamless indoor/outdoor communication. However, as the network provided weaker signal strength outside the buildings due to the wall penetration losses, the network capacity for outdoor calls was significantly less than the indoor capacity. The network capacity for mixed indoor/outdoor was marginally better than for indoor calls alone. The reason why the performance was not degraded, was because the outdoor calls only constituted 10 % of total calls, and the benefit of reduced interference compensated for the weaker signal strengths. This study indicated that a DECT/GSM portable could be served mainly by DECT in urban areas for pedestrian users, enabling dual mode phone users to enjoy the high capacity benefits of DECT with a backup of GSM when necessary in other city areas. Thus a GSM operator could install mainly DECT RPs and network them to facilitate handovers, and couple these DECT RPs into the GSM network for calls and billing (tariffed probably below that for GSM). The operator would save on infrastructure costs as DECT RPs are less expensive than GSM ones. Subscribers who are visiting the area and do not have dual mode phones

would communicate via wider area GSM cell sites. This strategy would perhaps encourage users to abandon tethered phones, using their dual mode phone wherever they are.

## 3.4 DECT-like radio interface for wireless ATM

Asynchronous transfer mode (ATM) has been regarded as an important technology for the wide area interconnection of heterogeneous networks. In ATM networks, the data is divided into a small, fixed length units called cells. The cell is 53 bytes including a 5 byte header and the actual data of 48 bytes. The most distinct feature of ATM is its flexibility, reliability and management capability of the quality of service (QoS) requirement specified by each application. The initial development of ATM assumed that fixed (optical) networks with high bandwidth and low error rates would be used. The promising performance characteristics as well as the popularity of ATM have encouraged investigations of possible wireless implementations. In the discourse we design a wireless ATM radio protocol based on the DECT technology. The objective of the protocol is to provide high quality radio links for ATM cell transmission between a BS and a MS.

Our system is required to operate over the band 1880 - 1900 MHz, which is allocated for the DECT system. The DECT transmission rate of 1.152 Mb/s and carrier spacing of 1.728 MHz were chosen in order to take advantage of inexpensive DECT filters. We used a Gaussian Minimum Shift Keying (GMSK) modulation method with the normalised 3 dB bandwidth of the premodulation Gaussian low pass filter (LPF), $B_bT$, being 0.5. The performance degradation due to the ISI effect of the premodulation Gaussian LPF, is small. Therefore, in order to reduce the complexity of the receiver, a one bit differential detector was employed.

As a result of the high transmission rate, the effect of time delay spread which can be regarded as a frequency selective fading effect, causes signal distortions and extra unwanted ISI in the detected signal and imposes an upper limit on BER performance of the system. Traditionally the effect of ISI is reduced by equalisation. As we considered the system performance for indoor picocells and street microcells in which delay spreads are general much less than the symbol duration an equaliser will not be required. Instead we studied the use of channel coding and interleaving in order to improve the BER performance when its value was not due to multipath effect. We

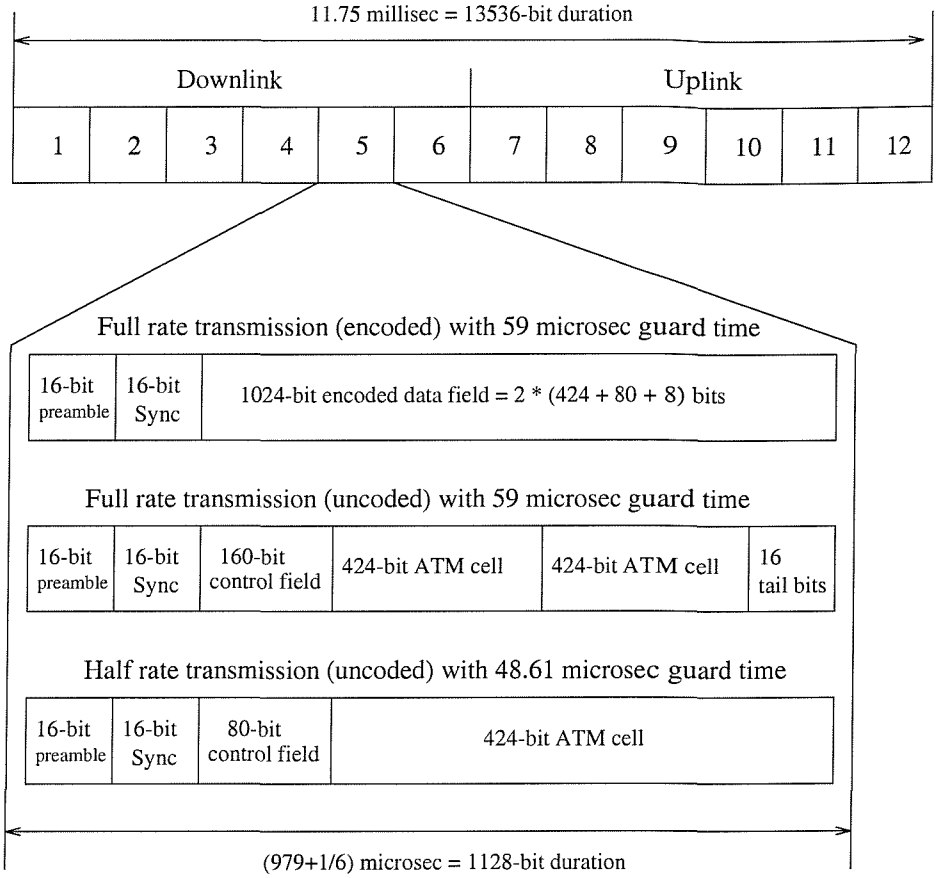


Figure 3.7: TDMA/TDD structure for a wireless ATM protocol

also considered halving transmission bit rate to 576 kb/s when the BER was due to the presence of significant multipath fading, a condition we considered to be relatively rare.

### 3.4.1 System overview

In this discourse, we studied a system which employs TDMA/TDD radio protocol. TDMA is an access technique in which signals from each transmission source are formed into packets and transmitted in bursts, typically once per time frame containing time slots. Other users send and receive in other slots using the same radio frequency carrier. Time division duplexing (TDD) is a technique which allows uplink transmissions, i.e. from a mobile to BS, and downlink transmissions, i.e. from the BS to MS, to occur in different slots on the same carrier.

Initially we design the radio protocol to support an ATM voice packet. An ATM

voice packet of 53 byte includes five byte header, 47 byte speech data and one byte for error control. The speech coding standard for ATM is 32 kb/s ADPCM, which is the same as the speech coder deployed by DECT. Figure 3.7 shows the TDMA/TDD frame structure. The TDMA/TDD frames of 11.75 *ms* duration are subdivided into 12 time slots, where slots number 0 to 5 and 6 to 11 are for the downlink and uplink transmission respectively. The frame length of 11.75 is obtained from dividing the number of speech data bit in a packet by the speech coding rate, i.e., (8*47)/32 = 11.75. Each TDMA slot lasts 979.17 $\mu s$. Three packet types are shown in Figure 3.7. The full rate packet with channel encoded data has three fields, which include a 16-bit preamble field, a 16-bit synchronizing field and a 1024-bit data field which is the encoded version of the concatenated of 80-bit control data and 424-bit ATM packet ( the extra eight bits of zero are added at the end of the precoded data). The full rate packet with uncoded data has six fields including a 16-bit preamble, a 16-bit synchronizing field, a 160-bit control field, two 424-bit ATM cells, and 16 tail bits. The packet for half bit rate transmission has four fields, namely, a 16-bit preamble field, a 16-bit synchronizing field, a 80-bit control field and 424-bit data field containing an ATM packet.

### 3.4.2 Interleaving and channel coding

For full rate transmission with channel coding, the control data and ATM packet are concatenated, channel coded and interleaved. The channel coding used is a half rate convolutional coding with a constraint length of seven. Eight tail bits of zero are added at the end of the precoded data to compensate the coding delay. A convolutional code is then generated by passing the whole data sequence through a linear finite-state shift register. The shift register consists of seven stages and two function generators, as shown in Figure 3.8 [52].

The convolutional code was designed for correcting errors which are statistically independent, as in the case of the additive white Gaussian noise (AWGN) channel. However, mobile radio channels exhibit bursty error characteristics. Signal fading due to time-variant multipath propagation often causes the signal to fall below the noise level, thereby resulting in a large number of bit errors, i.e., an 'error-burst'.

A block diagram of a system that employs symbol interleaving is shown in Figure 3.9 where the encoded data are reordered by the interleaver and transmitted over the channel. At the receiver, after demodulation (which may be either hard or soft

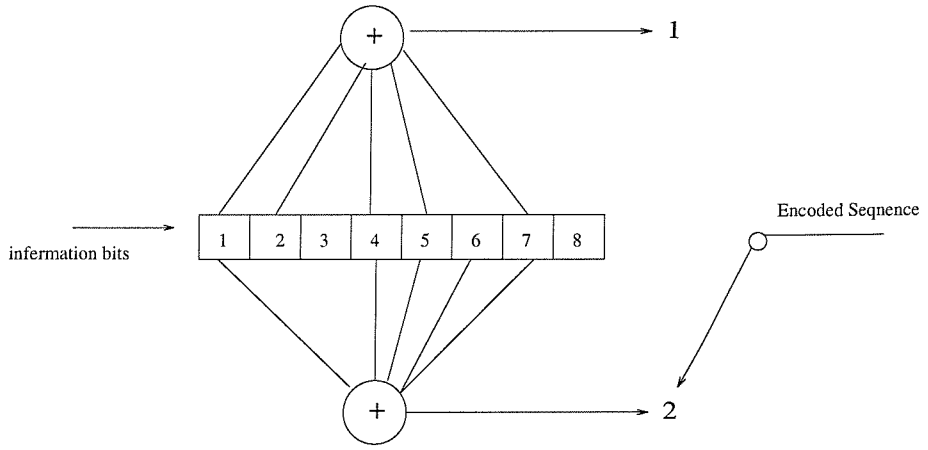


Figure 3.8: Optimal 1/2 rate convolutional encoder with a constraint length of seven

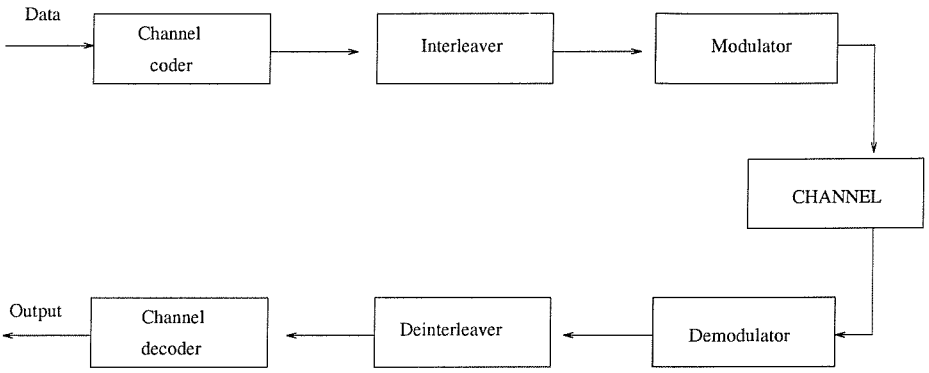


Figure 3.9: Block diagram of system employing interleaving for burst error

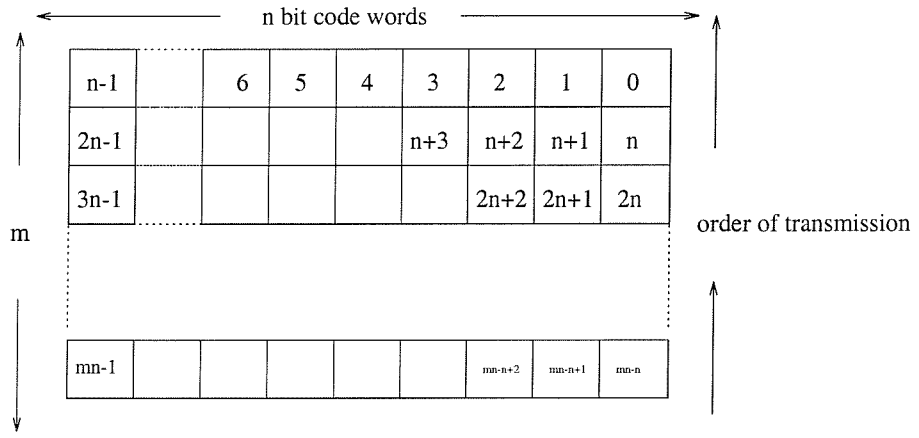


Figure 3.10: Block interleaving

decision), the deinterleaver renders the data in the proper sequence and passes it to the decoder. As a result of the interleaving/deinterleaving, error bursts are spread out in time at the receiver so that errors within a code word appear to be independent. The interleaving process is performed with in a single radio packet in order to minimise the latency of the wireless ATM interface. We employ a block interleaver illustrated in Figure 3.10 which formats the encoded data into a rectangular array of $m = 8$ rows and $n = 128$ columns. Usually, each row of the array constitutes a code word of length $n$, the array is read out column by column for transmission.

### 3.4.3 GMSK modulation

Gaussian Minimum Shift Keying (GMSK) modulation is a special case of a general class of continuous modulation, having a good bandwidth efficiency for a binary modulation scheme. In general, the transmitted GMSK radio signal can be expressed as

$$s(t) = \sqrt{\frac{2E}{T}} cos(2\pi f_c t + \phi(t,a) + \phi_0) \tag{3.5}$$

where $E$ is the energy of $S(t)$ within the symbol period $T$, and $f_c$ and $\phi_0$ are the frequency and initial phase of the carrier. The time varying phase carrying information is

$$\phi(t,a) = \sum_{i=-\infty}^{\infty} a_i \Phi(t - iT);\ -\infty \leq t \leq \infty \tag{3.6}$$

where $\alpha_i$ represents binary signaling , i.e., $\alpha_i = +1$ or $-1$. The phase function $\Phi(t)$ which determines the spectrum of the signal, is:

$$\Phi(t) = \begin{cases} 0 & t \leq 0 \\ G(t + \frac{T-LT}{2}) - G(t - \frac{T-LT}{2}) + \frac{\pi}{4} & 0 < t < LT \\ \frac{\pi}{2} & t \geq LT \end{cases} \tag{3.7}$$

$$G(x) = \frac{\pi\, x\, \mathrm{erf}(\alpha_n x)}{4T} + \frac{\exp(-\alpha_n^2 x^2)}{2\sqrt{\pi}\alpha_n T} \tag{3.8}$$

$$\alpha_n = \sqrt{\frac{2}{\ln 2}} B_b \pi = \sqrt{\frac{2}{\ln 2}} \frac{B_n \pi}{T} \tag{3.9}$$

where $L$ is the number of symbols over which an input symbol influences the modulated signal, since GMSK is a member of the family of continuous phase modulation (CPM) schemes. Furthermore, $B_b$ is the 3dB-down bandwidth of a low pass filter having Gaussian shape spectrum, and $B_n$ is the normalized bandwidth, $B_n = B_b T$.

The phase of the GMSK signal in the $n$th bit interval can be rearranged as

$$\begin{aligned}\phi(t,a) &= \sum_{i=n-L+1}^{n} a_i \Phi(t-iT) + \frac{\pi}{2}\sum_{i=-\infty}^{n-L} a_i \\ &= \theta(t,a) + \theta_n \end{aligned} \tag{3.10}$$

where $\theta(t,a)$ is the correlative state vector that depends on the $L$ most recent bits and $\theta_n$ is the phase state. In our study the symbol response length $L$ for $B_n = 0.5$ is set to two.

### 3.4.4 Channel model

Channels models which have accurate fading statistics are essential for the bit-by-bit error simulation. A discrete impulse response of the channel is,

$$h(kT_s) = \sum_{i=1}^{L_c} \alpha_i e^{j\theta_i} \delta(k\tau_s - \tau_i) \tag{3.11}$$

where $\tau_s$ is the fractional bit sampling period, $\alpha_i$ are independent and Rayleigh distributed, $\theta_i$ are independent and uniformly distributed over $(0, 2\pi)$, $\tau_i$ is the time delay of each Rayleigh fading component, and $L_c$ is the last component in the response. In general, the path weightings $\alpha_i$ are known to be Rician [53, 54], but we examine the worst case scenario where $\alpha_i$ are subjected to Rayleigh fading.

To model the discrete baseband impulse response $h(kT_s)$ of the wideband channel, we create $L_c$ narrowband baseband Rayleigh fading channel characterized by the Doppler fading spectrum

$$S(f) = \begin{cases} \frac{1}{\pi\sqrt{f_m^2 - f^2}} & \left\| \frac{f}{f_m} \right\| < 1 \\ 0 & \text{otherwise} \end{cases} \tag{3.12}$$

where $f_m = v/\lambda$ is the Doppler frequency in Hz, $v$ the mobile velocity and $\lambda$ the carrier wavelength. The spectrum corresponds to a vertical monopole antenna having a uniform distribution of the incident power. We employed a mobile velocity of 1.33 m/s (or 3 mph) for pedestrian mobiles and a propagation frequency of 1.9 GHz. This results in $f_m \approx 8$Hz.

The delay $\tau_i$ and the average power $E_i$ are chosen by extracting the impulse response of measurement results obtained from reference [55]. Figure 3.11 displays the channel impulse responses of rooms 4017 , in the Electronics and computer science building

at Southampton university . As the smaller impulses are less significant [32], we introduce a threshold of 20 $dB$ and discard all components whose power is below this threshold. Each impulse response component provides the average power of each delay component in the model, and the rms delay spread of the channel is 27 $ns$. The power sum of $E\{\alpha_i^2\}$ is set to unity in the simulation, so that the channel has unity average gain. The sampling rate of the impulse response measurement is 20 $ns$. The rms delay spread of the channel is defined as [2]

$$\sigma_\tau = \sqrt{\overline{\tau^2} - \overline{\tau}^2}, \tag{3.13}$$

where

$$\overline{\tau} = \frac{\sum_i P(\tau_i)\tau_i}{\sum_i P(\tau_i)}, \tag{3.14}$$

and

$$\overline{\tau^2} = \frac{\sum_i P(\tau_i)\tau_i^2}{\sum_i P(\tau_i)}. \tag{3.15}$$

Based on measurements reported in Figure 1.23 of reference [32] the rms delay spread for outdoor microcells was estimated to be about 115 $ns$. In order to investigate the protocol performance in outdoor microcell environments, we created a range of outdoor channel impulse response models by multiplying the associated delay of each impulse response tap in Figure 3.11 by a factor of two, three and four and obtained channel models exhibiting rms delay spreads of 54 $ns$, 81 $ns$ and 108 $ns$, respectively.

Coherence bandwidth of the radio channel is a measure of the transmission bandwidth at which distortion becomes appreciable. The coherence bandwidth can be derived from the rms delay spread as [32]:

$$B_c = \frac{1}{2\pi\sigma_\tau}. \tag{3.16}$$

Corresponding to the rms delay spreads of 27 $ns$ and 115 $ns$, the associated coherence bandwidths are 5.9 MHz, and 1.38 MHz, for an indoor picocell and a street microcell, respectively.

### 3.4.5 Results and discussion

All parameters used in our simulations are itemised in Table 3.1. Figure 3.12 shows the BER performances when hard decision decoding and soft decision decoding for the GMSK radio interface with channel coding were used. The hard decision and soft decision decoding systems had gains of 4 dB and 6 dB relative to the uncoded

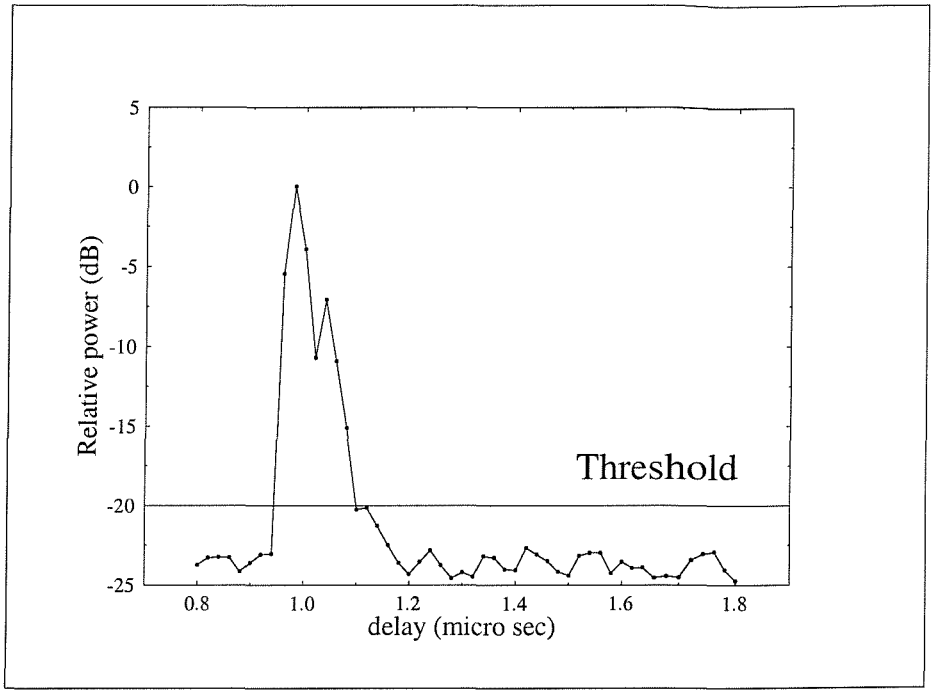


Figure 3.11: Discretised channel impulse response of room 4017 in building 53 at University of Southampton

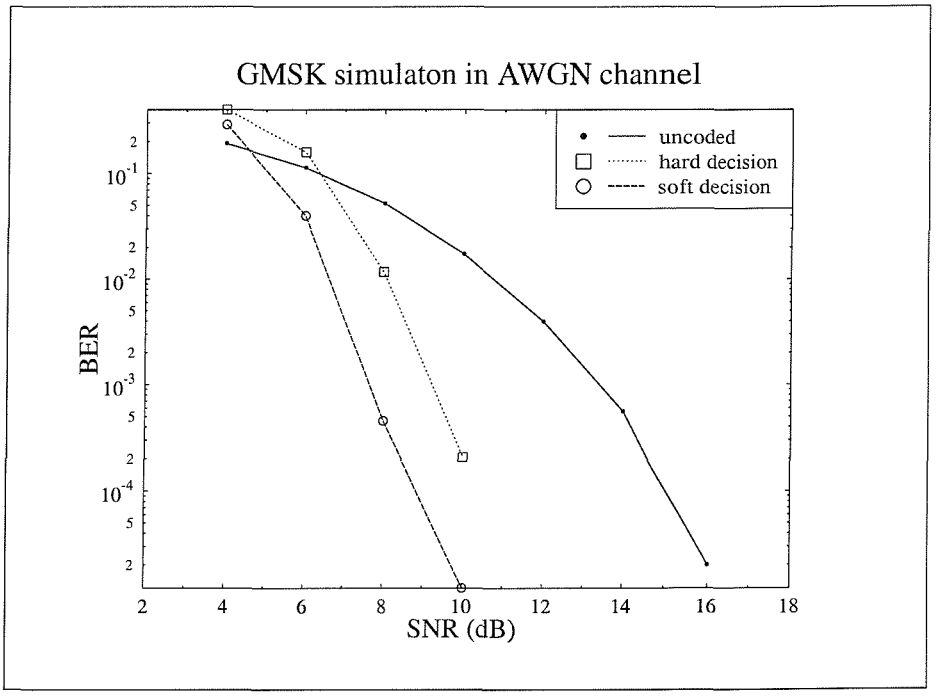


Figure 3.12: BER performance in an AWGN channel

| Symbol | Description | Value |
|---|---|---|
| $f_c$ | Carrier frequency | 1.9 GHz |
| $v$ | Mobile's velocity | 1.33 m/s |
| $T$ | Symbol period | 868 $ns$ |
| $B_n$ | Normalised bandwidth | 0.5 |
| $f_m$ | Doppler frequency | 8 Hz |
| $L$ | Length of symbol response | 2 |
| $P(\tau_1)$ | Average power of the 1st Rayleigh component relative to the peak component | -5.5 dB |
| $P(\tau_2)$ | Average power of the 2nd Rayleigh component | 0 dB |
| $P(\tau_3)$ | Average power of the 3rd Rayleigh component | -3.9 dB |
| $P(\tau_4)$ | Average power of the 4th Rayleigh component | -10.7 dB |
| $P(\tau_5)$ | Average power of the 5th Rayleigh component | -7.1 dB |
| $P(\tau_6)$ | Average power of the 6th Rayleigh component | -10.9 dB |
| $P(\tau_7)$ | Average power of the 7th Rayleigh component | -16.7 dB |
| $\tau_s$ | Fractinal bit sampling period | 20 $ns$ for $\sigma_\tau = 27$ $ns$<br>40 $ns$ for $\sigma_\tau = 54$ $ns$<br>60 $ns$ for $\sigma_\tau = 81$ $ns$<br>80 $ns$ for $\sigma_\tau = 108$ $ns$ |

Table 3.1: The value of parameters used in GMSK simulations

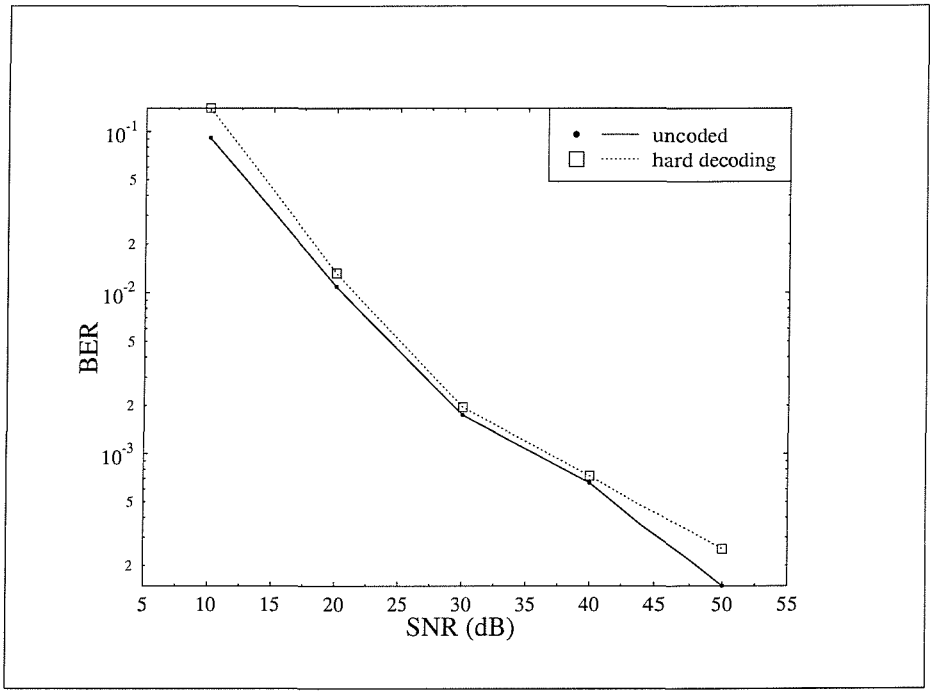


Figure 3.13: BER performance in a flat fading channel

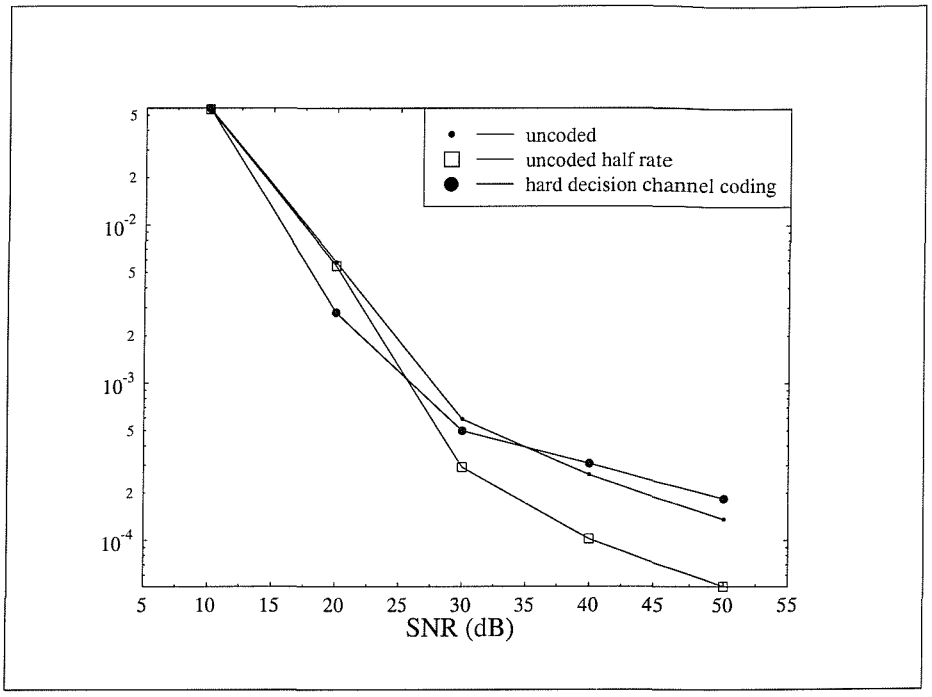


Figure 3.14: BER performance with in MB4017 channel, $\sigma_\tau = 27ns$

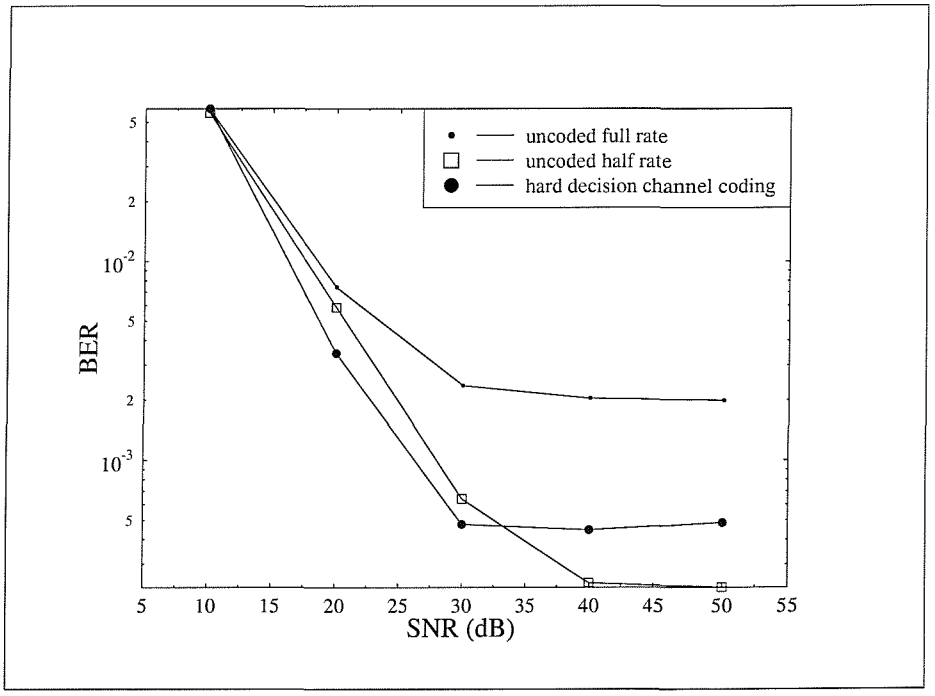


Figure 3.15: BER performance with rms delay spread of 54 $ns$

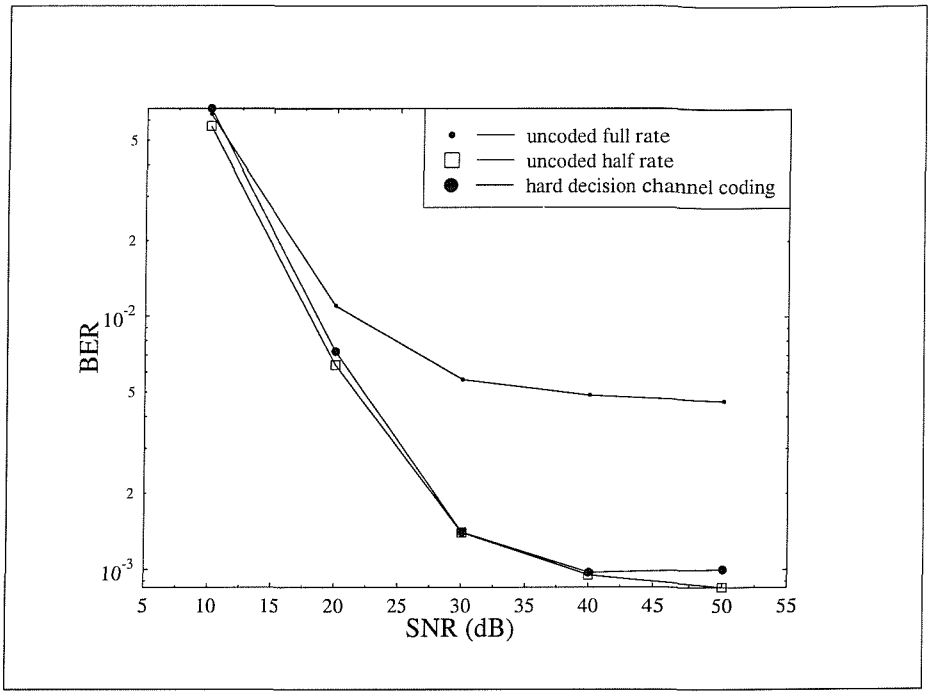


Figure 3.16: BER performance with rms delay spread of 81 *ns*

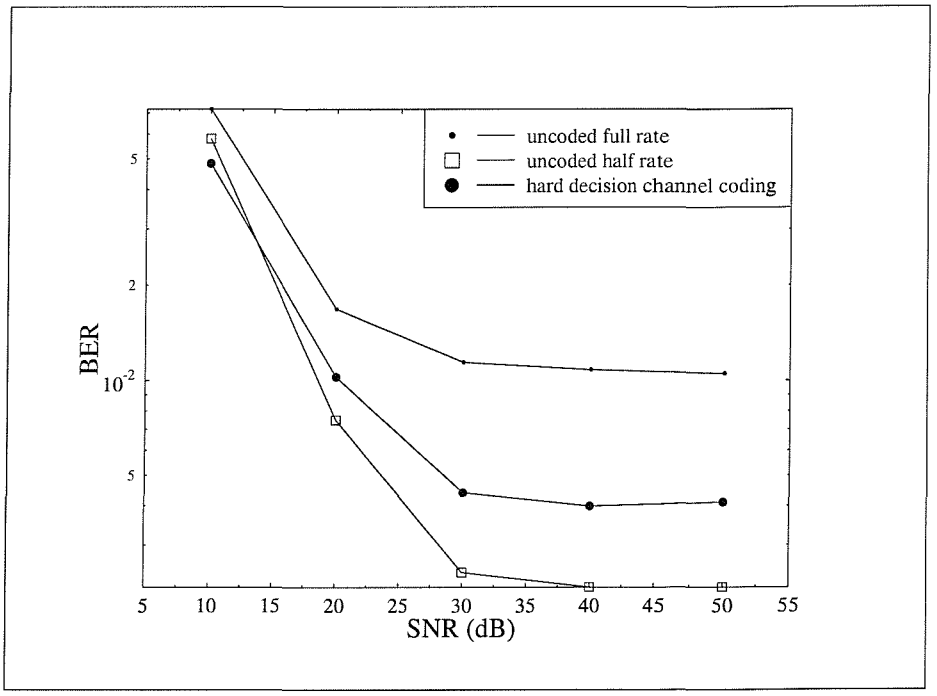


Figure 3.17: BER performance with rms delay spread of 108 *ns*

system. Figure 3.13 shows the BER performance of the hard decision coding in a flat fading Rayleigh channel. We had no gain for the channel coding, because the signal components of a given code word were not statistical independent. Although the interleaver was used, the separation distance of the interleaver was much less than the coherence time of the channel, $\approx 22\ ms$. Therefore, the signal components of each code bit did not fade independently. We use the definition of the coherence time by Steele [32] which is approximately as

$$T_c \approx \frac{9}{16\pi f_m} \tag{3.17}$$

where $f_m$ is the maximum Doppler shift frequency.

Figures 3.14 - 3.17 show the BER performance in wideband channels with different delay spreads. When the rms delay spread was 27 $ns$, all system can achieve BER $10^{-3}$. Both the halving transmission rate and channel coding have 2 dB gain at BER $10^{-3}$. However only the halving transmission rate improved the irreducible BER. When the rms delay spread of the channel is 54 $ns$, only the channel coding and the halving transmission rate can reach BER $10^{-3}$. Though the channel coding gained 2 dB more than the halving bit rate at BER $10^{-3}$, the halving transmission rate had lower irreducible BER. For the channel with 81 $ns$ rms delay spread, the halving transmission rate and the channel coding had almost the same performance and can achieve BER $10^{-3}$. When the rms delay spread was 108 $ns$, all systems fail to achieve BER $10^{-3}$, however the halving transmission rate outperformed the channel coding.

### 3.4.6 Conclusion

We conclude that for the excess delay spread considered, halving transmission rate is a better solution for improving BER performances of an ATM packet transmission, compared to introducing 1/2-rate convolutional coding and interleaving. The channel coding performance can be improved by using a considerably longer interleaver, i.e., longer than the coherence time of the channel, however, that results in undesirably long delays.

# Chapter 4

# Automatic Channel Allocation

## 4.1 Introduction

Third-generation (3G) mobile radio systems aim to support a wide range of services from voice and low-rate data up to high rate data services, including multimedia services. Both circuit-switched and packet-oriented transmissions will be implemented. 3G systems are expected to provide a much higher capacity than current systems and have some backward compatibility with the existing second-generation (2G) digital mobile radio systems, such as GSM.

As demand for mobile services increases, small cell systems including street microcellular and inbuilding picocellular networks, are likely to be deployed extensively in order to provide the necessary capacity. The high density of cells with their BSs will cause difficulties in frequency planning. The radio propagation environments in microcells and picocells are different from that of the conventional macrocellular system. The propagation environment is difficult to predict due to numerous types of clutter in and around buildings, making unified propagation models difficult to formulated. Furthermore, the radio interference from multistorey buildings adds a third dimension to the frequency reuse geometry. A conventional approach based on fixed channel allocation (FCA) with manual frequency planning may be costly and time consuming if a large number of small cells are to be deployed. In addition, the incremental growth in the number of cells required a reassessment of the whole frequency plan as each new BS is introduced. The above considerations emphasise the desirability of deploying channel allocation schemes that do not required field measurements and frequency planning.

3G systems need to provide a variety of data services in addition to mobile telephony, such as, wireless Internet, video communications, electronics fund transfer, mobile offices, etc. As these applications are characterised by bursty traffic, packet-switched access will give a more efficient utilisation of the transmission medium than circuit-switched connections. In packet-switched transmissions, capacity is allocated on demand thereby avoiding the waste of spectral resources during source inactivity. As a consequence, a higher number of connections can be supported by a statistical multiplexing gain. Among the various packet multiple access schemes proposed for mobile radio operations [56], we will concentrate in this Chapter on packet reservation multiple access (PRMA) [57, 58, 59, 60]

PRMA is a protocol for packet radio access which usually combines random access with time division access and employs voice activity detection to improve the multiplexing efficiency of speech traffic. Similar to TDMA, the transmission schedule is formed by frames, each containing a fixed number of time slots. No resource need be dedicated for channel access, when all the slots in a frame are information slots. Mobile terminals classify each slot as either "reserved", or "available". To access the channel, the mobile terminals contend for an available time slot by directly transmitting a data packet in the time slot at the beginning of each activity; if the access is successful the time slot is reserved for that talk-spurt (or data spurt) and released at its end. When the access is unsuccessful due to contention, then in order to minimise subsequent collision of the retransmission of contending packets, the access is reattemped according to a permission probability that depends on the state of a local pseudo random generator.

We are concerned in this Chapter with identifying channel allocation schemes that do not required frequency planning and are also suitable for PRMA operations. In the next section we give a brief overview and classification of some already existing channel allocation algorithms. Then we propose a new channel allocation scheme which can support PRMA applications, and compare it with existing channel allocation schemes that can be used by PRMA mobile radio systems. The remaining part of the Chapter deals with the performance investigation of different channel allocation algorithms for both circuit-switched and packet-oriented mobile radio operations in different radio environments.

## 4.2 Classification and overview of channel allocation schemes

Generally microcellular BSs are located extensively where there are high teletraffic demands. In fixed channel allocation schemes that require frequency planning, a number of BSs located close to each other are grouped into a cluster. The available radio spectrum is divided into sets of frequencies, and is reused in each cluster. Each frequency set having one or more carriers, with each carrier usually having more than one channel, is allocated to each BS in a cluster. The number of frequency sets is equivalent to the number BSs in the cluster. The number of BSs in a cluster relates to the distance between two BSs which have assigned the same frequency set, referred as "reuse distance", and is selected so that the co-channel interference is within acceptable limits. Other channel allocation schemes based on fixed channel allocation (FCA), such as channel borrowing [7, 8, 9] and hybrid channel allocation schemes [10, 11] have been suggested in order to provide a better grade-of-service (GOS) and a higher system capacity compared to conventional FCA. However, these algorithms still require frequency planning.

There are two alternative approaches for assigning channel sets without FCA. The first approach is an autonomous frequency planning (AFP) [12, 13] where the frequency reuse structure is self-organised by the network. The AFP is similar to the conventional FCA, in which the frequencies, and thereby channels, are preassigned to each BS and the reuse structure is quasi-static. Although AFP avoids the need of frequency planning, it is inadequate to cope with the unpredictable traffic bursts, which in microcells, introduce a higher variability in traffic demand than in larger cells. The other approach is to completely remove the requirement for a stable and structured frequency reuse pattern in a service area. Now all radio channels (combinations of time slots and carrier frequencies) may be available everywhere for every call. This approach is called dynamic channel assignment (DCA), where a channel is allocated to a cell on a call-by-call basis to achieve time-varying frequency reuse patterns.

### 4.2.1 Autonomous frequency planning

To provide an autonomous frequency planning (AFP), the system must automatically gather information necessary for allocating channels to each BS, and then make

the necessary channel allocations. Each BS is equipped with a channel allocation controller that autonomously gathers information on interference level of each carrier and allocates its channels. The advantage of this method is its implementation simplicity, as no central coordination among neighbouring BSs is required [12]. Cheng and Chuang [13] evaluated and compared several distributed measurement-based algorithms for the autonomous AFP, and suggested that a least interference algorithm (LIA), where the channel with the least received instantaneous interference power is selected, is the best algorithm. However, the algorithms used in those studies were based on the assumption of one carrier per BS. For a multi-carrier assignment, the co-site constraint exists as the frequency separation between assigned frequencies must be sufficient for the adjacent frequency interference to be acceptably low.

Moreover the studies in references [12, 13] assumed a macrocell-like propagation model where the propagation path loss was obtained from the distance of the direct path between a transmitter and its receiver. A BS measures interference level of each channel which relates directly to the distance from the co-channel BSs and shadow fading. Therefore the channel with the least interference is likely to be the channel with the longest distance from the co-channel BSs, and the co-channel interference level is minimised by using this channel. However, in street microcells the measured interference level of the channel being used by an adjacent BS can be very low, as some adjacent BSs may not have a direct path between them, and the interference level does not reflect the co-channel reuse distance. This phenomenon is called non-line-of-sight (NLOS) error. If a BS reuses a channel being used by its adjacent BSs, the level of co-channel interference may be unacceptably high, as their coverage boundaries are overlapped. Therefore, the measurement-based algorithm alone may not perform AFP efficiently in the microcellular and picocellular environments where a direct path between BSs is not guaranteed.

### 4.2.2 Dynamic channel allocation

Dynamic channel allocation (DCA) algorithms have been recognised as a mean of efficient utilisation of the limited spectrum compared to FCA. Many publications show that DCA can outperform FCA in terms of throughput capacities under the condition of nonuniform heavy traffic [14, 15, 16].

Conventional FCA divides the available radio channels into $C_s$ groups, where $C_s$ is a reuse cluster size, and assigns each group to each BS in a reuse cluster. This implies

some trunking inefficiencies in the use of the spectrum, as the maximum number of channel per cell is $N_C = (N_T \cdot N_{ts})/C_s$, where $N_T$ is the total number of available carriers and $N_{ts}$ is the number of traffic time-slot per carrier. However, with DCA, all channels are available in every cell, provided that the system-specific interference constraints are satisfied, and the maximum carried traffic per cell is $N_C = N_T \cdot N_{ts}$. In order to gain from a DCA scheme, the number of transceivers $N_{trx}$ at a BS must be greater than $N_T/C_s$, i.e., the number of transceivers required for an FCA scheme.

Most of the proposed DCA algorithms are based on an *a priori* knowledge of the mutual interference between different cells. This knowledge is usually formally described through a compatibility matrix [14, 61, 17] whose generic element $M_{i,j}$ may be zero or one, depending on whether cell $i$ and cell $j$ may use the same channel. These algorithms still need frequency planning as they are required to define the compatibility matrix. Furthermore, these algorithms require an intensive exchange of information among the BSs; the decision process which may be centralised or permitted at each BS, is based on the current status of the available channel in the potentially interfering cells. This amount of information signalling exponentially increases as the cell size decreases due to the large number of cells involved: this poses additional constraints on the DCA in that it should preferably involve information and decision processes that are all available at the BS level and only relate to the relevant cell.

A distributed DCA referred to as the local packing DCA (LPDCA) [62] is also a search based DCA method, but the searching process is distributed to each BS, which maintains a so-called augmented channel occupancy (ACO) table containing the current channel utilisation information of neighbouring BSs which may cause significant interference. Information exchange is local and within those BSs that can significantly interfere with each other.

Abdul-Haleem et al. [18] proposed a class of DCA called, "Fuzzy distributed DCA" (FDDCA). This is an extension of the LPDCA and considers a co-site carrier separation constraint and a knowledge of the instantaneous traffic condition by employing fuzzy logic as a decision maker. Upon receiving a call, the LPDCA algorithm assigns the channel that complies with the co-site constraint and co-channel constraint. However, the LPDCA and FDDCA algorithms are not fully automatic, since the algorithms cannot automatically determine the neighbouring cell constraints, which are location-specific and vary, depending upon the propagation environment. In addition,

the coordination of neighbouring BSs is required in order to enable the exchange of their channel usage status.

To avoid the coordination among neighboring BSs as required by previous mentioned DCA algorithms (which are often impractical to implement when there are a significant number of BSs) autonomous dynamic channel assignment algorithms, where each BS measure interference from other BSs and autonomously selects the carrier with the lowest interference, have been suggested in [19, 20, 21].

Akaiwa et al. [19] proposed a self-organized dynamic channel allocation scheme called "Channel segregation", where each BS maintains its channel ordering list which it obtains through learning from the history of frequency usage between it and the other BSs. Upon call arrival, the BS selects the highest order channel which is not being used by itself, nor in other interfering cells. The BS checks the channel availability by sensing the interference level of the channel. If the channel is available, the order of the channel is increased, otherwise, the order is decreased and the BS senses the availability of the next channel. However the carrier sensing algorithm does not consider intra-cell adjacent carrier interference (ACI) which can be significant if the carrier separation is too small.

Autonomous reuse partitioning (ARP) [20], proposed by Kanai is similar to the channel segregation algorithm except that all BSs are given the same channel order list in advance and this list is fixed. When a call arrives at a BS, channels are viewed in order and the first idle channel which satisfied the CIR threshold in both uplink and downlink is allocated. If there is no channel with sufficient CIR level, the call is blocked. Since channels are viewed in the same order, channels with higher order are used more frequently, and have larger interference levels. As a result, channels with high interference levels are mainly allocated to mobile stations (MSs) with strong received power, (i.e., those near their BSs). On the other hand, channels with low order, having small interference levels, are allocated to mobile stations with weak received power, (i.e., those far from their BSs). This allows formation of an efficient reuse pattern. Though original work suggested that the channel can be obtained by CIR measurement, which is very difficult in practice, later work used the measured interference power level to determine the channel availability, i.e., if the measured power is below or above a given threshold value, the channel is determined to be idle and busy, respectively. The call set-up time of the ARP may be slow when the number of channels is large due to a long channel search time. The carrier sensing

algorithm in ARP also does not consider the intra-cell ACI.

Chuang et al. [21] proposed a simple distributed measurement based DCA where the channel selections are based on the interference measurements made by each mobile and BS. Cheng and Chuang [22] also evaluated and compared several distributed measurement-based algorithms for DCA, and confirmed that a least interference algorithm (LIA) where the channel with the least received instantaneous interference power is selected, performs best. However, the LIA was not designed for systems with multi-transceiver BSs. As BS transceivers simultaneously transmit on different assigned carriers, the frequency separation between the carriers must be far enough to avoid ACI.

## 4.3 Autonomous adaptive frequency assignment

We propose a new channel allocation scheme called Autonomous Adaptive Frequency Assignment (AAFA), where not only the information from interference measurements is considered, but also the teletraffic information, such as the traffic loads and handover statistics are utilised. Although our proposed algorithm is designed for a GSM-like system structure, it can be applied in other systems with different multiple access technologies, such as FDMA and wideband CDMA. In our AAFA the licensed spectrum allocation is divided into $N$ TDMA equal-width frequency pairs (frequency division duplex). In small cell systems, such as street microcells and inbuilding picocells, several fixed stations may be interconnected and controlled by single base station controller (BSC).

Our algorithm is derived from the measurement-based LIA [12, 13], the local packing DCA (LPDCA) [23] and the fuzzy distributed DCA (FDDCA) [18]. The LIA algorithm calls for each BS to measure interference from other BSs and autonomously select the frequency with the lowest interference level. However, the co-site constraint for multi-carrier assignment is not taken into account in the algorithm. The other weakness of the LIA algorithm is that the measurement of interference level on downlink channels may not correctly address the co-channel constraint when an NLOS path exists between a desired BS and an interfering BS, as the interfering BS may cause excessive interference to a mobile connected to the desired BS, although the measuring interference level is low. Therefore, extra knowledge of the channel usage of BSs that are in the interfering range is required for frequency assignment. The LPDCA

and FDDCA algorithms assign channels by performing a channel search according to pre-determined co-site and co-channel constraint in a DCA fashion. However, the algorithms are not fully autonomous as the co-site and co-channel constraint must be pre-determined by the network planners.

The AAFA can be applied for both centralised and distributed network architectures. Current cellular systems based on macrocells employ a centralised system architecture, where a central controller assigns channels to multiple cells under their supervision. By contrast, current mobile cordless systems employs distributed architecture where each mobile station selects a channel for itself. Centralised architecture can provide better channel management than a distributed one because all the information from every cell is available for channel assignment. However, it demands greater signalling capacity and complexity due to the coordination requirement between cells. Generally the distributed architecture is preferred in small cell networks, because it is easier to manage and expand than the centralised one due to its simpler signalling protocol. Nevertheless, the centralised architecture is more cost effective than the distributed one where many cells are required in small areas in order to provide high traffic capacity, such as in an office building. The centralised architecture can be implemented by a radio-fibre microcellular network [63, 64] where a base transceiver station (BTS) consists of one central station, called the hub, and several radio ports (RPs) that radiate the RF signal. This arrangement reduces the cost and complexity of the network by concentrating the modem and control equipments of several cells at the hub. A BS at each cell is therefore a radio port, where incoming signals from the hub are simply amplified and radiated through the antenna. Figures 4.1 and 4.2 [65] show the distributed and the centralised microcellular architecture, respectively.

### 4.3.1 The algorithm

The AAFA algorithm offers fully automatic channel assignments and selects frequencies using the knowledge of interference levels and neighboring channel usage. Each BS selects $M$ frequencies out of the total available $N$ frequencies. The selected frequencies are then listed according to its usability index obtained from the frequency selection process.

Figure 4.3 shows the fiowchart for the procedure performed by each BS in reconfiguring its allocated frequency list. In each frequency assignment, a BS repeats the

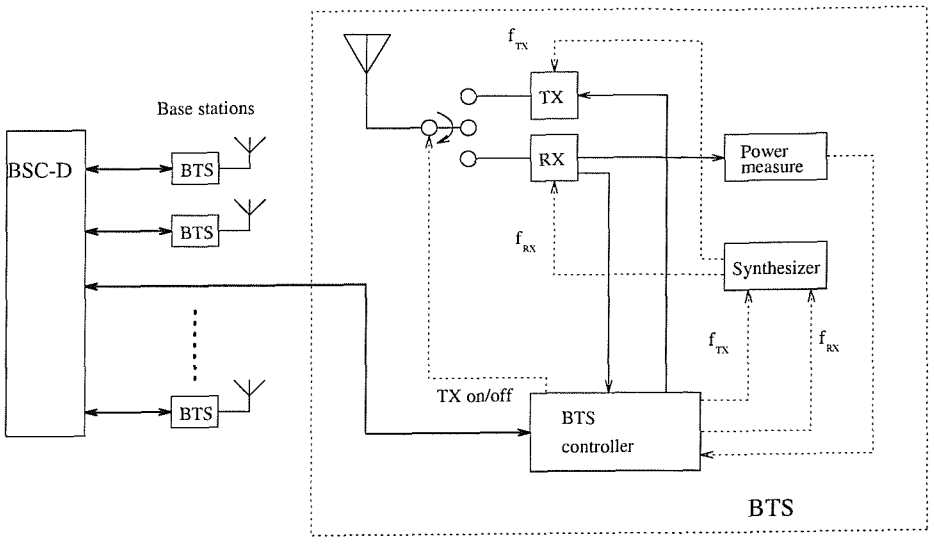


Figure 4.1: Distributed microcellular architecture

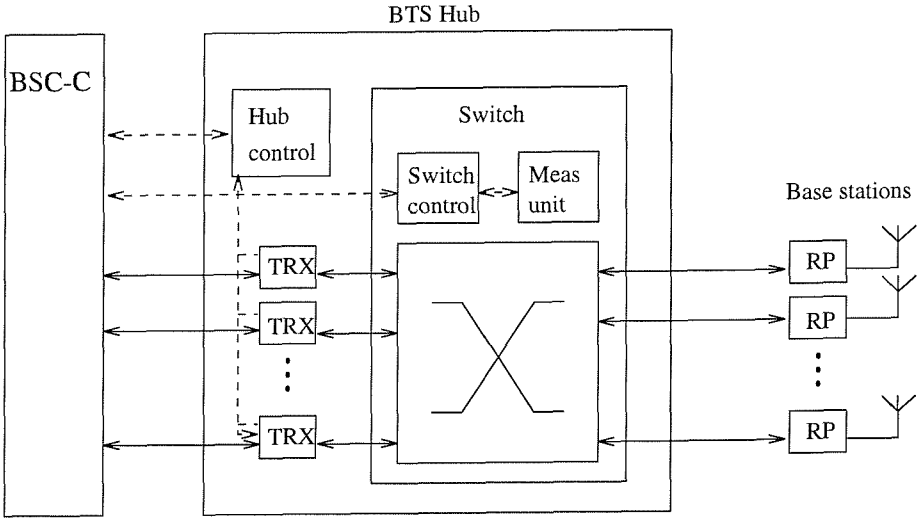


Figure 4.2: Centralised microcellular architecture

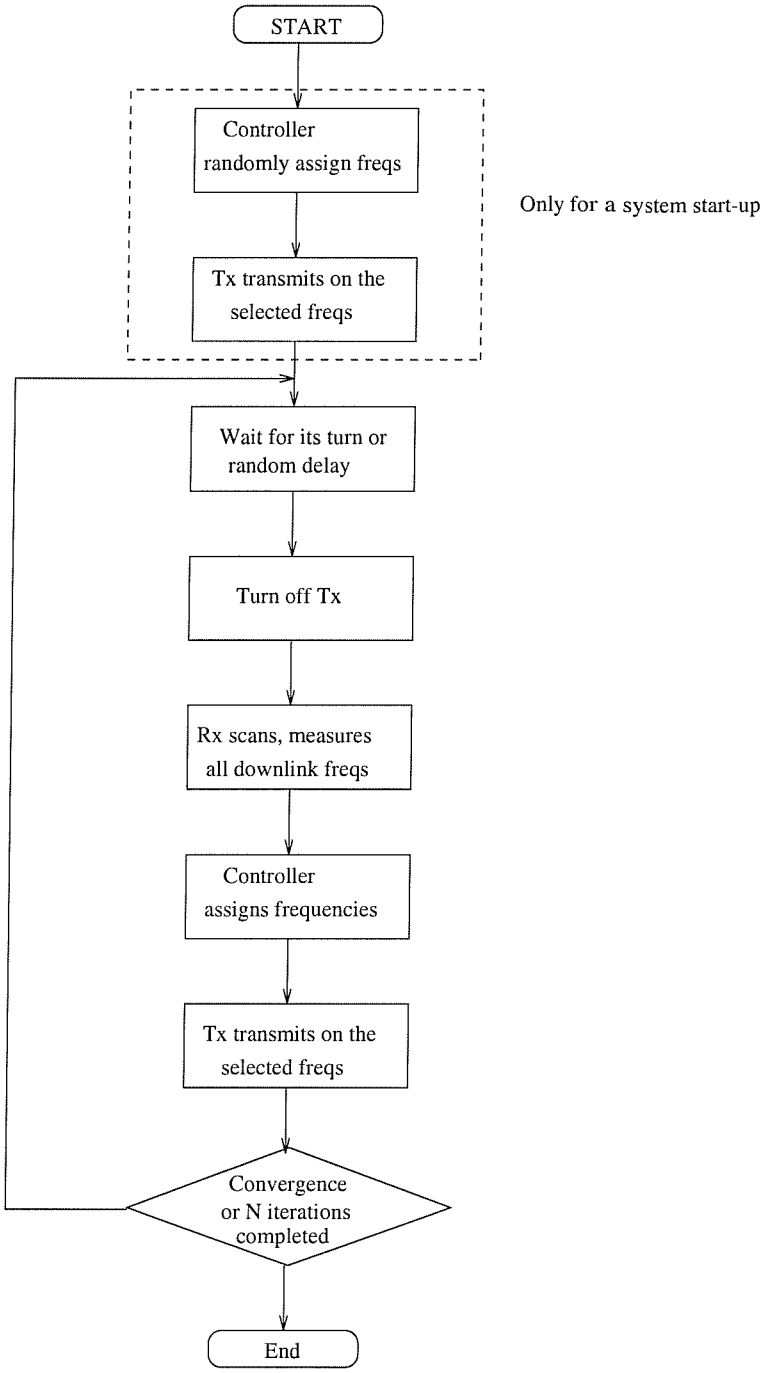


Figure 4.3: Flow chart of the frequency assignment procedures by a BS

frequency update procedure until a determined number of iterations is reached, or the selected frequency list converges, i.e., no change in the frequency list for two consecutive cycles. In the frequency update algorithm a BS must turn off its transmitter, and scan all downlink frequencies for interference measurements. In order to ensure that the interference from all other cells is measured, the probability that two BSs performing measurements at the same time must be minimised. This can be done by coordinating all BSs in the system so that they can update their frequency in turn, i.e., one BS turns off its transmitter and performs the interference measurements, while all other BSs transmit their on their allocated carriers. The coordination can be achieved by a simple "token passing" procedure in which a token can be passed from one BS to another. When a BS receives the token, it can update its frequency; otherwise , it must wait. Chuang [12] has shown that this procedure can be performed autonomously without coordination between BSs by using a random delay between each update. After scanning all downlink frequencies, the measurement data is fed to the channel assignment controller. The controller then selects $M$ frequencies, and the BS transmitter broadcasts on the selected frequencies.

Before the system start-up, all BSs are silent. The controller produces the artificial measurement data where the normalised interference level of each frequency is random, i.e., we use the value between 0 dB and -20 dB. The other information required by the controller is the knowledge of frequency usage by neighboring cells which may cause co-channel interference. The neighboring relationship of each cell is not known prior to the system start-up. The neighboring relationship can only obtained by the base station controller (BSC) after the system has been operated as the neighbouring relationship is evaluated from the statistics of call handover between cells. Once the neighboring relationship is known, the BSC is then able to supply the controller with the knowledge of the frequencies being used by the neighbouring cells.

The controller operates the channel assignment procedure in two stages. In the first stage, the controller approximates the usability entropy, $U$, of each frequency, i.e., $U_i$ represents the usability of $i$th frequency, by processing information of each frequency which includes the measured interference levels and its usage in neighbouring cells. If a BS only requires one frequency, the controller can simply assigned the frequency with the maximum usability entropy to the BS. If the BS requires $M$ frequencies, then to assign the $M$ frequencies with the highest usability entropy may cause adjacent channel interference if the assigned frequencies are not separated sufficiently.

Therefore the second step is needed to select $M$ frequencies with maximum usability and minimum adjacent channel interference. The number of frequencies required by a BS, M, is generally the number of transceivers installed at the BS, $N_{TRX}$, which is determined from a traffic demand in the cell coverage of the BS. In systems with frequency hopping, $M$ can be greater than $N_{TRX}$, as a number of frequencies are required for frequency hopping to ensure sufficient gain from interference diversity. The output of the first stage is then passed to the second stage, where the controller selects $M$ frequencies out of the $N$ available frequencies.

The channel assignment controller consists of two parts, namely the constraint processing unit and the channel assigning unit. We first specify the input and output variables of the constraint processing unit. The available frequencies are $F_N = (1, 2, ..., N)$. The input variables are the measured interference levels represented by a column matrix of size $N$, $I = \{I_i | i \in F_N\}$ and the neighbouring frequency usage, $J = \{J_i | i \in F_N\}$. The values of $I_i$ is the interference level of the $i$th frequency measured at the channel assignment controller, and is represented by a normalised interference level in dB, which is the ratio of the measured interference level, $S_i$, to the maximum interference level from all available frequencies, $S_{max}$, and is given by $I_i = S_{max} - S_i$, hence, $I_i \geq 0$ (dB). The value $J_i$ is one if the $i$th frequency is being used by at least one of the neighbouring cells, otherwise $J_i$ is zero.

The input data $J$ is then processed, and we obtained a set co-channel factors $C$, which is given by

$$\begin{aligned} C &= \{C_i | i \in F_N\}, \\ C_i &= \min_{\substack{j \in F_N \\ J_j > 0}} (N, g(i,j)) \end{aligned} \tag{4.1}$$

where $C_i$ is the co-channel factor of the $i$th frequency and $g(i,j)$ is the frequency separation distance given by $g(i,j) = |i - j|$. The output of the primary unit is the frequency usability given by

$$\begin{aligned} U &= \{U_i | i \in F_N\}, \ 0 \leq U_i \leq 1, \\ U_i &= \begin{cases} 0 & \text{if} \quad C_i < K_a \vee I_i \leq 0 \\ I_i / I_{th} & \text{if} \quad 0 < I_i < I_{th} \wedge C_i \geq K_a \\ 1 & \text{otherwise} \end{cases} \end{aligned} \tag{4.2}$$

where $K_a$ is the co-channel constraint, i.e., the adjacent cells must use frequencies which are separated by at least $K_a$ so that they do not interfere with each other. In addition, $I_{th}$ is the interval of the power measurement window, and is given by

$$I_{th} = \max((S_{max} - S_{min}), 20), \tag{4.3}$$

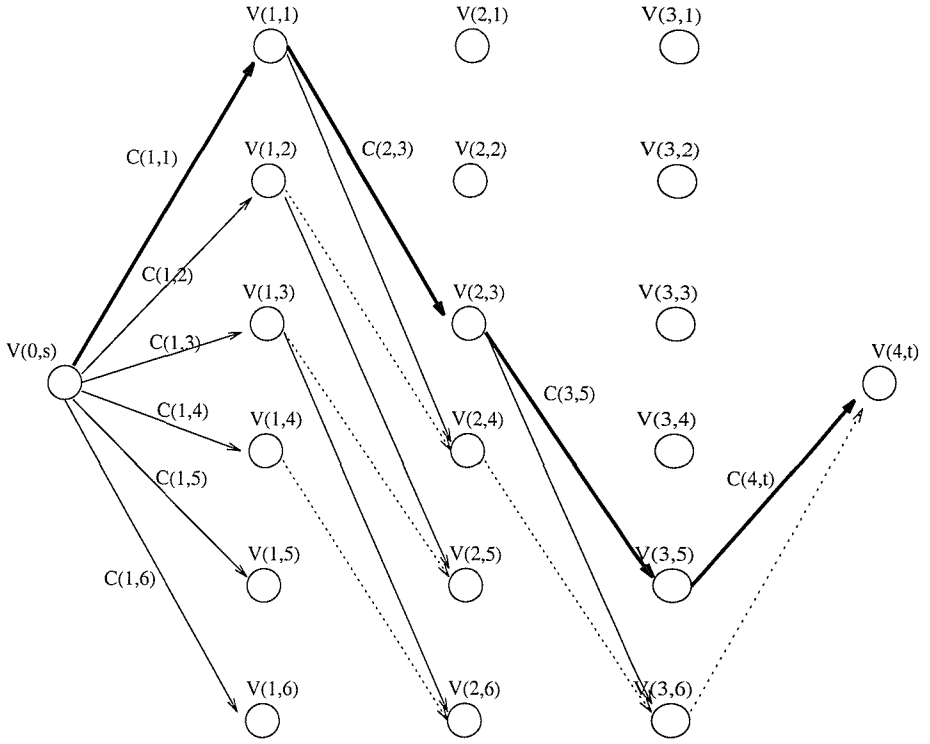


Figure 4.4: Five stage graph corresponding to a channel assignment problem

where $S_{max}$ and $S_{min}$ represent the maximum and minimum measured interference level, respectively. The minimum $I_{th}$ is arbitrarily set to 20 dB, i.e., 11 dB above the minimum required SIR of 9 dB ($\text{SIR}_{min}$ = 9dB). We discretise all values to reduce computation. The resolution of $I_i$, $C_i$ and $U_i$ in our experiment are one dB, one carrier-width and 0.01, respectively. Next the usability matrix, $U$, is fed into the channel assignment unit of the controller.

The channel assignment problem can be formulated as a multistage graph problem [66]. The problem is to allocate $M$ frequencies, $F_M = (F_1, F_2, ..F_M)$, to a cell in such a way as to maximise the combined set usability, and adjacent channel interference (ACI). We formulate this problem as an $M + 2$ stage graph $G = (V, E)$ which is a directed graph in which the vertices are partitioned into $M + 2$ disjoint sets $V_i$, $0 \leq i \leq M + 1$. Stage $i$, $1 \leq i \leq M$ represents frequency $i$. Hence, there are $N$ vertices $V(i, j)$, $0 \leq j \leq N$ associated with stage $i$, $1 \leq i \leq M$. Stages 0 and $M + 1$ each have one vertex $V(0) = s$ and $V(M + 1) = t$, respectively. Vertex $V(i, j)$, $1 \leq i \leq M$ represents the state in which $j$th frequency is allocated to $F_i$. The edges in $G$ are of the form $\langle V(i, j), V(i + 1, l)\rangle$ for all $1 \leq j < N$ and $0 \leq i \leq M$. The edge

$\langle V(i,j), V(i+1,l)\rangle$ is assigned a weight of $U_l$ and corresponds to allocating $l$ to $F_{i+1}$.

The resulting graph for a channel assignment problem with $M = 3$ and $N = 6$ is shown in Figure 4.4. An optimum allocation of frequencies is defined by a maximum weight $s$ to $t$ path, provided that no ACI violation occurs in the path. This is converted into minimum cost problem by changing the sign of all the edge costs, i.e., the cost of $\langle V(i,j), V(i+1,l)\rangle$ is given by $c(j,l) = -U_l$.

A dynamic programming formulation for $M+2$ stage graph problem is obtained by first noticing that every $s$ to $t$ path is a result of a sequence of $M$ decisions. The $i$th decision involves determining which vertex in $V_{i-1}$, $2 \leq i \leq M+2$, is to be on the path. Observe that the principle of optimality holds. Let $P(i,j)$ be a minimum cost path from vertex $s$ to vertex $j$ in $V_i$, and COST$(i,j)$ be the cost of this path. Using the backward approach, we obtain

$$\text{COST}(i,j) = \min_{\substack{l \in V_{i-1} \\ \langle j,l\rangle \in E}} \{\text{COST}(i-1,l) + c(l,j)\} \tag{4.4}$$

as COST$(1,j) = c(1,j)$ if $\langle s,j\rangle \in E$, and COST$(1,j) = \infty$ if $\langle s,j\rangle \notin E$, Equation 4.4 can be solved for COST$(M+2,t)$ by first computing COST$(1,j)$ for all $j \in V_1$ , then COST$(2,j)$ for all $j \in V_2$, etc., and finally COST$(M+2,t)$. Let $K_0$ is a minimum co-site frequency separation required to avoid ACI. We only need to consider the $L$ frequencies with the highest usability, and $L$ is given by $L = MK_0 + 1$. Therefore, $U_{th}$ is the value of $L$th highest usability. $P(i,j)$ is a non-ACI minimum cost path from vertex $s$ to vertex $j$ in $V_i$, and $P(i,j)$ is defined as

$$P(i,j) = \{P(i-1, D(i,j)), j\}, \tag{4.5}$$

where $D(i,j)$ is the value of $l$ which minimises COST$(i-1,l) + c(l,j)$ (see Equation 4.4). With the above consideration we limit the member of $E$ to those edges $\langle V(i,j), V(i+1,l)\rangle$ that comply with the following conditions:

1. $U_l \geq U_{th}$,
2. $U_l \leq U_j$,
3. $\min_{k \in P(i,j)}(|k-l|) \geq K_0$.

In Figure 4.4 we have $N = 6$, $M = 3$ and $K_0 = 2$, and assume that $U_1 > U_2 > U_3 > U_4 > U_5 > U_6 > U_{th}$. The optimal allocation of channels is defined by the $s$ to $t$ path with minimum cost.

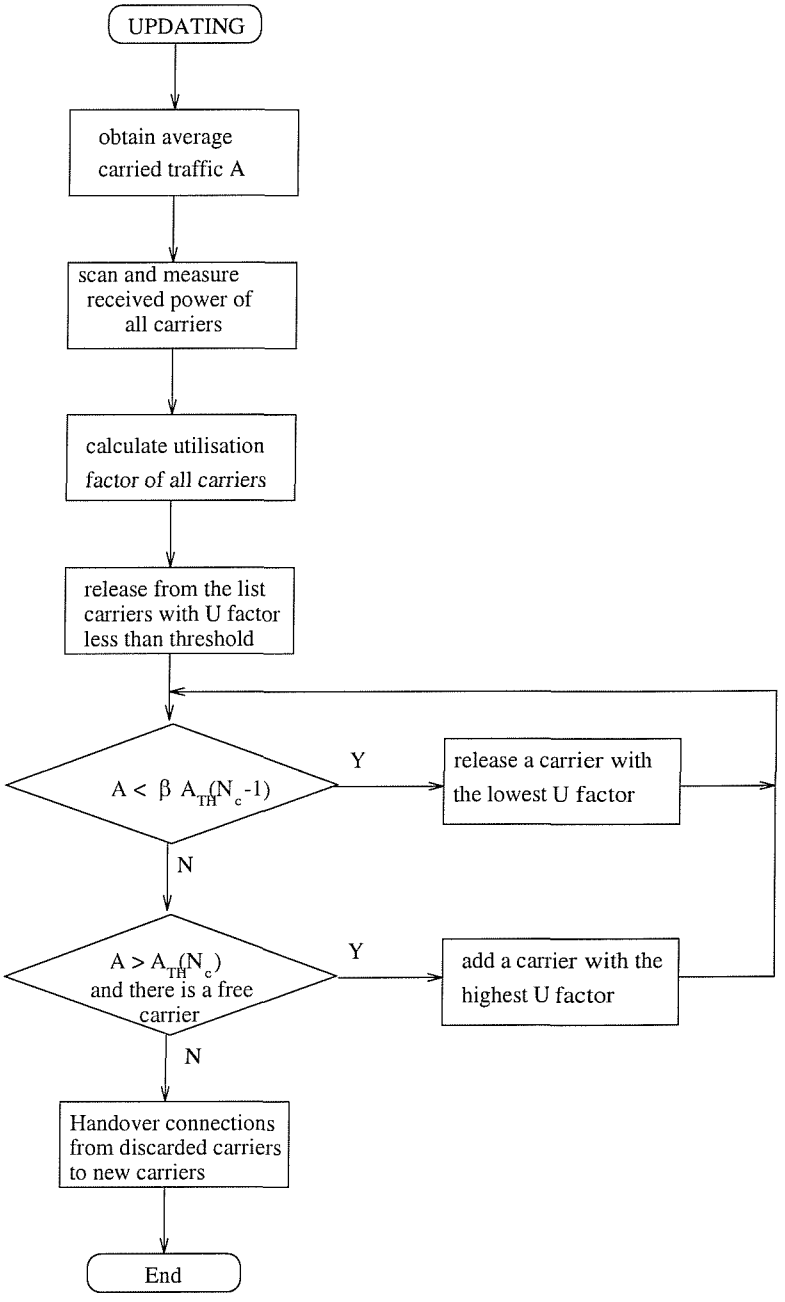


Figure 4.5: The AAFA carrier updating algorithm

After the initial channel assignment, each BS dynamically updates its channel allocation list according to changes in the propagation environments and the spatial distribution of users and the traffic demand. In order to provide a fast network response we introduce a channel updating algorithm as shown in Figure 4.5. Each BS continuously determines its average carried traffic load $A_C$ during a monitoring interval, and measures the downlink interference levels on all carriers. The usability of each carrier is then calculated according to Equation 4.2, and the BS removes carriers with a usability lower than the threshold, $U_{th}$, from its frequency list. Here we determine $U_{th}$ by assuming that the allowable reuse distance is at least twice the distance from the BS to the nearest base site, therefore $U_{th}$ is given by

$$U_{th} = (10\gamma \log(2))/I_{th}, \tag{4.6}$$

where $\gamma$ is a propagation factor and $I_{th}$ is the interference window given by Equation 4.3. The propagation factor $\gamma$ is subjected to each cellular environment. For macrocells, we assume that the BS antenna height is relatively high, and there is no obstruction between BS, hence $\gamma$ is set to two, i.e., free space propagation factor. We also set $\gamma$ to two for microcells, as some micro BSs may also experience line-of-sight with their neighboring BSs. For picocells, where BSs are separation by floors and walls, we set $\gamma$ to 3.5.

After adjusting the frequency list according to the propagation environment, the BS then update the frequency list according to the traffic requirement. The BS compares its average carried traffic, $A_C$, with a traffic threshold $A_{TH}(M_c - 1)$, where $M_c$ is the current number of carriers allocated to the cell. If $A_C < \beta \cdot A_{TH}(M_c - 1)$, then the carrier with the least usability is removed from the frequency list, where $A_{TH}(j)$ is the carried traffic threshold function, and $\beta$ is the factor for stabilising the adaptive algorithm and is set to 0.9. This process is repeated until the above condition is no longer met, or $M_c$ reaches the minimum number of carriers at a BS, $M_{c_{min}}$. Here we set $M_{c_{min}}$ to unity. The BS then compares $A_C$ with $A_{TH}(M_c)$. If $A_C > A_{TH}(M_c)$, an available carrier with a maximum usability is added, i.e., its usability must be equal or higher than the threshold, $U_{th}$. This process is repeated until the condition is no longer met or there is no more available carrier to allocate. After updating the frequency list, all the calls associated with the discarded carrier are handovered to the allocated carriers. The definition of $A_i$ and $A_{TH}(j)$ depends on types of carried traffic, i.e., speech, video or data, and the medium access control protocol associated with the system. In the next section we give some examples of defining these parameters

for circuit-switched access and PRMA access for the telephony service. Generally, in order to cope with the time-variant and geographical traffic fluctuations, the system must update its channel assignments as often as possible. However, in GSM the update period is limited by the affordable relative frequency of signal measurements. In this thesis we set the update interval to one minute.

## 4.4 Macrocellular simulation

### 4.4.1 System model

Consider a two-dimensional service area with 16 base sites placed on an equally spaced hexagonal grid as shown in Figure 4.6. Each base site forms three hexagonal cells, and is located six kilometres apart, consequently each macrocell sectors has a radius of two kilometres. Accordingly, the total coverage area provided by these base sites is approximately 500 $km^2$, i.e., the simulation area is 24 km by 20.78 km. In order to avoid edge-effects we use a wrap-around technique, where each end of the geographical region adjoins to its opposite end. Cells shown in shade experience heavy traffic load during some period of a day, as they contain sections of main roads or motorways which are congested in rush hour. To model this uneven traffic scenario, some percentage of the total incoming traffic is distributed uniformly in a 200-m strip lying across the service area, as used in reference [67], while the rest of the incoming calls are distributed across the whole coverage area. There are a total of 48 carriers available. For the FCA scheme, cells are arranged into clusters of 4/12 (4 cells with 12 sectors), with each sector having four carriers. For the AAFA scheme, each sector is equipped with eight transceivers, and consequently a sector is capable of handling twice the capacity of an FCA cell, if eight carriers or more are assigned to the AAFA cell.

There are three types of mobiles: highway cars, local-road cars and pedestrians. Highway cars travel in both directions along the highway strip at a fixed speed of 72 km/h(=50 mph). Local-road cars travel in uniformly distributed directions at fixed speeds of 36 km/h, and change direction according to a PDF having an exponentially distributed distance with a mean of 500 m. Pedestrians walk in random directions at a fixed speed of 1 m/s, and change direction according to an exponential PDF with a mean of 50 m.

Two traffic distribution scenario are considered, namely, uniform traffic scenario

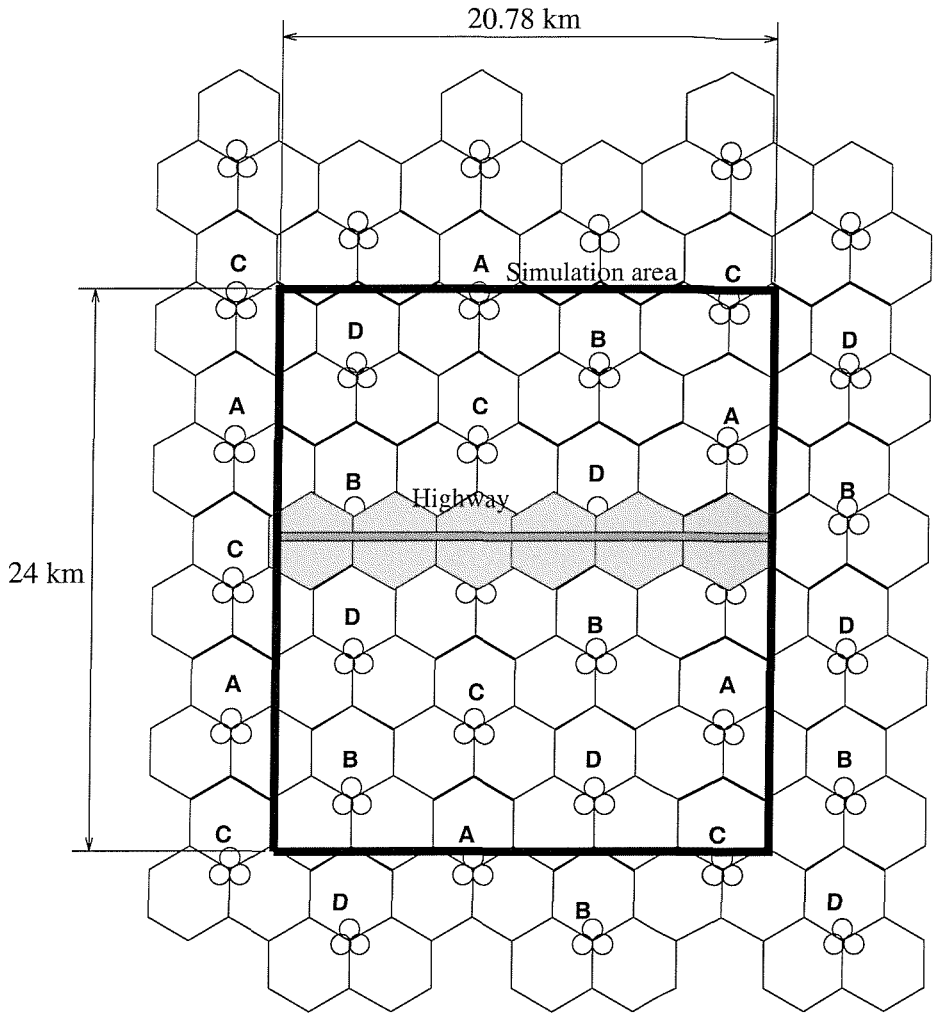


Figure 4.6: The macrocell layout with 3 sectors per cell and 4 cells per cluster. Each BS is labelled by its allocated frequency set

and non-uniform traffic scenario. In the uniform traffic scenario, we do not take into account the highway strip; 50% of the mobiles are cars on local roads, and 50% are roving pedestrian. In the non-uniform traffic scenario, 50% of the mobiles are highway cars, 25 % are local-road cars, and 25% are pedestrians. Each mobile generates 0.05 Erlang of traffic. The duration of a call is exponentially distributed with a mean of 100 s. Thus each mobile makes approximately makes an average of two calls per hour.

The simulator closely models the actual behaviour of the GSM system. The system operational aspects models include call setup, call completion, location updating, channel assignment, handover procedure, etc. Discrete event driven simulation was chosen for the model representation. Three classes of events were selected to describe

the system behaviour as follows:

1. call arrival events that represent the random arrival of calls at each MS;
2. call monitoring events for location updating and handover of active MSs;
3. call completion events that occur at the end of a call (successful completion).

Calls arrive according to a Poisson distribution with the arrival rate related to the total offered traffic. When a call arrives at an MS, it finds the strongest BS and requests a call set-up. If there are channels available at the BS, the call is established. Otherwise, the call is blocked. During the call the BS continuously checks the link SIR. If the SIR falls below a certain threshold, ($\text{SIR}_{min} = 9\text{dB}$), or the MS moves into a new BS coverage, the MS makes a handover attempt. The handover can be either between different cell sites or within the same cell site. We call the former as 'inter-cell handover' and the latter as 'intra-cell handover'. If the handover is unsuccessful, and the SIR remains below the threshold, the MS repeatly retries during a five second timeout period. After this period the call is terminated. Each BS continuously monitors the traffic it is handling, and channel assignment updating is implemented every 60 seconds.

### 4.4.2 Propagation models

The average received power $P_r$ (in dBm) at a given receiver, from a given transmitter, is calculated using the formula

$$P_r = P_{tx} + G_T + G_R - L_{path} - L_{shd}, \tag{4.7}$$

where $P_{tx}$ is an average transmitted power (dBm), $G_T$ is a transmitter antenna gain (dB), $G_R$ is a receiver antenna gain (dB), $L_{path}$ is a path loss (dB) and $L_{shd}$ is a shadow fading (dB). Multipath fading is not included in our model since our study concerns only the local mean signal, which has the multipath fading averaged out, say by some form of diversity. The decibel value of the shadow fading, $L_{shd}$, is assumed to follow a zero-mean Gaussian statistics with a standard deviation of 6 dB.

For path losses of radio links between a mobile and a base station, we employ the model Hata model and the Walfish-Ikegami model [41], which are the works of the European cooperation in the field of scientific and technical research (EURO-COST) subgroup COST-231 models. We use the COST-231-Walfish-Ikegami model for path

lengths from 20 metres to 5 km, and the COST-231-Hata model for path lengths more than 5 km. The COST-231-Hata model is the extension of the Hata's formula [33] to the frequency band 1500-2000 MHz. The path loss formula (dB) is

$$L_H = A + B\log(d) + C \tag{4.8}$$

where

$$\begin{aligned} A &= 46.3 + 33.9\log(f_c) - 13.82\log(h_b) - a(h_m) \\ B &= 44.9 - 6.55\log(h_b) \\ C &= \begin{cases} 0 & \text{medium city and suburban areas} \\ & \text{with moderate tree density} \\ 3 & \text{for metropolitan centres} \end{cases} \\ a(h_m) &= (1.1\log(f_c) - 0.7)\,h_m - (1.56\log(f_c) - 0.8) \end{aligned}$$

The carrier frequency, $f_c$ (MHz) is restricted to 1500-2000 MHz. The MS antenna height $h_m$ (m) is restricted to 1-10 metres. The BS antenna height $h_b$ (m) is limited to 30-200 metres and must be above the roof tops. The distance between MS and BS, $d$ (km), is restricted to 1-20 km.

The COST-231-Walfish-Ikegami model takes into account the propagation over a row of buildings by multi-screen diffraction, and diffraction from the roof near the MS down to street level where the MS is roving [2]. The model works best when the BS antenna is installed several metres above the maximum roof top of adjacent buildings and within a radius of some hundred metres from a MS. We use only NLOS propagation of the model as we assume that the MSs are always in NLOS. The path loss for NLOS is express in terms of building height $h_{roof}$ (m), street widths $w$ (m), building separation $b$ (m) and road orientation $\phi$ with respect to the direct radio path. The path loss is composed of three terms, viz.,

$$L_W = \begin{cases} L_0 + L_{rts} + L_{msd} & \text{for} \quad L_{rts} + L_{msd} \geq 0 \\ L_0 & \text{for} \quad L_{rts} + L_{msd} < 0 \end{cases} \tag{4.9}$$

where $L_0$ is the free-space loss, $L_{rts}$ is the rooftop-to-street diffraction and scatter loss, and $L_{msd}$ is the multiscreen diffraction loss. The free-space loss is

$$L_0 = 32.4 + 20\log(d) + 20\log(f_c). \tag{4.10}$$

The rooftop-to-street diffraction and scatter loss is

$$L_{rts} = -16.9 - 10\log(w) + 10\log(f_c) + 20\log\Delta h_m + L_{ori} \tag{4.11}$$

where

$$L_{ori} = \begin{cases} -10 + 0.354(\phi), & 0 \leq \phi \leq 35^o \\ 2.5 + 0.075(\phi - 35), & 35 < \phi \leq 55^o \\ 4.0 - 0.114(\phi - 55), & 55 < \phi \leq 90^o \end{cases} \tag{4.12}$$

and

$$\Delta h_m = h_{roof} - h_m$$

The multi-screen diffraction loss is

$$L_{msd} = L_{bsh} + k_a + k_d \log(d) + k_f \log(f_c) - 9 \log b \tag{4.13}$$

where

$$\begin{aligned} L_{bsh} &= \begin{cases} -18 \log(1 + \Delta h_b), & h_b > h_{roof} \\ 0, & h_b \leq h_{roof} \end{cases} \\ k_a &= \begin{cases} 54, & h_b > h_{roof} \\ 54 - 0.8\Delta h_b, & d \geq 0.5 \text{ km and } h_b \leq h_{roof} \\ 54 - 0.8\Delta h_b d/0.5, & d < 0.5 \text{ km and } h_b \leq h_{roof} \end{cases} \\ k_d &= \begin{cases} 18, & h_b > h_{roof} \\ 18 - 15\Delta h_b / h_{roof}, & h_b \leq h_{roof} \end{cases} \\ k_f &= \begin{cases} -4 + 0.7(f_c/925 - 1), & \text{medium city and suburban} \\ -4 + 1.5(f_c/925 - 1), & \text{metropolitan area} \end{cases} \end{aligned}$$

and

$$\Delta h_b = h_b - h_{roof}.$$

The term $k_a$ represents the increase in the path loss for BS antennae below the rooftops of adjacent buildings. The terms $k_d$ and $k_f$ control the dependence of the multi-screen diffraction loss on distance and radio frequency, respectively. The model is valid for the following ranges of parameters: $800 \leq f_c \leq 2000$ (MHz), $4 \leq h_b \leq 50$ (m), $1 \leq h_m \leq 3$ (m), and $0.02 \leq d \leq 5$ (km). If no data on the structure of the buildings and roads are available, the following default values are recommended, $b = 20...50$ (m), $w = b/2$, $\phi = 90^o$, and $h_{roof} = 3 \cdot$ number of floors + roof (m), where roof = 3 (m) pitched and 0 (m) flat. For the macrocellular scenario (see Table 4.1), the following path losses are obtained:

$$\begin{aligned} L_{path} &= \begin{cases} L_W & \text{for} \quad 0.02 \leq d < 5 \text{ km} \\ L_H & \text{for} \quad d \geq 5 \text{ km} \end{cases} \\ L_H &= 137.5 + 34.4 \log d \\ L_W &= 133.8 + 38 \log d \end{aligned} \tag{4.14}$$

| Parameter | Value |
|---|---|
| $f_c$ | 1800 MHz |
| $\lambda$ | 0.167 |
| $h_b$ (macro) | 40 m |
| $h_b$ (micro) | 6 m |
| $h_b$ (pico) | 1.5 m above a floor |
| $h_m$ | 1.5 m |
| $h_{roof}$ | 27 m |
| Area | Metropolitan |
| $w$ | 28 |
| $b$ | 100 |
| $D_b$ | 216 m |
| $F_b$ | 18 dB |

Table 4.1: System parameters for our propagation models.

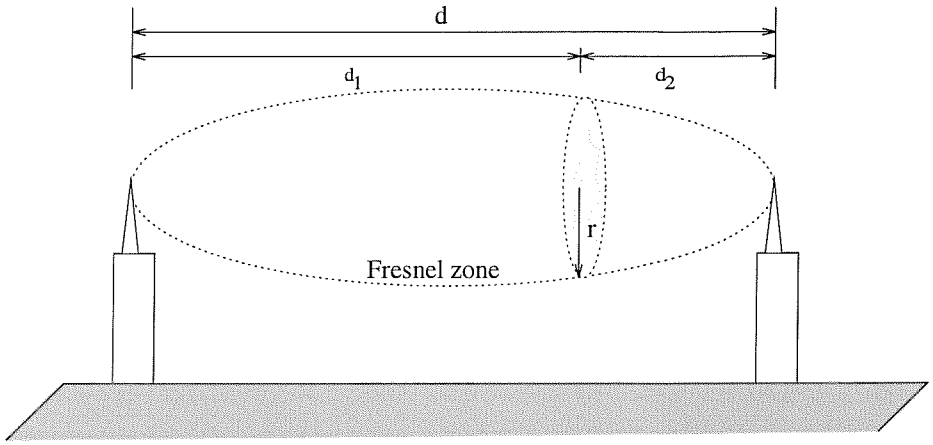


Figure 4.7: The first fresnel zone between two macrocellular BS antennae

To calculate path loss of a radio link between two BSs, we use a free space propagation model, $L_{path} = 20\log(d)$, where $d$ is a distance between the BS antennas. Figure 4.7 shows a simple radio link path, and the dotted line defining the region known as the "first Fresnel zone". In order to satisfy the free space propagation condition, the direct path between the two antennas and the first fresnel zone must be clear of obstructions [68]. We consider a plane normal to the line-of-sight path at a given point between the two BSs, the radius of the first fresnel zone is given by

$$r = \sqrt{\frac{\lambda d_1 d_2}{d_1 + d_2}}. \tag{4.15}$$

From above equation the maximum radius, $r_{max}$ occurs when $d_1 = d_2$. In our simulation the maximum concerned distance between BSs is 25 kilometres, consequently, $r_{max}$ is approximately 32 metres which is still below our BS antenna height of 40 metres. Note that we do not consider any man-made or any other obstructions between macrocellular BSs, and the free space propagation model is therefore justified.

Our study uses horizontally sectored antennas with a broad vertical radiation pattern. To obtain a circular shape cell from a sectored site antenna, we use a simple antenna pattern model given by

$$G(\theta) = \alpha + \cos^{\gamma}\theta \tag{4.16}$$

where $G$ is the gain of the antenna at azimuth angle $\theta$ from its maximum lobe, $\gamma$ is the path loss exponent of the macrocellular propagation model ($\gamma = 3.44$). $\alpha$ is a factor related to the antenna front-back ratio and is given by

$$\alpha = 1/(10^{F_b/10} - 1), \tag{4.17}$$

where $F_b$ is the front-to-back ratio of the base-site antenna in dB.

## 4.5 Microcellular simulation

### 4.5.1 System model

We use a city model with 32 microcellular BSs uniformly located over a two-dimensional area of one km$^2$ with a pattern of rectilinear streets as shown by Figure 4.8. There are 64 equal size city office blocks. Each building is 72 metres square. The streets are 28 metres wide, including 4 metre wide pavements on each side of the streets. As

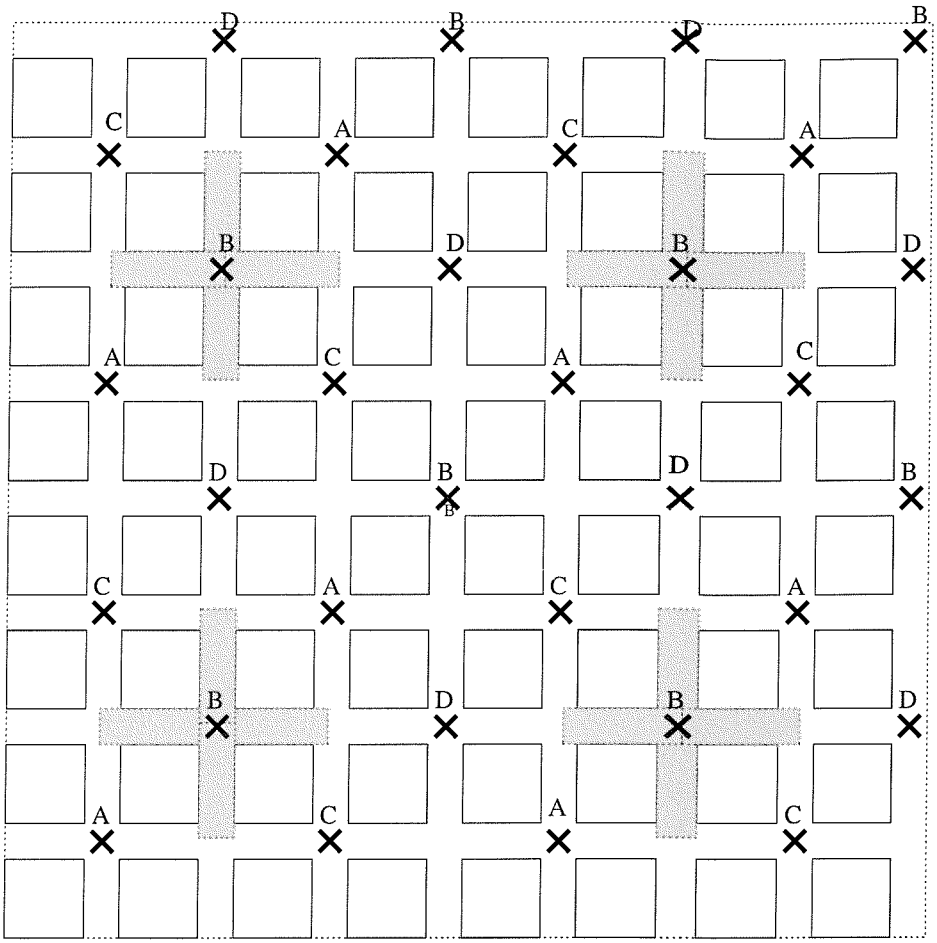


Figure 4.8: The microcellular network layout with hot spot area shown in shaded. Each BS is labelled by its allocated frequency set

in the macrocellular simulation, the wrap-around technique is employed in order to avoid edge effects. The areas shown shaded are expected to experience heavy traffic load during the peak hour. Two traffic distribution models are considered, namely the uniform traffic scenario and the non-uniform traffic scenario. In the uniform traffic scenario all arrival calls are from mobiles uniformly distributed across the city area. To model the non-uniform traffic scenario, 50% of the total incoming traffic is originated from mobiles located in the shaded area, while the rest of the calls are uniformly distributed across the city area. There are a total of 16 carriers allocated for the microcellular network. For the FCA scheme, cells are grouped into clusters of four, consequently each BS is assigned four carriers. For the AAFA scheme each BS is equipped with 8 transceivers, hence its traffic capacity is doubled if eight or more

carriers are available at the cell.

Microcellular users are randomly located on the footpath around buildings. Only 10% of them are stationary while engaged in calls. The speeds of the users are normally distributed with a mean and variance of 1.0 and 0.5 m/s, respectively. Their speed are regularly updated at time intervals of 1 s. The minimum and maximum speed is 0 and 2 m/s, respectively. When the users reach a junction, we randomly pick a the new junction from the surrounding junctions. All adjacent junctions have an equal probability of being chosen. As in the macrocellular simulation, each mobile station generates 0.05 Erlang of traffic. The duration of a call is exponentially distributed with a mean of 100 s. The other system operation is the same as in the macrocellular simulation.

### 4.5.2 Propagation model

For ranges less than 500 m and antenna heights less than 20 m, empirical measurements have shown that the received signal strength for line-of-sight (LOS) propagation along city streets can be described by a two-slope model [69]. The LOS path loss is

$$L_{LOS} = \begin{cases} 20\log(4\pi d/\lambda), & \text{if} \quad d < D_b \\ 20\log(4\pi d^2/\lambda) - 20\log(D_b), & \text{if} \quad d \geq D_b \end{cases} \tag{4.18}$$

where $d$ is the BS to MS horizontal separation distance, and $D_b$ is a slope breaking distance given by $D_b = 4h_b h_m/\lambda$ . Our non line-of-sight (NLOS) path loss model is derived from the model proposed by Erceg et al. [38]. The Erceg's model fitted 2.0 GHz measurements taken in New York, which has approximately the same street and building block dimensions as our city centre model, making it a good choice for our application. The NLOS path loss is defined as

$$L_{NLOS} = \begin{cases} 20\log(4\pi d_c/\lambda) + 10B\log(d/d_c) + A, & \text{if} \quad d_c < D_b \\ 20\log(4\pi d_c^2/\lambda) + 10B\log(d/d_c) & \\ -20\log(D_b) + A, & \text{if} \quad d_c \geq D_b \end{cases} \tag{4.19}$$

where $d_c$ is the horizontal distance from the BS to a corner, and $d$ is the total horizontal distance from a BS to an adjacent BS via a diffracting corner. The NLOS attenuation slope, $B$, is $B = d_c/50 + 2$, if $d_c > 100$, otherwise $B = 4$. The NLOS corner loss, $A$,

is

$$A\ (dB) = \begin{cases} 10, & \text{if } d_c < 50\ m, \\ 13, & \text{if } 50 \leq d_c < 100\ m \\ 17, & \text{if } 100 \leq d_c < 150\ m \\ 19, & \text{if } 150 \leq d_c < 200\ m \\ 22, & \text{if } 200 \leq d_c < 300\ m \\ 23, & \text{if } 300 \leq d_c < 400\ m \\ 25, & \text{if } d_c \leq 400\ m. \end{cases}$$

In microcells, shadowing of the buildings becomes evident when a mobile turns a corner and loses line-of-sight with its BS. However, even when a mobile experiences line-of-sight transmissions, there is a variation in the received signal level that is due to the irregularities of the buildings, vehicles in the streets, street furniture, etc, which constitute a slow fading effect that has a log-normal distribution with a standard deviation of 4 dB.

To calculate pathloss of a radio link between two given BSs, we use the same propagation model as for microcellular radio links between a BS and a mobile, but with $D_b$ set to $D_b = 4h_b h_b/\lambda$. All microcellular BSs employ omni-directional antennas, with an antenna gain of unity.

## 4.6 Picocellular simulation

### 4.6.1 System model

A picocellular model comprises a cluster of four office buildings located in the city centre of the microcellular model described in the previous section. Each building is 72 metres square and nine-floors high. Figure 4.9 shows a building floor plan where each floor has four corridors and 144 square shaped offices [70]. There are nine BSs installed on each floor. The position of a BS is indicated by dots in Figure 4.9. Therefore, the four buildings have a total of 324 picocells. We assume that the ground floor of each building is a shopping complex, and the picocells in these areas experience heavy traffic during some period of the day. We consider two traffic distribution scenarios, namely, uniform traffic scenario and non-uniform traffic scenario. In the uniform traffic scenario, calls are originated from mobiles uniformly distributed over the picocellular service area. In the non-uniform traffic model, 50% of the total calls originate from mobiles on the ground floors and the rest of the calls originate from

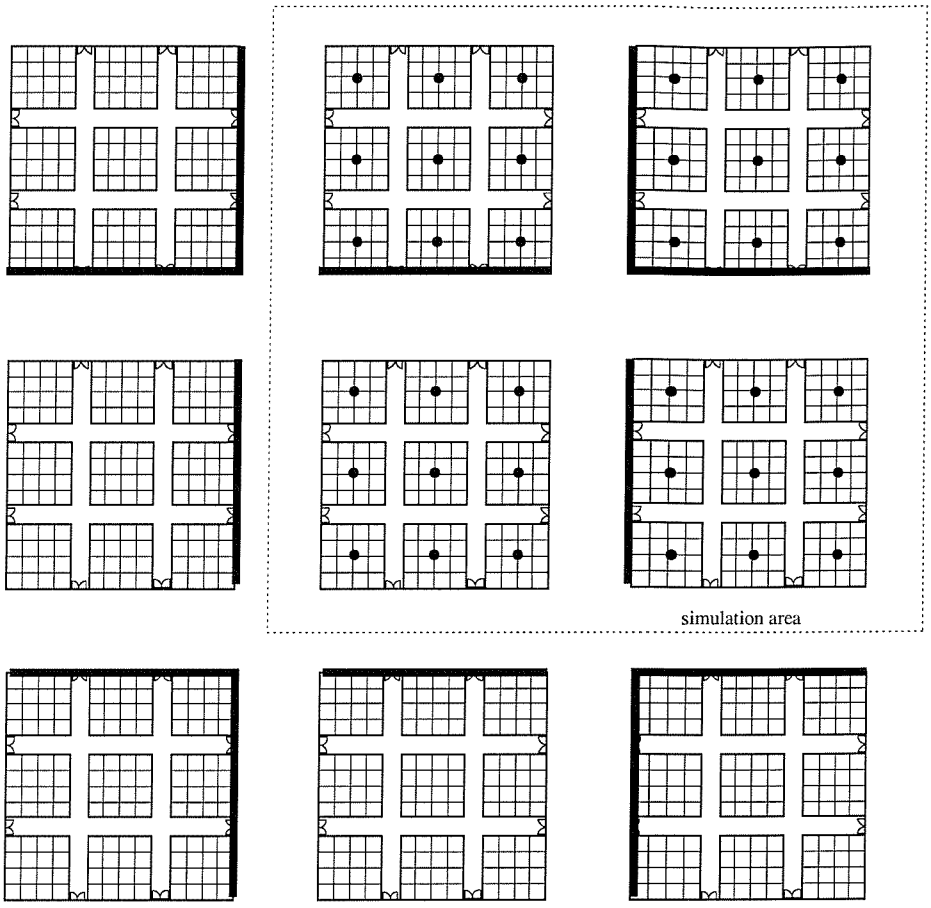


Figure 4.9: Picocellular network layout

mobiles uniformly distributed over picocellular service area. Each mobile generates 0.2 Erlang of traffic. The duration of a call is exponential distributed with a mean of 180 s. Thus each mobile makes approximately an average of 4 calls per hour. The other system operation is the same as in the macrocellular simulation.

### 4.6.2 Propagation model

The radio propagation into and within buildings uses a combined direct and reflection ray model. We use the direct ray model where a path loss is given by

$$L_D = L_f + L_w, \tag{4.20}$$

where $L_f$ is calculated using the free space propagation formula:

$$L_f = 20 \log(4\pi d/\lambda) \tag{4.21}$$

and $d$ is the free space distance from MS to BS antennae. The loss $L_w$ is the sum of the penetration losses of the walls and floors intersected by the path joining the BS antenna and the MS antenna. The corridor walls have a penetration loss of 8 dB. The glass doors between the corridors and the street have a 4 dB loss. The internal office partitions have a loss of 3 dB. The building floors have a 15 dB loss. The penetration losses used here are similar to those used in Chapter 3.

To account more accurately for propagation into and out of buildings, the external walls of buildings (not glass doors) are given an incident-angle-dependent penetration loss. The external wall loss is given by

$$W_{loss} = W_e + (1 - \sin\theta)^2 \cdot W_{ge}, \tag{4.22}$$

where $W_e$ is the perpendicular incident penetration loss set to 12 dB, $W_{ge}$ is the difference between $W_e$ and the grazing incident penetration loss, set to 20 dB, and $\theta$ is the angle between the incident ray and the plane containing the wall.

We consider only a single reflection as the multiple reflections are less significant due to the extra ray travelling distance and reflection loss. The reflection loss of the external walls and the glass doors are set to 3 and 30 dB, respectively. Fig. 4.9 also shows the surfaces considered as reflectors, highlighted by thick lines, for the picocell BSs in the middle building and a microcell BS located beside the the middle building. A reflected ray pathloss is given by

$$L_R = L_f + L_w + L_r, \tag{4.23}$$

where $L_f$ is calculated using Equation 4.21 with $d$ replaced by the reflected ray path length between MS and BS, $d_r$ , and $L_r$ is the reflection loss of the reflecting surface. The total path loss including the direct and reflected ray is given by

$$L = \left|10\log(10^{-L_D/10} + 10^{-L_R/10})\right|. \tag{4.24}$$

## 4.7 Results

There are several performance matrices that can be used to quantify the performance and or quality of service provided by a particular channel allocation algorithms. We are concerned with identifying the performance matrices and the carried traffic threshold function $A_{TH}(j)$, for mobile radio systems with circuit-switched access and with PRMA access. Communication systems are generally evaluated on the basis of their

| Parameter | Macrocell value | Microcell value | Picocell value |
|---|---|---|---|
| $A_u$ (Erlang) | 0.05 | 0.05 | 0.2 |
| $\mu_c^{-1}$ (second) | 100 | 100 | 180 |
| Number of base site | 36 (108 sectors) | 32 | 324 |
| Coverage area | 10.4 km$^2$/sector | 10416 m$^2$/cell | 576 m$^2$/cell |
| Bandwidth (MHz) | 20 | 7 | 13 |
| VAF (PRMA only) | | 43 % | |

Table 4.2: The values of system parameters used in simulations

maximum carried traffic, provided that quality requirements are satisfied. Accordingly, we define the performance matrices and results for circuit-switched systems and PRMA systems separately in the following subsections.

### 4.7.1 Circuit-switched access

In fixed networks the most relevant cause of impairment is the blocking of new calls when no free channel is available. The carried traffic, $A_C$, is the fraction of the offered traffic $A_T$ and is expressed as:

$$A_C = A_T(1 - P_B) \tag{4.25}$$

where $P_B$ is the probability that a new call is blocked,

$$P_B = \frac{\text{number of blocked calls}}{\text{number of new calls}}. \tag{4.26}$$

The offered traffic is expressed by

$$A_T = \lambda_c/\mu_c = N_u A_u, \tag{4.27}$$

where $\lambda_c$ is a new call arrival rate, $\mu_c^{-1}$ is an average call duration, $N_u$ is the total number of users and $A_u$ is an average offered traffic per user. The system parameters use in our simulations are summarised in Table 4.2

In mobile radio systems an additional impairment arise; these are mainly related to failures of handover (HO) attempts. Handover are required when the received signal is too weak because users have moved out of cell coverage, or when the interference coming from other users resulting in a carrier-to-interference ratio CIR lower than the minimum required carrier-to-interference ratio $\text{CIR}_{min}$. Under these circumstances, if the call cannot be handovered within a certain time limit, the users are forced to

| no. of carriers, j | 1 | 2 | 3 | 4 | 5 | 6 | 7 | 8 | 9 | 10 |
|---|---|---|---|---|---|---|---|---|---|---|
| $N_{TCH}(j)$ | 7 | 14 | 22 | 30 | 37 | 45 | 53 | 61 | 69 | 77 |
| $A_{TH}(j)$ | 3 | 9.7 | 17 | 25 | 32 | 40 | 48 | 56 | 64 | 72 |

Table 4.3: Traffic threshold in Erlang and a number of traffic channels for a current number of carrier at a GSM base station

terminate their calls. Therefore, for mobile radio systems an additional parameter is defined as the call dropping probability, $P_D$, or the probability that calls are forced to terminate $P_F$,

$$P_D = P_F = \frac{\text{number of calls being forced to terminate}}{\text{number of successful new calls}}. \tag{4.28}$$

Due to these capacity impairments, the carried traffic, $A_C$, is further reduced to

$$A_C = A_T(1 - P_B - P_F + P_B P_F). \tag{4.29}$$

In order to assess the performance of our algorithm, we use a reference channel allocation algorithms, namely the fixed channel allocation (FCA) with no handover priority. The new call blocking probability $P_B$ can be approximated by the Erlang-B formula [31, 71, 32]

$$P_B = E_B(N, A_T) = \frac{(A_T)^N/N!}{\sum_{k=0}^{N}(A_T)^k/k!} \tag{4.30}$$

where $N$ is the number of channels allocated to a cell, and $A_T$ is the total traffic requested given by Equation 4.27.

The measured carried traffic $A_i$ is quantified in terms of average number of busy channels during the $i$th interval. The traffic threshold, $A_{TH}(j)$ is obtained by calculating a carried traffic that corresponds to the required GOS of the system. Note that the GOS is the probability that calls, including new calls and handover calls, fail to obtain channels from a BS. Here we maintain the GOS below 5%. Due to low GOS value, we set $A_{TH}(j)$ to the carried traffic, $A_C$, that gives $P_B = E[N_{TCH}(j), A_T]$ = 5%, where $N_{TCH}(j)$ is the number of traffic channels for $j$ carriers, $E[N, A]$ is the Erlang-B formula, $A_T = A_C/(1 - P_B)$ is the mean offered traffic in Erlang, and $P_B$ is a probability that a new call will be blocked. We use the GSM parameters in our study, and $N_{TCH}(j)$ and $A_{TH}(j)$ values are tabulated in Table 4.3.

The macrocellular network uses a GSM bandwidth of 20 MHz that accommodates 48 carriers for uplink and 48 carriers for downlink. Each sector covers an area of 10.4

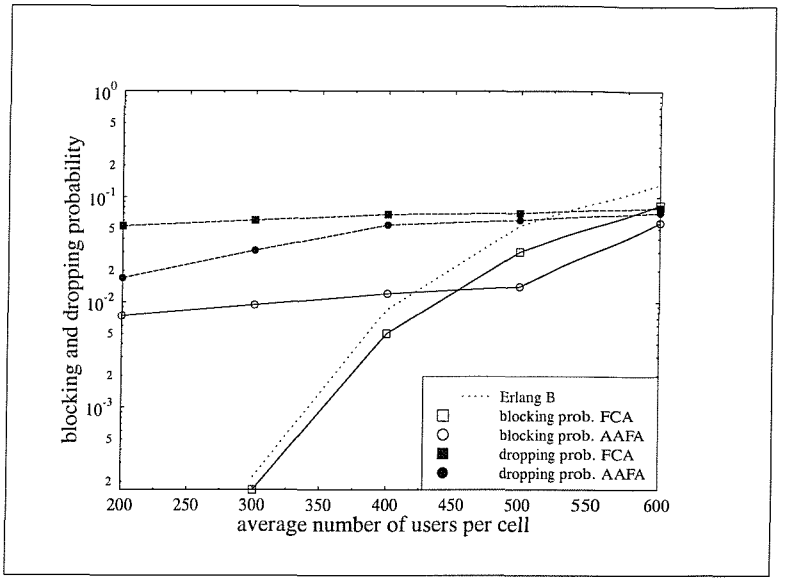


Figure 4.10: GOS performance comparison for macrocells with uniform traffic distribution

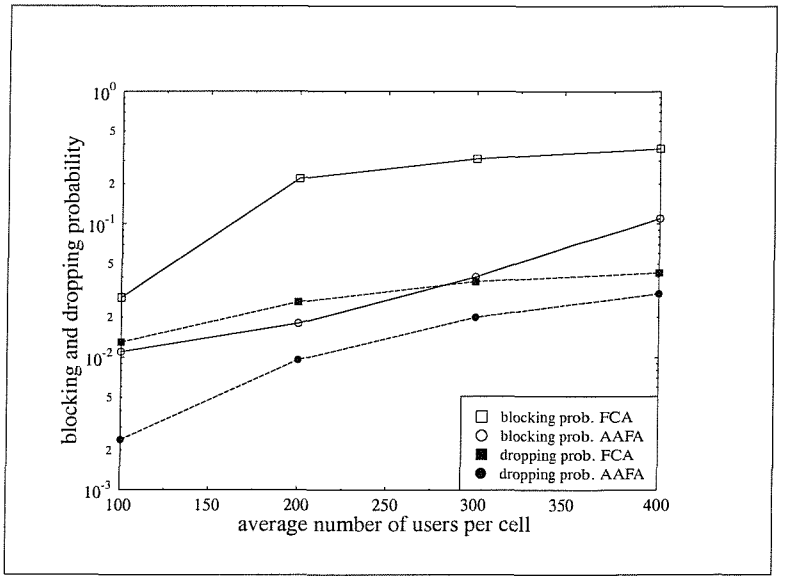


Figure 4.11: GOS performance comparison for macrocells with non-uniform traffic distribution

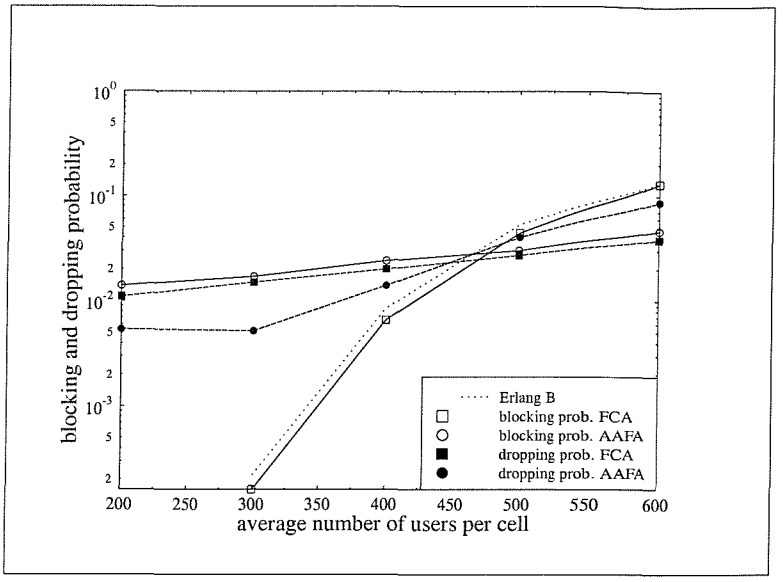


Figure 4.12: GOS performance comparison for microcells with uniform traffic distribution

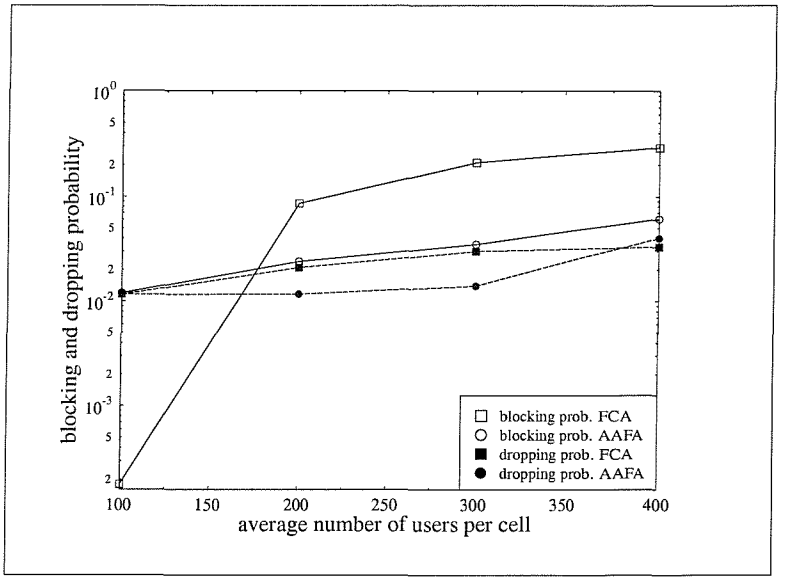


Figure 4.13: GOS performance comparison for microcells with non-uniform traffic distribution

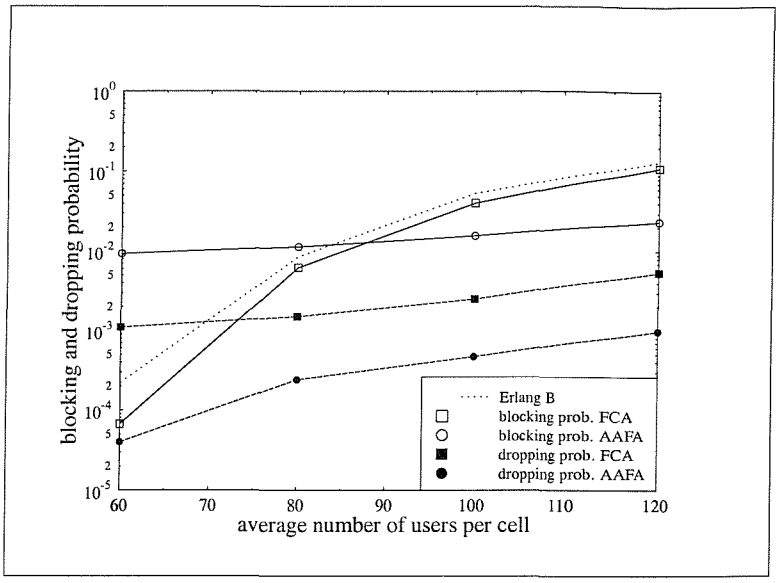


Figure 4.14: GOS performance comparison for picocells with uniform traffic distribution

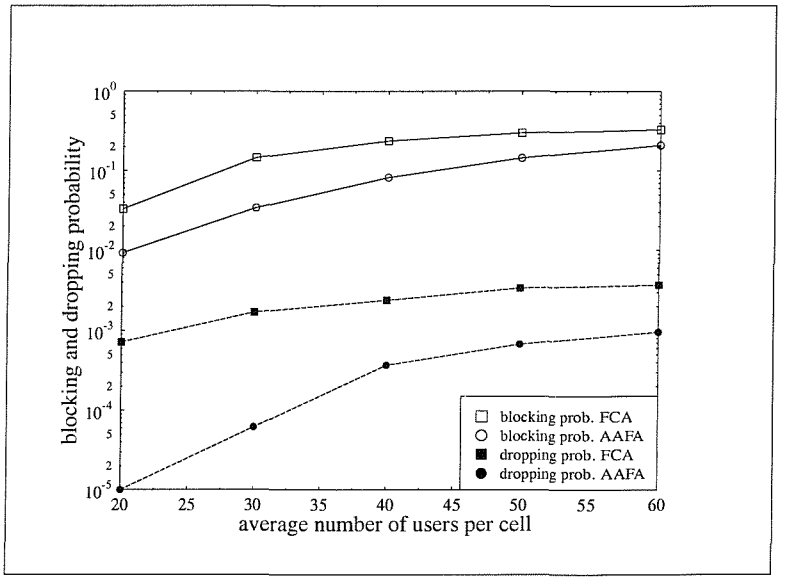


Figure 4.15: GOS performance comparison for picocells with non-uniform traffic distribution

$km^2$. In the FCA system, each sector is allocated with 4 carriers, that is equivalent to 30 traffic channels, according to Table 4.3. Figure 4.10 shows the variation of the probability of a new call being blocked,$P_B$ ,and the probability of a call being forced to terminate, $P_F$, versus the average number of users per cell under the uniform traffic scenario for the AAFA and FCA macrocellular network. The Erlang B curve is slightly higher than the $P_B$-FCA curve, due to the effect of call dropping. However the $P_B$-FCA curve is found to be in agreement with the Erlang B curve. From this figure it can be seen that the AAFA network offered superior blocking performance when traffic load is high, i.e., more than 450 users per cell. However, when the traffic is low to medium, the $P_B$ of the AAFA system is higher than the $P_B$ of the FCA system, and is maintained at around one percent. The call dropping performance of the AAFA system is better than the FCA system, especially in the low traffic region. For a GOS of $P_B = 5\%$, the AAFA system enhances the system capacity by nine percent, i.e, from 550 users per cell to 600 users per cell, comparing to the conventional FCA system.

Figure 4.11 shows the GOS comparison for the non-uniform traffic scenario. The AAFA system provides a significant improvement of $P_B$ and $P_F$ performance compared to the FCA system. For a GOS of $P_B = 5\%$, the system capacity is improved by 180%, i.e., from 125 users per cell to 350 users per cell. This is equivalent to an improvement of mean carried teletraffic from 57 to 160 mErlang/MHz/$km^2$.

The microcellular networks use a radio bandwidth of 7 MHz, accommodating 16 carrier pairs, and each BS in the FCA system is allocated four carrier pairs. Each microcellular BS provides a coverage of 10416 $m^3$ in the streets. Figure 4.12 shows the $P_B$ and $P_F$ performance versus the average number of users per microcell for the microcellular networks under the uniform traffic scenario. From this figure, the AAFA network is seen to have a superior blocking performance at high traffic load, i.e., when the average number of users per cell is higher than 475, and a poorer blocking performance at low to medium traffic loads. However, the call dropping rate of the AAFA system is lower than of the FCA system when the average number of users per cell is lower than 450. When the traffic load exceeds 450 users/cell the call dropping rate of the AAFA system is marginally higher than of the FCA system. For the GOS of $P_B = 5\%$, the AAFA improves the system capacity over the FCA system by 20%, i.e., from 500 users per cell to 600 users per cell.

Figure 4.13 shows the performance of the AAFA system under the non-uniform

traffic scenario. The blocking performance of the AAFA system is superior to the FCA system at medium to high traffic loads, i.e, when the average number of user exceeds 175 users per cell. The call dropping performance of the AAFA system is marginally better than the FCA system for the range of our simulation, i.e., 100-400 average users per cell. For a GOS of $P_B = 5\%$, the AAFA increases the system capacity by 80 %, i.e., from 190 to 360 users per cell. This is equivalent to a carried teletraffic of 248 and 345 Erlang/MHz/km$^2$, respectively.

The picocellular network uses a bandwidth of 13 MHz, accommodating 32 GSM carriers pairs. This provides the FCA system with four carrier pairs per BS. Each BS achieves an inbuilding coverage of 576 m$^2$. Figure 4.14 shows the new call blocking performance and the call dropping performance for the AAFA picocellular network and the FCA picocellular network under the uniform traffic scenario. The AAFA system provides superior blocking performance at high traffic load, i.e., average number of users per cell is higher than 89. The dropping performance of the AAFA system is also significantly better than the FCA system. For the GOS of $P_B = 2\%$ the AAFA system improves the system capacity by 20%, i.e., an improvement from 95 users per cell to 115 users per cell.

Figure 4.15 shows the system performance of the AAFA system and the FCA system under the non-uniform traffic scenario. The AAFA system provides better call blocking performance and lower call dropping rate compared to the FCA system. For the GOS of $P_B = 5\%$ the AAFA improves the system capacity by 50%, i.e., from 22 to 33 users per cell. This is equivalent to a carried teletraffic of 1395 and 2093 Erlang/MHz/km$^2$/floor, respectively.

### 4.7.2 PRMA access

In PRMA, the system can serve more users than the available channels because of statistical multiplexing of the users. Calls in a PRMA system are not blocked as in conventional systems when new calls are blocked when no channels are available. However, there is an upper limit to the number of users, $M_{max}$, for acceptable system operation [72].

In mixed service operation, of voice and data, the upper limit on the number of users for each service is different. Voice packets cannot be delayed for too long as speech quality will be degraded significantly; hence, voice packets are discarded by the receiver if they have been delayed longer than a maximum packet holding time, $\tau_{max}$.

In data packet transmission, by contrast, there may be no such severe limits on the maximum packet holding time. For some services, data packets may be delayed until they can be successfully transmitted. Thus in case of congestion, voice packets suffer from being discarded because of excessive delay, while other data packets merely suffer from delay. Consequently, the system does not collapse when an overload occurs as the degradation is rather smooth. Let us define an overload probability, $P_O$ as [72]:

$$P_O = \text{fraction of time with } M_u > M_{max}, \tag{4.31}$$

where $M_u$ is the number of ongoing calls in a cell. In a PRMA system, we will not concern ourselves with handover failure as we assume that a handover to a new BS is done during the interval between talk spurts, by means of an appropriate signalling process, which is out of the scope of our study. A new talk-spurt is then addressed to the new BS, and the number of connected users of the new BS increases. If this number exceeds the upper limit of the number of users, the new BS is overloaded, and this impairment is taken into account by the overload probability.

In a PRMA system, a user's access to an available channel is done rapidly, and there is generally no reliable prediction of the quality of the channel. Furthermore, channel quality monitoring cannot normally be performed due to the short duration of talk spurts, comparing to the averaging periods typically required for quality measurements. If the co-channel interference coming from other users results in a packet carrier-to-interference ratio, CIR, that is lower than the minimum required carrier-to-interference ratio, $\text{CIR}_{\text{req}}$, the packet is corrupted. We define an interference probability as

$$P_I = \frac{\text{number of corrupted packets}/s}{\text{total number of transmitted packets}/s} \tag{4.32}$$

Therefore, the most relevant constraints on PRMA performance comes from overload and interference probabilities. The maximum offered traffic which can be handled is given by:

$$A_{T_{max}} = \min(A_O, A_I) \tag{4.33}$$

where $A_O$ and $A_I$ are the upper values of offered traffic satisfying the constraint of $P_O$ and $P_I$.

We use the results reported in references [58, 73], where a PRMA carrier with a framelength of 16 ms and 20 time slots per frame can support up to 37 simultaneous users with an acceptable grade-of-service (packet dropping probability = 1%). Nanda also shows in reference [73] that it is possible to achieve within 10% of the maximum

channel utilisation with as few as 18 source channels. From this finding we formulate an upper limit $M_{max}(j)$ for PRMA with FCA as $M_{max} = 37N/20$, $N \geq 18$, where $N$ is the number of available channels in a cell. The overload probability $P_O$ is evaluated considering that call statistics follow a Poisson distribution [74], that is:

$$\begin{aligned} P_O &\triangleq \Pr\{M > M_{max}\} = 1 - \Pr\{M \leq M_{max}\} \\ &= 1 - \sum_{M=0}^{M_{max}} A_T^M \exp(-A)/M!, \end{aligned} \tag{4.34}$$

where $A_T$ is an offered traffic in a cell, and $M$ is a number of current connections.

For systems employing flexible channel allocation schemes, where the number of channels available at a cell is varied according to traffic load, $M_{max}$ is the function of a number of channels at a cell. We consider a system where channel allocation is based on the GSM-carrier assignment, and the number of traffic channels $N_{TCH}(j)$ for $j$ carriers assigned to a cell is shown in Table 4.4.

Results from reference [73] shows that for seven and 14 slots per frame on each direction (uplink and downlink), corresponding to one and two allocated GSM carrier pairs, the system examined can supported nine and 23 conversations, respectively. From this finding we formulate an upper limit $M_{max}(j)$ for a PRMA base station with $j$ available carriers as

$$M_{max}(j) = \begin{cases} 9 & \text{if } j = 1 \\ 23 & \text{if } j = 2 \\ 37N_{TCH}(j)/20 & \text{if } j > 2 \end{cases} \tag{4.35}$$

Generally, the traffic threshold $A_{TH}(j)$ is obtained by calculating the carried traffic corresponding to the required GOS. In this case, we consider the GOS as the probability that the system is overloaded, $P_O$. We do not consider $P_I$ because it is not easy to calculate $P_I$ as there are too many parameters involved. We maintain the GOS of $P_O \leq 1\%$ by setting $A_{TH}(j)$ to the offered traffic, $A_T$, that gives $P_O$ equal to 1%. The traffic thresholds for the PRMA system are tabulated in Table 4.4.

We performed a simulation of a packet network in a microcellular environment. The network was allocated with 7 MHz bandwidth, accommodating 16 GSM carrier pairs. The speech activity was 43% according to references [58, 73]. Each BS in the FCA system was allocated four carriers. Each microcellular BS provided the coverage in the streets of 10416 $m^2$.

Figure 4.16 shows the $P_O$ and $P_I$ performance versus the average number of users per microcell for the microcellular networks under the uniform traffic scenario. From

| no. of carriers, j | 1 | 2 | 3 | 4 | 5 | 6 | 7 | 8 | 9 | 10 |
|---|---|---|---|---|---|---|---|---|---|---|
| $N_{TCH}(j)$ | 7 | 14 | 22 | 30 | 37 | 45 | 53 | 61 | 69 | 77 |
| $M_{max}(j)$ | 9 | 23 | 40 | 49 | 68 | 83 | 97 | 112 | 127 | 142 |
| $A_{TH}(j)$ | 4.1 | 14 | 27.5 | 35 | 51 | 64 | 76.4 | 89.7 | 103 | 116.5 |

Table 4.4: Traffic threshold in Erlang, the number of traffic channels and the upper limit numbers of simultaneous conversations for a current number of carriers at a PRMA base station

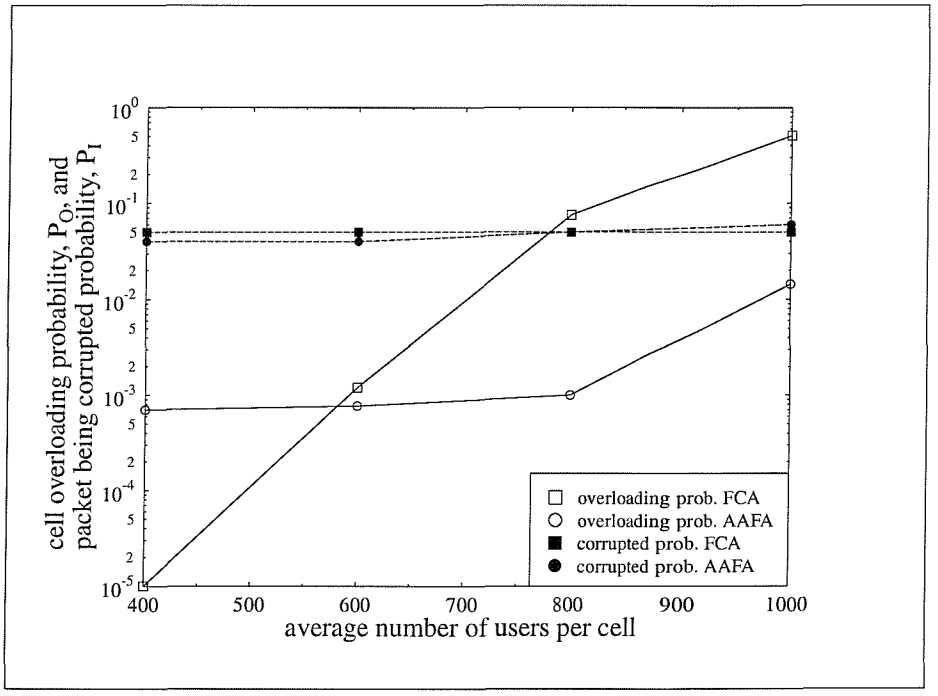


Figure 4.16: GOS performance comparison for PRMA microcells with uniform traffic distribution

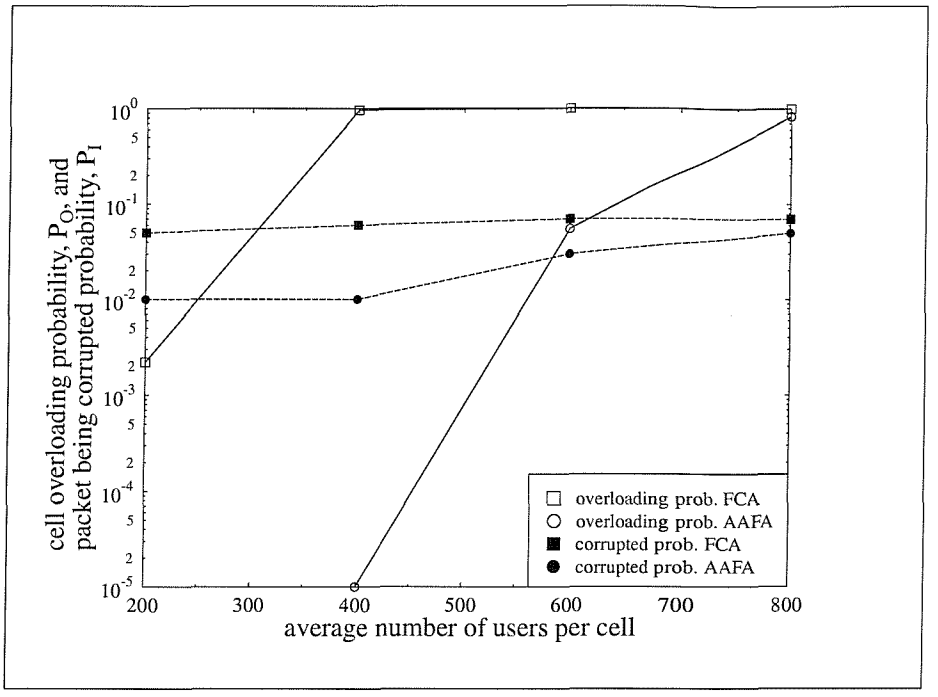


Figure 4.17: GOS performance comparison for hot-spot PRMA microcells with non-uniform traffic distribution

this figure, the AAFA system provided better overloading performance when the traffic load was higher than 580 users per cell, but with a poorer overloading performance at lower traffic loads.

However the packet corrupting performance of the AAFA network was the same as the FCA network. For the GOS of $P_I = 1\%$, the AAFA improved the system capacity over the FCA network by 38%, i.e., from 700 users per cell to 970 users per cell.

Figures 4.17 and 4.17 show the performance of the AAFA under the non-uniform traffic scenario. Figure 4.17 is the teletraffic performance at the hot-spot microcells, where the majority of users visit and are shown in shaded areas in Figure 4.8. The other microcells not shown in shaded areas are the cold-spot cells. The overloading performance of the AAFA network is superior than the FCA network in both the hot-spot cells and the cold-spot cells. The call dropping performance of the AAFA network is marginally better than the FCA network for the hot-spot microcells, and is the same as the FCA network for the cold-spot microcells. For GOS of $P_I = 1\%$ in the hot-spot cells, the AAFA network increases the system capacity by 120 %, i.e., from 250 to 550 users per cell. This is equivalent to carried teletraffic of 342 and 754

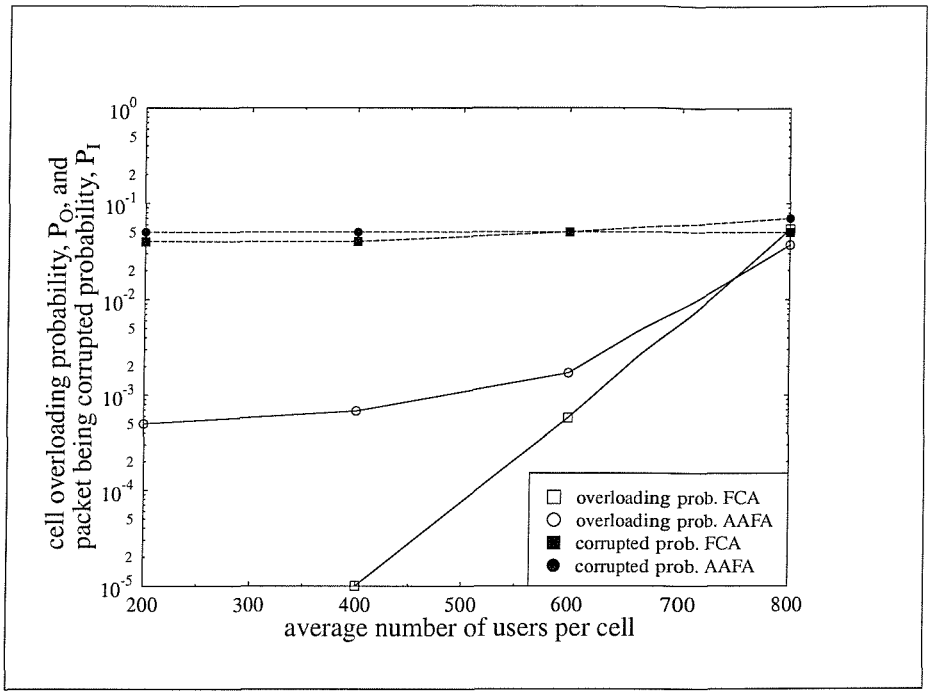


Figure 4.18: GOS performance comparison for cold-spot PRMA microcells with non-uniform traffic distribution

Erlang/MHz/km$^2$, respectively.

## 4.8 Conclusion

A novel method of channel allocation for mobile communication networks is presented and studied in this Chapter. The algorithm is called adaptive autonomous frequency assignment (AAFA), as is inspired from an earlier work of autonomous frequency planning [12]. The algorithm is designed to update channel allocations according to the changes in the propagation environment and the traffic distribution. We have created a simulation model to test the performance of our algorithm in different cellular environments, including macrocellular networks, microcellular networks and picocellular networks. We also simulated a packet mobile communication microcellular network based on a PRMA protocol. The results shows that the AAFA network provides robustness and higher system capacity than the conventional FCA system in all cellular environments. The results of the PRMA simulation also indicates that the AAFA algorithm is suitable for packet radio access as well as circuit-switched

wireless system.

Although the performance results advocate DCA-based implementations, there are still many practical problems associated with the introduction of DCA to existing systems, such as GSM. In particular, further research is required as to how the information exchanges among BSs and BSCs can be implemented. Further related notes on the application of DCA in the context of GSM-based cellular networks can be found for example in reference [75]. Finally, it is worth stressing that in high capacity multilayer cellular systems, where the teletraffic generated by the users is non-uniformly distributed over the service area, there is always a chance that the system becomes congested and a gradual upgrading of the network is a necessity. This implies that in addition to deploying multilayer cells DCA could be introduced in the various areas, as soon as they become congested.

# Chapter 5

# Spectrum Sharing for Multilayer System

## 5.1 Introduction

In the early stages of deploying a mobile cellular network the emphasis is on radio coverage and large macrocells are deployed. So at start-up the number of base stations are kept to a minimum and so is the infrastructure costs and the number of users, and hence the income is small. However, with the rapid growth of cellular subscribers the network operator needs to increase the system capacity. There are many strategies to do this, such as to employ sectorised antennae, where each cell site is split into several sectors, for example, three sector cells are obtained by using 120 degree sectorised antennae. The sectorised cell structure reduces the interference facilitating smaller reuse clusters where each cell can reuse channels more efficiently. Thus the system capacity is increased without installing extra base stations. For example, if a conventional macrocell required a reuse structure of 7 cells per cluster, and a sectorised cell structure with three sectors per cell could operate with only four cells per cluster, then the capacity is increased by 43 %.

Another strategy to increase capacity is to employ an underlay-overlay technique, where each cell site participates in two cell clusters, i.e., the underlay is the inner coverage area, and the overlay is the outer coverage area of a cell. The system capacity is increased because the required reuse cluster size of the underlay cells is smaller than overlay cell cluster while the signal-to-interference ratio experienced by mobile stations is approximately the same. The study in reference [76] shows that

in GSM networks the underlay-overlay system can provide 25-40 % improvement in system capacity.

The capacity enhancement strategy, called multiple reuse partition (MRP), proposed by Ericsson has been shown to double a capacity of a conventional macrocells with 12 cells per cluster [77]. The basic principle of MRP is to divide the spectrum into subbands having a different number of carrier frequencies. These subbands are then planned and allocated to each cell separately, and with different frequency reuse patterns. The interference may vary greatly between different frequencies due to the difference of the reuse. However, the MRP system relies on frequency and interference diversity resulting from frequency hopping to ensure that link quality is maintained in spite of the tight reuse of some frequencies.

Fractional loading is another strategy of increasing system capacity [3, 78]. The method does not require frequency planning, and all frequencies are allocated to each cell site which are sectorised by at least six sectors per cell in order to maintain the same capacity as of the sectorised cell system with three sectors per cell under the uniform traffic scenario, as explained in Chapter 2. Apart from the benefit of not required frequency planning, fractional loading, however, provided a significant capacity increase with non-uniform traffic distributions. For example, compared with a sectorised cell system with four cells per cluster, the capacity improvement is up to four times greater than sectorisation, and 12 times greater than a conventional macrocell structure, assuming a non-uniform traffic condition. We consider that the fractional loading is the best method of increasing the system capacity without installing additional BSs.

Cell splitting [1, 49] is a capacity enhancement method that requires additional BSs that results into a shorter distance between cells, and therefore cell radii and cell sizes are smaller. The system capacity is increased as the spectrum is reused more frequently over the same area. However, in urban centers with their tall buildings, the spectrum can be reuse more efficient by employing microcells where BS antennae are mounted below rooftop levels on lamp posts or on the outside walls of buildings. A microcell reuse cluster may be smaller than a macrocell reuse cluster, because of the buildings acting as electromagnetic shields between co-channel cells [24].

Early cellular networks were designed for mobile users in cars, and consequently the radio coverage was concentrated in streets. However, due to the life style of mobile users they tend to rely on their mobile phones more than on other communication

methods, and most cellular calls are made from inbuildings nowadays. The advent of personal communication systems (PCS's) required an extensive mobile cellular service within building from mobile cellular operators. Cordless systems and wireless PBX are competitors of indoor cellular systems, but their roaming capability is extremely limited. Enormous traffic capacity is required to fulfill the traffic demand within buildings, where the user density is very high. Currently macrocells offer limited indoor coverage, but this is often insufficient in the centre areas of city blocks. The indoor coverage of microcells may required the deployment of many microcells as transmission power levels are relatively low. A number of different solutions have been proposed. The straight forward solutions which have been implemented in many networks are distributed antennae [5] with inbuilding picocells to provide the capacity [79, 80, 81].

From the above discussion, we envisages that high capacity cellular networks require the deployment of macrocells, microcells and picocells. Microcells and picocells are located where there is a great demand of traffic capacity, such as the urban areas and office buildings. The network that contains microcells and picocells in additional of macrocells is defined as a multilayer network, where different cells have overlapping coverage. Here we consider a network with three layers, the macrocell layer, the microcell layer and the picocell layer.

There are two main methods for allocating spectrum for different cell layers, namely, frequency partitioning and spectrum sharing. Frequency partitioning splits the radio bandwidth and allocates each subband to each layer [62]. However, this approach may lead to a loss of trunking efficiency. For operators with small bandwidth allocation, this may lead to a significant loss of capacity in the macrocellular layer as the available frequencies for each layer becomes unacceptably low. Spectrum sharing allows the same frequencies to be used by different layers continuously. In reference [82], a channel borrowing algorithm allows the under-layer to use the free channels of adjacent macrocells. However, channel borrowing is only effective when the surrounding macrocells have light traffic. When all the macrocells have heavy traffic, not many free channels can be used by under-layer microcells. A fixed frequency planning scheme that allows the microcells at some locations to reuse macrocell channels, is presented in reference [83], where the position of the microcells is restricted to a certain area. Furukawa demonstrated in reference [84] that a distributed dynamic channel assignment scheme associated with power control enables the microcells to reuse some of

the macrocellular channels. The DCA scheme involves a carrier sensing on a call by call basis which requires a longer call setup, and handover period. In addition, the channel priority of each channel is set according to the successful rate of channel requisition. In other words, the more frequent the channel is acquired, the higher its priority becomes within the channel priority list. Consequently, it may take a long time to stabilise the channel priority list. Grandhi proposed a frequency scavenging algorithm that selects some macrocell carriers to be use by microcells, by measuring the interference level of macrocell carriers, and determining the carriers where probability of being interfered by macrocells is low [85]. The scheme requires a long setup time to perform the channel assignment, and needs some coordination between microcells in order to form a microcell reuse cluster.

A DCA scheme with channel exclusion is proposed in reference [86] in order to enable microcells to use excluded macrocell channels. Several exclusion schemes are studied. A common exclusion scheme, equivalent to frequency partitioning, where each macrocell refrains from using the same frequency set, perform worst, and a random exclusion where the exclusion channel list of each macrocell is randomly selected, gives the best performance. A simulation study in reference [87] shows that microcells can reuse some macrocell frequencies, as long as the microcells are small enough compared to the macrocells. Coombs and Steele investigated a combined macrocellular network and microcellular network, and observed that the frequency partitioning provides a better spectrum efficiency that sharing the same spectrum between the microcells and macrocells [88]. Their results are pessimistic, because they did not take into account of the effects of electromagnetic shielding caused by the low antenna elevation of micro-BS. Consequently, the inter-layer interference of the uplink microcells and downlink macrocells is inherently low.

A study by Rappaport provides a simulation method to determine the channel availability for sharing between inbuilding and outdoor cellular systems [89]. Picocellular systems were assumed to operate with radio frequency (RF) power levels low enough that they cause negligible interference to the outdoor macrocellular systems. Field strength measurement information of macrocellular systems at a 42 floor building were used to determine the downlink channel interference to the indoor picocellular system caused by the macrocellular network. Results show that indoor reuse is practical as long as interference levels of about -85 dBm from the outdoor macrocellular can be tolerated.

In this Chapter we investigate some practical issues of sharing spectrum between macrocellular systems, street microcellular systems and inbuilding picocellular systems. These issues including channel allocation and power setting problems. The remain of the chapter is arranged in six sections. In Section 5.2 we describe the system architecture and develop a theoretical framework to determine channel allocation and power setting for microcells. In Section 5.3 we proposed a method of sharing spectrum between overlaying macrocells and underlaid cells, namely a fixed spectrum sharing algorithm (FSSA). Channel allocation and power setting of street microcells and inbuilding picocells are analysed using mathematical modelling. In Section 5.4, we propose an automatic scheme of channel allocation for underlaid microcells and underlaid picocell, namely a dynamic spectrum sharing algorithm (DSSA). A summary of the work and our conclusion are given in Section 5.5.

## 5.2 System architecture

Generally the channel allocation of any cellular mobile radio systems is governed by the minimum tolerable signal-to-interference ratio ($\text{SIR}_{min}$). The major interference is co-channel interference which is from different users occupying the same channels. The value of $\text{SIR}_{min}$ is the minimum SIR that can still provide the acceptable bit error rate. It is system dependent, related to a number of system specifications including the multiple access scheme, the modulation, the speech coding, and the channel coding. Our analysis is based around a GSM-like system. The $\text{SIR}_{min}$ required for the system is set to 12 dB.

### 5.2.1 Macrocellular network

We use a hexagonal macrocellular model, where hexagonal-shaped macrocells are tessalated to provide contiguous service coverage, as shown in Figure 5.1 for macrocells with omni-directional antennae. A cell cluster is outlined in bold and replicated over the coverage area. The frequency reuse distance $D$ between co-channel cell sites is related to the cell radius $R$ and the cluster size $K$, and is given by $D = R\sqrt{3K}$ [1]. If the cells are formed by omni-directional antennae, interference is received from all six significant co-channel cells. In the sectorised cells with directional antennae being deployed, the number of significant interfering cells is reduces to two. In both cases,

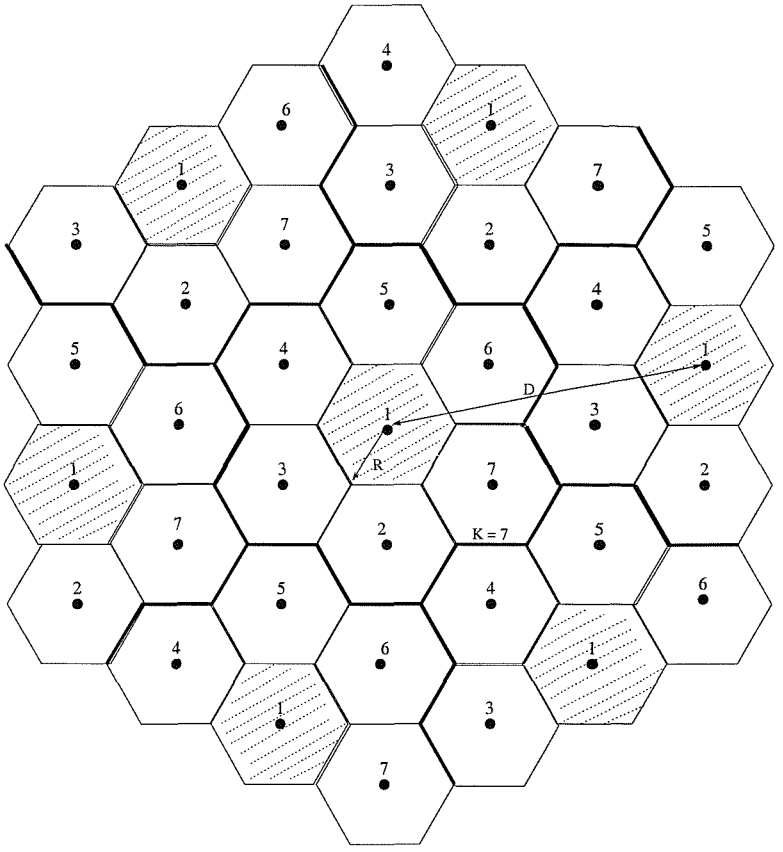


Figure 5.1: Illustration of the cellular frequency reuse concept. Cells with the same number use the same set of frequencies.

the SIR or the system is given by [1]

$$\mathrm{SIR}_{macro} = \frac{(D/R)^{\gamma}}{N} = \frac{(\sqrt{3K})^{\gamma}}{N}, \tag{5.1}$$

where $\gamma$ is the path loss exponent, and $N$ is the number of significant co-channel cells.

### 5.2.2 Microcellular network

Microcells are introduced into a macrocellular network and are organised in cluster sizes of $K_m$. We use the rectilinear street microcellular network shown in Figure 2.11b, where the microcells are arranged with a cluster size $K_m$ of 4. The reuse distance is expressed by

$$D_m = 2R_m\sqrt{K_m}, \tag{5.2}$$

where $R_m$ is the LOS distance from a BS to its cell boundary. The LOS coverage of microcells and the two slope path loss law [70] having a break distance of $D_b =$

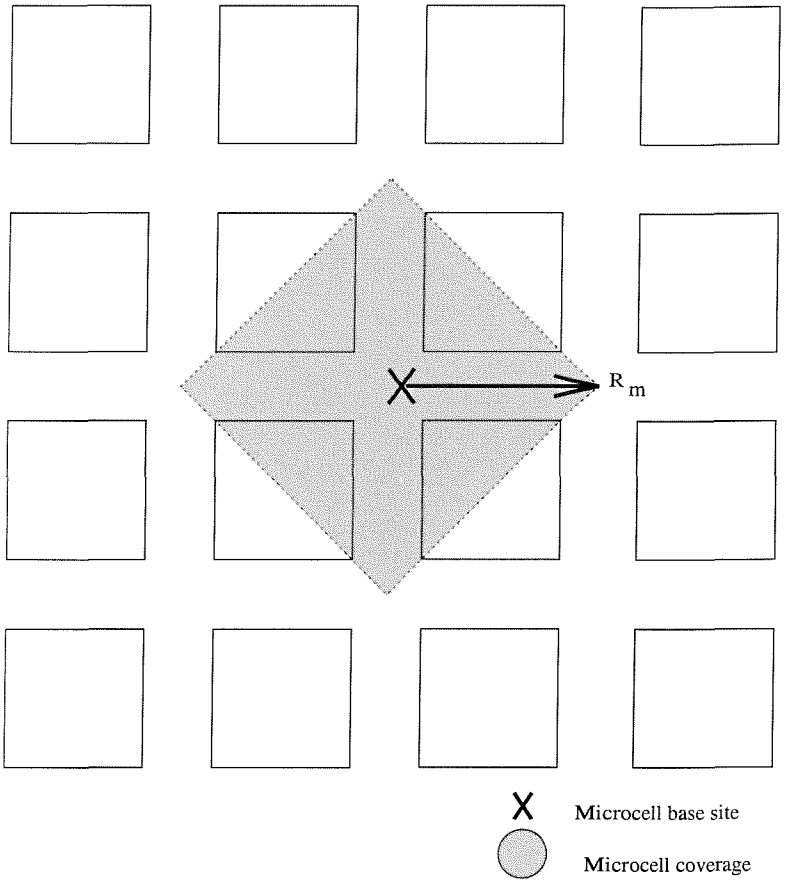


Figure 5.2: Illustration of the coverage area of a street microcell

$4h_b h_m/\lambda$ is used in our analysis. The height of base station antennas and mobile station antennas is $h_b$ and $h_m$, respectively, and $\lambda$ is the carrier wavelength. The power received at a mobile from a microcell base station at a distance $d$ away is given by

$$P_R = \begin{cases} P_T(4\pi d/\lambda)^{-2}, & \text{if } d < D_b \\ P_T D_b^2(4\pi d^2/\lambda)^{-2}, & \text{if } d \geq D_b \end{cases} \tag{5.3}$$

where $P_T$ is the transmission power. For an operating frequency of 1.8 GHz, a BS antenna height of 6 metres and a MS antenna height of 1.5 metres, the value of $D_b$ is 216 metres. We assume that the BS antenna is positioned such that $R_m$ is within $D_b$, i.e., $R_m \leq D_b$, and the co-channel reuse distance is always beyond $D_b$, i.e., $D_m > D_b$. The received power of an MS located at $d = R_m$ is

$$S = P_T(4\pi R_m/\lambda)^{-2}. \tag{5.4}$$

From Figure 2.12, we can see that there are two significant interferers, and the separation distance between the microcell and its significant co-channel microcells is set to $D_m$. The combined received interference from the two interferers is therefore given by

$$I = 2P_T D_b^2 (4\pi D_m^2/\lambda)^{-2}, \tag{5.5}$$

and by substituting $D_m$ in Equation 5.2 the SIR is

$$\text{SIR}_{micro} = 8R_m^2 D_b^{-2} K_m^2. \tag{5.6}$$

### 5.2.3 Picocellular network

We consider a rectangular office building illustrated by Figure 2.24 and 2.25. Our picocells have a square shape with a width of $2R_p$, where $R_p$ is the nearest distance from the pico-BS to its cell boundary. The received power of an MS located at the horizontal distance of $d = R_p$, is

$$S = P_T (4\pi R_p/\lambda)^{-2} 10^{\frac{L_w R_p + L_f N_f W_r}{10 W_r}}, \tag{5.7}$$

where $L_f$ is the floor loss, $N_f$ is the number of floors between the transmitter and the receiver, $L_w$ is the wall loss, and $W_r$ is the room width. We consider the reuse planning described in Chapter 2, with a horizontal cluster size of $K_h$ and the vertical cluster size of $K_v$. The total picocellular cluster size is $K_p = K_h K_v$. The horizontal co-channel reuse distance is $D_p = 2R_p\sqrt{K_h}$. and we have the total received interference as

$$I = N_h P_T (4\pi D_p/\lambda)^{-2} 10^{\frac{L_w D_p}{10 W_r}} + N_v P_T (4\pi R_p/\lambda)^{-2} 10^{\frac{L_w R_p + L_f K_v W_r}{10 W_r}}, \tag{5.8}$$

where $N_h$ is the number of the significant horizontal co-channel interferers and $N_v$ is the number of the significant vertical co-channel interferers. The SIR is therefore given by

$$\text{SIR}_{pico} = (0.25 N_h K_h^{-1} 10^{\frac{L_w R_p (2\sqrt{K_h} - 1)}{10 W_r}} + N_v 10^{\frac{L_f N_v}{10}})^{-1}. \tag{5.9}$$

### 5.2.4 Choosing a reuse cluster size

Basically the cluster size of cellular systems are chosen to satisfy the condition of

$$\text{SIR} \geq 10^{\Lambda/10}, \tag{5.10}$$

where $\Lambda$ represent the required SIR in dB. By substituting the SIR term using Equations 5.1, 5.6, and 5.9, we obtain $K$, $K_m$ and $K_p$, respectively.

## 5.3 Fixed spectrum sharing algorithm

In this section, we consider a spectrum sharing algorithm, namely the so-called farthest reuse technique, which was used in Reference [84], suggesting to invoke underlaid microcells or picocells, in order to reuse channels assigned to the farthest macrocells in the same cluster. We begin by analysing the reuse structure of the spectrum sharing algorithm in different macrocell cluster sizes. Then we analyse the SIR performance of an underlaid microcellular network sharing some macrocellular channels, and also the SIR performance of the overlaying macrocells. Next we address the SIR performance of the inbuilding picocellular network sharing macrocellular channels, and the SIR performance of the overlaying macrocellular networks.

### 5.3.1 Farthest reuse algorithm

For a macrocell in the macrocellular network with a cluster size of at least nine cells per clusters, there are always at least two macrocells in the same cluster that are not adjacent to the macrocell. Figure 5.3 shows macrocellular planning with different cluster sizes. If microcells and picocells are required to be deployed in a macrocell labelled $A$ in Figure 5.3, the frequencies assigned to macrocells which are not adjacent to macrocell $A$, i.e., macrocells outside the dotted boundary, may be reused by the underlaid microcells and picocells. For $K = 9$, the farthest macrocells in the same cluster is macrocell $B1$ and $B2$. Hence the channel sets assigned to $B1$ and $B2$, could be reused by the underlaid cells in cell $A$. That is, two channel sets out of the total nine are available for sharing between overlaying macrocells and underlaid cells, i.e., approximately 20 % of radio resource is shared. We collectively call these channels as "channel set B".

We observe that the number of significant interlayer macrocell interferers is three. Cells labelled B1 with dotted circles in Figure 5.3 are the nearest interferers that use channel set $B1$. The interlayer reuse distance for $K = 9$ is three times the cell radius, $3R$, For macrocells with a cluster size of 12, cells $B1$ and $B2$ are the farthest cells with an interlayer reuse distance of $3.46R$. For $K = 16$, there are three macrocells being the farthest cells, i.e., $B1$, $B2$ and $B3$, The number of significant interferers of channel set $B$ is two, and the interlayer reuse distances for channel set $B$ is $3.46R$. For $K = 19$, the number of the farthest cells is six, i.e., cells $B1$ to $B6$, with an interlayer reuse distance of $3.46R$, and the number of significant interferers is two. For $K = 21$,

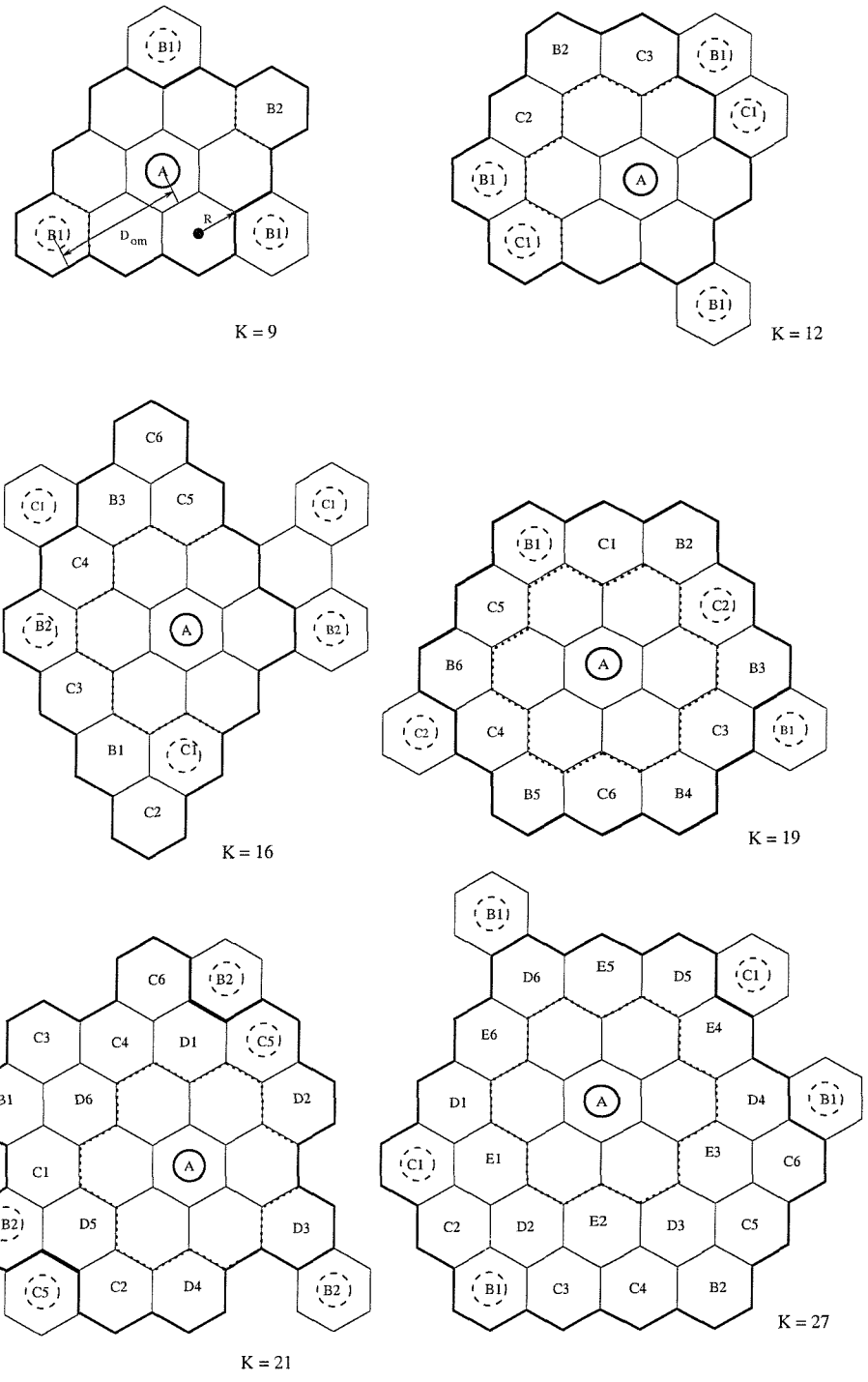


Figure 5.3: Clusters of hexagonal cells; $K = 9, 12, 16, 19, 21, 27$.

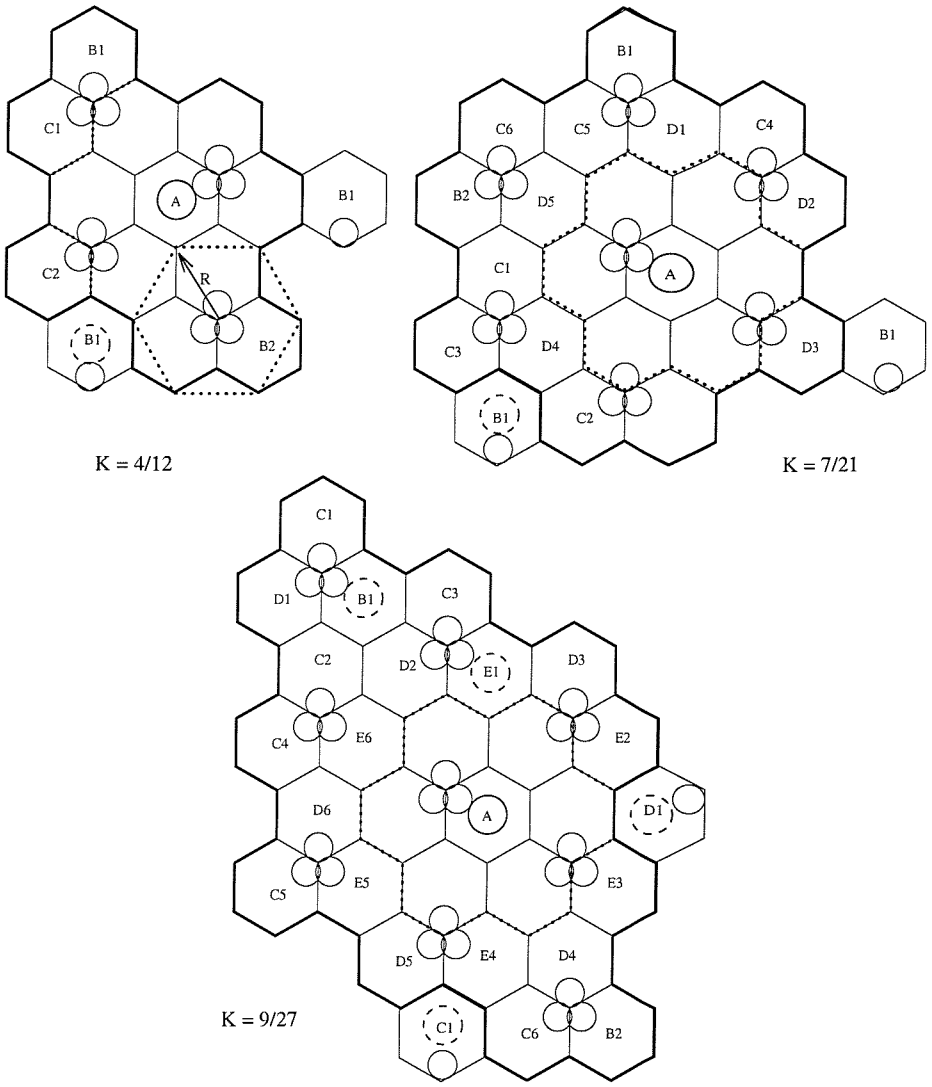


Figure 5.4: Clusters of sectorised cells; $K = 4/12, 7/21, 9/27$.

cells $B1$ and $B2$ can be reused with the interlayer reuse distance of $4.61R$, and the number of significant interferers of three. For $K = 27$ we have two cells, $B1$ and $B2$, with the interlayer reuse distance of $5.2R$. The number of significant interferers of channel set $B$ is three.

Table 5.1 summarises the planning parameters for macrocells with different cluster size, including the number of frequency sets available for interlayer reuse, $M_a$, the number of interlayer macrocell interferers, $N_{om}$, the macrocell co-channel reuse factor, $Q = D/R$ ($D$ is the co-channel reuse distance and $R$ is the macrocell radius, and the overlay co-channel reuse factor, $Q_{om} = D_{om}/R$. $D_{om}$ is the distance from overlay

| Cluster size | $Q$ | $Q_{om}$ | $N_{om}$ | $M_a$ |
|---|---|---|---|---|
| 9 | 5.2 | 3 | 3 | 2 |
| 12 | 6 | 3.46 | 3 | 2 |
| 16 | 6.9 | 3.46 | 2 | 3 |
| 19 | 7.5 | 3.46 | 2 | 6 |
| 21 | 7.94 | 4.61 | 3 | 2 |
| 27 | 9 | 5.20 | 3 | 2 |
| 4/12 | 3.46 | 2 | 1 | 2 |
| 7/21 | 4.58 | 2.66 | 1 | 2 |
| 9/27 | 5.2 | 3 | 1 | 2 |

Table 5.1: Frequency planning parameters for spectrum sharing systems

macrocell interferers to the co-channel microcell.

Figure 5.4 shows frequency planning with different cluster sizes for sectorised macrocellular systems. Each base site employs three directional antennas and is arranged into three sectors shown. The original cell shapes before being sectorised are shown by dotted hexagons of radius $R$. After being sectorised the coverage area of one base site becomes three small hexagons attached together with the base station located at its center. Firstly, we consider a 4/12 planning, i.e., the cluster size is formed by four base sites covering 12 sectors. The intra-layer reuse distance, $Q$, is $3.46R$. Observing that at a sector labelled $A$, the farthest sectors away from sector $A$ is $B1$ and $B2$. The interlayer reuse distance is $2R$, which is approximated from the middle of sector $A$ to the middle of sector $B$. The cell radius $R$ shown in Figure 5.4 is

$$R = D_b/\sqrt{3}, \tag{5.11}$$

where $D_b$ is the separating distance between two nearest base sites. For 7/21 planning, a macrocell cluster is formed by seven base sites covering 21 sectors. The interlayer and intra-layer reuse distances are 4.58 and $2.66R$, respectively. The intra-layer and intra-layer reuse distances for 9/27 planning, where a macrocell cluster of nine base sites is used, are $5.3R$ and $3R$, respectively.

### 5.3.2 Introducing street microcells into macrocellular network

One of the problems associated with designing the spectrum sharing system is to assign power to the microcells such that the microcells do not cause excessive interference to the macrocells. In addition, the microcell transmission power must sufficiently strong to combat successfully the co-channel interference from the macrocells. The results from reference [87] suggest that the micro-downlink is the critical link as most MSs experience high interference from macro-BSs, while the micro-BSs which are isolated from macro MSs by electromagnetic shielding of the buildings notice very little interference from macro-MSs. For the macrocells, the uplink is the critical link while the downlink is almost unaffected, due to the isolation of the micro-BSs.

In order to determine the practicality of deploying the spectrum sharing scheme we determine the SIR performance of the critical links, including the macro-uplink and the micro-downlink. The SIR of the macro-uplink is extended to

$$\begin{aligned} \mathrm{SIR}_{mac-u} &= \frac{S}{I_{mac}+I_{mic}} \\ &= \frac{P_{mac}R^{-\gamma}}{NP_{mac}D^{-\gamma}+P_{mic}N_{im}D_{om}^{-\gamma}} \\ &= (NQ^{-\gamma}+\Delta P N_{im}Q_{om}^{-\gamma})^{-1}, \end{aligned} \tag{5.12}$$

where $N$ is the number of significant interfering macrocells, $N_{im}$ is the number of significant interfering microcells, and $\Delta P$ is the power ratio between the transmissions from the microcells and macrocells, i.e., $\Delta P = P_{mic}/P_{mac}$. We have $Q = D/R$ and $Q_{om} = D_{om}/R$, which are the intra-layer and the inter-layer co-channel reuse factors, respectively. To determine the upper limit of $\Delta P$ we substitute Equation 5.12 into Equation 5.10. The maximum microcell power ratio is

$$\Delta P \leq \Delta P_{max} \equiv \frac{1-10^{\Lambda/10}NQ^{-\gamma}}{10^{\Lambda/10}N_{im}Q_{om}^{-\gamma}} \tag{5.13}$$

We also consider the SIR of micro-downlink which is expressed by

$$\begin{aligned} \mathrm{SIR}_{mic-d} &= \frac{S}{I_{mic}+I_{mac}} \\ &= \frac{P_{mic}R_m^{-2}10^{L_{1-m}/10}}{2P_{mic}D_b^2D_m^{-4}10^{L_{1-m}/10}+P_{mac}N_{om}D_{om}^{-\gamma}10^{L_{1-km}/10}} \\ &= (0.125R_m^{-2}D_b^2K_m^{-2}+\Delta P^{-1}N_{om}R_m^2R^{-\gamma}Q_{om}^{-\gamma}10^{\Delta L/10})^{-1} \end{aligned} \tag{5.14}$$

where $N_{om}$ is the number of significant macrocell interferer, $D_{om} = Q_{om}R$ is the distance from the macrocell interferers, and $\Delta L$ is the decibel path loss difference between the microcell pathloss at one metre and the macrocell pathloss at one kilometer,

i.e.,

$$\Delta L = L_{1-km} - L_{1-m}. \tag{5.15}$$

In the previous chapter, the Hata's macrocell pathloss at one km is -137.5 dB, and the microcell pathloss at one metre is -37.5 dB, therefore $\Delta L$ is -100 dB. Note that the unit of $R_m$ and $D_b$ is in metre and the unit of $R$ is in kilometre. By substituting Equation 5.14 into Equation 5.10, we have the minimum microcell power ratio as

$$\Delta P \geq \Delta P_{min} \equiv \frac{N_{om} R_m^2 R^{-\gamma} Q_{om}^{-\gamma} 10^{\Lambda/10} 10^{\Delta L/10}}{1 - 0.125 R_m^{-2} D_b^2 K_m^{-2} 10^{\Lambda/10}} \tag{5.16}$$

Considering that the total extra capacity provided by microcells, $A_m = A_{mc} N_{im} K_m$, must be greater than the required extra teletraffic capacity, $A_i$, where $A_{mc}$ is the traffic capacity per microcell in Erlang and is a function of the number of carriers available at a microcell, $N_{fm}$. For GSM-like system, $A_{mc}$ is given by the function $A_{TH}(N_{fm})$ in Table 4.3, which the offered traffic for 5% call blocking probability. $N_{fm}$ can be obtain from

$$N_{fm} = \text{integer} \left\{ \frac{N_T M_a}{K K_m} \right\} \tag{5.17}$$

where $N_T$ is the total number of carriers, and $M_a$ is the number of frequency sets available for spectrum sharing between layers given in Table 5.1. We then obtain the minimum number of microcell clusters that satisfies the traffic requirement as $N_{im-t}$ which is obtain by rounding the following value up to the nearest integer;

$$N_{im-t} = \text{integer} \left( \frac{A_i}{A_{mc} K_m} \right). \tag{5.18}$$

To satisfy the SIR requirement at both the microcells and the macrocells, the condition $\Delta P_{min} \leq \Delta P_{max}$ must be satisfied. Using Equations 5.16 and 5.13, we obtain the range of $R_m$ for a microcell as,

$$R_{m-min} \leq R_m \leq R_{m-max}, \tag{5.19}$$

where

$$\begin{aligned}
R_{m-min} &= \sqrt{\frac{b}{1+\sqrt{1-bN_{im}/a}}}, \\
R_{m-max} &= \min \left( D_b, \sqrt{\frac{b}{1-\sqrt{1-bN_{im}/a}}} \right), \\
a &= \frac{R^{\gamma} Q_{om}^{2\gamma} (1 - 10^{\Lambda/10} N Q^{-\gamma})}{2 N_{om} 10^{2\Lambda/10} 10^{\Delta L/10}}, \\
b &= 0.25 D_b^2 K_m^{-2} 10^{\Lambda/10}.
\end{aligned}$$

We set the maximum $R_m$ to $D_b$, in order to comply with the propagation assumption used in this analysis. We observe that the condition, $(bN_{im}/a) < 1$, must be met

so that $R_{m-min}$ and $R_{m-max}$ are real numbers. To determine the number of $N_{im}$ we must consider the service area provided by the microcell network. Note that we use a diamond-shaped microcell as illustrated in Figure 5.2, and each microcell has a coverage of $2R_m^2$. The total area served by microcells, $S_m = 2R_m^2 N_{im} K_m$, must be greater than the area in which extra teletraffic capacity is required, $S_i$, i.e., $S_i \leq 2R_m^2 N_{im} K_m$, and the distance $R_m$ for a microcell is

$$R_m = \sqrt{\frac{S_i}{2K_m N_{im}}}. \tag{5.20}$$

By substituting $R_m$ given by the above equation into Equation 5.19, we obtain the range of the number of microcell clusters for the service area $N_{im-a}$ as

$$N_{im-min} \leq N_{im} \leq N_{im-max}, \tag{5.21}$$

where

$$N_{im-min} = \begin{cases} \frac{S_i}{2bK_m} & \text{if } S_i < 2aK_m \text{ and } K_m > \sqrt{0.25 \cdot 10^{\Lambda/10}}, \\ \frac{S_i}{bK_m} - \frac{S_i^2}{4abK_m^2} & \text{if } S_i \geq 2aK_m \text{ and } K_m > \sqrt{0.25 \cdot 10^{\Lambda/10}}, \\ \frac{S_i}{2K_m D_b^2} & \text{otherwise,} \end{cases}$$

$$N_{im-max} = \begin{cases} \frac{S_i}{bK_m} - \frac{S_i^2}{4abK_m^2} & \text{if } S_i < 2aK_m, \\ \frac{S_i}{2bK_m} & \text{if } S_i \geq 2aK_m, \end{cases}$$

and the terms $a$ and $b$ are given in Equation 5.19. Next we select the minimum number of microcell clusters required as

$$N_{im} = \max(N_{im-t}, N_{im-min}). \tag{5.22}$$

After that the upper limit of $R_m$ is obtained by substituting $N_{im}$ into Equation 5.19. The upper power limit and lower power limit are also calculated from Equations 5.13 and 5.16, respectively.

When the selected $N_{im}$ is greater than $N_{im-max}$, we have to increase $N_{im-max}$ in order to cope with the demand $N_{im}$. This can be achieved by decreasing the terms $b$, which is a function of the breaking distance $D_b$ as given in Equation 5.19. $D_b$ is a function of the height of the micro-BSs and is given by $D_b = 4h_b h_m/\lambda$ where $\lambda$ is the carrier wavelength, $h_b$ and $h_m$ are the heights of the micro BS antennas and micro MS antennas, respectively. Using this approach can increase $N_{im-max}$ up to $(h_{b0}/h_{b-min})^2$ times, where $h_{b0}$ is the original micro-BS antenna height, and $h_{b-min}$ is the minimum micro-BS antenna height. If $N_{im-t} \leq N_{im-max}(h_{b0}/h_{b-min})^2$, we obtain

the number of microcell clusters $N_{im} = N_{im-t}$, and the range of the new micro-BS antenna height as

$$h_{b-min} \leq h_{b-new} \leq h_{b0}\sqrt{\frac{N_{im-max}}{N_{im-t}}}. \tag{5.23}$$

However, if $N_{im-t} > N_{im-max}(h_{b0}/h_{b-min})^2$, lowering the micro-BS antenna height alone cannot provide enough microcell capacity. Observing Equation 5.21, parameters $K_m$ and $a$ need to be considered. We can increase $N_{im-max}$ by decreasing $K_m$, however, this approach is not practical because it will increase the amount of co-channel interference between the microcell clusters. Improving the microcell traffic capacity by changing the terms $a$ is not straight forward, although increasing $a$ raises $N_{im-max}$. This is because increasing $a$ involves increasing the macrocell cluster size $K$, and this reduces the number of channels per macrocell, and subsequently reduces the number of channels to be reused by the microcells. The number of channels available per microcell after increasing the macrocell cluster size from $K_0$ to $K_1$ is given by

$$N_{cm1} = N_{cm0}\frac{K_0}{K_1}, \tag{5.24}$$

where $N_{cm0}$ is the number of channels per microcell for $K_0$ macrocell cluster size. By not considering the loss of trunking efficiency due to the reduction of number of channels, the required number of microcell clusters becomes

$$N_{im-t-1} = N_{im-t-0}\frac{N_{cm0}}{N_{cm1}} = N_{im-t}\frac{K_1}{K_0}. \tag{5.25}$$

If $a_0$ and $a_1$ are the values of $a$ for $K = K_0$ and $K = K_1$, respectively, then from Equation 5.19 we obtain

$$a_1 = a_0\left(\frac{Q_{om1}^{2\gamma}N_{om0}(1 - 10^{\Lambda/10}N_1Q_1^{-\gamma})}{Q_{om0}^{2\gamma}N_{om1}(1 - 10^{\Lambda/10}N_0Q_0^{-\gamma})}\right), \tag{5.26}$$

where the parameters with subscript 0 and 1 are for $K = K_0$ and $K = K_1$, respectively. We simplify the above equation using the following assumptions;

- $N_0 = N_1 = N$,
- $N_{om0} = N_{om1}$,
- $Q_{om0} = \sqrt{K_0}$ and $Q_{om1} = \sqrt{K_1}$
- $Q_0 = \sqrt{3K_0}$ and $Q_1 = \sqrt{3K_1}$

and therefore we have

$$a_1 = a_0 \left( \frac{(3K_1)^{\gamma/2} - 10^{\Lambda/10}N}{(3K_0)^{\gamma/2} - 10^{\Lambda/10}N} \right). \tag{5.27}$$

We calculate the optimum value of $K_1$ which supports the maximum number of underlaying microcell traffic capacity, by solving the following differential equation

$$\frac{\mathrm{d}(N_{im-max-1}/N_{im-t-1})}{\mathrm{d}K_1} = 0, \tag{5.28}$$

where $N_{im-t-1}$ is given by Equation 5.25 and $N_{im-max-1}$ is given by

$$N_{im-max-1} = \frac{S_i}{bK_m} - \frac{S_i^2}{4a_1 bK_m^2}. \tag{5.29}$$

with the micro BS antenna height set to $h_{b-min}$. Equation 5.28 can be reduced to

$$\begin{aligned} & K_1^{\gamma+2} - K_1^{\gamma} - 2 \cdot 3^{-\gamma/2} \cdot 10^{\Lambda/10} N K_1^{2+\gamma/2} \\ & + 3^{-\gamma/2}(2 \cdot 10^{\Lambda/10}N - A(\gamma+2)/2)K_1^{\gamma/2} \\ & +3^{-\gamma} \cdot 10^{2\Lambda/10} N^2 K^2 + 3^{-\gamma} 10^{\Lambda/10} N(A - 10^{\Lambda/10}N) \;\; = \;\; 0 \end{aligned} \tag{5.30}$$

where

$$A = \frac{S_i((3K_0)^{\gamma/2} - 10^{\Lambda/10}N)}{4a_0 K_m}$$

Finally we select the number of microcell clusters as

$$N_{im} = \min(N_{im-t-1}, N_{im-max-1}), \tag{5.31}$$

and $N_{im-max-1}$ is the upper limit of the number of underlaying microcell clusters. The range of the micro-BS antenna heights is therefore given by

$$h_{b-min} \leq h_b \leq \max(h_{b-min}, (h_{b-min}\sqrt{N_{im-max-1}/N_{im-t-1}}). \tag{5.32}$$

The process of designing a spectral sharing for microcells underlaying macrocells described above is illustrated in the form of a flow chart in Figure 5.5.

### 5.3.3 Introducing inbuilding picocells into macrocellular network

In order to reuse the macrocell carrier frequencies in the picocellular systems, the transmitting power level of both the picocellular BSs and MSs must be low enough not to cause excessive interference to the existing macrocellular system. The interference

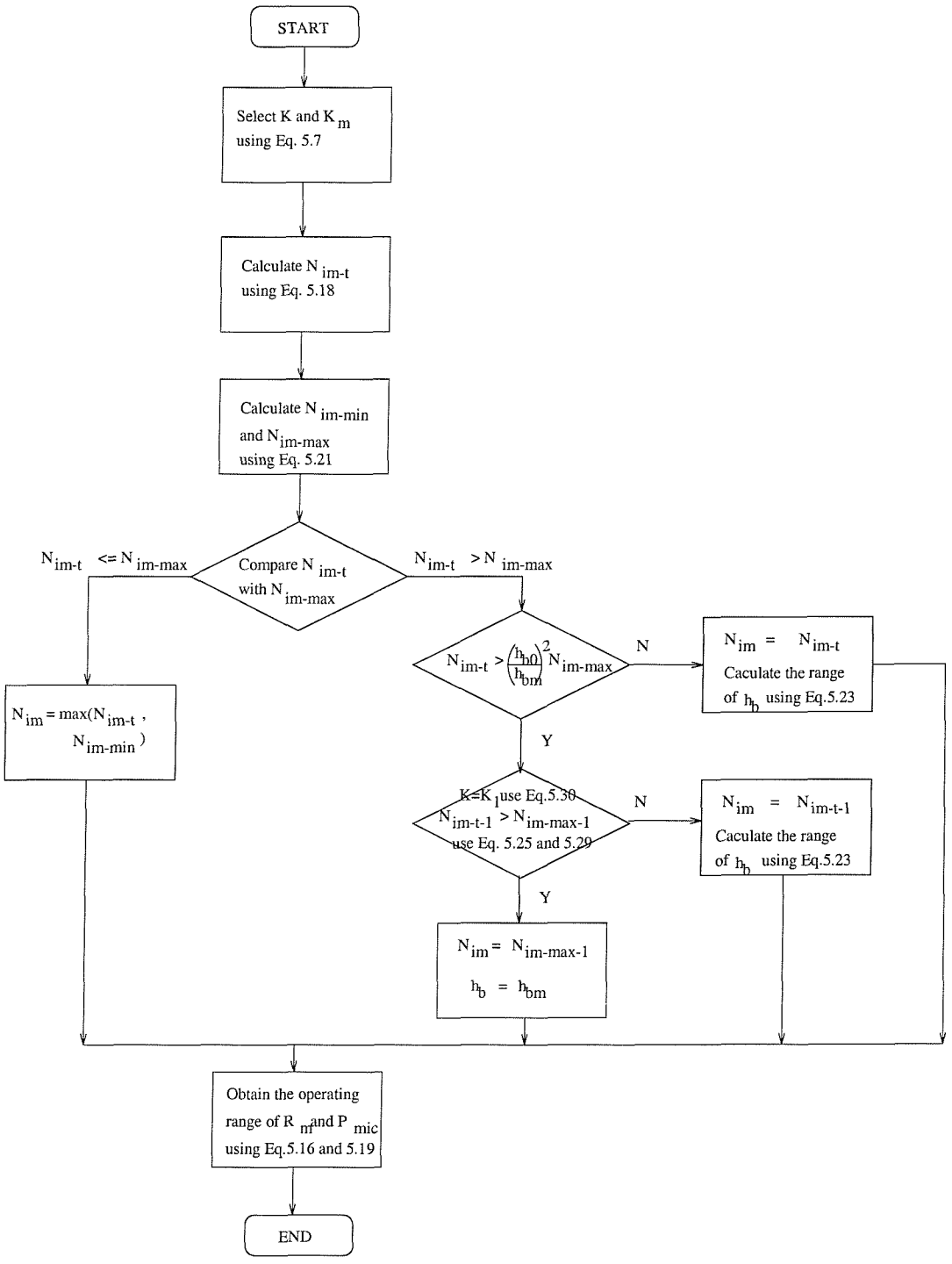


Figure 5.5: Flowchart illustrating the designing methodology of Fixed Spectrum Sharing Algorithm (FSSA)

from the picocells are likely to affect macrocell uplink more than macrocell downlink, because the high elevation of the macrocell BSs. Therefore we consider the macrocell uplink as the critical link in a macrocell for the spectrum sharing system. For the same reason, a picocell downlink is likely to suffer from macrocell interferers more than a picocell uplink, and we consider the picocell downlink as the critical link. Measurements of the signal strength received inside of buildings due to an external transmitter, suggested that the signal strength received inside a building increases with height [90, 91, 92, 93, 2]. At the lower floors of a building, the urban clutter induces greater attenuation and reduces the level of radio penetration. At higher floors, a LOS path may exist, thus causing a stronger incident signal at the exterior walls of the building. RF penetration loss has been found to be a function of frequency as well as height within the building. Measurements on the ground floor of a building by Turkmani [91] showed penetration loss of 14.2 dB, 13.4 dB and 12.8 dB for 900 MHz, 1800 MHz, and 2300 MHz, respectively. Turkmani [90] also reported that the building penetration loss decreases at a rate of 2 dB per floor from the ground level up to the ninth floor and then increases above the ninth floor. Similar results were also reported by Walker [92] and Durante [93]. Measurements have also shown that there are other parameters which influence the penetration loss, such as the percentage of window, compared to the building exterior surface area, and the presence of metallic tinted windows which can provide up to 30 dB penetration loss [2]. From the above reported measurements we conceive a simple model for building penetration loss in dB as,

$$L_b(F) = L_{bg} + FL_{bd}, \tag{5.33}$$

where $L_{bg}$ is the penetration loss at the ground floor of a building and is set to -13.4 dB for 1800 GHz transmission, $F$ is the number of floors, i.e., $F = 0, 1, 2, 3, ...$, and $L_{bd}$ is the penetration floor factor set to two dB. The validity of this model is up to the ninth floor of the building, as the measurements suggest. The signal strength received within the building due to macrocell BS is therefore obtained by adding the building penetration loss to the existing macrocell propagation model. The SIR of the macrocell-uplink when picocells reuse the same channel is given by

$$\begin{aligned} \text{SIR}_{mac-u} &= \frac{S}{I_{mac}+I_{pic}} \\ &= \frac{P_{mac}R^{-\gamma}}{NP_{mac}D^{-\gamma}+P_{pic}N_{ip}D_{om}^{-\gamma}10^{L_b/10}} \\ &= (NQ^{-\gamma} + \Delta PN_{ip}Q_{om}^{-\gamma}10^{L_b/10})^{-1}, \end{aligned} \tag{5.34}$$

where $N_{ip}$ is the number of significant interfering picocells, and $\Delta P$ is the power ratio between picocells and macrocells , i.e., $\Delta P = P_{pic}/P_{mac}$. We have $Q_{om} = D_{om}/R$, which is the inter-layer co-channel reuse factor. To determine the upper limit of $\Delta P$ we substituting Equation 5.34 into Equation 5.10. The maximum allowed picocell power ratio is found as,

$$\Delta P \leq \Delta P_{max} \equiv \frac{1 - 10^{\Lambda/10} N Q^{-\gamma}}{10^{(L_b+\Lambda)/10} N_{ip} Q_{om}^{-\gamma}}. \tag{5.35}$$

The SIR of picocell downlink with interference from macrocells is given by

$$\begin{aligned} \mathrm{SIR}_{pic-d} &= \frac{S}{I_{pic-h}+I_{pic-v}+I_{mac}} \\ &= (P_{pic}R_p^{-2}10^{\frac{L_w R_p}{10W_r}+\frac{L_{1-m}}{10}})(N_h P_{pic} D_p^{-2} 10^{\frac{L_{1-m}}{10}+\frac{L_w D_p}{10W_r}} \\ &\quad + N_v P_{pic} R_p^{-2} 10^{\frac{L_{1-m}}{10}+\frac{L_w R_p}{10W_r}+\frac{L_f K_v}{10}} + N_{om} P_{mac} D_{om}^{-\gamma} 10^{\frac{L_{1-km}+L_b}{10}})^{-1} \\ &= (0.25 N_h K_h^{-1} 10^{\frac{L_w R_p (2\sqrt{K_h}-1)}{10W_r}} + N_v 10^{\frac{L_f N_v}{10}} \\ &\quad + \Delta P^{-1} N_{om} Q_{om}^{-\gamma} R^{-\gamma} R_p^2 10^{\frac{(\Delta L+L_b)}{10}-\frac{L_w R_p}{10W_r}})^{-1}. \end{aligned} \tag{5.36}$$

Details of the parameters are already described in the previous section. Note that the unit of $R_p$ is in metre. By substituting the above equation into Equation 5.10, we have the minimum picocell power ratio as

$$\Delta P \geq \Delta P_{min} \equiv \frac{N_{om} Q_{om}^{-\gamma} R^{-\gamma} R_p^2 10^{\frac{\Delta L+L_b+\Lambda}{10}-\frac{L_w R_p}{10W_r}}}{1 - 0.25 N_h K_h^{-1} 10^{\frac{L_w R_p (2\sqrt{K_h}-1)}{10W_r}+\frac{\Lambda}{10}} - N_v 10^{\frac{\Lambda+L_f N_v}{10}}}. \tag{5.37}$$

Considering a scenario of installing a picocellular network in $N_{bld}$ buildings. Each building has $N_{off}$ offices, and each office has a traffic demand of $A_{off}$ Erlangs. The required number of picocell clusters to provide the traffic demand is

$$N_{ip} = \frac{N_{bld} N_{off} A_{off}}{A_{pc} K_h K_v}, \tag{5.38}$$

where $A_{pc}$ is the traffic capacity of a picocell. Similar to the microcell section $A_{pc}$ is given by $A_{TH}(N_{fp})$, where $N_{fp}$ is the number of carriers available at a picocell, and is expressed by

$$N_{fp} = \text{integer}\left\{\frac{N_T M_a}{K K_h K_v}\right\}. \tag{5.39}$$

With each office as a square of width $W_r$, and each picocell has a square-shape with $2R_p$ width, the area of a picocell is therefore $4R_p^2$, and the office area is $W_r^2$. The amount of traffic demand in a picocell can be obtained from

$$A_{pd} = A_{off} \frac{4R_p^2}{W_r^2}. \tag{5.40}$$

With the condition that the traffic capacity in a picocell must be equivalent or greater than the demand traffic, $A_{pc} \geq A_{pd}$, we obtain the upper-bound of $R_p$ as

$$R_p \leq \frac{W_r}{2}\sqrt{\frac{A_{pc}}{A_{off}}}. \tag{5.41}$$

The minimum and maximum picocell transmission power ratio can be obtained from Equation 5.37 and 5.35, respectively, using $R_p$ given by Equation 5.41 and $N_{ip}$ given by Equation 5.38.

We observe that to satisfy the SIR requirement of both macrocells and picocells, the condition $\Delta P_{min} \leq \Delta P_{max}$ must be applied, and we find the lower bound of the building penetration loss required to operate the spectrum sharing system is

$$L_b \leq L_{b-min} \equiv 5\log(c), \tag{5.42}$$

where

$$c = \frac{(1 - 10^{\Lambda/10}NQ^{-\gamma})(1 - 0.25N_hK_h^{-1}10^{\frac{L_wR_p(2\sqrt{K_h}-1)}{10W_r}+\frac{\Lambda}{10}} - N_v10^{\frac{\Lambda+L_fN_v}{10}})}{(N_{ip}N_{om}Q_{om}^{-2\gamma}R^{-\gamma}R_p^2 10^{\frac{\Delta L+2\Lambda}{10}-\frac{L_wR_p}{10W_r}})}.$$

We therefore consider the possibility of deploying the spectrum sharing by the measurement of building penetration loss. If a building has a penetration loss higher than $L_{b-min}$ threshold, a picocellular system reusing macrocell channels can be deployed within the building.

### 5.3.4 Case study for microcells underlying macrocells

We consider a GSM-like system which require a minimum SIR of 12 dB. In the areas having high density traffic demand, sectorised macrocellular networks are likely to be deployed due to their higher spectrum efficiency compared to conventional omni-macrocellular networks. Using Equations 5.1 and 5.10 we found that a 4/12 frequency cellular structure, i.e., four BS per cluster with each BS having three sectors, satisfies the minimum SIR requirement. If a total of 20 MHz of bandwidth is allocated to the system, and the carrier are spaced by 200 kHz, the total number of carriers (for each link) available for the system usage is 48, i.e., two carriers at the edge of the bandwidth are left unused to create guard bands. The number of carriers available for each sector is therefore four, i.e., four carriers per frequency set. We will assume that the BS separation distance is 10 km, giving hexagonal cells of radius 5.8 km.

| Symbol | Description | Value |
|---|---|---|
| $f_c$ | carrier frequency | 1.8 GHz |
| $\lambda_c$ | wavelength | 0.167 m |
| $S_i$ | total area with heavy traffic demand | 1 km$^2$ |
| $A_i$ | total extra demand offered traffic | 200 Erlangs |
| $K$ | macrocellular cluster size | 4/12 |
| $K_m$ | microcellular cluster size | 4 |
| $\Lambda$ | minimum SIR required | 12 dB |
| $\gamma$ | macrocell pathloss exponent | 3.44 |
| $L_{1-km}$ | macrocell pathloss at 1 km | -137.5 dB |
| $L_{1-m}$ | microcell pathloss at 1 m | -37.5 dB |
| $N$ | number of macrocell co-channel interferers | 2 |
| $N_{om}$ | number of interlayer macrocell co-channel interferers | 1 |
| $Q$ | macrocell co-channel reuse factor | 3.46 |
| $Q_{om}$ | interlayer co-channel reuse factor | 2 |

Table 5.2: The values of parameters used in the case study

Each macrocell provides a traffic capacity of 21.8 Erlangs with the GOS of 5 %, i.e, the blocking probability $P_B = 0.05$.

We consider a scenario where an increase of teletraffic of $A_i = 200$ Erlangs occurs in an area of $S_i = 1$ km$^2$ in a macrocell, i.e., in the cell with city centre coverage. If a signal-to-interference ratio of 12 dB is required for satisfactory channel performance, and from Equations 5.6 and 5.10, the minimum microcell cluster size is four. Therefore, we deploy a microcellular network of $K_m = 4$ to enhance the traffic capacity in the area of high traffic demand. All parameters used in the calculation are itemised in Table 5.2.

We have two channel sets available for the under-layer system, that is eight carriers. With the microcell planning of $K_m = 4$, each microcell is assigned two carriers, $N_{fm} = 2$, and provides a traffic capacity of 8.2 Erlangs, $A_{mc} = 8.2$. Using Equation 5.18, the number of microcell clusters required to meet the teletraffic demand is $N_{im-t} = 7$. Originally we set the micro-BS antenna height at six metres, and using Equation 5.21 we obtain that an acceptable $N_{im}$ is within the range $12 \leq N_{im} \leq 22$. Hence we choose to deploy 12 microcells per cluster. Using Equation 5.19 we obtain the minimum and maximum allowed $R_m$ distance for a microcell as 75 metres and 215 metres, respectively. The minimum transmitting power for microcells is calculated from Equation 5.16 as -74.8 dB relatve to the maximum macrocell transmitting power,

and the maximum microcell transmitting power is obtained from Equation 5.13 as -17.2 dB relative to the maximum macrocell transmitting power. We conclude that spectrum sharing with clusters of $K$ and $K_m$ is feasible.

### 5.3.5 Case study for inbuilding picocells underlying macrocells

For the same macrocellular network as used in the the microcell case study, and with the inbuilding picocell model described in Chapter 2, then from Equations 5.9 and 5.10, we find that the horizontal reuse cluster is four and the vertical reuse cluster is two in order to satisfy the SIR requirement. The total pico-cluster size is therefore eight. The number of carriers available for reuse in a building is also eight carriers, i.e., from two frequency sets, $M_a = 2$. With the picocell reuse cluster size of eight, each picocell is assigned one carrier and has a traffic capacity of 2.9 Erlangs. Each building has 10 floors where each floor contains 144 offices. The office width is five by five meters, and the office partition loss is -3 dB. The average traffic demand in an office is 0.5 Erlang. We obtain the upper bound of $R_p$ as 6 metres. The number of significant horizontal interferers, $N_h$, and significant vertical interferers, $N_v$, is set to three and two, respectively. If there are 50 buildings to be installed with picocellular systems, the minimum number of picocell clusters is given by Equation 5.38 as 1562. We choose to install 2248 picocellular clusters with $R_p = 5$, within 50 buildings, and we obtain the lower bound of the building attenuation, $L_{b-min}$, from Equation 5.42 as 36.7 dB, i.e., the signal strength received within the building must not be above 36.7 dB relative to the signal strength received outside the building at street level. For the picocell at the top floor of the buildings, $L_b = 4.6$ dB, which is lower than $L_{b-min}$, and the maximum and minimum picocell transmitting power is -42.3 dB and -100.7 dB, relative to the macrocell maximum transmitting power, respectively.

### 5.3.6 Capacity enhancement of the algorithm

Firstly we consider the upper limit of channel availability for the spectrum sharing system. The underlaid system should not reuse the channels being used by adjacent microcells, as the interference between these cells could be significant, especially for macro-MS and the under-layer systems near the macrocell border, i.e., macro-MSs connecting to the adjacent macrocell can be very close to a micro-BS, and excessive

| Cluster size | $Q$ | $Q_{om}$ | $N_{om}$ | $M_a$ | Cluster size | $Q$ | $Q_{om}$ | $N_{om}$ | $M_a$ |
|---|---|---|---|---|---|---|---|---|---|
| 9 | 5.2 | 3 | 3 | 2 | 4/12 | 3.46 | 2 | 1 | 2 |
| 12 | 6 | 3.46 | 3 | 2 | | | 1.73 | 1 | 5 |
| | | 3 | 2 | 5 | 7/21 | 4.58 | 2.66 | 1 | 2 |
| 16 | 6.9 | 3.46 | 2 | 3 | | | 2 | 1 | 8 |
| | | 3 | 3 | 9 | | | 1.73 | 1 | 14 |
| 19 | 7.5 | 3.46 | 2 | 6 | 9/27 | 5.2 | 3 | 1 | 2 |
| | | 3 | 1 | 12 | | | 2.66 | 1 | 8 |
| 21 | 7.94 | 4.61 | 3 | 2 | | | 2 | 1 | 14 |
| | | 3.46 | 2 | 8 | | | 1.73 | 1 | 20 |
| | | 3 | 1 | 14 | | | | | |
| 27 | 9 | 5.20 | 3 | 2 | | | | | |
| | | 4.61 | 2 | 8 | | | | | |
| | | 3.46 | 1 | 14 | | | | | |
| | | 3 | 1 | 20 | | | | | |

Table 5.3: Frequency planning parameters for spectrum sharing systems with extra channels for underlaid cellular systems

downlink interference could occur if they are using the same channels. We observe that in the farthest reuse algorithm, when $K \leq 7$, the farthest macrocells in the same cluster is always adjacent to the considered macrocell, therefore, no channels can be reuse by the underlaying systems. For a macrocellular system with $K > 7$, using the farthest reuse algorithm, the number of available channels for the under-layer systems is $N_{bf} = M_a N_c$, where $M_a$ is the number of available channel sets given by Table 5.1, and $N_c$ is the number of channel assigned to each macrocell. However, for macrocellular systems with $K > 9$, there are macrocells in the same cluster which are not the farthest and are not adjacent to the overlaying macrocell. The underlaid systems may reuse their channels provided that the SIR performance at the co-channel macrocells and the underlaid system is satisfied. Table 5.3 is the extended version of Table 5.1 and include the reuse parameters for channels other than the farthest reuse. For each $K$, there are a number of possible reuse scenarios, i.e., for $K = 12$, the under-layer cells can reuse two channels sets, i.e., $M_a = 2$, with the interlayer reuse factor of $Q_{om} = 3.46$, or can reuse five channels sets, $M_a = 5$, with the worst case interlayer reuse factor of three, $Q_{om} = 3$.

Figure 5.3 and 5.4 illustrates the spectrum sharing for omni-macrocellular networks

and sectorised macrocellular networks, respectively. For $K = 12$, the underlaid system in cell $A$ (see Figure 5.3) can reuse the channels assigned to cell $B1$ and $B2$ (collectively called channel set $B$) which are the farthest cells in the same cluster as cell $A$. Channels assigned to cells $C1$ to $C3$ (collectively called "channel set $C$), which are outside the neighbouring boundary, may also be reused by the underlaid systems in cell $A$ with an interlayer reuse distance of $3R$. The number of significant interfering macrocells for channel set $B$ and $C$ are three and two, respectively.

For $K = 16$, there are three macrocells being the farthest cells, i.e., $B1$ to $B3$, and six macrocells being the second farthest cells, i.e., $C1$ to $C6$. The number of significant interfering macrocells of channel set $B$, and $C$ are two and three, respectively. The interlayer reuse distances for channel sets $B$ and $C$ are $3.46R$ and $3R$, respectively.

For $K = 19$, the number of the farthest cells is six, i.e., cells $B1$ to $B6$. Channel set $B$ can be reused with an interlayer reuse distance of $3.46R$, and the number of significant interfering macrocells is two. Cells $C1$ to $C6$ is the second farthest cells, and channel set $C$ can be reused with an interlayer distance of $3R$, and two significant interfering macrocells. Although the interlayer reuse distance of the two significant interfering macrocells are slightly different, we approximate them to the lesser one.

For $K = 21$, channel set $B$ (channels assigned to cells $B1$ to $B2$) can be reused with an interlayer reuse distance of $4.61R$, and the number of significant interfering macrocells is three. Channel set $C$ (channels assigned to cells $C1$ to $C6$) can be reused with an interlayer reuse distance of $3.46R$ and the number of significant interfering macrocells is two. Channel set $D$ (channels assigned to cells $D1$ to $D6$) can be reused with an interlayer reuse distance of $3R$ and the number of significant interfering macrocells is one.

For $K = 27$ we can reuse channels assigned to $B1$ and $B2$, with an interlayer reuse distance of $5.2R$. Channels assigned to $C1$ to $C6$, can be reused with an interlayer reuse distance of $4.61R$. Channels assigned to $D1$ to $D6$ can be reused with an interlayer reuse distance of $3.46R$. Channels assigned to $E1$ to $E6$ can be reused with an interlayer reuse distance of $3R$. The number of significant interfering macrocells of channel sets $B$, $C$, $D$ and $E$ are three, two, one and one, respectively.

For $K = 4/12$ the extra channels, belong to cells $C1$ to $C3$, can be reuse by the under-layer system in cell $A$ with an interlayer reuse distance of $1.73R$, and the number of significant interfering macrocells is one. In the case where $K = 7/21$, channels assigned to cells $C1$ to $C6$, can be reused with an interlayer reuse distance

of $2R$, and channels assigned to cells $D1$ to $D6$ can be reused an interlayer reuse distance of $1.73R$.

For $K = 9/27$, channels assigned to cells $C1 - C6$ can be reused with an interlayer reuse distance of $2.66R$, channels assigned to cells $D1 - D6$ can be reused with an interlayer reuse distance of $2R$, and channels assigned to $E1 - E6$ can be reused with an interlayer reuse distance of $1.73R$. The number of significant interfering macrocells for all cases is unity.

We consider an upper limit of the fixed spectrum sharing algorithm underlaid macrocells as the scheme where the under-layer systems reuse all channels that are not assigned to the overlaying macrocell and its adjacent macrocells, seven cells altogether. Therefore, the maximum number of available channel for underlaid system, $N_{bm}$, is

$$N_{bm} = \begin{cases} (K-7)N_c & \text{for } K > 7 \\ 0 & \text{otherwise} \end{cases} \tag{5.43}$$

For sectorised macrocellular planing, $K$ is the number of sectors in a cluster. From the above equation we observe that if $K \leq 7$, no channels can be reuse by the under-layer system. This is because all channels are used by either the over-layer macrocell or by the adjacent macrocells. Suppose that in order to provide enough channels for the under-layer systems, we have to increase the cluster size to $K'$, when the number of channels available in a macrocell becomes

$$N_c' = \frac{N_c K}{K'}. \tag{5.44}$$

The number of channels available for underlaid systems obtained from Equations 5.43 and 5.44 is

$$N_{bm}' = \frac{(K'-7)}{K'} K N_c. \tag{5.45}$$

In the bandwidth partitioning scheme a portion of the channels are dedicated solely to the under-layer systems. The number of channels assigned to each macrocell before frequency partitioned and after frequency partitioned are $N_c$ and $N_c'$, respectively. Therefore the number of channels available for underlaid systems is

$$N_{bp} = K(N_c - N_c'). \tag{5.46}$$

In order to compare the performance of the spectrum sharing algorithm with the frequency partition scheme, we compare the number of available channels for the underlaid systems while letting the number of channels for a macrocell to be the

same. To do that we substitute $N'_c$ in Equation 5.46 by $N'_c$ given by Equation 5.44, and we obtained

$$N'_{bp} = \frac{(K' - K)}{K'} K N_c. \tag{5.47}$$

By comparing $N'_{bm}$ and $N'_{bp}$, we observe that $N'_{bm}$ is equivalent to $N'_{bp}$ for $K = 7$, $N'_{bm}$ is greater than $N'_{bp}$ for $K > 7$, and $N'_{bm}$ is smaller than $N'_{bp}$ for $K < 7$. This suggests that for the macrocell layer with small cluster size, i.e., $K < 7$, the frequency partition scheme gives a higher capacity. However, for macrocellular networks that require big reuse cluster sizes, i.e., $K > 7$, the spectrum sharing scheme provides better capacity performance than the frequency partition scheme. For $K = 7$, the capacity performance of both schemes are similar.

In order to assess the improvement of the system performance of the enhanced spectrum sharing scheme we reconsider the macrocellular layer with its 4/12 frequency planning described in the previous case studies. We retain the use of all parameters, except that the number of available channel sets is now five, i.e., $M_a = 5$, $Q_{om} = 1.73$, and $N_{om} = 1$. We have five channel sets available for the underlaid system, that is 20 carriers. With the microcell planning of $K_m = 4$, each microcell is assigned two carriers, $N_{fm} = 5$, and can provide a traffic capacity of 28 Erlangs, $A_{mc} = 28$. Using Equation 5.18, the number of microcell clusters required to meet the teletraffic demand is $N_{im-t} = 2$. Originally we set the micro-BS antenna height at six metres, and using Equation 5.21 we observe that the range remains unchanged as $12 \leq N_{im} \leq 22$. Therefore we opt to deploy 12 microcell clusters. Using Equation 5.19 we find the minimum and maximum allowed microcell radii as 75 metres and 215 metres, respectively. The minimum transmitting power for microcells is calculated from Equation 5.16 as -74.8 dB relative to the maximum macrocell transmitting power, and the maximum microcell transmitting power is obtained from Equation 5.13 as -17.2 dB relative to the maximum macrocell transmitting power. Although the required number of microcell clusters is not changed compared to the original algorithm, the traffic capacity per microcell increased by 240% upon using the enhanced algorithm.

Next we consider the scenario when the underlaid system is clusters of inbuilding picocells. With a picocell reuse cluster size of eight, each picocell is assigned three carriers and has a traffic capacity of 15 Erlangs. Each building has 10 floors where each floor contains 144 offices. The office size is five by five meters, and the office partition loss is -3 dB. The average traffic demand in an office is 0.5 Erlang. We obtain the upper bound of $R_p$ as 13.7 metres. If there are 50 buildings ready to

be install picocellular systems, the minimum number of picocell clusters given by Equation 5.38 is reduced to 300 by using the enhanced algorithm. We choose to install 562 picocellular clusters with $R_p = 10$, in 50 buildings and we obtain the lower bound of the building attenuation, $L_{b-min}$, from Equation 5.42 as 31.1 dB, i.e., the signal strength received within the building must not be greater than 31.1 dB compared to the signal strength received outside the building at street level. For the picocell at the top ffoor of the buildings, $L_b = 4.6$ dB, which is lower than $L_{b-min}$, and the maximum and minimum picocell transmitting power is -38.5 dB and -91.5 dB relative to the maximum transmitting power of the macrocell BSs, respectively.

When both microcells and inbuilding picocells are required to be deployed under the cover of a macrocell, the channels available for the under-layer system must be partitioned into two groups, one for microcells, and one for picocells, in order to avoid the co-channel interference between the two systems. The picocell signal received outside the building can be particularly strong, as suggested by Reference [70]. For instance, in the macrocellular networks with the 4/12 cellular arrangement described earlier, the number of available channel sets of five is divided into two and three channel sets, for microcells and picocells, respectively.

So far only co-channel interference is considered. However, the interference resulting from signals which are adjacent in frequency to the desired signal, or so called "adjacent channel interference" can be particular serious if a transmitter is transmitting on an adjacent frequency that is very close to the mobile receiver attempting to receive a signal from a base station. The problem of adjacent channel interference in spectrum sharing systems can be particular serious between a macrocell and its under-layer cells if the under-layer microcells or picocells have MSs that are transmitting on adjacent channels that are very close to those used by a macrocell mobile user. In order to minimise the effect in the spectrum sharing system, the under-layer system must not reuse the channels that are adjacent to the channels being used by the overlaying macrocell. Figure 5.6 shows the example of the arrangement of channel sets such that the channel set that are allowed to be reused in the underlaid system are not adjacent to the channel set assigned to the overlaying macrocell. The channels available to the system are arranged into 12 channel sets such that channel set one is adjacent to channel set two, channel set two is adjacent to channel set one and three, and so on. They key of assigning the channel sets is to begin assigning the first channel set, i.e., channel set one, to the channel sets which are expected to have

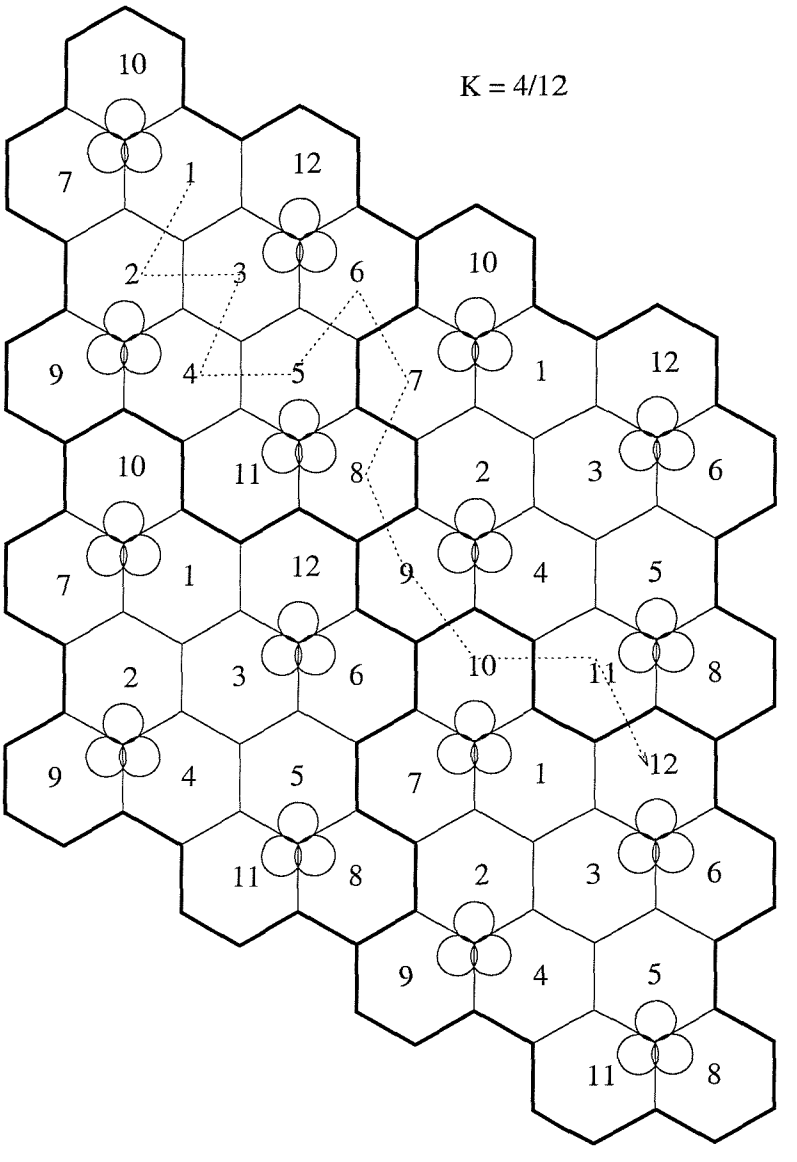


Figure 5.6: Channel sets assignment for a macrocell cluster with $K = 4/12$.

the highest density in the under-layer system. Then we continue to assign channels, traversing through the adjacent cells, which have not been assigned and do not have adjacent channel restrictions with respect to the current cell.

## 5.4 Dynamic spectrum sharing algorithm

In the previous section we described the fixed spectrum sharing algorithm where the number of channels available for each layer is planned in advance and fixed, and the channel assignment used by each layer is assumed to be FCA. However, if the macrocell layer employs a dynamic channel assignment scheme where the number of channel assigned to each cell is varied according to its teletraffic demand, the number of channels available for the underlaid systems in each macrocell is no longer fixed and is equivalent to the number of channels which are not assigned to the overlaying macrocells and its adjacent macrocells. Therefore, the capacity of the underlaid cells is time-varying and is dependent on the channel assignment process at the macrocellular level, and vice versa, i.e., the channel assignment in the macrocellular layer must also take into account of the channel usage in the underlaid system, in order to prevent excessive interference between the layers.

In the city centre area where only microcells and picocells handle a significant amount of teletraffic, the traffic demand between microcells and picocells is likely to be time-varying, because of the small cell sizes and the effect of users' mobility. For instance, in the early morning when people are on their way to work, most calls made are likely to be served by microcells; during office hours, inbuilding picocells are likely to handle most of the calls; while during lunch time or in the evening, microcells could play the major roles in serving users in a city centre area. The fixed spectrum sharing that divides channels available for the underlaid cells into two groups, one for microcells, and one for picocells, may not provide enough traffic capacity for this non-uniform and time varying traffic distribution.

In the previous chapter we have described a number of dynamic channel allocation algorithms where the channel assignment is able to adapt to the variation of traffic demand between cells in the same layer. However those DCA algorithms alone cannot cope with different cellular structures in multilayer networks. In this context we propose a dynamic spectrum sharing algorithm that can be integrated into dynamic channel allocation schemes, and enable the channel assignment of each cell in each

layer to agree with its teletraffic demand. Our algorithm is derived from the studies in References [87] and [86]. References [87] suggested that each underlaid microcells reuse the channels which are not used in three nearest macrocells. We observe that this method of excluding the channels used in the three nearest macrocell can be embedded into a dynamic channel assignment algorithm of the underlaid system, provided that each underlaid cell has a capability of identifying the three nearest macrocells, their occupying channels and channels adjacent to the occupying channels.

However, in a macrocellular network where macrocells employ dynamic channel assignment, especially when a macrocell overlaying the underlaid cells is highly loaded, the number of channels available for the under-layer systems is decreased dramatically because most channels is assigned to the overlaying macrocell and cannot be used by the under-layer systems. Therefore we required a spectrum sharing scheme that ensures a certain number of available channels for all underlaid systems, including microcells and picocells. Reference [86] introduced a new class of DCA algorithm, called the co-existence DCA (CE-DCA), which supports the co-existence of macrocells and underlaid microcells. In the classic DCA algorithm each cell is free to choose any channel that meets an interference constraint from the universal set of channels available to the network. To avoid mutual interference between the two systems, each macrocell excludes a random subset of channels from the universal set. However the algorithm presented in both references [87] and [86] did not support the time-varying traffic demand between layers. We set out to design an adaptive spectrum sharing algorithm which ensures that the channel assignment algorithm of all layers share the spectrum efficiently with an adaptive capability to meet the time-varying traffic demands between layers.

### 5.4.1 System architecture

In this context we derive our spectrum sharing algorithm from a carrier-by-carrier channel assignment, such as AAFA described in the previous chapter. When microcells and picocells are introduced into an existing macrocellular network, the total number of available carriers $N_T$, are divided into two subgroups, $S_A$ for microcell reuse and $S_B$ for picocell reuse, in order to avoid mutual interference between the microcell layer and the picocell layer. Firstly we consider a macrocellular network with FCA having $K$ cells per cluster. The minimum number of carriers assigned to

$S_A$ is

$$N_{A-min} = \text{ceil}(\frac{K_m}{K-8})K, \tag{5.48}$$

where ceil$(a)$ is a function which gives a round up integer of $a$, and $K_m$ is the required reuse cluster size for the microcells. We assume that for each microcell there are eight carrier sets which belong to the three nearest macrocells and their adjacent carriers. Similarly the minimum number of carriers assigned to $S_B$ is

$$N_{B-min} = \text{ceil}(\frac{K_p}{K-8})K, \tag{5.49}$$

where $K_p$ is the required reuse cluster size for the picocells. Hence, in order to provide spectrum sharing for both microcells and picocells underlaying a macrocellular network, we required at least $N_{T-min}$ carriers, given by

$$N_{T-min} = N_{A-min} + N_{B-min}. \tag{5.50}$$

Accordingly, each macrocell must hold at least $N_{ac} = N_{A-min}/K$ carriers of carrier subgroup $A$, and $N_{bc} = N_{B-min}/K$ carriers of carrier subgroup $B$. If $N_T > N_{T-min}$, the extra carriers can be adaptively assigned to each subgroup, according to traffic demands in the microcell layer and picocell layer.

We devise an adaptive algorithm where the spectrum sharing mechanism is governed by the traffic demand of inbuilding picocells, as we envisage that if the multilayer networks are widely deployed, the majority of traffic may be handle by the inbuilding picocells. Figure 5.7 shows the control algorithm for deciding the number of carriers for $S_A$ and $S_B$. At the beginning, we set $N_B$ equal to $N_{B-min}$, and the rest of the available carriers are assigned to $S_B$. The subgroup assignment is then updated periodically, i.e, say every few minutes. When a picocell detects a traffic overload, it sends an overload request to the three nearest macrocells. The corresponding macrocells then inform other macrocells within their neighboring area to decrease their $N_A$ and increase their $N_B$, provided that $N_A \geq N_{A-min}$. Picocells send the overload request when the channels available for the picocell layer are exhausted, i.e., there is a traffic overload in a picocell and the picocell cannot acquire an extra carrier for itself. By contrast if a microcell senses that it has been overloaded for a period of time, and it also sends an overload request to the corresponding macrocells. Each macrocell executes these overload requests, and gives priority to the requests from picocells, if picocells are lightly loaded, In other words, when there are no overload requests from picocells for a specified interval, say ten minutes, the macrocell then adjusts the parameters, $N_A$ and $N_B$ in favour of microcells.

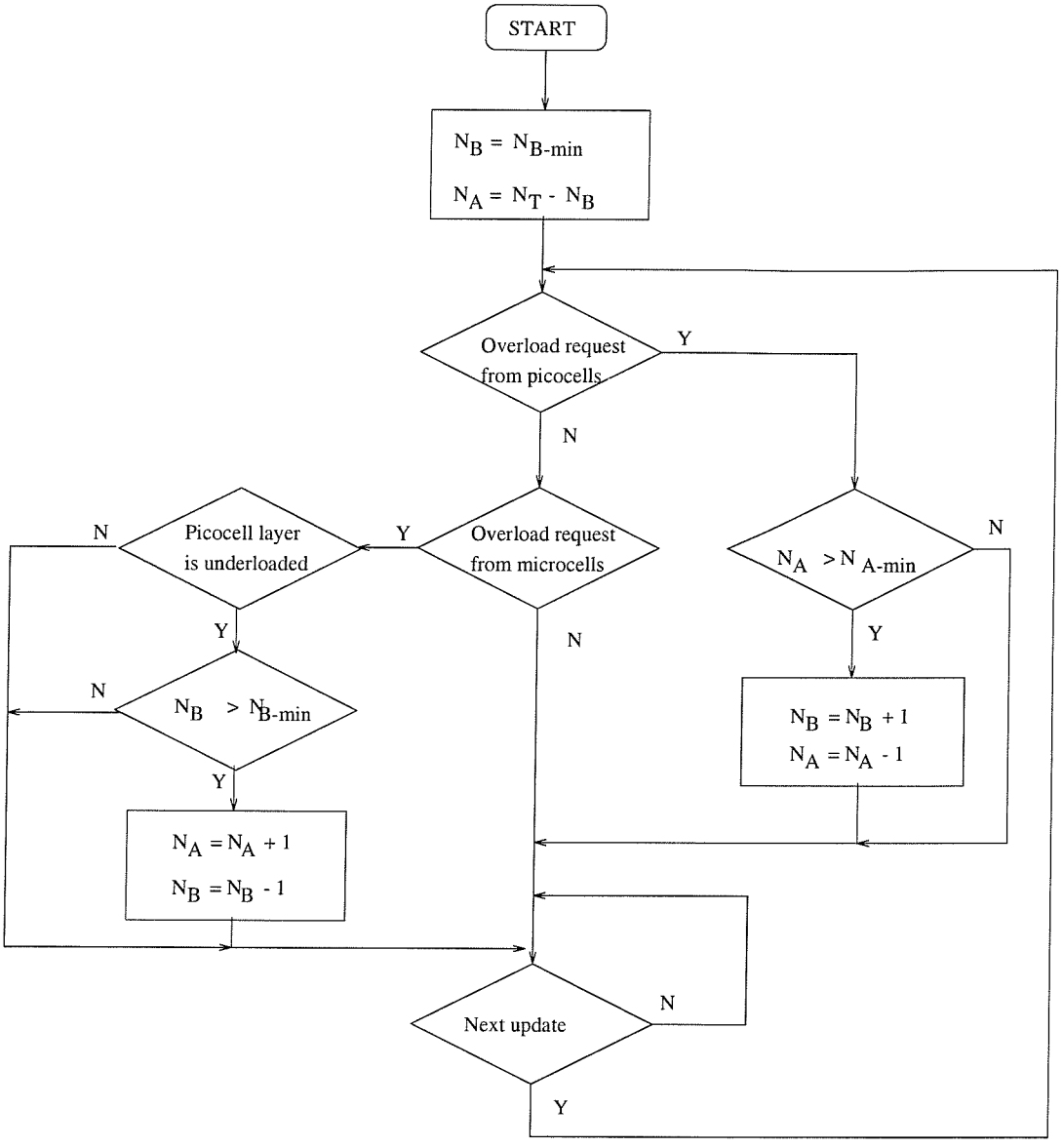


Figure 5.7: Flowchart illustrating Dynamic Spectrum Sharing Algorithm (DSSA)

When a microcell, is introduced into a macrocellular network, it scans to identify the three nearest macrocells, and acquires an available carrier list for its dynamic channel assignment process, i.e., those carriers in $S_A$ which are not assigned to the corresponding macrocells and are not adjacent to their assigned carriers. The microcell then informs its carrier available list, $F_{A-micro}$, to the macrocells, and the macrocells update their carrier excluding lists for microcells, $E_A$, to include those in the microcell available list, and their adjacent carriers. When a picocell is introduced, the picocell performs the same process as the microcell does with the macrocell layer, but the available carrier list $F_{A-pico}$ is obtained from the carriers in $S_B$ which are not assigned to the corresponding macrocells and are not adjacent to their assigned carriers. The macrocells then update their excluding list for picocells, $E_B$, to contain those carriers in the picocell available list, and their adjacent carriers. The available carrier list of macrocells is, therefore,

$$F_{A-macro} = F_N \cap E_A \cap E_B, \tag{5.51}$$

where $F_N$ is the set of all carriers available for the network.

Referring to the AAFA described in the previous chapter, with this spectrum sharing algorithm, the frequency usability $U$, given by Equation 4.2 is modified to

$$\begin{aligned} U &= \{U_i | i \in F_N\}, \ 0 \leq U_i \leq 1, \\ U_i &= \begin{cases} 0 & \text{if} \quad C_i < K_a \ \vee \ I_i \leq 0 \ \vee \ i \notin F_A \\ I_i/I_{TH} & \text{if} \quad 0 < I_i < I_{TH} \ \wedge \ C_i \geq K_a \ \wedge \ i \in F_A \\ 1 & \text{otherwise} \end{cases} \end{aligned} \tag{5.52}$$

where $F_A$ is the list of available carriers, $I_i$ is the interference level of the $i$th frequency, $I_{TH}$ is the power measurement window, $C_i$ is the co-channel factor and $K_a$ is the co-channel constraint. More details of these parameters can be founded in Chapter 4.

### 5.4.2 System analysis

We analyse the SIR performance of the spectrum sharing system based on a macrocellular network with FCA having 4/12 cell structure, as described in the previous case study. Figure 5.8 shows a model of the coverage area for the macrocellular network. We observed that the area can be divided into tessalated triangles, in which microcells and picocells are associated with the same three strongest macrocells. Within a macrocell cluster we label each cell site by an uppercase letter representing its assigned frequency set. Table 5.4 represents the frequency planning derived from Figure 5.6.

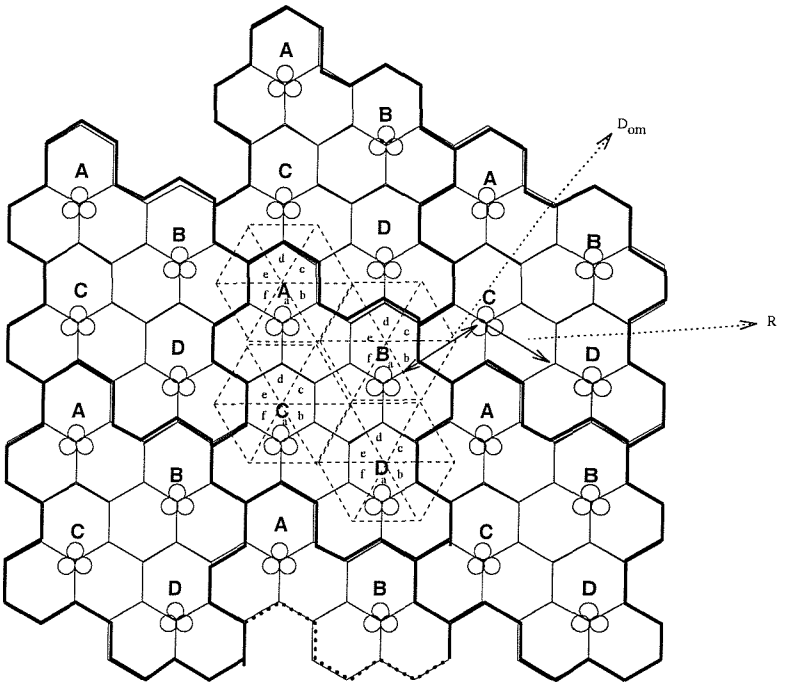


Figure 5.8: The proposed microcell/macrocell overlaying system

| Frequency set | Top sector | Left sector | Right sector |
|---|---|---|---|
| A | 10 | 7 | 1 |
| B | 12 | 3 | 6 |
| C | 2 | 9 | 4 |
| D | 5 | 11 | 8 |

Table 5.4: Frequency planning for macrocells

Each macrocell cluster is composed of 24 triangles. We label these triangles by forming six triangles into hexagons around the top sector of each base site; each sector of the hexagon is labelled by a lowercase letter; and we refer to each triangle by its associated base site and the sector label, i.e., sector $a$ in a hexagon associated with base site $A$ is called $A_a$. Table 5.5 shows the available carriers to be used by under-layer cells in different areas.

We observe that in area $D_a$, the number of available carriers for reuse in the under-laid cells is only three. Therefore, the earlier assumption that the number of available carriers for the under-layer cells is always four or more as the number of carrier sets used by the three nearest macrocells and their adjacent carriers is at most eight, is

| Area | Interfering macrocells | Interfering frequency sets | Available frequency sets |
|---|---|---|---|
| $A_a$ | $A_{top}$, $A_{left}$, $A_{right}$ | 10,7,1 | 3,4,5,12 |
| $A_b$ | $A_{top}$, $A_{right}$, $D_{left}$ | 10,1,11 | 3,4,5,6,7 |
| $A_c$ | $A_{top}$, $D_{left}$, $C_{right}$ | 10,11,4 | 1,2,6,7,8 |
| $A_d$ | $A_{top}$, $C_{right}$, $C_{left}$ | 10,4,9 | 1,2,6,7,12 |
| $A_e$ | $A_{top}$, $C_{left}$, $B_{right}$ | 10,9,6 | 1,2,3,4,12 |
| $A_f$ | $A_{top}$, $B_{right}$, $A_{left}$ | 10,6,7 | 1,2,3,4,12 |
| $B_a$ | $B_{top}$, $B_{left}$, $B_{right}$ | 12,3,6 | 1,8,9,10 |
| $B_b$ | $B_{top}$, $B_{right}$, $C_{left}$ | 12,6,9 | 1,2,3,4 |
| $B_c$ | $B_{top}$, $C_{left}$, $D_{right}$ | 12,9,8 | 1,2,3,4,5,6 |
| $B_d$ | $B_{top}$, $D_{right}$, $D_{left}$ | 12,8,11 | 1,2,3,4,5,6 |
| $B_e$ | $B_{top}$, $D_{left}$, $A_{right}$ | 12,11,1 | 3,4,5,6,7,8,9 |
| $B_f$ | $B_{top}$, $A_{right}$, $B_{left}$ | 12,1,3 | 5,6,7,8,9,10 |
| $C_a$ | $C_{top}$, $C_{left}$, $C_{right}$ | 2,9,4 | 6,7,11,12 |
| $C_b$ | $C_{top}$, $C_{right}$, $B_{left}$ | 2,4,3 | 6,7,8,9,10,11,12 |
| $C_c$ | $C_{top}$, $B_{left}$, $A_{right}$ | 2,3,1 | 5,6,7,8,9,10,11,12 |
| $C_d$ | $C_{top}$, $A_{right}$, $A_{left}$ | 2,1,7 | 4,5,9,10,11,12 |
| $C_e$ | $C_{top}$, $A_{left}$, $D_{right}$ | 2,7,8 | 4,5,10,11,12 |
| $C_f$ | $C_{top}$, $D_{right}$, $C_{left}$ | 2,8,9 | 4,5,6,11,12 |
| $D_a$ | $D_{top}$, $D_{left}$, $D_{right}$ | 5,11,8 | 1,2,3 |
| $D_b$ | $D_{top}$, $D_{right}$, $A_{left}$ | 5,8,7 | 1,2,3,10,11,12 |
| $D_c$ | $D_{top}$, $A_{left}$, $B_{right}$ | 5,7,6 | 1,2,3,9,10,11,12 |
| $D_d$ | $D_{top}$, $B_{right}$, $B_{left}$ | 5,6,3 | 1,8,9,10,11,12 |
| $D_e$ | $D_{top}$, $B_{left}$, $C_{right}$ | 5,3,4 | 1,7,8,9,10,11,12 |
| $D_f$ | $D_{top}$, $C_{right}$, $D_{left}$ | 5,4,11 | 1,2,7,8,9 |

Table 5.5: Interfering and available frequency sets for microcells in different area

not applicable for area $D_a$. However, in general, the assumption of excluding eight carriers sets is still valid. In our analysis we consider the worst case scenario, and we have the number excluding carriers is nine, including three carrier sets which are assigned to the three nearest macrocells, and six adjacent carrier sets. Hence, the number of frequency sets available for underlaid systems is

$$M_a = K - 9. \tag{5.53}$$

Consider the worst case scenario at area $B_a$ where the number of significant interfering macrocells, $N_{om}$ is unity, and the co-channel interlayer reuse distance, $D_{om}$, is $1.25R$, where $R$ is the maximum distance from a BS to its cell boundary as illustrated in Figure 5.8. Accordingly the interlayer co-channel factor $Q_{om}$ is 1.25.

When a microcell uses a channel assigned to a macrocell, extra interference between layers must be taken into account, and must be kept to a minimum or below an acceptable level. The microcell can overcome this interference by adjusting the transmitted power of its BSs to a sufficient level that does not to cause significant interference to the co-channel macrocells. In order to determine the upper limit of microcell BS transmitting power, we consider the macrocellular structure as 4/12 with 12 macrocells per cluster deployed as in Section 5.3.4, but with $M_a = 3$, $Q_{om} = 1.25$ and $N_{om} = 1$. The minimum transmitting power for microcells obtained from Equation 5.16 is -70 dB relative to the maximum macrocell BS transmitting power, and the maximum microcell transmitting power is obtained from Equation 5.13 as -22.1 dB relative to the maximum macrocell BS transmitting power.

Next we consider the scenario when 562 picocell clusters are deployed as described in Section 5.3.6, and the parameter $Q_{om}$ is set to 1.25. We obtain the lower bound of the building attenuation, $L_{b-min}$, from Equation 5.42 as 26.2 dB, i.e., the signal strength received within the building must not be above 26.2 dB relative to the signal strength received outside the building at street level. For the picocell on the top floor of the buildings, $L_b = 4.6$ dB, which is lower than $L_{b-min}$, and the maximum and minimum picocell transmitting power is -43.4 dB and -86.6 dB relative to the macrocell maximum transmitting power, respectively.

### 5.4.3 Enhancing picocellular capacity by underlay-overlay

In the previous subsection, microcells and picocells use similar approaches of identifying the available carriers by determining the three strongest macrocells. However, in a macrocellular network with a large BS separation distance, some picocells in a building with high penetration loss may not be able to identify the second and third strongest macrocells. Therefore we propose in this section a spectrum sharing algorithm where a picocell obtains its $F_A$ list by identifying only the strongest macrocell, and chooses carriers in the $S_B$ of the corresponding macrocell which is not assigned to the macrocell, and is not adjacent to the macrocell carriers. The minimum number of carriers assigned to $S_B$ becomes

$$N_{B-min} = \text{ceil}(K_p/(K-3))K, \tag{5.54}$$

as the number of carrier sets which belong to the nearest macrocells are counted as one carrier set and their adjacent carriers are counted as two carrier sets, hence a

total of three carrier sets. If the same number of carriers are assigned to $S_B$ of all macrocells in the same cluster, the number of carriers available for each picocells is increased by $5/(K-8)$ times.

However, at picocells that are located near a cell boundary and do not exclude carriers being used by the second and third strongest macrocells, the chances are high that macro-MSs associated with the neighboring macrocells are very close to the picocells and cause significantly interference (due to the high transmission power level used by macrocells) In order to avoid this circumstance, an underlay-overlay scheme [1] is applied in each macrocell sector as shown in Fig. 5.9. The underlay is the inner hexagon and the overlay is the outer hexagon. Each macro-BS limits the use of carriers in subgroup $S_B$, within its underlay perimeter, in other words, all macro-MSs near a cell boundary are prevented from using the carriers in $S_B$, which are to be reuse by picocells. Therefore picocells near a cell boundary will not experience interference from macro-MSs in the neighboring macrocells. The maximum transmitted power level for the carrier in the $S_B$ subgroup can also be reduced by

$$\Delta P_u(\text{dB}) = 10\gamma \log(R_u/R) = 10\gamma \log(\alpha), \tag{5.55}$$

where $\gamma$ is the path loss exponent, $R_u$ is the radius of the underlay area, $R$ is the macrocell radius, and $\alpha = R_u/R$ is the under-overlay ratio of macrocells. We may obtain $\alpha$ by assuming that users in macrocells are uniformly distributed, and we choose $\alpha$ such that the available channel density for the underlay area is equal to the channel density in the overlay area of a macrocell. That is

$$\frac{N_B}{\pi R_u^2} = \frac{N_T}{\pi R^2}. \tag{5.56}$$

Hence $\alpha$ is given by

$$\alpha = \sqrt{\frac{N_B}{N_T}}. \tag{5.57}$$

We consider the SIR performance of a picocellular system located at a cell boundary for the arrangement depicted in Figure 5.9. The number of significant macrocell interferers to the picocells, $N_{om}$ is unity, and the co-channel interlayer reuse distance, $D_{om}$, is given by $D_{om} = R$, where $R$ is the maximum distance from a BS to its cell boundary. Accordingly, the interlayer co-channel factor $Q_{om}$ is unity. For the underlay spectrum sharing system, the SIR of the macro-uplink when picocells reuse the same channel, given by Equation 5.34, is modified by replacing the distance from BS to

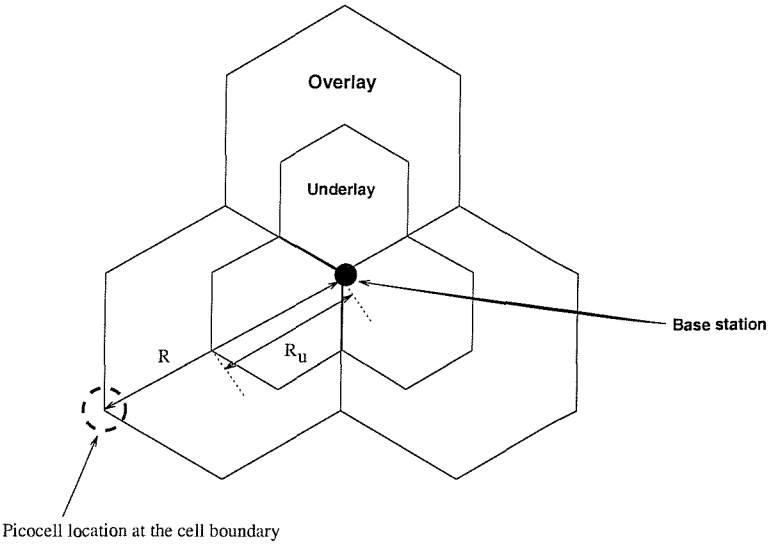


Figure 5.9: Underlay-overlay in sector cells

the macrocell radius, $R$, with an underlay radius, $R_u$, and substituting $Q_{om} = 1$, We have

$$\begin{aligned} \mathrm{SIR}_{mac-u} &= \frac{S}{I_{mac}+I_{pic}} \\ &= \frac{P_{mac}R_u^{-\gamma}}{NP_{mac}D^{-\gamma}+P_{pic}N_{ip}D_{om}^{-\gamma}10^{L_b/10}} \\ &= \alpha^{-\gamma}(NQ^{-\gamma}+\Delta P N_{ip}10^{L_b/10})^{-1}, \end{aligned} \tag{5.58}$$

where $\Delta P$ is the power ratio between picocells and macrocells. Consequently, the maximum allowed picocell power ratio becomes

$$\Delta P \leq \Delta P_{max} \equiv \frac{\alpha^{-\gamma} - 10^{\Lambda/10}NQ^{-\gamma}}{10^{(L_b+\Lambda)/10}N_{ip}Q_{om}^{-\gamma}}, \tag{5.59}$$

and the lower bound of the building penetration loss required to operate the spectrum sharing system for the underlay spectrum sharing system is given by

$$L_b \leq L_{b-min} \equiv 5\log(c), \tag{5.60}$$

where

$$c = \frac{(\alpha^{-\gamma} - 10^{\Lambda/10}NQ^{-\gamma})(1 - 0.25N_hK_h^{-1}10^{\frac{L_wR_p(2\sqrt{K_h}-1)}{10W_r}+\frac{\Lambda}{10}} - N_v10^{\frac{\Lambda+L_fN_v}{10}})}{(N_{ip}R^{-\gamma}R_p^2 10^{\frac{\Delta L+2\Lambda}{10}-\frac{L_wR_p}{10W_r}})}.$$

We assess the system performance by considering the scenario when 562 picocells clusters are deployed into the macrocellular network as described in the previous section. Suppose that the number of carriers assigned to $S_B$ subgroup is half the total

carriers, hence, we have $\alpha = 0.707$. We obtain the lower bound of the building attenuation, $L_{b-min}$, from Equation 5.60 as 30 dB, i.e., the signal strength received within the building must not be above 30 dB relative to the signal strength received outside the building at street level. For the picocell at the top floor of the buildings, $L_b = 4.6$ dB, which is lower than $L_{b-min}$, and the maximum and minimum picocell transmitting power is -39.6 dB and -90.4 dB relative to the macrocell maximum transmitting power, respectively. We observe that by employing an underlay-overlay arrangement, the spectrum sharing performance is improved in terms of better dynamic range of picocell transmitting power, and minimising the possible severe co-channel and adjacent channel interference, especially for picocells located near the macrocell boundary. However, the underlay-overlay algorithm may degrade some traffic capacity of macrocells as the available channels at a macrocell are divided into smaller subgroups, and may lead to the loss of trunking efficiency.

## 5.5 Conclusion

In this chapter we have described the system architecture of multilayer communication networks, which include wide area macrocells, street microcells and inbuilding picocells. We proposed two spectrum sharing algorithms, namely the fixed spectrum sharing algorithm (FSSA) and the dynamic spectrum sharing algorithm (DSSA) for multilayer cellular communication networks. By using a mathematical modelling method, we delivered a method for deploying the spectrum sharing algorithm, and some important system parameters for the FSSA multilayer networks, including the minimum reuse cluster size required for each layer, and the suitable power setting for street microcells and inbuilding picocells. The performance of the FSSA was compared with the frequency partitioning scheme. We found that the spectrum sharing system gives a better spectrum efficiency if the minimum required reuse cluster size of macrocells, $K$, is more than seven. When $K < 7$, the frequency partitioning yields better spectrum efficiency. For DSSA, we also used mathematical modelling to analyse the SIR performance of the worst case interference scenario. We proposed the application of the DSSA with the AAFA system, where the number of available carriers in each layer, and the number of carriers assigned to each cell adapt to their traffic demands.

In the derivation of the results, we did not take into account the effects of shadow

fading. These results should therefore only be considered as guidance for designing a spectrum sharing system. Shadow fading can degrade the SIR of radio links within the spectrum sharing system. For a qualitative study of the effects of shadowing on the signal quality, a statistical model with realistic shadowing characteristics should be employed, which is beyond the scope of this thesis.

# Chapter 6

# Summary and conclusions

## 6.1 Summary

In order to achieve high user capacity, multilayer architectures have been proposed for efficient management of network radio resource. Multilayer cellular networks provide radio coverage to the same area by overlapping cells of different sizes. Three-layer cellular systems consist of street microcell clusters, inbuilding picocell clusters and the over-layer macrocell clusters. Three system architectures were proposed for deploying multilayer networks for the global system for mobile communication. The first method is frequency partitioning where the allocated GSM spectrum is divided into subbands, and each band is allocated to each cell layer. The second method is to employ a cordless system to provide indoor picocellular networks and street microcellular networks leaving the GSM system to provide macrocellular coverage. The last method is spectrum sharing where microcells and picocells reuse the spectrum allocated to the macrocellular layer.

The spectral efficiency of the frequency partitioning architecture is evaluated. Using the latest propagation models that we know of each type of cellular environment, the spectral efficiency and the minimum reuse cluster size required for each cellular layer are determined by mathematical analysis and computer simulation. The macrocell cellular networks we envisage are characterised by the following features that are some what arbitrary but selected to illustrated our concepts. The macrocellular layer is formed by an hexagonal grid. Each cell site has a BS that is sectorised with three sectors per cell. The microcellular network is deployed in a dense urban rectilinear street grid environment. The cell-site antennas are located at street level, well below

the rooftops of surrounding buildings. The inbuilding picocellular network is installed within square buildings having four corridors and 144 square offices. Each floor has nine office areas and also nine picocell sites, where each picocell is located in each office area. For typical GSM link quality requirements, the macrocellular reuse cluster size is four, and the maximum spectral efficiency of the macrocellular network is 0.88 Erlangs/MHz/km$^2$. This figure is based on the maximum trunking efficiency when each BS is equipped with ten transceivers. For BSs with a small number of transceivers, the spectral efficiency is lower, e.g., for a BS with two transceivers the spectral efficiency is reduced to 60 % of the maximum. The reuse cluster size for macrocellular networks is varied from two to seven, according to network structures. The maximum spectral efficiency of the microcellular networks is also varied from 237 to 1480 Erlangs/MHz/km$^2$. The required reuse cluster size for inbuilding picocellular networks is eight, and the spectral efficiency for our inbuilding model is 7845 Erlangs/MHz/km$^2$. In our analysis, power control and frequency hopping did not directly improve system capacity, as the required reuse cluster size is unchanged. However, unnecessary high transmission power is reduced by power control, and with the interference diversity achieved by frequency hopping, the method of fractional loading allows the network to use smaller reuse structures. In the macrocellular networks with three and six sectors per cell, the single cell cluster provides an acceptable link quality with with 25% and 50% fractional loading, respectively, assuming 50% voice activity.

To deploy an under-layer cellular network in a macrocell using frequency partitioning scheme, system planners must dedicate a portion of macrocellular spectrum to the under-layer system. As the system capacity of each cellular layer is related to the infrastructure and the system bandwidth, the system planners must carefully assign the amount of spectrum bandwidth to each cellular layer and also consider the number of cell sites which attributes to the infrastructure cost. The analysis in this thesis, therefore, provides, a practical guidelines to system planning in multilayer cellular systems with frequency partitioning scheme.

Another approach of deploying multilayer cellular systems is to allocate the entire GSM spectrum to the macrocellular networks, and to use the digital enhanced cordless telecommunication (DECT) network in street microcells and in inbuilding picocells. This approach is suitable for operators with relatively limited spectrum for a GSM network, as the under-layer capacity is maintained by the DECT networks.

However, the system requires dual-mode mobile terminals, namely GSM/DECT terminals, in order to access both radio interfaces. Enhancements to a DECT system operating in an office environment is proposed. A minicell with an adaptive handover channel strategy results in an improvement in the GOS of ten times rising more than a thousand times as the number of users per picocell decreases from 40 to below 32, respectively. A joint street microcell/office picocell model is used to evaluate a DECT system providing outdoor as well as indoor radio coverage from indoor radio ports. The indoor DECT network was able to provide seamless communication within the city area with no capacity loss, provided that the majority of calls were originated from indoors. We propose an adaptive DECT-like radio interface for wireless ATM system. The adaptive transmission rate strategy is proposed in order to improve the bit error rate (BER) performance in the frequency selective fading channels.

The deployment of small cell systems with densely populated BSs results in complex planning issues. The radio propagation environment in microcells and picocells are different from those in conventional macrocellular systems in two major respects: i) there are more variations in the propagation environment due to the numerous reflectors and diffractors in and around the buildings, and a unified propagation model of wide area and localised is difficult to formulated; and ii) the radio interference from multistorey buildings adds a third dimension to the frequency reuse difficulties. Traditional frequency planning of fixed channel allocation (FCA) may be costly and time consuming if a large number of small cells are to be deployed. To realise frequency reuse without frequency planning, the radio protocol which will enable the channel allocation to be automatically done by the network needs to be invented. Therefore, we proposed a novel channel allocation algorithm, namely adaptive autonomous frequency assignment (AAFA). AAFA was designed to automatically update channel assignment periodically according to the changes in the propagation environment and traffic conditions. The algorithm was tested using computer simulation on different cellular system models, i.e., macrocells, microcells and picocells. We obtained the AAFA algorithm performance in both circuit-switched access mode and packet radio access mode. Comparing with the conventional FCA system, the capacity of the cellular systems employing the AAFA algorithm increased by up-to 20% and 180%, for uniform and non-uniform traffic scenario, respectively.

The deployment of an under-layer cells using the frequency partitioning scheme,

reduced the system capacity of the macrocellular layer because a portion of macrocellular spectrum was given to the under-layer cellular system. In order to investigate the possibility of maintaining the macrocell's capacity while deploying the under-layer networks, we proposed two spectrum sharing algorithms that allow the macrocellular layer and the under-layer cellular network to use the same radio bandwidth. Fixed spectrum sharing algorithm (FSSA) uses a principle that when an under-layer is deployed in a macrocellular network, only the macrocells within the interfering range of the under-layer cells, i.e., the overlaying macrocell and other surrounding macrocells within the same reuse cluster, must refrain from using the spectrum using by the under-layer cells. For a macrocell in the macrocellular network with at least nine cells per cluster, there are always at least two macrocells in the same cluster that are not adjacent to the macrocell, and the channels assigned to the non-adjacent macrocells may be reused by the under-layer cells in the macrocell. We analysed several case studies of the spectrum sharing system with the macrocellular cluster size of 4/12. To deploy the microcellular system with a reuse cluster size of four within a macrocell, the minimum and maximum transmitting power for microcells were limited to -74 dB and -17.2 dB relative to the maximum macrocell transmitting power, respectively. For the picocell at the ninth-floor of the buildings, the minimum and maximum transmitting power is -100.7 dB and -42.3 dB relative to the macrocell maximum transmitting power, respectively. FSSA gives better spectrum efficiency than the frequency partitioning scheme when the macrocellular system has a reuse cluster size of greater than seven. When the reuse cluster size is less than seven, the frequency partitioning gives better spectrum efficiency. The spectrum efficiency for both schemes are the same for the reuse cluster size of seven. We proposed the dynamic spectrum sharing algorithm (DSSA) where the channel allocation is related to teletraffic demands in each layer. DSSA can be apply to the cellular systems with dynamic channel assignment. The performance of DSSA was analysed in terms of SIR performance.

The research presented in this thesis covers three different approaches of deploying multilayer cellular systems for existing macrocellular network operators. Frequency partitioning is suitable for a macrocellular network of which a reuse cluster is less than or equal to seven. For the multilayer system with macrocellular reuse cluster of greater than seven, spectrum sharing yields better spectrum efficiency. The dual mode system where a GSM network provides wide area coverage and DECT systems provide

local high density coverage, is suitable for the GSM operator with small bandwidth. A novel adaptive autonomous channel assignment scheme which is compatible with both circuit-switched radio systems and packet radio systems, have been proposed.

## 6.2 Conclusions

In conclusion, multilayer mobile communication systems attain enormous spectral efficiency improvements over conventional cellular systems. In some circumstances - as demonstrated in the thesis - the improvement could exceed a factor of 10 000. The proposed solutions are attractive for mobile network designers in resolving capacity problems. At the same time, they introduce the problem of controlling inter-layer interference and bandwitdth management between the layers. Frequency partitioning is a solution that successfully solves the inter-layer interference problem by dividing the network's bandwidth into subbands and by assigning a subband to each layer. However, due to the paucity of bandwidth and the high cost of bandwidth licencing, frequency partition may not be practical, since not all operators can afford a sufficiently high bandwidth for frequency partitioning. Our main contribution was the proposal of spectrum sharing algorithms. The thesis analysed several possible spectrum sharing scenarios, from both a theoretical and practical perspective, including channel assignment problems, and the distinct characteristics of inter-layer and intra-layer cellular environments. An alternative approach of deploying the multilayer system structure was suggested in the context of the GSM/DECT dual mode system for an operator posessing a relatively low bandwidth, which would be too low for invoking spectrum sharing schemes. Some aspects of this system, such as capacity enhancements, wireless ATM based applications and the effects of cordless outdoor propagation, were also addressed.

## 6.3 Suggestion for further work

In multilayer cellular systems, efficient traffic management including call admission and handover strategies are required because mobile terminals may be within service coverage of many BSs in different cellular layers. In order to maximise the system capacity and the quality of service, we must consider several issues such as user mobility, traffic condition at each BS and types of service requested. It would be

interest to establish a mathematical relationship between the grade-of-service and user's mobility, for different cellular layer and different types of service, i.e., telephony, mobile Internet and etc. Further work is, therefore, necessary to deliver and to compare different traffic management algorithms.

It is envisaged that wireless Internet service will play a significant role in shaping the future mobile cellular systems. The high bit-rate traffic demand from users travelling on some public transports such as bus and train could be very high, as several passengers may surfing the Internet during their trip. More public transport system will provide on-board wireless services by deploying on-board picocells. We may term these on-board cells as "moving picocells". To deploying moving picocells within a macrocellular network, more work is needed to evaluate the spectrum efficiency and system performance.

# Glossary

| | |
|---|---|
| **3G** | Third generation mobile radio systems |
| **AAFA** | Adaptive autonomous frequency assignment |
| **ACI** | Adjacent carrier interference |
| **AFP** | Autonomous frequency planning |
| **ATM** | Asynchronous transfer mode |
| **AWGN** | Additive white Gaussian noise |
| **BER** | Bit error rate |
| **BS** | Base station |
| **CCI** | Co-channel interference |
| **CDMA** | Code division multiple access |
| **CEPT** | European posts and telecommunications standards body |
| **CIR** | Carrier-to-interference ratio |
| **CT** | Cordless telecommunication |
| **dB** | Decibel |
| **DCA** | Dynamic channel allocation |
| **DCS** | Digital communication system |
| **DECT** | Digital enhanced cordless telecommunication |
| **DSSA** | Dynamic spectrum sharing algorithm |
| **DTX** | Discontinuous transmission |

| | |
|---|---|
| **FCA** | Fixed channel allocation |
| **FDMA** | Frequency division multiple access |
| **FEC** | Forward error correction |
| **FSSA** | Fixed spectrum sharing algorithm |
| **GHz** | GigaHertz |
| **GMSK** | Gaussian minimum shift keying |
| **GOS** | Grade of service |
| **GSM** | Global system for mobile communication |
| **HO** | Handover |
| **ISI** | Intersymbol interference |
| **KHz** | KiloHertz |
| **LOS** | Line-of-sight |
| **LPF** | Low pass filter |
| **MHz** | MegaHertz |
| **MS** | Mobile station |
| **NLOS** | Non-line-of-sight |
| **PCS** | Personal communication system |
| **PDF** | Probability density function |
| **PRMA** | Packet reservation multiple access |
| **QoS** | Quality of service |
| **RP** | Radio port |
| **RSSI** | Received signal strength indicator |
| **SIR** | Signal-to-interference ratio |

| | |
|---|---|
| **SNR** | Signal-to-noise ratio |
| **TDD** | Time division duplexing |
| **TDMA** | Time division multiple access |
| **VAD** | Voice activity detector |
| **VAF** | Voice activity factor |
| **WLL** | Wireless local loop |

# List of Symbols

## Chapter 2

| | |
|---|---|
| $\chi$ | Fraction of channels allocated for signalling |
| $\eta_B$ | Bandwidth efficiency |
| $\eta_C$ | Spatial efficiency |
| $\eta_S$ | Spectral efficiency |
| $\eta_T$ | Trunking efficiency |
| $\gamma$ | Propagation exponent |
| $\gamma_0$ | Path loss exponent of the desired signal |
| $\gamma_i$ | Path loss exponent of the $i$th interferer |
| $\gamma_I$ | Approximated path loss exponent |
| $\lambda$ | Carrier wavelength |
| $\lambda_h$ | Handover call arrival rate |
| $\lambda_n$ | New call arrival rate |
| $\mu$ | Call departure rate |
| $\mu_c$ | Channel service rate |
| $\mu_h$ | Outgoing handover rate |
| $\mu_m$ | Reciprocal of a mean unencumbered call duration |
| $\mu_b$ | Mean boundary crossing rate |
| $\mu_d$ | Average of normalised BS-MS distance in a cell |
| $\mu_v$ | Average of the inverse of log-normal variables |

| | |
|---|---|
| $\mu_{bc}$ | Mean boundary crossing rate for a circular cell model |
| $\mu_{bl}$ | Mean boundary crossing rate for a highway cell model |
| $\mu_{bs}$ | Mean boundary crossing rate for a street microcell model |
| $\mu_I$ | Approximated mean of the sum of log-normal fading variables |
| $\mu_j$ | Mean of log-normal variables |
| $\mu_k$ | Mean of $V_i(k)$ |
| $\mu_f$ | Mean of $V_f$ |
| $\nu$ | Voice activity factor |
| $\omega$ | Penalty factor |
| $\sigma_f$ | Standard deviation of $V_f$ |
| $\sigma$ | Standard deviation of log-normal fading |
| $\sigma_I$ | Approximated standard deviation of the sum of log-normal fading variables |
| $\sigma_j$ | Standard deviation of log-normal variables |
| $\sigma_k$ | Standard deviation of $V_i(k)$ |
| $\sigma_\xi$ | Standard deviation of shadow fading variables |
| $\theta$ | Angle between the mobile position vector and the antenna direction vector |
| $\zeta$ | Loading factor |
| $A$ | Median path loss |
| $A_I$ | Approximated median path loss |
| $A_{CT}$ | Total traffic carried by a network |
| $A_0$ | Median path loss of the desired signal |
| $A_i$ | Median path loss of the $i$th interferer |

| | |
|---|---|
| $B_c$ | Bandwidth per carrier |
| $B$ | Breakpoint distance |
| $C$ | Number of on ongoing calls in a cell |
| $C_s$ | Number of cells per cluster |
| $C_{s1}$ | Reuse cluster size of a 1-D microcell layout |
| $C_{s2}$ | Reuse cluster size of a 2-D microcell layout |
| $d$ | Distance from the desired BS to the desired mobile |
| $d_{eq}$ | Distance between transceivers normalised by an antenna gain |
| $d_{eq0i}$ | Normalised distance to the connected station of $i$th interferer |
| $D_{b_{NLOS}}$ | NLOS separation distance between adjacent BSs |
| $D_{b_{LOS}}$ | LOS separation distance between adjacent BSs |
| $D_{bv}$ | Vertical BS separation |
| $D_{ch}$ | Nearest horizontal co-channel cell-site separation distance |
| $D_{bh}$ | Horizontal BS separation |
| $D_{cv}$ | Nearest vertical co-channel cell-site separation |
| $D_b$ | BS separation distance |
| $D_c$ | Co-channel reuse distance |
| $D_i$ | Distance between the desired mobile and the $i$th interferer |
| $G_c$ | Carried traffic per channel |
| $h_b$ | BS antenna height |
| $h_m$ | MS antenna height |
| $H_f$ | Floor height |
| $I$ | Average interference |

| | |
|---|---|
| $I_f$ | Interference level at each hop |
| $k$ | Number of first tier interferers |
| $K$ | Number of sectors per cell |
| $L$ | Path loss |
| $L_0$ | Loss at the reference point |
| $L_w$ | Wall loss |
| $L_f$ | Floor loss |
| $L_{h\mu}$ | BS separation distance for highway microcells |
| $L_{s\mu}$ | BS separation distance for street microcells |
| $M_h$ | Number of significant horizontal interferers |
| $M_v$ | Number of significant vertical interferers |
| $M$ | Number of first tier interferers |
| $N_v$ | Vertical reuse distance |
| $N_f$ | Transmitter-to-receiver floor difference |
| $N$ | total number of traffic channels assigned to a cell |
| $N_g$ | Number of channels reserved for handovers only |
| $N_n$ | Number of channels being used by either new calls or handover calls |
| $N_{tc}$ | Total number of carriers allocated to a network |
| $N_{trx}$ | Number of transceivers per cell |
| $N_{ts}$ | Number of time slots per carrier |
| $p_i$ | Probability that the system is in state $i$ |
| $p_k(k)$ | PDF of $k$ |
| $P_B$ | Probability that a new call is blocked |

| | |
|---|---|
| $P_c$ | Proportion of pedestrians leaving a microcell by road crossing |
| $P_d$ | Proportion of pedestrians delayed at the intersection of those who trying to cross |
| $P_F$ | Probability that a handover call is forced to terminate |
| $P_{fh}$ | Probability that a handover is blocked |
| $P_H$ | Probability that a call which already have a successful handover will required another handover before completion |
| $P_N$ | Probability that a new call, which is not blocked will required at least one handover before completion |
| $P_R$ | Received signal power |
| $P_T$ | Transmitted signal power |
| $R$ | Cell radius |
| $R_{LOS}$ | LOS distance to the cell boundary along a street of a microcell |
| $R_{NLOS}$ | NLOS distance to a microcell boundary |
| $\Re$ | Reliability |
| $S_c$ | Sector area |
| $S_T$ | Total area covered by a mobile network |
| **SIR** | Signal-to-interference ratio |
| $\mathbf{SIR}_{min}$ | Minimum signal-to-interference ratio |
| $T_d$ | Average delay time a pedestrian spends waiting at the intersection of to cross the road |
| $T_h$ | Time during which a mobile resides in the cell after a handover |
| $T_m$ | Unencumbered call duration |
| $T_n$ | Time from the onset of a call to when the MS leaves the cell, while still engaged in a call |
| $v_s$ | Mobile's speed |

| | |
|---|---|
| $v$ | Log-normal fading variable |
| $V_i(k)$ | The sum of $k$ log-normal variables |
| $V_f$ | Approximated log-normal random variable of frequency hopping scenario |
| $V_0$ | Shadow fading of the desired signal |
| $V_i$ | Shadow fading of the $i$th interferer |
| $V_{max}$ | Maximum mobile's speed |
| $V_I$ | The sum of log-normal variables |
| $W$ | Total available bandwidth allocated to a network |
| $W_o$ | Width of each office area |
| $W_c$ | Corridor width |
| $W_r$ | Room width |
| $(x_i, y_i)$ | Coordinate of the desired mobile with reference to the $i$th co-channel microcell site in the first tier |
| $(x_{0i}, y_{0i})$ | Coordinate of the $i$th interferer with reference to its connected station |

## Chapter 3

| | |
|---|---|
| $\alpha_i$ | Rayleigh fading variable |
| $\lambda$ | Wavelength |
| $\omega$ | penalty factor |
| $\phi_0$ | Initial phase of the carrier |
| $\phi(t, a)$ | Carrier phase |
| $\Phi(t)$ | Phase function |
| $\sigma_\tau$ | RMS delay spread |
| $\tau_s$ | Fraction bit sampling period |
| $\tau_i$ | Time delay of each Rayleigh fading component |
| $\theta_i$ | Phase variable |
| $\theta(t, a)$ | Correlative state vector that depends on the $L$ most recent bits |
| $\theta_n$ | Phase state |
| $a_i$ | Binary signalling |
| $A$ | Average traffic load |
| $A_t$ | Traffic threshold |
| $A_i$ | Offered traffic per indoor RP |
| $A_o$ | Offered traffic per outdoor RP |
| $A_{pi}$ | Offered traffic of each indoor user |
| $A_{po}$ | Offerer traffic of each outdoor user |
| $B_b$ | 3 dB bandwidth of a low pass filter |
| $B_n$ | Normalised bandwidth |

| | |
|---|---|
| $B_c$ | Coherence bandwidth |
| $d$ | Distance between a RP and a portable |
| $E$ | Energy of $S(t)$ with a symbol period |
| $E_i$ | Average power |
| $f_c$ | Carrier frequency |
| $f_m$ | Doppler frequency |
| $F$ | Floor attenuation |
| $h_1$ | Office RP antenna height |
| $h_2$ | Portable antenna height |
| $h(kT_s)$ | Discrete impulse response of the channel |
| $k$ | Number of floors between a RP and a portable |
| $L$ | Length of symbol response |
| $L(\nu)$ | Clutter loss factor |
| $L_c$ | Number of components in the impulse response |
| $L_{dist}$ | Distance dependent dual slope path loss |
| $L_{walls}$ | The sum of penetration losses of the wall intersected by the path joining a RP and a portable. |
| $n$ | Decay index |
| $N_i$ | Total number of indoor RPs |
| $N_o$ | Total number of outdoor RPs |
| $N_{RP}$ | Total number of RPs |
| $N_{h,i}$ | Number of channels reserved for handover at the $i$th interval |
| $N_{h,max}$ | Maximum number of channels reserved for handover |
| $N_{block}$ | Number of calls being blocked |

| | |
|---|---|
| $N_{drop}$ | Number of calls being dropped |
| $N_{arrival}$ | Total number of call arrivals |
| $P_b$ | Call blocking probability |
| $P_d$ | Call dropping probability |
| $PL$ | Path loss |
| $S(f)$ | Doppler fading spectrum |
| $S(t)$ | Transmitted GMSK radio signal |
| $t$ | Time variable |
| $T$ | Symbol period |
| $T_c$ | Coherence time |
| $v$ | mobile's speed |

## Chapter 4

| | |
|---|---|
| $\beta$ | Stabilising factor |
| $\gamma$ | Propagation factor |
| $\lambda$ | Wavelength |
| $\lambda_c$ | Call arrival rate |
| $\mu_c$ | Call departure rate |
| $A_C$ | Carried traffic |
| $A_T$ | Offered traffic |
| $A_{TH}$ | Traffic threshold |
| $A_u$ | Average offered traffic per user |
| $A_{T_{max}}$ | Maximum offered traffic that a system can handle |
| $A_I$ | Upper value of offered traffic satisfying the constraint of $P_I$ |
| $A_O$ | Upper value of offered traffic satisfying the constraint of $P_O$ |
| $b$ | Building separation |
| $c(j,l)$ | Cost of allocating $l$ after allocating $j$ |
| $C$ | Set of co-channel factors |
| $C_i$ | Co-channel factor of the $i$th frequency |
| $\mathbf{COST}(i,j)$ | Cost of $P(i,j)$ |
| $d$ | Distance between BS and MS |
| $d_c$ | Horizontal distance from a BS to a corner |
| $D_b$ | Breaking distance |
| $f_c$ | Carrier frequency |

| | |
|---|---|
| $F_b$ | Front-back ratio |
| $F_N$ | Set of available carriers |
| $F_i$ | The $i$th allocated frequency |
| $g(i,j)$ | Frequency separation distance between $i$ and $j$ |
| $G$ | Set of edges in the dynamic graph problem |
| $G_T$ | Transmitter antenna gain |
| $G_R$ | Receiver antenna gain |
| $G(\theta)$ | Antenna gain |
| $h_b$ | BS antenna height |
| $h_{roof}$ | Building height |
| $h_m$ | MS antenna height |
| $i,j,k,l$ | Frequency numbers |
| $I$ | Set of measured interference levels |
| $I_{th}$ | Interference threshold |
| $I_i$ | Measured interference level of the $i$th carrier |
| $J$ | Set of neighbouring frequency status |
| $J_i$ | Neighbouring frequency status of the $i$th carrier |
| $K_0$ | Minimum co-site frequency separation required to avoid ACI |
| $K_a$ | Co-channel constraint |
| $L$ | Number of frequencies considered in dynamic graph |
| $L_R$ | Reflected path loss |
| $L_r$ | Reflection loss of the reflecting surface |
| $L_W$ | Walfish-Ikegami's path loss formula |

| | |
|---|---|
| $L_{LOS}$ | LOS path loss |
| $L_{path}$ | Path loss |
| $L_{shd}$ | Shadow fading |
| $L_H$ | Hata's path loss formula |
| $L_{rts}$ | Rooftop-to-street diffraction |
| $L_0$ | Free-space loss |
| $L_{msd}$ | Multiscreen diffraction loss |
| $L_D$ | Direct path loss |
| $L_w$ | The sum of the penetration losses of the walls and the floors intersected by the path joining the BS antenna and the MS antenna |
| $L_f$ | Free-space propagation loss |
| $M_c$ | Number of carriers assigned to a cell |
| $M_{c_{min}}$ | Minimum number of carries assigned to a cell |
| $M$ | Number of frequencies assigned to a cell |
| $M_u$ | Number of ongoing calls |
| $M_{max}$ | Maximum number of calls for acceptable PRMA system operation |
| $N_{TCH}$ | Current number of carrier at a BS |
| $N_u$ | Total number of users |
| $N$ | Number of available carriers |
| $P(i,j)$ | Minimum cost path from vertex $s$ to vertex $j$ in $V_i$ |
| $P_r$ | Average received power |
| $P_{tx}$ | Averaged transmitted power |
| $P_B$ | Call blocking probability |

| | |
|---|---|
| $P_D$ | Call dropping probability |
| $P_F$ | Probability that a call is forced to terminate |
| $P_O$ | Overloading probability |
| $P_I$ | Interference probability |
| $r$ | Cross section radius of the first Fresnel zone |
| $s$ | Beginning vertex |
| $S_i$ | Received power of the $i$th carrier |
| $S_{min}$ | Minimum measured interference level |
| $S_{max}$ | Maximum measured interference level |
| $S_i$ | Normalised measured interference level of the $i$ carrier |
| $t$ | Ending vertex |
| $U$ | Set of the frequency usability values |
| $U_{th}$ | Usability threshold |
| $U_i$ | Usability of the $i$th frequency |
| $V_i$ | Vertices at stage $i$ |
| $V(i,j)$ | Vertice at stage $i$ and frequency $j$ |
| $w$ | Street width |
| $W_{loss}$ | External wall loss |

## Chapter 5

| | |
|---|---|
| $\alpha$ | Underlay-overlay ratio |
| $\lambda$ | Wavelength |
| $\Lambda$ | Required SIR |
| $A_{off}$ | Traffic demand within each office |
| $A_{pc}$ | Traffic capacity per picocell |
| $A_{pd}$ | Traffic demand per picocell |
| $A_i$ | Extra traffic capacity required in a macrocell |
| $A_{mc}$ | Traffic capacity per microcell |
| $C_i$ | Co-channel factor of the $i$ carrier |
| $d$ | Distance from a micro-BS to a mobile |
| $D$ | Co-channel reuse distance |
| $D_{om}$ | Distance from the nearest macrocell interferers to the co-channel microcells |
| $D_m$ | Co-channel reuse distance |
| $D_b$ | Breaking distance |
| $D_p$ | Horizontal co-channel reuse distance |
| $E_A$ | Carrier excluding list for microcells |
| $E_B$ | Carrier excluding list for picocells |
| $F_{A-macro}$ | Available carrier list for the overlaying macrocell |
| $F_{A-micro}$ | Available carrier list for microcells |
| $F_{A-pico}$ | Available carrier list for picocells |
| $F_N$ | Set of carriers available in the network |

| | |
|---|---|
| $F$ | Number of floors |
| $h_{b0}$ | Original microcell antenna height |
| $h_{b-min}$ | Minimum microcell antenna height |
| $h_{b-new}$ | New microcell antenna height |
| $h_b$ | BS antenna height |
| $h_m$ | MS antenna height |
| $i$ | Carrier number |
| $I_i$ | Interference level of the $i$th carrier |
| $I_{TH}$ | Interference threshold |
| $I_{pic}$ | Interference from picocells |
| $I$ | Received interference |
| $I_{mac}$ | Interference from macrocell layer |
| $I_{mic}$ | Interference from microcell layer |
| $K$ | Cluster size |
| $K_a$ | Co-channel constraint |
| $K_0$ | Original macrocell cluster size |
| $K_1$ | New macrocell cluster size |
| $K_h$ | Horizontal cluster size |
| $K_m$ | Microcell cluster size |
| $K_v$ | Vertical cluster size |
| $L_f$ | Floor loss |
| $L_w$ | Wall loss |
| $L_{1-m}$ | Median path loss at 1 metre |

| | |
|---|---|
| $L_{1-km}$ | Median path loss at 1 km |
| $L_{bg}$ | Penetration loss at the ground floor of buildings |
| $L_b$ | Inbuilding path loss |
| $L_{bd}$ | Penetration loss floor factor |
| $L_{b-min}$ | Lower bound of the building attenuation |
| $\Delta L$ | Decibel path loss different between $L_{1-m}$ and $L_{1-km}$ |
| $M_a$ | Number of frequency sets available for spectrum sharing between layers |
| $N$ | Number of significant co-channel interferers |
| $N_{cm1}$ | Number of channels available per microcell for $K = K_1$ |
| $N_{cm0}$ | Number of channels available per microcell for $K = K_0$ |
| $N_{fm}$ | Number of carriers available at a microcell |
| $N_{ip}$ | Number of picocell clusters |
| $N_T$ | Total number of carriers |
| $N_{im}$ | Number of significant interfering microcells |
| $N_{om}$ | Number of significant interfering macrocells |
| $N_{im-max}$ | Maximum number of microcell clusters allowed |
| $N_{im-min}$ | Minimum number of microcell cluster allowed |
| $N_{im-t}$ | Minimum number of microcell clusters that satisfies the traffic requirement |
| $N_{off}$ | Number of offices |
| $N_{bld}$ | Number of buildings |
| $N_{fp}$ | Number of carriers available at a picocell |
| $N_c$ | Number of channel assigned to each macrocell |

| | |
|---|---|
| $N_{bm}$ | Maximum number of channels available for under-layer system for spectrum sharing system |
| $N_{bp}$ | Maximum number of channels available for under-layer system for frequency partitioning system |
| $N_{A-min}$ | Minimum number of carriers assigned to $S_A$ |
| $N_{B-min}$ | Minimum number of carriers assigned to $S_B$ |
| $N_{T-min}$ | Minimum number of carriers for spectrum sharing system |
| $N_{ac}$ | Minimum number of carriers used at each microcell |
| $N_{bc}$ | Minimum number of carriers used at each picocell |
| $N_A$ | Number of carriers assigned to $S_A$ |
| $N_B$ | Number of carriers assigned to $S_B$ |
| $N_f$ | Number of floors between a transmitter and a receiver |
| $N_h$ | Number of significant horizontal co-channel interferers |
| $N_v$ | Number of significant vertical co-channel interferers |
| $P_R$ | Average received power |
| $P_T$ | Average transmitted power |
| $P_{mac}$ | Macrocell transmitting power |
| $P_{mic}$ | Microcell transmitting power |
| $P_{pic}$ | Picocell transmitting power |
| $\Delta P_u$ | Power ratio between transmitting on underlay carriers and overlay carriers |
| $\Delta P$ | Power ratio |
| $\Delta P_{max}$ | Maximum power ratio allowed |
| $\Delta P_{min}$ | Minimum power ratio allowed |
| $Q$ | Macrocell co-channel reuse factor |

| | |
|---|---|
| $Q_{om}$ | Overlay co-channel reuse factor |
| $R_{m-min}$ | Minimum allowed value of $R_m$ |
| $R_{m-max}$ | Maximum allowed value of $R_m$ |
| $R$ | Cell radius |
| $R_m$ | LOS distance from a micro-BS to its cell boundary |
| $R_p$ | Nearest distance from a pico-BS to its cell boundary |
| $S$ | Received power at a cell boundary |
| $S_A$ | Microcell carrier subgroup |
| $S_B$ | Picocell carrier subgroup |
| $S_i$ | Total area served by microcells |
| $U$ | Usability list |
| $U_i$ | Usability of the $i$th carrier |
| $W_r$ | Room width |

# Bibliography


[1] W. C. Y. Lee, *Mobile cellular telecommunications systems*, McGrawhill, 1990.

[2] T.S. Rappaport, *Wireless Communications Principles and Practice*, Prentice Hall, 1996.

[3] M. Frullone et al., "Advanced planning criteria for cellular systems," *IEEE Personal Communications*, pp. 10–15, Dec. 1996.

[4] P. Chow et al., "Performance advantages of distributed antennas in indoor wireless communication systems," *Proc. VTC'94*, pp. 1522–1526, 1994.

[5] K. J. Kerpez, "A radio access system with distributed antennas," *IEEE Trans. Veh. Technol.*, vol. 45, no. 2, pp. 265–275, May 1996.

[6] G. K. Chan and F. A. Razaqpur, "Spectrum requirements of an indoor pico-cell radio system," *IEEE Trans. Veh. Technol.*, vol. 44, no. 1, 1995.

[7] J. S. Engel and M. M. Peritsky, "Statistically-optimum dynamic server assignment in systems with interfering servers," *IEEE Trans. Veh. Technol.*, vol. VT-22, pp. 203–209, Nov. 1973.

[8] L. G. Anderson, "A simulation study of some dynamic channel assignment algorithms in high capacity mobile telecommunications systems," *IEEE Trans. Veh. Technol.*, pp. 210–217, Nov. 1973.

[9] S. M. Elnoubi et al., "A new frequency channel assignment algorithm in high capacity mobile communication systems," *IEEE Trans. Veh. Technol.*, vol. VT-31, no. 3, pp. 125–131, Aug. 1982.

[10] T. J. Kahwa and N. D. Georganes, "A hybrid channel assignment scheme in large-scale cellular-structured mobile communication systems," *IEEE Trans. Commun.*, vol. COM-26, no. 4, pp. 432–438, Apr. 1978.

[11] J. Tajima and K. Imamura, "A strategy for flexible channel assignment in mobile communication systems," *IEEE Trans. Veh. Technol.*, vol. 37, pp. 92–103, May 1988.

[12] J. C.-I. Chuang, "Autonomous adaptive frequency assignment for TDMA portable radio system," *IEEE Trans. Veh. Technol.*, vol. 46, pp. 627–635, Aug. 1991.

[13] M. M.-L. Cheng and J. C.-I. Chuang, "Distributed measurement-based quasi-fixed frequency assignment for TDMA personal communications systems," *IEICE Trans Commun.*, vol. E78-B, pp. 1179–1186, Aug. 1995.

[14] D. C. Cox and D. O. Reudink, "Dynamic channel assignment in high capacity mobile communication system," *Bell Syst. Tech. J.*, vol. 50, no. 6, pp. 1833–1857, July–Aug. 1971.

[15] J. Zander and H. Erikson, "Asymptotic bounds on the performance of a class of dynamic channel assignment algorithms," *IEEE J. Select. Areas Commun.*, vol. 11, no. 6, pp. 926–923, Aug. 1993.

[16] K. Sivarajan and R. McEliece, "Dynamic channel assignment in cellular radio," *Proc. IEEE Veh. Technol. Conf., VTC 1990*, pp. 631–637, May 1990.

[17] D. C. Cox and D. O. Reudink, "A comparison of some channel assignment strategies in large-scale mobile communications systems," *IEEE Trans. Commun.*, vol. 20, pp. 190–195, Apr. 1972.

[18] M. Abdul-Haleem et al., "Fuzzy logic based dynamic channel assignment," *Proc. IEEE ICCS*, vol. 2, pp. 773–777, Nov. 1994.

[19] Y. Akaiwa and H. Andoh, "Channel segregation-a self-organized dynamic channel allocation method: application to TDMA/FDMA microcellular system," *IEEE J. Select. Areas Commun.*, vol. 11, pp. 949–954, Aug. 1993.

[20] T. Kanai, "Autonomous reuse partitioning in cellular systems," *Proc. IEEE Veh. Technol. Conf., VTC 1992*, pp. 782–785, 1992.

[21] J. C.-I. Chuang, "Performance issues and algorithms for dynamic channel assignment," *IEEE J. Select. Areas Commun.*, vol. 11, pp. 955–963, Aug. 1993.

[22] M. M.-L. Cheng and J. C.-I. Chuang, "Performance evaluation of distributed measurement-based dynamic channel assignment in local wireless communications," *IEEE J. Select. Areas Commun.*, vol. 14, pp. 698–710, May 1996.

[23] C. I and P. Chao, "Local packing-distributed dynamic channel allocation at cellular base station," *Proc. IEEE GLOBECOM, 1993*, vol. 1, pp. 293–301, Nov. 1993.

[24] R. Steele et al., "Teletraffic performance of GSM900/DCS1800 in street microcells," *IEEE Commun. Mag.*, pp. 102–108, Mar. 1995.

[25] G. L. Stüber, *Principles of mobile communication*, Kluwer academic publisher, 1996.

[26] M. Mouly and M-B. Pautet, *The GSM system for mobile communications*, M. Mouly and M-B Pautet, 1992.

[27] K. L. Yeung and S. Nanda, "Channel management in microcell/macrocell radio systems," *IEEE Trans. Veh. Technol.*, vol. 45, no. 4, 1996.

[28] H. Xie and S. Kuek, "Priority handoff analysis," in *Proc. IEEE Veh. Technol. Conf., VTC93, New Jersey*, May 1993, pp. 855–862.

[29] D. Hong and S. S. Rappaport, "Traffic model and performance analysis for cellular mobile radio telephone systems with prioritized and non prioritized handoff procedures," *IEEE Trans. Veh. Technol.*, vol. VT-35, pp. 77–91, Aug. 1986.

[30] S. A. El-Dolil et al., "Teletraffic performance of highway microcells with overlay macrocell," *IEEE J. Select. Areas Commun.*, vol. 7, no. 1, pp. 71–78, Jan. 1989.

[31] R. Steele and M. Nofal, "Teletraffic performance of microcellular personal communication network," *IEE Proc.-I*, vol. 139, no. 4, pp. 448–449, Aug. 1992.

[32] R. Steele(Ed) and L. Hanzo(Ed), *Mobile radio communications, 2nd Edition*, John Wiley and Son, 1999.

[33] M. Hata, "Empirical formula for the propagation loss in land mobile radio services," *IEEE Trans. Veh. Technol.*, vol. VT-29, pp. 317–325, 1980.

[34] Y. S. Yeh and S. C. Schwartz, "Outage probability in mobile telephony due to multipath log-normal interferers," *IEEE Trans. Commun.*, vol. COMM-32, pp. 380–388, Apr. 1984.

[35] C. C. Lee and R. Steele, "Signal-to-interference calculations for modern TDMA cellular communication systems," *IEE Proc.-Commun.*, vol. 142, pp. 21–30, Feb. 1995.

[36] M. V. Clark et al., "Reuse efficiency in urban microcellular networks," *IEEE Trans. Veh. Technol.*, vol. 46, pp. 279–289, May 1997.

[37] L. F. Fenton, "The sum of log-normal probability distributions in scatter transmission system," *IRE Trans. Commun. Syst.*, vol. CS-8, pp. 57–67, Mar. 1960.

[38] V. Erceg et al., "Urban/suburban out-of-sight propagation modelling," *IEEE Commun. Mag.*, pp. 56–61, June 1992.

[39] M. Au and R. Steele, "Teletraffic performance of a city street microcellular system using equalised base station loading for TDMA/FCA," *Electronics Letters*, vol. 30, no. 20, pp. 1649–1650, Sept. 1994.

[40] A. Goldsmith and L. J. Greenstein, "A measurement-based model for predicting coverage areas of urban microcells," *IEEE J. Select. Areas Commun.*, vol. 11, pp. 1013–1022, Sept. 1993.

[41] J. E. Berg, "Urban transmission loss models for mobile radio in the 900- and 1800-MHz bands," Tech. Rep. COST 231 TD (90) 119 Rev. 1, EURO-COST, Jan. 1991.

[42] W. H. W. Tuttlebee ed., *Cordless telecommunication worldwide*, Springer, 1996.

[43] D. Raychaudhuri and D. Wilson, "ATM-based transport architecture for multiservices wireless personal communication networks," *IEEE Journal on Selected Areas in Communications*, vol. 12, no. 8, pp. 1401–1413, Oct. 1994.

[44] U. Black, *ATM : Foundation for broadband networks*, Prentice Hall, 1995.

[45] "A guide to DECT features that influence the traffic capacity and the maintenance of a high radio link quality, including the results of simulationa," Tech. Rep., ETFI draft technical report, 1992.

[46] R. Steele, M. Nofal and S. El-Dolil, "Adaptive algorithm for variable teletraffic demand in highway microcells," *Electronics letters*, vol. 26, no. 14, pp. 988–990, July 1990.

[47] H. Hashemi, "The indoor radio propagation channel," *Proceedings of the IEEE*, vol. 81, no. 7, pp. 943–968, July 1993.

[48] J. D. Parsons, *The Mobile Radio Propagation Channel*, Pentech Press, 1991.

[49] T. S. Rappaport, *Wireless Communications Principles and Practice*, Prentice Hall, 1996.

[50] D. Molkdar, "Review on radio propagation into and within buildings," *IEE Proceedings-H*, vol. 138, no. 1, pp. 61–73, February 1991.

[51] F. C. Owen and C. D. Pudney, "In-building propagation at 900 MHz and 1650 MHz for digital cordless telephones," in *Sixth International Conference on Antennas and Propagation (ICAP 89), Coventry, Engl, 04-07 Apr 1989*, IEE, London, Engl., 1989, pp. 276–280.

[52] J. P. Odenwalder, "Optimal decoding of convolutional codes," Tech. Rep., Ph.D. dissertation, School of Engineering and Applied Science, UCLA, 1970.

[53] A. R. Tharek and J. P. McGeehan, "Indoor propagation and bit error rate measurement at 60 GHz using phase-locked oscillators," in *Proc. IEEE Veh. Technol. Conf., VTC88, Philadelphia*, June 1988, pp. 127–133.

[54] P. Karlsson and H. Borjesson, "Measurement system for indoor narrowband radio propagation at 1700 MHz and some results," in *Proc. IEEE Veh. Technol. Conf., VTC92, Miami*, May 1992, pp. 625–628.

[55] J. Dawes, "Factors affecting the impulse response of the indoor radio channel," Tech. Rep., Private communication, May 1995.

[56] J. Dunlop, "Packet access mechanisms for cellular radio," *Electron. & Commun. Eng. Journal*, pp. 173–179, June 1993.

[57] D. J. Goodman, R. A. Valenzuela, K. T. Gayliard, B. Ramamurthi, "Packet reservation multiple access for local wireless communication," *IEEE Trans. Commun.*, vol. 37, no. 8, pp. 885–890, Aug. 1990.

[58] D. J. Goodman and S. X. Wei, "Efficiency of packet reservation multiple access," *IEEE Trans. Veh. Technol.*, vol. 40, no. 1, pp. 170–176, Feb. 1991.

[59] J. Dunlop and J. Y. Khan, "Performance of packet reservation multiple access for digital mobile radio using variable rate speech coder," *Electronics Letters*, pp. 2071–2076, Dec. 1990.

[60] A. Arregui and J. Dunlop, "Stability analysis of the contention mechanism of the PRMA++ protocol," *Proc. IEEE Veh. Technol. Conf. 1998*, vol. 3, pp. 2124–2128, 1998.

[61] D. C. Cox and D. O. Reudink, "The behavior of dynamic channel-assignment mobile communications systems as a function of number of radio channels," *IEEE Trans. Commun.*, vol. 20, pp. 471–479, June 1972.

[62] C.-L. I, L. J. Greenstein and R. D. Gitlin, "A microcell/macrocell cellular architecture for low- and high mobility wireless users," *IEEE J. Select. Areas Commun.*, vol. 11, no. 6, pp. 885–891, Aug. 1993.

[63] A. J. Cooper, "Fibre/radio for the provision of cordless/mobile telephony services in the access network," *Electronics letters*, vol. 26, no. 24, pp. 2054–2056, Nov. 1990.

[64] T-S. Chu and M. J. Gans, "Fibre optic microcellular radio," *IEEE Trans. Veh. Technol.*, vol. 40, no. 3, pp. 599–606, Aug. 1991.

[65] M. I. Silventoinen and H. Posti, "Radio resource management in a novel indoor GSM base station system," *Proc. The 8th IEEE International Symposium on Personal, Indoor and Mobile Radio Communications, PIMRC'97*, vol. 3, pp. 776–780, Sept. 1997.

[66] E. Horowitz and S. Sahni, *Computer algorithms*, Computer Science Press, 1978.

[67] Y. Argyropoulos et al., "Dynamic channel allocation in interference-limited cellular systems with uneven traffic distribution," *IEEE Trans. Veh. Technol.*, vol. 48, no. 1, pp. 224–232, Jan. 1999.

[68] J. D. Parsons, *The mobile radio propagation channel*, Pentech Press, 1992.

[69] P. Harley, "Short distance attenuation measurements at 900 MHz and 1.88 GHz using four antenna heights for microcells," *IEEE J. Sel. Areas Commun.*, vol. 7, pp. 5–11, Jan. 1989.

[70] C. Phongphanphanee, T. Mitchell and R. Steele, "DECT coverage of indoor/outdoor environment," *IEEE Communications Letters*, vol. 3, no. 6, pp. 161–163, June 1999.

[71] S. S. Kuek and W. C. Wong, "Approximate analysis of a dynamic-channel-assignment with handoffs," *IEE Proc.-Commun.*, vol. 141, no. 2, Apr. 1994.

[72] M. Frullone et al., "On the performance of packet reservation multiple access with fixed and dynamic channel allocation," *IEEE Trans. Veh. Technol.*, vol. 42, no. 1, Feb. 1993.

[73] S. Nanda, D. J. Goodman and U. Timor , "Performance of PRMA: A packet voice protocol for cellular systems," *IEEE Trans. Veh. Technol.*, vol. 40, no. 3, pp. 584–598, Aug. 1991.

[74] M. Frullone et al., "Comparisons of multiple access schemes for personal communication systems in a mixed cellular environment," *IEEE Trans. Veh. Technol.*, vol. 43, no. 1, Feb. 1994.

[75] F. D. Priscoli et al., "Application of dynamic channel allocation strategies to the GSM cellular network," *IEEE J. Select. Areas Commun.*, vol. 15, no. 8, pp. 1558–1567, Oct. 1997.

[76] A. Sathyendran, "Multi-layered underlay overlay frequency planning scheme for cellular networks," *Proc. VTC'97*, pp. 1277–1281, 1997.

[77] S. Engstrom et al., "Multiple reuse patterns for frequency planning in GSM networks," *Proc. IEEE Veh. Technol. Conf., VTC 1998*, vol. 3, pp. 2004–2008, 1998.

[78] J. Wigard et al., "Capacity of a GSM network with fractional loading and random frequency hopping," *IEEE International Symposium on Personal, Indoor and Mobile Radio Communications, PIMRC,*, vol. 2, pp. 723–727, 1996.

[79] R. Steele and V. K. Prabhu, "Mobile radio cell structure for high user density and large data rates," *Proc. IEE, Part F*, , no. 5, pp. 396–404, Aug. 1985.

[80] R.Steele, "Towards a high capacity digital cellular mobile radio system," *Proc. IEE, Part F*, , no. 5, pp. 405–415, Aug. 1985.

[81] R. Steele, "The cellular environment of lightweight handheld portables," *IEEE Commun. Mag.*, vol. 27, no. 7, pp. 20–29, July 1989.

[82] T.-S. P. Yum and W. S. Wong, "Hot-spot relief in cellular systems," *IEEE J. Select. Areas Commun.*, vol. 11, pp. 934–940, 1993.

[83] L.-C. Wang, G. L. Stüber and C.-T. Lea, "Architecture design, frequency planning and performance analysis for a microcell/macrocell overlaying system," *IEEE Trans. Veh. Technol.*, vol. 46, no. 4, pp. 836–848, Nov. 1997.

[84] H. Furukawa and Y. Akaiwa, "A microcell overlaid with umbrella cell system," *Proc. IEEE Veh. Technol. Conf., VTC 1994*, pp. 1455–1459, 1994.

[85] S. A. Grandhi et al., "Spectrum scavenging for indoor microcells," *Proc. IEEE Veh. Technol. Conf., VTC 1996*, pp. 462–466, 1996.

[86] C-L. I and M. A. Haleem, "Co-existence DCA: dynamic channel allocations allowing underlaying autonomous microcells," *Proc. IEEE Veh. Technol. Conf., VTC 1997*, pp. 1455–1459, 1997.

[87] M. Almgren et al., "Channel allocation and power settings in a cellular system with macro and micro cells using the same frequency spectrum," *Proc. IEEE Veh. Technol. Conf., VTC 1996*, pp. 1150–1154, 1996.

[88] R. Coombs and R. Steele, "Introducing microcells into macrocellular networks," *IEEE Trans. Commun.*, vol. 47, no. 4, 1999.

[89] T. S. Rappaport and R. A. Brickhouse, "A simulation of cellular system growth and its effect on urban in-building parasitic frequency reuse," *IEEE Trans. Veh. Technol.*, vol. 48, no. 1, pp. 286–294, Jan. 1999.

[90] A. M. D. Turkmani and A. F. de Toledo, "Radio transmission at 1800 MHz into and within, multistory buildings," *IEE Proc.-I*, vol. 138, no. 6, pp. 577–584, Dec. 1991.

[91] A. M. D. Turkmani and A. F. de Toledo, "Propagation into and within buildings at 900, 1800 and 2300 MHz," *IEEE Vehicular Technology Conference*, 1992.

[92] E. H. Walker, "Penetration of radio signals into buildings in cellular radio environments," *IEEE Vehicular Technology Conference*, 1992.

[93] J. M. Durante, "Building penetration loss at 900 MHz," *IEEE Vehicular Technology Conference*, 1973.

# Author Index

## X



## Y



## Z